3
2002

This is to certify that the
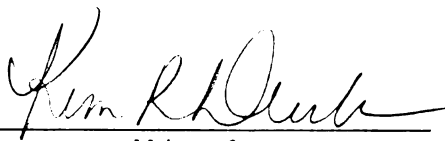
dissertation entitled

MAGNETIC ARCHITECTURES BASED ON METAL CYANIDE
INTERACTIONS:
MIXED METAL CLUSTERS AND POLYMERIC ARRAYS

presented by

Jennifer Ann Smith

has been accepted towards fulfillment
of the requirements for

_____Ph.D._____ degree in __Chemistry__

_____
Major professor

Date _December 8, 2001_

0-12771

**LIBRARY
Michigan State
University**

PLACE IN RETURN BOX to remove this checkout from your record.
TO AVOID FINES return on or before date due.
MAY BE RECALLED with earlier due date if requested.

DATE DUE	DATE DUE	DATE DUE

MAGNETIC ARCHITECTURES BASED ON METAL CYANIDE

INTERACTIONS:

MIXED METAL CLUSTERS AND POLYMERIC ARRAYS

By

Jennifer Ann Smith

A DISSERTATION

Submitted to

Michigan State University

in partial fulfillment of the requirements

for the degree of

DOCTOR OF PHILOSOPHY

Department of Chemistry

2002

ABSTRACT

MAGNETIC ARCHITECTURES BASED ON METAL CYANIDE INTERACTIONS:

MIXED METAL CLUSTERS AND POLYMERIC ARRAYS

By

Jennifer A. Smith

Many magnetic materials, most notably the three dimensional Prussian blue cubic solids, are based on the cyanide ligand. The interest in these systems stems, in part, from the fact that the linear bridging mode of cyanide allows for strong magnetic exchange coupling between paramagnetic metal centers. The interaction favors antiferromagnetic interactions when the magnetic orbitals of the two metals in the M-CN-M' linkage are of the same symmetry, and ferromagnetic interactions when the magnetic orbitals are orthogonal. The ability to predict the nature of the magnetic coupling through the CN^- ligand is one of the main advantages of using this two atom bridge rather than the oxide bridge whose magnetic interactions are highly dependent on the M-O-M' angle.

Research in our laboratory focuses on the building-block approach for preparing specific structural motifs, such as the molecular square and cube, and on using cyanometallates to create new polymeric arrays or discrete clusters. A series of 3d transition metal compounds were prepared with two bidentate ligands along with two weakly coordinating ligand or two cyanide ligands for generating a molecular square motif. An example of this type of reaction is the combination of the cis-M(N-N)$_2$(CN) with cis-[M'(N-N)$_2$(OH$_2$)$_2$]$^{n+}$ in which the H$_2$O ligands are displaced in favor of the nitrogen end of the cyanide ligands. One possible outcome of the reaction is formation of a bimetallic molecular square. In another approach, the transition metal complexes were protected with a facially capping ligand and coordinated to three acetonitrile or cyanide ligands with the aim of preparing molecular cubes.

Another aspect of the project involves the reaction of hexacyanometallate ions [M(CN)$_6$]$^{n-}$ with metal cations M^{2+} (M = Mn, Co and Ni), in the presence of bidentate ligands, such as 2,2'-bipyridine, 1,10-phenanthroline or 2,2'-bipyrimidine. In this manner, a variety of novel bimetallic clusters and low-dimensional polymeric species with distinctive topologies and magnetic properties were obtained.

ACKNOWLEDGEMENT

He never drinks milk, only Coca-Cola, which he said, is the remedy for any illness. He is the reason why I will graduate, his guidance and understanding of the chemistry led the way for my last minute results.

I would like to thank Matt for teaching me how to use a Schlenk line. I have been very fortunate for the friends I made while in graduate school, Jennifer Hess, Jennifer Aitken, Elizabeth, Shannon and Amanda from our aerobic exercise to tae-bo and our shopping excursions. I really miss doing the crossword puzzles with you all everyday at lunch. Our ice cream breaks were delicious and so satisfying. I would also like to thank Paul and Brad for listening to me. I enjoyed our sports conversations and thanks for being my punching bags. I would also like the thank Cristian and the newer group members for some really fun and interesting times in Texas, Karn, Eric, Merv, Curtis, Meijong and Lindsey.

I would also like to thank Joy Heising and Teresia Möller for making my time in Texas so special. I enjoyed our weekend adventures from Tina Turner to squishing frogs that are jumping all over the road while driving to Memphis and using bubble gum to mend our windshield wiper back together at 2 am in pouring rain.

I also would like to give credit to my feline companions, Simba and Bogey. Whenever I had a bad day, I could come home to them and they

would entertain me, almost instantly changing my mood. Most importantly, I want to give my deepest appreciation to my husband, parents and grandparents for their support and understanding.

TABLE OF CONTENTS

x

LIST OF TABLES

xvi

LIST OF FIGURES

LIST OF COMPOUNDS

(1) ---------- $[(2,2'\text{-bpym})_2\text{Mn}(\text{OH}_2)_2](\text{BF}_4)_2$

(2) ---------- $[(2,2'\text{-bpym})_2\text{Fe}(\text{OH}_2)_2](\text{BF}_4)_2$

(3) ---------- $[(2,2'\text{-bpym})_2\text{Co}(\text{OH}_2)_2](\text{BF}_4)_2$

(4) ---------- $[(2,2'\text{-bpym})_2\text{Ni}(\text{OH}_2)_2](\text{BF}_4)_2$

(5) ---------- $[(2,2'\text{-bpy})_2\text{Mn}(\text{CH}_3\text{CN})_2](\text{BF}_4)_2$

(6) ---------- $[(2,2'\text{-bpy})_2\text{Co}(\text{CH}_3\text{CN})_2](\text{BF}_4)_2$

(7) ---------- $[(2,2'\text{-bpy})_2\text{Ni}(\text{CH}_3\text{CN})_2](\text{BF}_4)_2$

(8) ---------- $[(\text{phen})_2\text{Ni}(\text{CH}_3\text{CN})_2](\text{BF}_4)_2$

(9) ---------- $[(2,2'\text{-bpy})_2\text{Ni}(\text{CH}_3\text{CN})_2](\text{PF}_6)_2$

(10) --------- $(2,2'\text{-bpy})_2\text{Mn}(\text{CF}_3\text{SO}_3)_2$

(11) --------- $(2,2'\text{-bpy})_2\text{Co}(\text{CF}_3\text{SO}_3)_2$

(12) --------- $(\text{phen})_2\text{Mn}(\text{CF}_3\text{SO}_3)_2$

(13) --------- $[(2,2'\text{-bpy})_2\text{Ni}(\text{OH}_2)_2](\text{CF}_3\text{SO}_3)_2$

(14) --------- $(\text{phen})_2\text{Mn}(\text{NO}_3)_2$

(15) --------- $(\text{phen})_2\text{Co}(\text{NO}_3)_2$

(16) --------- $(2,2'\text{-bpy})_2\text{Mn}(\text{CN})_2$

(17) --------- $(2,2'\text{-bpy})_2\text{Co}(\text{CN})_2$

(18) --------- $[(4,4'\text{-Me}_2\text{-}2,2'\text{-bpy})_2\text{CrCl}_2]\text{Cl}$

(19) --------- $[(4,4'\text{-Me}_2\text{-}2,2'\text{-bpy})_2\text{FeCl}_2]\text{Cl}$

(20) --------- $[(4,4'\text{-}Me_2\text{-}2,2'\text{-}bpy)_2Fe(CN)_2](PF_6)$

(21) --------- $[(4,4'\text{-}{}^tBu\text{-}2,2'\text{-}bpy)_2Co(CN)_2](PF_6)$

(22) --------- $[TpFe(CH_3CN)_3](CF_3SO_3)$

(23) --------- $K[TpFe(CN)_3]$

(24) --------- $[TpCo(CH_3CN)_3](BF_4)$

(25) --------- $[TpCo(CH_3CN)_3](CF_3SO_3)$

(26) --------- $[TpCo(CH_3CN)_3](PF_6)$

(27) --------- $[Et_4N]_2[TpCo(CN)_3]$

(28) --------- $[TpNi(CH_3CN)_3](BF_4)$

(29) --------- $[TpNi(CH_3CN)_3](CF_3SO_3)$

(30) --------- $[TpNi(CH_3CN)_3](PF_6)$

(31) --------- $NiTp_2$

(32) --------- $[(9S3)Co(CH_3CN)_3](PF_6)_2$

(33) --------- $(9S3)CoCl_2$

(34) --------- $[Co(9S3)_2]Cl_2$

(35) --------- $[FeTp_2](BF_4)$

(36) --------- $\{Mn(H_2O)_2[Mn(2,2'\text{-}bpym)(H_2O)]_2[Fe(CN)_6]_2\}$

(37) --------- $\{[Co(2,2'\text{-}bpy)_2]_3[Fe(CN)_6]_2\}^+$

(38) --------- $\{[Ni(2,2'\text{-}bpy)_2(H_2O)][Ni(2,2'\text{-}bpy)_2]_2[Fe(CN)_6]_2\}$

(39) --------- $\{[Zn(phen)_3][Zn(phen)_2]_2[Fe(CN)_6]_2\}$

(40) --------

{[Zn(phen)$_2$][Fe(CN)$_6$]}$_2${[Zn(phen)$_2$(OH$_2$)][Zn(phen)$_2$][Fe(CN)$_6$]}$_2$

LIST OF ABBREVIATIONS

CH_3CN	acetonitrile
Å	Angstrom
br	broad
2,2'-bpy	2,2'-bipyridine
2,2'-bpym	2,2'-bipyrimidine
μ	bridging ligand, micro
°C	Celsius
dien	diethylenetriamine
4,4'-Me$_2$-2,2'-bpy	4,4'-dimethyl-2,2'-bipyridine
v	frequency
g	gram
X	halide
$(PF_6)^-$	hexafluorophosphate
h	hour
IR	infrared spectroscopy
m	medium intensity
mL	milliliter
mmol	millimole
M	molarity (moles per liter)

mol	mole
N-N	2,2'-bipyridine, 2,2'-bipyrimidine or 1,10-phenanthroline
$(NO_3)^-$	nitrate
NMR	nuclear magnetic resonance
$(ClO_4)^-$	perchlorate
phen	1,10-phenanthroline
[K-18-C-6]	potassium 18-C-6 ether
s	singlet, strong intensity
S	solvent molecule
4,4'-^{t}Bu-2,2'-bpy	4,4'-*tert*-butyl-2,2'-bipyridine
$[Bu_4N]$	tetrabutylammonium
$[Et_4N]$	tetraethylammonium
$(BF_4)^-$	tetrafluoroborate
THF	tetrahydrofuran
$(CF_3SO_3)^-$	triflate
Tp	tris(1-pyrazolyl)borohydride
9S3	1,4,7-trithiacyclononane
λ	wavelength
cm^{-1}	wavenumber
w	weak intensity

Chapter 1

INTRODUCTION

INTRODUCTION

1. History of Molecular Magnetism

The use of soluble transition metal coordination complexes as precursors to materials is a rapidly expanding area of inorganic chemistry with many potential applications. Topological arguments that take into consideration the geometrical preferences of the metals and ligands have allowed chemists to design new molecule-based solids, including porous,[1] magnetic,[2] conducting[3] and conducting materials that possess magnetic centers.[4]

Molecular magnetism originated with the discovery of Wickman and co-workers[5] who reported that the complex $FeCl(L-L)_2$ (L-L = N,N-diethyldithiocarbamate) with an S = 3/2 ground state orders ferromagnetically at a T_c of 2.5 K. Since then, the study of molecule-based magnets has emerged as a new field, with notable breakthroughs by Kahn[6] who reported the first inorganic-based molecular magnet ferrimagnetic chain of Mn(II)Cu(II) centers and by Miller and co-workers,[7] who discovered the first organic based molecular magnet, $[FeCp*_2][TCNE]^-$ (TCNE = tetracyanoethylene). Since these developments, advancements in this field include the discovery of high T_c ferromagnets based on the Prussian Blue motif,[8] spin-crossover compounds that undergo abrupt transitions near room

ter

m

s

#2

use

lau

p

temperature,[9] compounds that superconduct in the presence of localized magnetic moments,[10] and high spin clusters that mimic the properties of a single domain magnet (single molecule magnets).[11]

2. Prussian Blue

Among the more impressive magnetic solids based on coordination compounds are those based on the three-dimensional, face-centered cubic solid, $[Fe_4[Fe(CN)_6]_3 \cdot xH_2O$ (x = 14-16), called Prussian blue (PB), which was discovered in 1704 by Diesbach, a Berlin artist.[12] This material has been used extensively in the manufacturing of paints, lacquers, printing inks, laundry chalks and other color uses. The continued popularity of this pigment is attributed to its low cost, deep bright shade, high color strength and resistance to the action of water, organic media and acids.

An intriguing issue about PB that has fascinated chemists from the beginning is that two virtually colorless ions, namely $[Fe(H_2O)_6]^{3+}$ and $[Fe(CN)_6]^{4-}$, react in water to produce an intensely colored blue precipitate. It is now recognized that the color is due to a charge-transfer transition from the Fe(II) to the Fe(II) ion through the cyanide bridge. The structure of PB has also been the subject of great interest in the last century. The solid-state structure consists of alternating ferrous and ferric metal ions at the corner of a cubic lattice with edges of 5.1 Å.[12a] The cyanide groups lie along the edges

of the cubes connecting each metal atom. In spite of how long the material has been known, the first single crystal X-ray study of Prussian Blue, $Fe_4[Fe(CN)_6]_3 \bullet 14H_2O$ was not reported until 1977 by Ludi and co-workers.[13]

As the previous paragraph alludes, there are two basic environments for the metal centers in the Prussian Blue framework, assigned M^A and M^B in the general formula $M^A_x[M^B(CN)_6]_y$.[14] The M^A metals are coordinated to the N atom of six cyanide ligands, creating a weak ligand field, whereas M^B metals are bound through the carbon atoms which creates a strong ligand field. In the specific case of PB, $Fe_4[Fe(CN)_6]_3 \bullet xH_2O$ (x = 14-16) (Figure 1.1.), the Fe(II) ions are coordinated to the carbon end of CN^- and thus are low-spin d^6 ions whereas the Fe(III) ions are coordinated to the nitrogen end of CN^- and are high-spin d^5 ions. This situation results in only one type of paramagnetic site on PB, namely the L.S. Fe(III) S=1/2 centers which undergo ferromagnetic coupling through the diamagnetic Fe(II) centers. The first indication of the ferromagnetic ordering at T_c = 5.5 K was detected by Mössbauer spectroscopy.[15,16] Later Mayoh and Day concluded that, in spite of the long distances that separate the Fe^{III} centers, the intervening Fe^{II} sites participate in the magnetic interaction by providing a through bond-pathway.[17]

4

A. Background Magnetic Properties

In order to understand the factors involved in molecular *magnetism,*[18] some basic magnetic phenomena must first be understood. *In ferromagnets,* the individual spins are oriented in parallel fashion. In both antiferromagnets and ferrimagnets, the spins are coupled antiparallel to each other. The coupling constant J, describes the isotropic interaction between two spins S_1 and S_2, and is defined by the spin Hamiltonian $H = -2J(S_1 \bullet S_2)$. The energy separation between the singlet and the triplet states is J. For ferromagnetic coupling, $J > 0$, while for antiferromagnetic coupling, $J < 0$. If the orbitals containing the unpaired electron(s) are orthogonal to each other, then the magnetic orbitals cannot interact and Hund's rule keeps the spins parallel; in this situation, ferromagnetic coupling between the two spins occurs (Figure 1.2.). If direct overlap between the orbitals occurs as is the case when the magnetic orbitals have the same symmetry, the antiparallel alignment will be favored. A type of ordering called ferrimagnetism occurs when the local anti ferromagnetically interacting spins are not of equal magnitude but the residual spins order in the same manner as a ferromagnet.
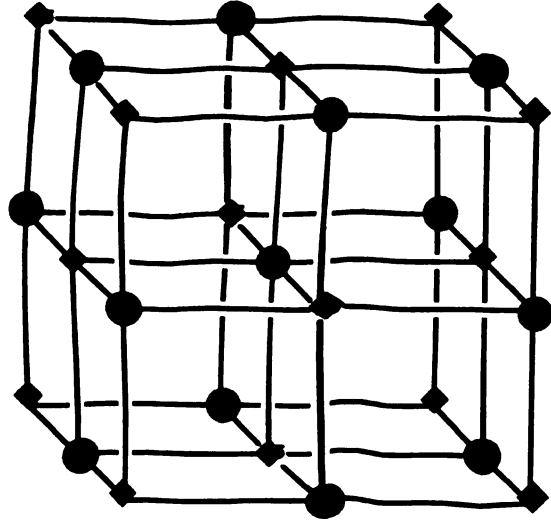
Face-Centered Cubic
Three-Dimensional Solids

● - Fe(II) (C_6 coordination)

◆ - Fe(III) (N_6 coordination)

Figure 1.1. Schematic diagram depicting the unit cell of the Keggin and Miles model of Prussian Blue. (Image is presented *in color*)

CN⁻ binds first at the C end ──→ Low-Spin

The second metal binds to N ──→ High-Spin

$L_nCr^{II}-CN-Mn^{II}L_n$

L.S.   H.S.

$t_{2g}^4 e_g^0$ $t_{2g}^3 e_g^2$

S=1   S=5/2

Direct overlap
of the t_{2g} orbitals so
unpaired electrons in these
orbitals **pair up**

ANTIFERROMAGNETIC
COUPLING

Net Spin (S = 3/2)

$L_nCr^{II}-CN-Ni^{II}L_n$

L.S.   H.S.

$t_{2g}^4 e_g^0$ $t_{2g}^6 e_g^2$

S=1   S=1

NO direct overlap of the
t_{2g} and e_g orbitals
(orthogonality) so unpaired
electrons in these orbitals
do not pair up

FERROMAGNETIC
COUPLING

Net Spin (S = 2)

Figure 1.2. Schematic diagram representing *antiferromagnetic* and ferromagnetic coupling of open-shell transition metals bridged by cyanide.

7

3. Prussian Blue Analogues

Within the past ten years, researchers have opened up new venues for Prussian-blue type chemistry by introducing a variety of metal atoms into the cubic structure afforded by octahedral $[M(CN)_6]^{n-}$ building blocks The aim is to increase magnetic ordering temperatures, and, indeed, several Prussian blue analogues have been prepared that exhibit T_c values above room temperature.[8] Prussian Blue analogues with metals other than iron are currently playing a major role in the research of magnets that order at high temperatures (Table 1.1.). An example of a Prussian Blue analogue is $Mn[Mn(CN)_6] \cdot 1.14H_2O$, which exhibits Curie paramagnetism between 140 and 300 K and a magnetic phase transition at 49 K due to ferrimagnetic ordering of this mixed valence system.[19] The M^A site is occupied by high-spin Mn(II) ions ($t_{2g}^3 e_g^2$, $S_A = 5/2$) whereas the M^B site is occupied by Mn(IV) ions (t_{2g}^3, $S_B = 3/2$). The three unpaired electrons in the t_{2g} orbitals are antiferromagnetically coupled, the net result of which is that two unpaired electrons from the Mn(II) centers are not cancelled. This magnetic behavior is dominated by the antiferromagnetic superexchange interaction through the cyanide ligand.

Table 1.1 *Prussian blue and PB analogues with their* T_c *values.*

Complex	T_c	Magnetic	ref
$V^{II}[Cr^{III}(CN)_6]_{0.66} \cdot 3.5H_2O \cdot 0.1[Et_4N][OTf]$	376	ferri	32a
$K_{0.058}V^{II/III}[Cr^{III}(CN)_6]_{0.79} \cdot (SO_4)_{0.058} \cdot 0.93H_2O$	372	ferri	32b
$K_{0.50}V^{II/III}[Cr(CN)_6]_{0.95} \cdot 1.7H_2O$	350	ferri	32b
$Cs_{0.82}V^{II}[Cr^{III}(CN)_6]_{0.94} \cdot 3H_2O \cdot 0.4[Et_4N][OTf]$	337	ferri	32a
$KV^{II}[Cr^{III}(CN)_6] \cdot 2H_2O \cdot 0.1KOTf$	330	ferri	32a
$Cs_{0.82}V^{II}_{0.66}[V^{IV}O]_{0.34}[Cr^{III}(CN)_6]_{0.92}[SO_4]_{0.203} \cdot 3.6H_2O$	315	ferri	8d, 32c
$V^{II}_{0.42}V^{III}_{0.58}[Cr(CN)_6]_{0.86} \cdot 2.8H_2O$	315	ferri	32d
$V^{II}_{0.45}V^{III}_{0.53}[V^{IV}O]_{0.02}[Cr^{III}(CN)_6]_{0.69}[SO_4]_{0.23} \cdot 3H_2O \cdot 0.02K_2SO_4$	310	ferri	8d, 32c
$[Cr_5(CN)_{12}] \cdot 10H_2O$	240	ferri	32e
$[Et_4N]_{0.5}Mn_{1.25}[V(CN)_6] \cdot 2H_2O$	230	ferri	32f
$Cs_{0.75}[Cr_{2.125}(CN)_6] \cdot 5H_2O$	190	ferri	32e
$Cs_2Ni[V(CN)_6]$	125	ferri	32f

9

Table 1.1 (*con't*)

$CsMn[Cr(CN)_6] \cdot H_2O$	90	ferri	32g
$CsNi[Cr(CN)_6] \cdot 2H_2O$	90	ferri	8a
$[Me_4N]Mn[Cr(CN)_6]$	59	ferri	32g
$Mn^{II}[Mn^{IV}(CN)_6] \cdot 1.14H_2O$	48.7	ferri	19
$K_2Mn[Mn(CN)_6]$	41	ferri	32h
$Mn_3[Mn(CN)_6]_2 \cdot 12H_2O$	37	ferri	32h
$CsMn[Mn(CN)_6] . 1/2H_2O$	31	ferri	32h
$Ni_3[Fe^{III}(CN)_6]$	23.6	ferro	32i
$Cu_3[Fe^{III}(CN)_6]_2$	20	ferro	32
$Co^{II}_3[Fe^{III}(CN)_6]_2$	14	ferri	32i
$Mn^{II}_3[Fe^{III}(CN)_6]_2$	9	antiferro	32
$Fe_4[Fe(CN)_6] \cdot xH_2O \ x = 14\text{-}16$	5.5	ferro	15, 16

ferri = ferrimagnetic, ferro = ferromagnetic, antiferro = antiferromagnetic

10

4. Controlled Syntheses of Specific Motifs

Nearly all of the d-block metals are known to form *compounds of* cyanide in which the ligand exhibits different binding modes *(Figure 1.3.).*[14] Homoleptic and mixed ligand cyanide complexes with a wide range of oxidation states and coordination numbers ranging from two to eight are known. The bidentate, linear nature of cyanide gives rise to extended structures with 1-D, 2-D and 3-D motifs, the exact nature of which depends on the coordination number and arrangement of ligands around the metal centers.

One particular motif of interest in our laboratory is the molecular square. Molecular squares composed of four metals bridged by four cyanides have been known since the early 20th century, the most common of which is based on square planar metal complexes with two *cis* protecting groups *(Figure 1.4.).*[20] Molecular squares can be prepared by a number of different routes, but the one of interest in this thesis involves the self-assembly of four octahedral precursors each with two *cis* chelating ligands (N-N). There are two types of precursors, namely those that contain two *cis* cyanides in addition to the two N-N ligands (donor positions) and those that contain solvent or leaving groups (acceptor positions) as depicted in Figure 1.5. In a reaction between precursors of this type, $[(N-N)_2M(CN)_2]^n$ and
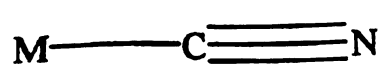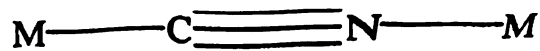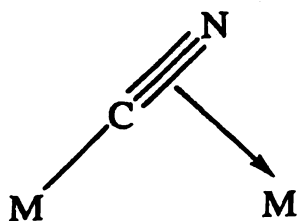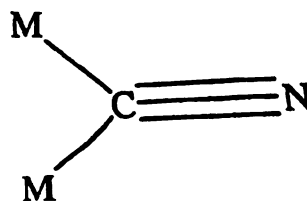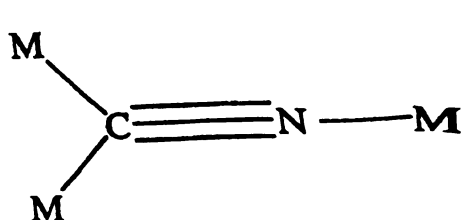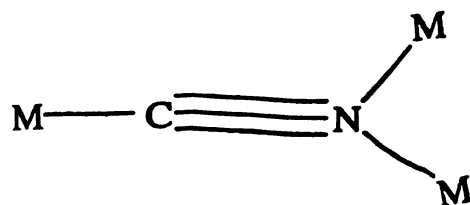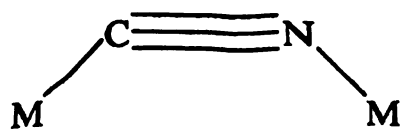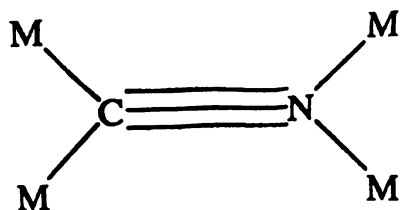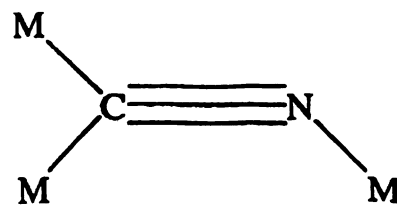
Figure 1.3. Coordination modes of the cyanide ion.
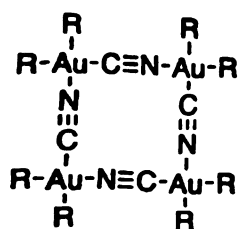
Phillips & Powell, 1939
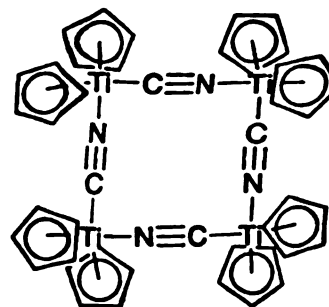
Schinnerling & Thewalt, 1992
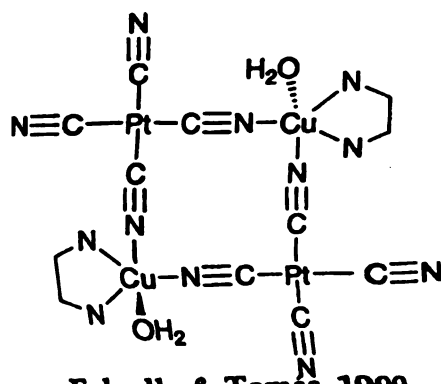
Falvello & Tomás, 1999
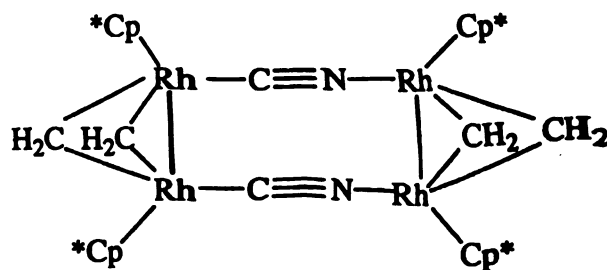
Maitlis et al., 1991
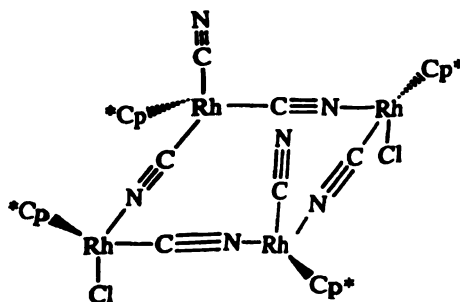
Rauchfuss, 1998
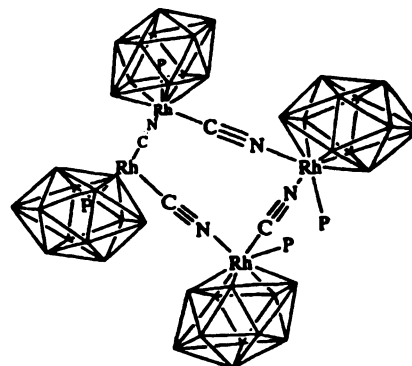
Hawthorne, et al., 1982

Figure 1.4. Examples of cyclic metal cyanide clusters characterized by X-ray diffraction studies.
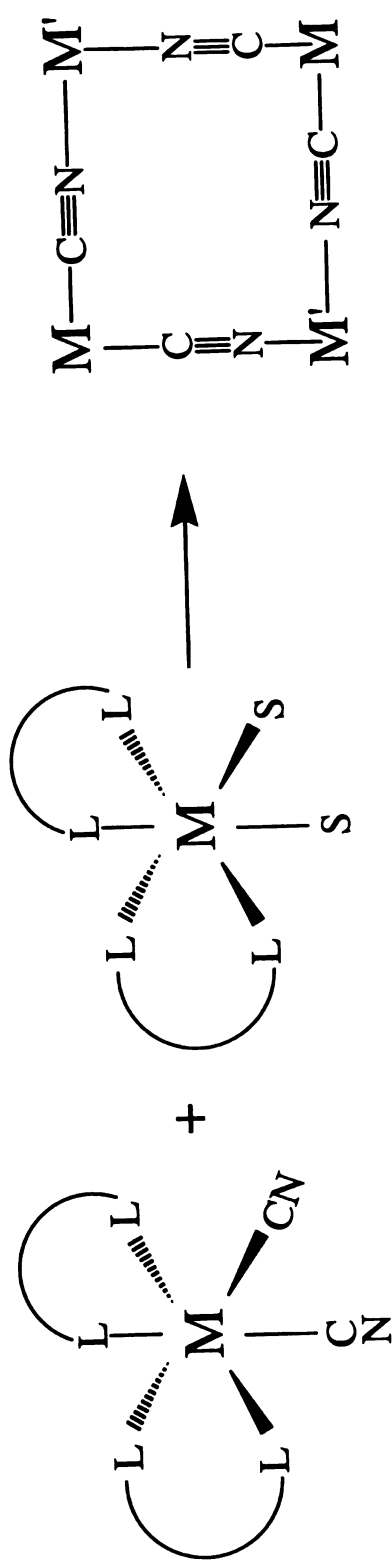
Figure 1.5. Schematic diagram representing the molecular square assembly process.

$\bigcap$ L — L = 2,2'-bipyrimidine, 2,2'-bipyridine or 1,10-phenanthroline

$S = OH_2$, CH_3OH, NO_3^-, $O_3SCF_3^-$ or CH_3CN

$[(\text{N-N})_2M'(\text{S})_2]^n$, the S ligands are displaced in favor of the nitrogen end of the cyanide ligands with one potential outcome being a molecular square. Molecular squares with octahedral 3d transition metal building blocks have been prepared, but they are far less common than the square planar 4d and 5d metals.[20d] In terms of magnetic behavior, a homometallic square would exhibit antiferromagnetic coupling, but by applying the orthogonality principle as a guide in selecting metals for a heterometallic square, ferromagnetic coupling can be favored.

In the vein of preparing open-shell molecular squares, Oshio and co-workers reported $[\text{Fe}_2^{II}\text{Cu}_2^{II}(\mu\text{-CN})_4(\text{bpy})_6](\text{PF}_6)_4 \bullet 2\text{H}_2\text{O} \bullet 4\text{CHCl}_3$ and $[\text{Fe}_2^{III}\text{Cu}_2^{II}(\mu\text{-CN})_4(\text{bpy})_6](\text{PF}_6)_6 \bullet 4\text{CH}_3\text{CN} \bullet 2\text{CHCl}_3$ (Figure 1.6.)[20i] whose magnetic properties are that of a simple paramagnet with noninteracting Cu^{II} centers in the $\text{Fe}_2^{II}\text{Cu}_2^{II}$ with low-spin Fe^{II} (S = 0) and S = 1/2 Cu^{II} centers. On the other hand, the $\text{Fe}_2^{III}\text{Cu}_2^{II}$ square with two S = 1/2 Fe^{III} centers in addition to two S = 1/2 Cu^{II} centers exhibits ferromagnetic coupling between the open shell Fe and Cu centers which gives rise to a total ground state for the molecule of S = 2.

A logical extension of the molecular square family of compounds into a third dimension is to molecular cubes, which have the potential for possessing higher magnetic moments due to the presence of eight rather than
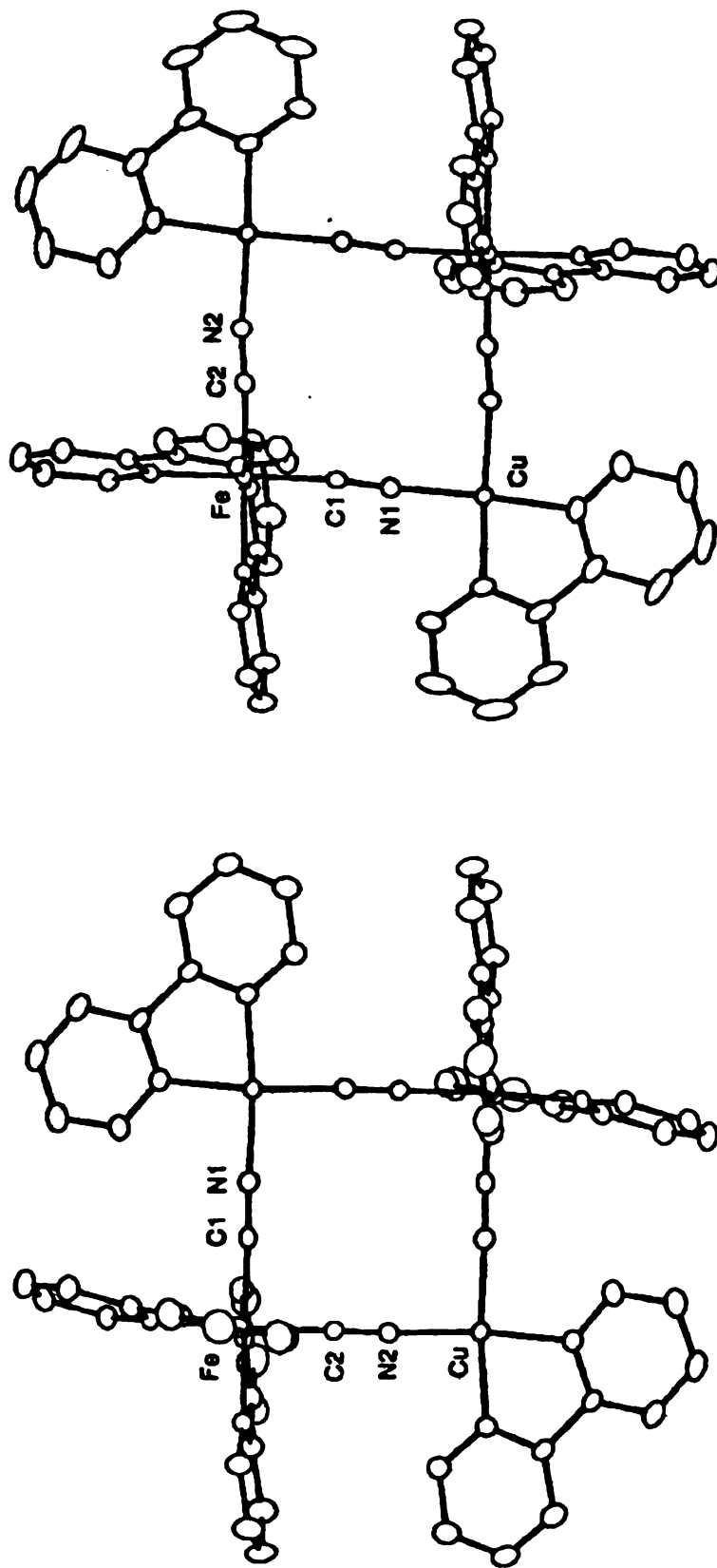
Figure 1.6. Structural representations of the molecular squares a) $[Fe_2^{II}Cu_2^{II}(\mu\text{-}CN)_4(bpy)_6](PF_6)_4 \bullet 2H_2O \bullet 4CHCl_3$ and b) $[Fe_2^{III}Cu_2^{II}(\mu\text{-}CN)_4(bpy)_6](PF_6)_6 \bullet 4CH_3CN \bullet 2CHCl_3.^{[20i]}$

only four metal centers. Molecular cubes were recently prepared independently by Rauchfuss and Long, in which the corners consist of eight metal atoms with bridging cyanides along the twelve edges. The remaining three coordination sites on the metal centers are occupied by a facial capping ligand, such as C_5H_5, C_5Me_5 or the triazacyclononane (tacn) ligand. In this manner, Rauchfuss and co-workers prepared the molecular cube, $[(Cp)_4(C_5(CH_3)_4(CH_3CH_2))_4Co_4Rh_4(CN)_{12}](PF_6)_4$ (Figure 1.7.), which exhibits interesting host-guest behavior.[21] The molecule was characterized by single crystal X-ray diffraction studies and found to have face diagonal distances of 7.1 and 7.4 Å with an interior volume estimated to be ~132 $Å^3$. The covalent radii of the cube framework prohibit access to the interior since six CH_3CN molecules are located near the cube faces, which are neither bound to nor inserted into the cube.

In a more interesting example, the same research group demonstrated the inclusion ability of $[Et_4N]_3\{M[(Cp^*)Rh(CN)_3]_4[Mo(CO)_3]_4\}$ (M = K, Cs) (Figure 1.8.) with alkali metals.[22] In the presence of an alkali metal cation, these cubes form in solution from the reaction of $(C_6H_3(CH_3)_3)Mo(CO)_3$ and $[Et_4N][(Cp^*)Rh(CN)_3]$. By replacing the Co(III) ion with the larger Mo(0) atom, it was possible to obtain a much larger cube framework such that alkali metal inclusion was possible. Competition experiments revealed that

17

the cube has a higher affinity for Cs^+ than K^+, thereby demonstrating the feasibility for selective host-guest chemistry.

It is important to point out that performing Rauchfuss and co-workers selected metals for their cube corners on the basis of size and relative inertness with respect to substitution. The Co(III) Rh(III) and Mo(0) ions/atoms used as cube corners are *diamagnetic*, which, of course, precludes the molecules from having any magnetic properties. In contrast, the work being conducted in our laboratories and those of Long and co-workers is focused on the preparation of heterometallic cyanide cubes with *paramagnetic* transition metal centers.

The work of Long and co-workers has led to some key results in the area, beginning with their report of the diamagnetic molecular cube, $[(tacn)_8Co_8(CN)_{12}](CF_3SO_3)_{12}$ (Figure 1.9.) which was structurally characterized by single crystal X-ray diffraction methods.[23] Although the compound is not paramagnetic, it serves as a proof of concept that first row transition metals can form such closed structures. The same group later reported the reaction of $[(tacn)Cr(H_2O)_3](CF_3SO_3)_3$ and $[(tacn)Co(CN)_3]$ to yield the paramagnetic cube, $[(tacn)_8Cr_4Co_4(CN)_{12}](CF_3SO_3)_{12} \cdot 8H_2O$ which was characterized by electrospray mass spectrometry. Unfortunately, no single crystals were obtained. Magnetic susceptibility measurements
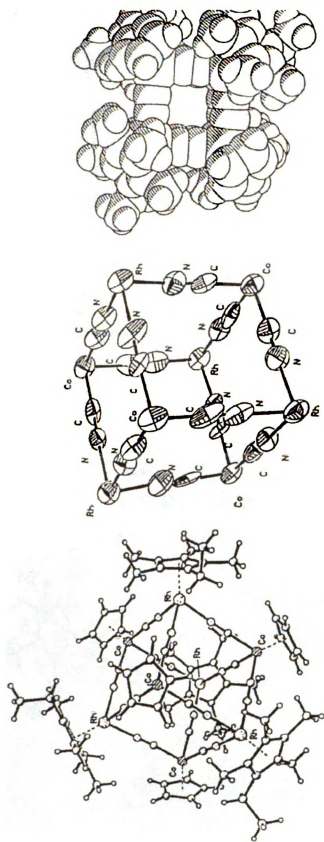
Figure 1.7. Thermal ellipsoid plots of $[(Cp)_4(C_5(CH_3)_4CH_3CH_2)_4Co_4Rh_4(CN)_{12}](PF_6)_4$ depicted (a) with corner protecting Cp and Cp* ligands, (b) skeletal view and (c) space filling diagram.[21]
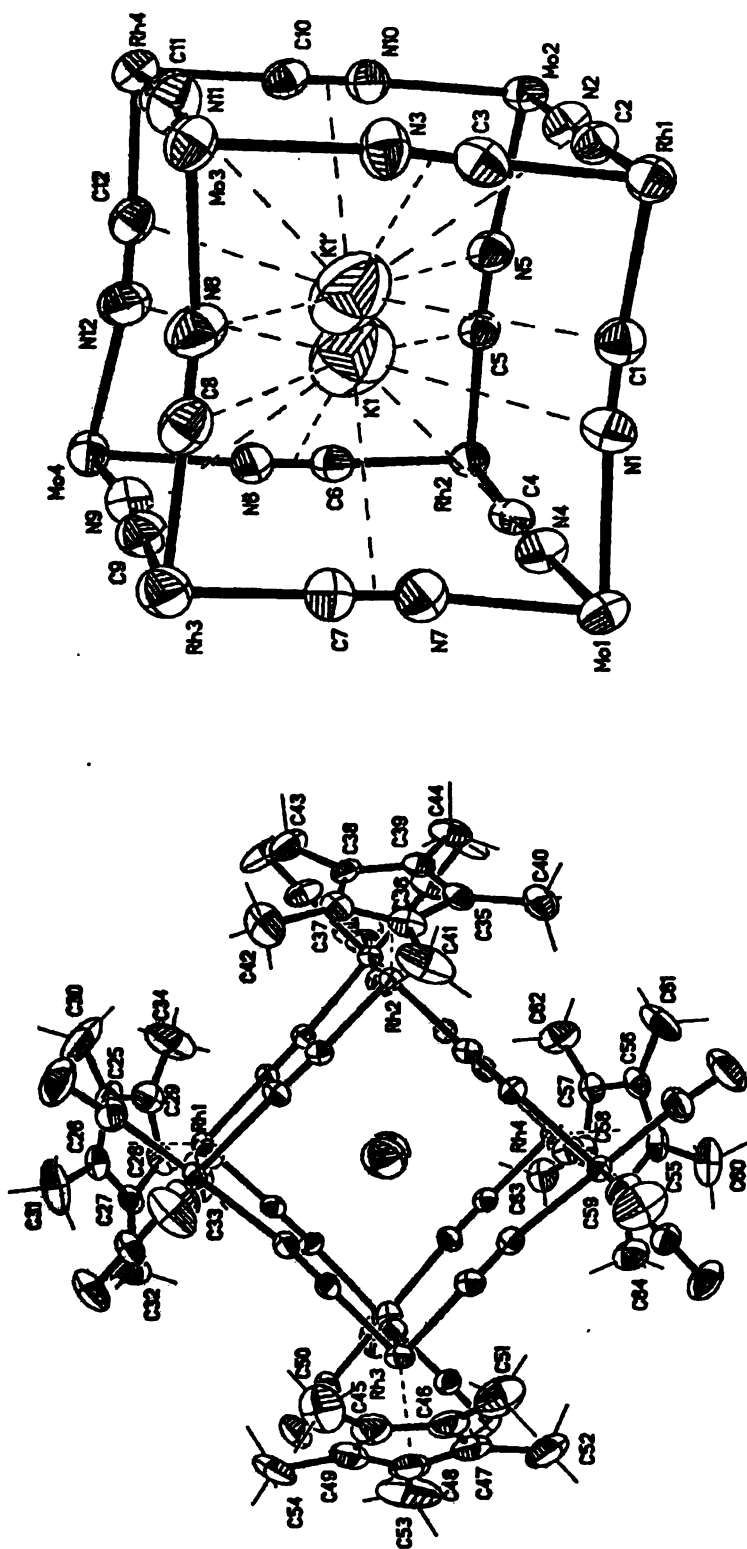
Figure 1.8. Thermal ellipsoid plots of K[(Cp*)$_4$(CO)$_{12}$Rh$_4$Mo$_4$(CN)$_{12}$] (a) with the corner protecting Cp* groups and (b) skeletal view. The potassium atom is disordered over two sites.[22]
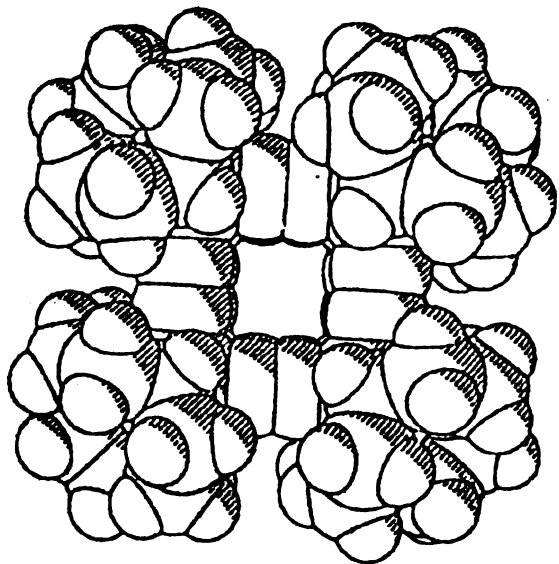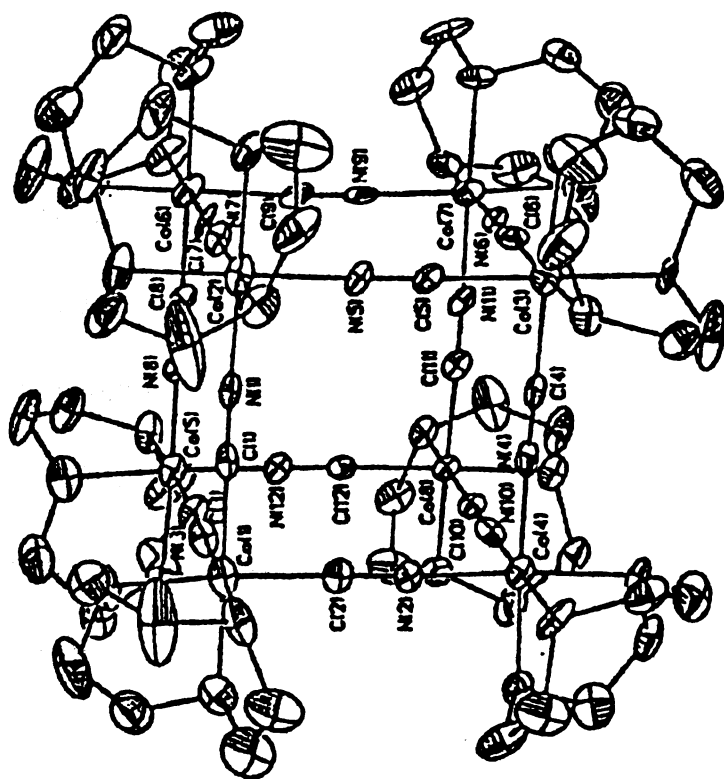
Figure 1.9. Thermal ellipsoid plot of the molecular cube structure [(tacn)$_8$Co$_8$(CN)$_{12}$](O$_3$SCF$_3$)$_3$ and a space filling diagram.[23]

revealed a room temperature μ_{eff} value of 7.51 B.M. with a g value of 1.97, which is consistent with four isolated S = 3/2 Cr(III) centers per cube. Evidently the diamagnetic Co(III) centers prevent coupling between the Cr(III) centers.

Despite the lack of magnetic coupling exhibited by the compound [(tacn)$_8$Cr$_4$Co$_4$(CN)$_{12}$](O$_3$SCF$_3$)$_{12}$•8H$_2$O, it is important to continue to prepare molecules of this type in order to test the possibility of having high moments that lead to interesting magnetic behavior. Although the compounds are not cyanide-based, it is important to point out that several mixed-valence manganese oxide clusters[24] (Figure 1.10.) with high ground state spin values exhibit what is referred to as single molecule magnetism (SMM). Unfortunately, it is not possible to predict the compositions or magnetic superexchange of oxide clusters that form in aqueous solution due to pH dependent redox reactions. In contrast, metal cyanide chemsitry is under much more synthetic control, as evidenced by the results presented in the aforementioned paragraphs.

Apart from the manganese oxide/carboxylate clusters, there are other metal oxide molecules that exhibit the slow magnetic relaxation characteristic of single molecule magnetism. A single molecule magnet (SMM) is defined as a compound with discrete non-interacting molecules

that exhibit sufficiently large magnetic moments and axial magnetic anisotropy (D) such that the molecule has an easy axis of alignment with an external field with a barrier converting between the equal energy states of magnetization parallel "↑" to the field to magnetization antiparallel "↓" to the field. The presence of a thermal barrier to reorienting the magnetization means that below a threshold temperature (the blocking temperature), the molecules function as a magnetic switch. In response to an external magnetic field, the magnetic moment of the SMM can be magnetized with its spin either "up" or "down" along the axial magnetic anisotropy axis. After the magnetic moment of this molecular species is oriented in an external field, and when the external field is then removed, the moment of the molecule will only very slowly reorient if the temperature is below the "blocking temperature". The key to making an SMM with an energy barrier for the magnetic moment reversal that exhibits a slow relaxation is to build in a ground state with high spin, S and negative axial magnetic anisotropy, *i.e.*, D < 0, since the barrier height for magnetization reversal scales as $S^2|D|$. A diagram of this double-well potential energy barrier for $[Mn_{12}O_{12}(O_2CCH_3)_{16}(H_2O)_4] \cdot 2(HO_2CCH_3) \cdot 4H_2O$ (S = 10) is depicted in Figure 1.11.[24d] Specifically for the Mn_{12} cluster, S = 10 and D = -0.50 cm^{-1} which leads to a barrier height of ~50 cm^{-1}. At 2 K, the Mn_{12} complex has a
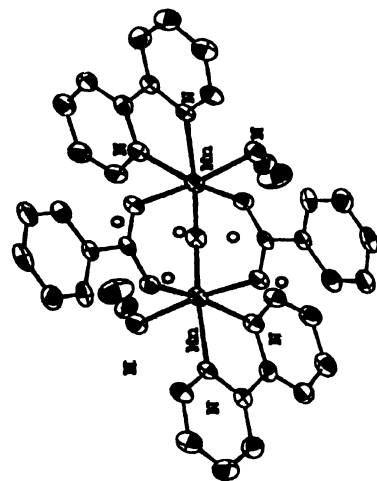
a) [Mn₂O(O₂CPh)₂(N₃)₂(bpy)₂]
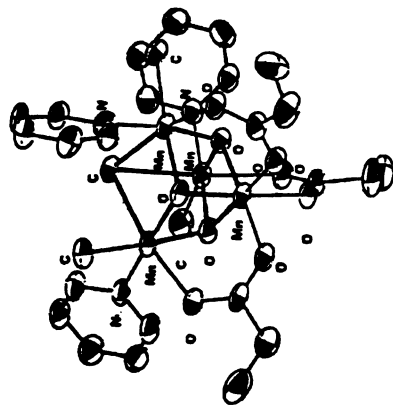
b) [Mn₄O₃Cl(O₂CCH₂CH₃)₃(py)₃]•5/2CH₃CN
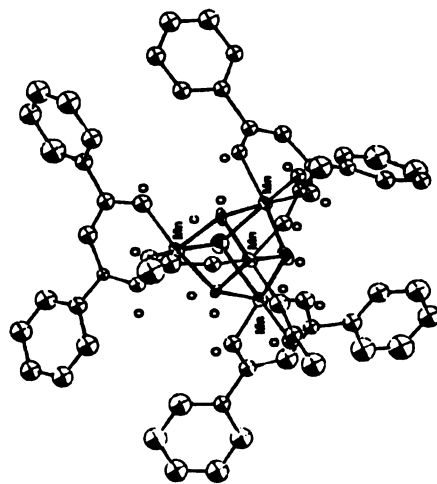
c) [Mn₄O₃Cl(OAc)₃(dbm)₃]
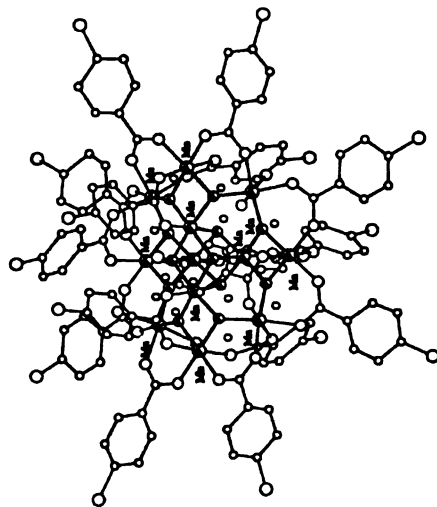
d) [Mn₁₂O₁₂(O₂CC₆H₄-p-Cl)₁₆(H₂O)₄]•8CH₂Cl₂

Figure 1.10. Examples of manganese carboxylate clusters.

24
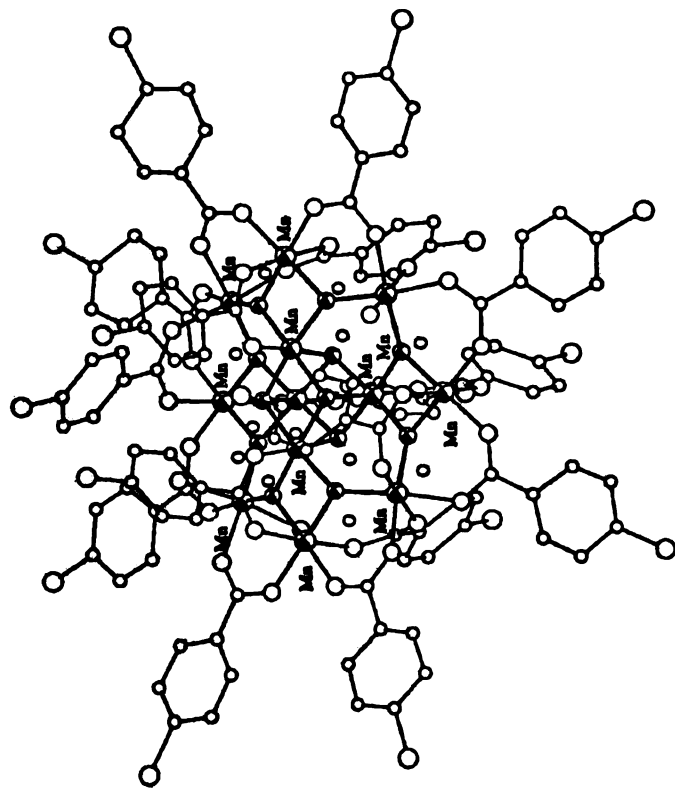
Figure 1.11. Double-well potential energy versus magnetization direction diagram for $[Mn_{12}O_{12}(O_2CCH_3)_{16}(H_2O)_4]\bullet2(HO_2CCH_3)\bullet4H_2O$ (S = 10). The thermal barrier height for magnetization reversal scales as $S^2|D|$ (100D with D = -0.50 cm^{-1}).
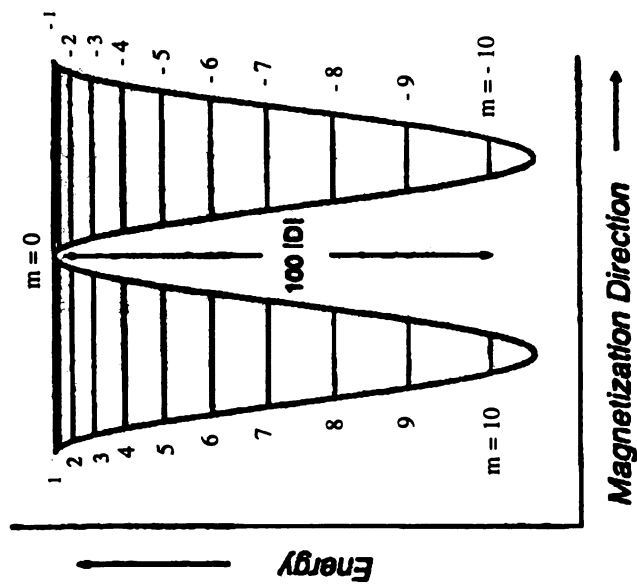
magnetization relaxation half-life on the order of 2 months.

In order to explore the possibility of using such molecules as data storage media, new clusters displaying larger values of S and D must be prepared to significantly increase the barrier height for re-orienting the magnetization of a particular molecule. In principle, a maximum of S = 10 is possible with the eight metal atom molecular cube if the corners are composed of alternating metal ions with electronic configurations of $t_{2g}^3 e_g^0$ and $t_{2g}^6 e_g^2$. As mentioned earlier, the orthogonality principle would dictate that all of the local unpaired spins in this molecule are ferromagnetically coupled. In considering the parameters that lead to a thermal barrier to reorienting the total magnetic moment of a molecule, one must consider the shape of the cluster as well as single ion anisotropy. If the single ion values are large and negative, *viz.*, they exhibit –D values, the symmetrical distribution of such ions in a molecule is likely to lead to a cancellation of the effects of local anisotropy. So a restatement of the requirements for increasing magnetic anisotropy can be rephrased to read "use metal atoms with large negative single ion anisotropy (-D) and create molecular shapes that are not highly symmetrical". Whether highly symmetrical molecular cubes will exhibit single molecule magnetic behavior or not is still an open question in the community. Since only a small number of single molecule

magnets are known it is not possible, at the present time, to predict how high-spin transition metal cyanide cubes will behave.

5. Building Polymeric Assemblies and Clusters with Hexacyanometallates

The spontaneous generation of well-defined architectures, for example molecular squares or cubes, occur by self-assembly of molecular building blocks with specific functionalities and geometries. Chapters II and III of this dissertation describe the preparation of convergent precursors and their reactions to form molecular squares and cubes. In Chapter IV an approach that employs both convergent and divergent precursors is described. This latter approach is based on the use of protecting groups on one metal center, $[(N-N)_2M(S)_2]^{n+}$, in reactions with hexacyanometallates, $[M(CN)_6]^{n-}$. Okāwa and co-workers first reported the synthesis of a compound based on this concept which is a 1-D rope ladder polymer from the reaction of $[Fe^{III}(CN)_6]^{3-}$ and $trans$-$Ni^{II}Cl_2(en)_2$.[2e] The asymmetric unit of the structure of $[Ni^{II}(en)_2]_3[Fe^{III}(CN)_6]_2$ consists of two $[Fe^{III}(CN)_6]^{3-}$ anions, two cis-$[Ni^{II}(en)_2]^{2+}$, one $trans$-$[Ni^{II}(en)_2]^{2+}$ and two water molecules (Figure 1.12.). These units produce polymeric zigzag chains by the connection of $[Fe^{III}(CN)_6]^{3-}$ and cis-$[Ni^{II}(en)_2]^{2+}$ ions which are further stitched together by the linkage $trans$-$[Ni^{II}(en)_2]^{2+}$. The result is the existence of rope-ladder

chains that run along the c axis. The chains align along the diagonal line of the ab plane to form 2-D sheets. The observation of the r.t. magnetic moment of $\chi_m T = 4.95$ cm^{3}Kmol^{-1} for the magnetic unit Fe$_2$Ni$_3$ coupled with the fact that an abrupt increase of the moment occurs at a maximum at of T = 14 K led the authors to conclude that a powdered sample (presumed to be the same as the crystals) was an ordered magnet. Later, the researchers published a series of crystallographically identical compounds, [Ni^{II}(en)$_2$]$_3$[M^{III}(CN)$_6$]$_2$•2H$_2$O (M^{III} = Fe, Mn, Cr, and Co),[25] which did not exhibit magnetic ordering due to antiferromagnetic intermolecular interactions between the pseudo 2-D sheets. The magnetic data for the first sample was performed on a precipitate and not on crystals, but when the crystals were finally measured, the compound was found to be metamagnetic which means that the material switches from antiferromagnetic to ferromagnetic coupling in the presence of a field. This study points out that magnetic data must be obtained on crystalline samples, as powders may have a different structure/composition or even degree of crystallinity (disorder versus order) that can give rise to different magnetic properties.

In another example of chemistry related to this thesis work, Okāwa and co-workers synthesized the 2-D bimetallic assembly, [Ni^{II}(pn)$_2$]$_2$[Fe^{III}(CN)$_6$]ClO$_4$•2H$_2$O by combining [Fe^{III}(CN)$_6$]$^{3-}$ with
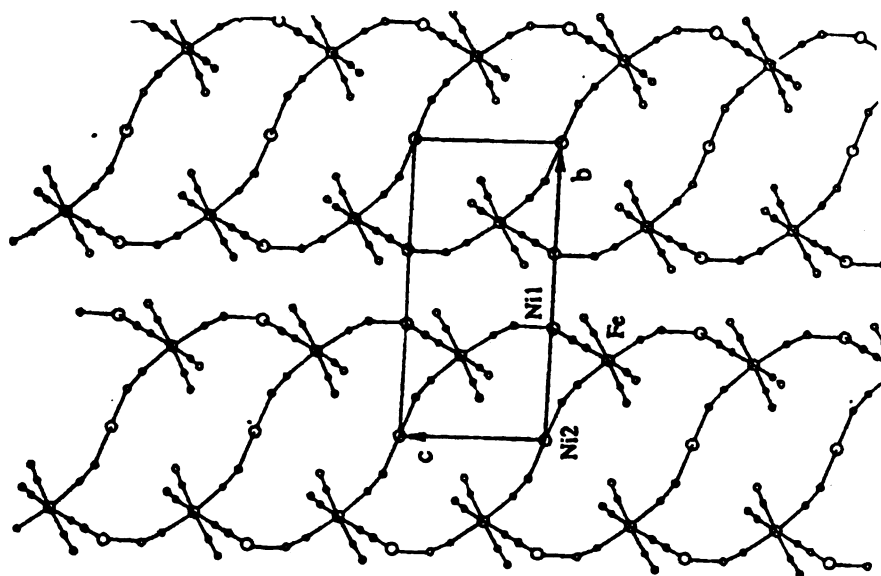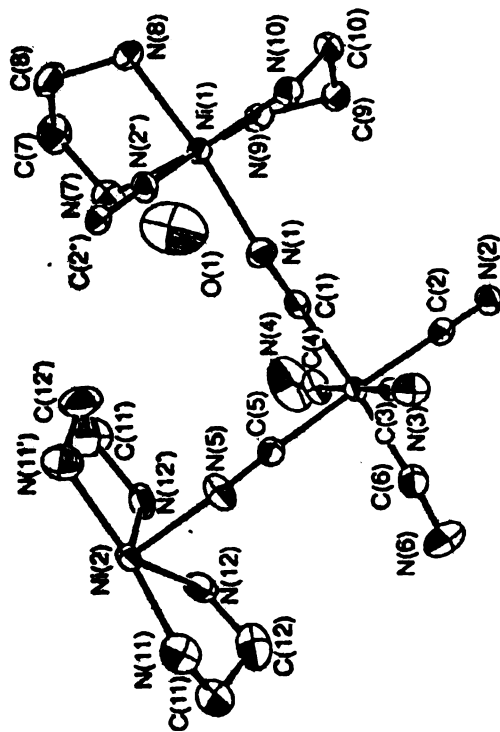
Figure 1.12. An ORTEP drawing of the asymmetric unit of [Ni(en)₂]₃[Fe(CN)₆]₂•2H₂O (above), projection of the polymeric structure onto the *bc* plane, the ethylenediamine molecules were omitted (right).

$[Ni^{II}(R,S-pn)_2](ClO_4)_2$ (pn = 1,2-diaminopropane) (Figure 1.13.).[26] At r.t the moment $\chi_M T$ is 3.21 cm^{3}Kmol^{-1} per FeNi$_2$ which increases with decreasing temperature up to the maximum value at 9 K for the ferromagnetically coupled FeNi$_2$ units.

In related work, a 3-D molecular ferrimagnet, $[Ni^{II}(tren)]_3[Fe^{III}(CN)_6]_2\bullet 6H_2O$ (tren = tris(2-aminoethyl)amine), was synthesized by Gatteschi and co-workers(Figure 1.14.).[27], The magnetic moment for the material is $\chi_M T$ = 4.96 cm^{3}Kmol^{-1} at 225 K which is close to the expected value for an uncoupled Ni$_3$Fe$_2$ unit. Further magnetic measurements were obtained to characterize the magnetic ordering which ultimately confirmed that a magnetically ordered state is achieved at 8 K.

In the previous cases, the dimensionality of the materials was either 1-D or 2-D, but Okãwa and co-workers have also prepared a 3-D bimetallic ferrimagnet, namely $[Mn(en)]_3[Cr(CN)_6]_2\bullet 4H_2O$ (en = ethylenediamine), which exhibits a T$_c$ = 69 K.[28] This ordering temperature is the highest among structurally characterized molecule-based magnets other than those in the Prussian blue family. The crystal structure of the material reveals that all of the cyanide groups of $[Cr(CN)_6]^{3-}$ are involved in the coordination to adjacent Mn^{2+} ions. Each Mn^{2+} ion is coordinated to one ethylenediamine group and four cyanide nitrogen atoms from adjacent $[Cr(CN)_6]^{3-}$ units
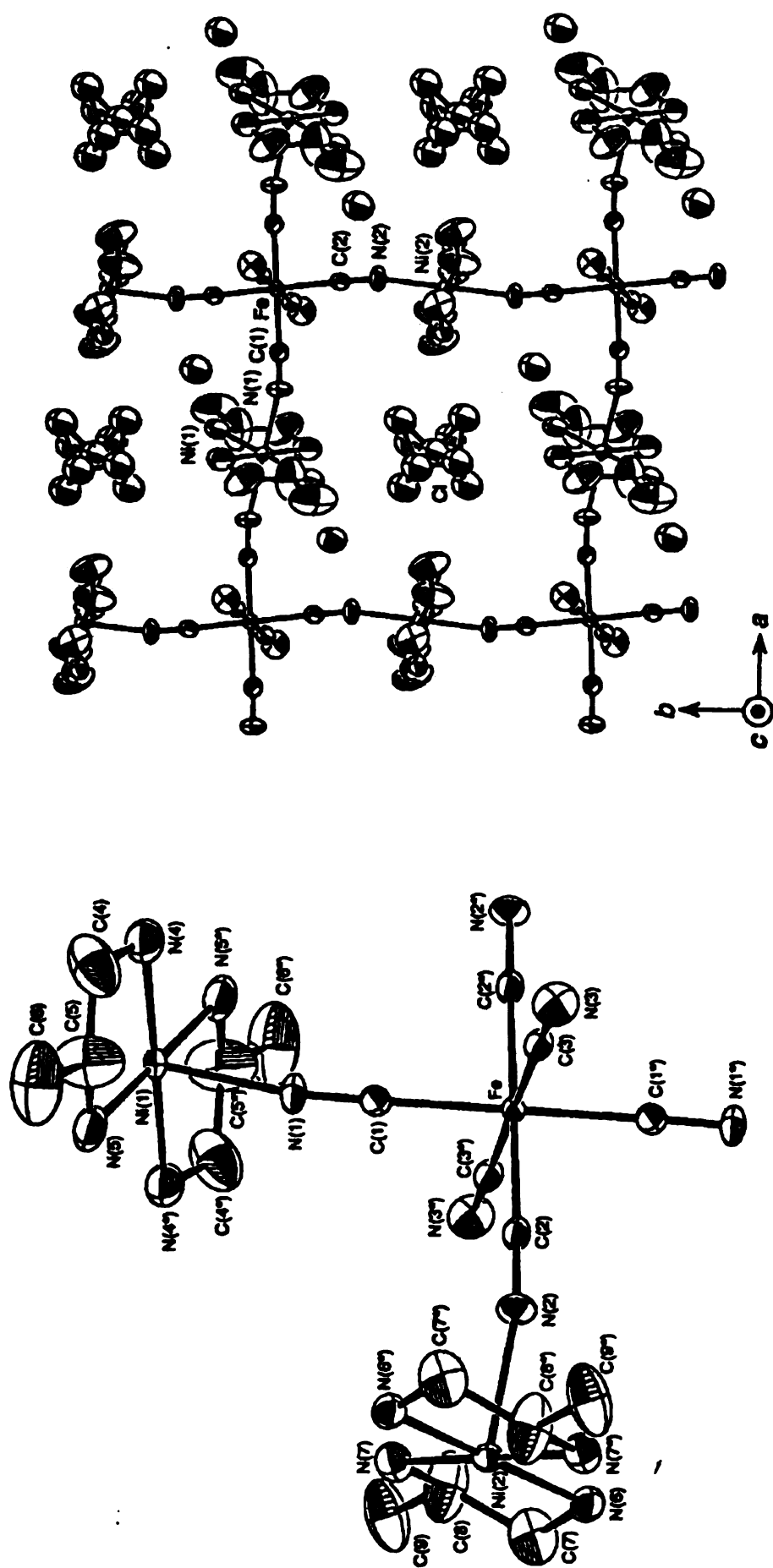
Figure 1.13. An ORTEP plot of the asymmetric unit in {[Ni(pn)$_2$]$_2$[Fe(CN)$_6$]}$^+$ and a projection of the Fe$^{III}_4$Ni$^{II}_4$ squares along the *c* axis of the 2-D network.
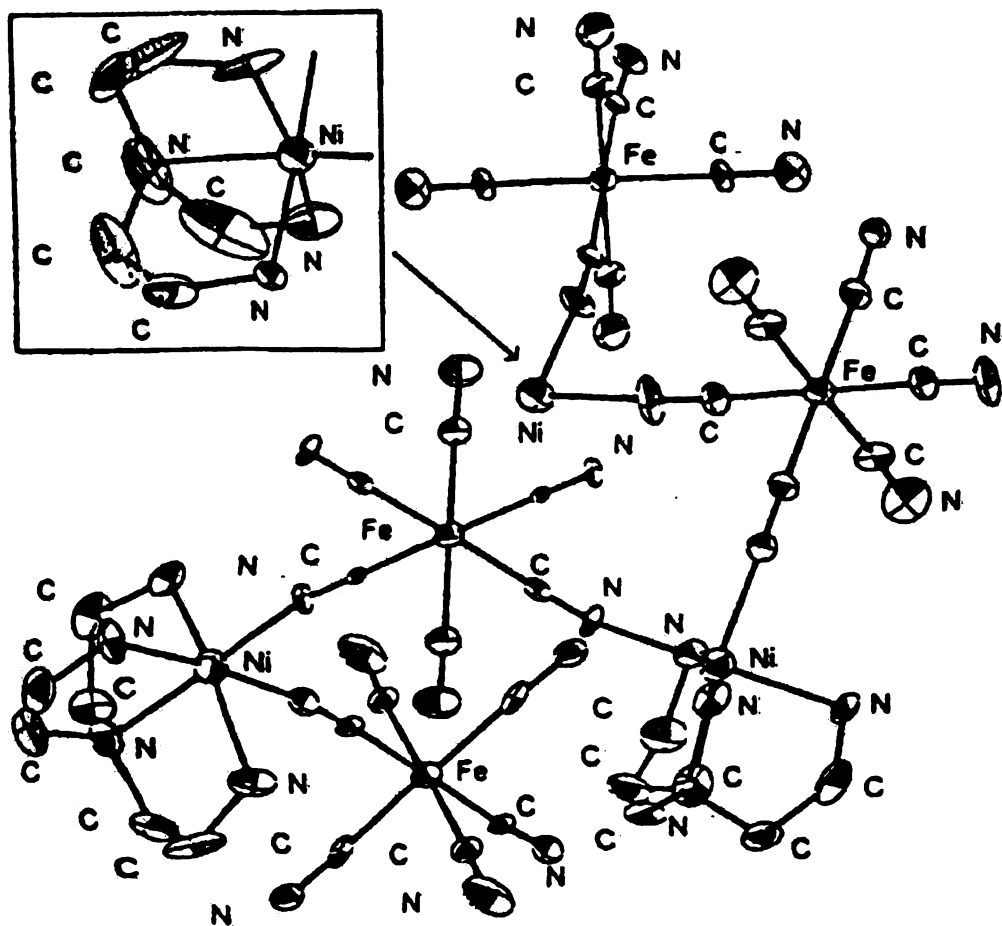
Figure 1.14. An ORTEP plot of the connectivity in the compound
$[Ni(tren)]_3[Fe(CN)_6]_2 \cdot 6H_2O$.

(Figure 1.15.). The $\chi_M T$ at room temperature is 13.08 cm^{3}Kmol^{-1} per Mn$_3$Cr$_2$.

There are many more examples of polymeric arrays that have been obtained by the aforementioned approach, but, more to the point of this thesis, hexacyanometallate anions can also be used to yield discrete structures as well. For example, Murray and co-workers reported the pentanuclear cluster, [Ni^{II}(bpm)$_2$]$_3$[Fe^{III}(CN)$_6$]$_2$•7H$_2$O (bpm = Bis(1-pyrazolyl)methane)) which the authors claim exhibits long range magnetic ordering through hydrogen bonding.[29] The cluster is composed of two [Fe^{III}(CN)$_6$]$^{3-}$ moieties in which three *fac* cyanides are connected to three different [Ni^{II}(bpm)$_2$]$^{2+}$ groups (Figure 1.16.). The geometry around the nickel atoms is a *cis* arrangement. The three remaining CN$^-$ ligands on each Fe atom are monodentate, but are involved in hydrogen-bonding networks to water molecules. The r.t. magnetic moment $\chi_M T$ value is 5.12 cm^{3}Kmol^{-1} per Ni$_3$Fe$_2$, with the signature of long-range magnetic ordering occurring at 23 K. Interestingly, there are two additional pentanuclear clusters that are said to be structurally identical to the previously mentioned cluster but without the network of hydrogen bonding. One is the pentanuclear cluster, [Ni(IM2-py)$_2$]$_3$[Cr(CN)$_6$]$_2$•7H$_2$O (IM2-py = 2-(2-pyridyl)-4,4,5,5-tetramethyl-4,5-dihydro-1H-imidazolyl-1-oxy) with a S = 9 ground state.[30] The compound

33

(a)

(b)

(c)

Figure 1.15. (a) ORTEP drawing of the heptanuclear unit of $[Mn(en)]_3[Cr(CN)_6]_2 \bullet 4H_2O$, (b) a Cr_3Mn_4 defective cubane unit, and (c) projection of the polymeric structure onto the *ac* plane (H_2O and en are omitted for clarity).

34
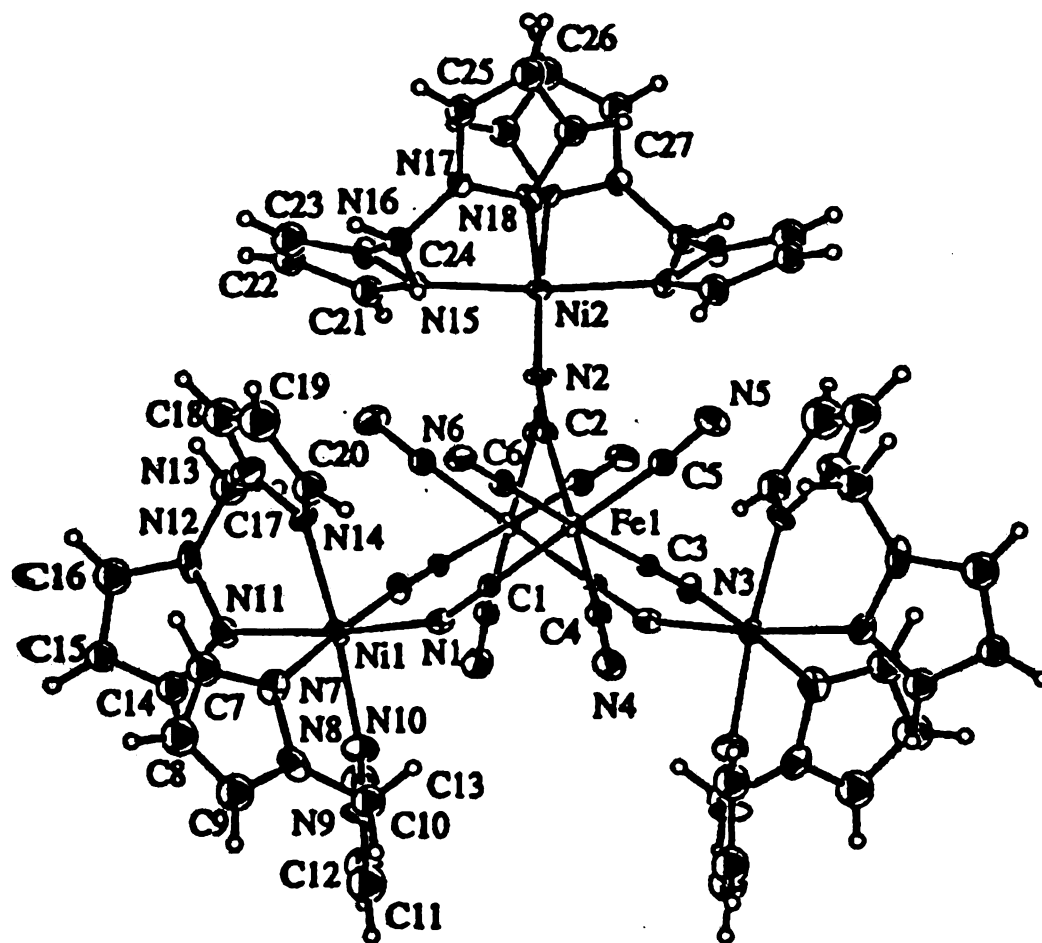
Figure 1.16. A thermal ellipsoid plot of the discrete, neutral pentamer cluster, $[Ni(bpm)_2]_3[Fe(CN)_6]_2 \cdot 7H_2O$.

was identified on the basis of elemental analysis, thermogravimetric analysis, infrared and UV-visible spectroscopy, and magnetic data. No crystal structure of the compound was obtained to confirm the proposed structure. The pentanuclear Fe(III) analog, $[Ni^{II}(IM2-py)_2]_3[Fe^{III}(CN)_6]_2 \bullet 4H_2O$, was also reported and exhibits a ground state of S = 7 $\_^{31}$ At room temperature, $\chi_M T$ is ~10 cm³Kmol⁻¹ which corresponds to the unit $[Ni(IM2-py)_2]_3Fe_2$.

Chapter IV of the thesis describes the use of new octahedral precursors prepared in our laboratories that contain only leaving groups, denoted S, namely $[(N-N)_2M(S)_2]^n$ and $[(L_3)M(S)_3]^n$ to build molecules with bridging $[M(CN)_6]^{n-}$ anions. This research led to the discovery of new architectures with interesting magnetic properties, which will be described. These compounds in this thesis add to our growing understanding of the synthetic methodologies that one can use to prepare new molecular magnetic materials based on cyanide linkages. These systems are of high interest for their potential to exist with large ground spin state (S) values and large molecular anisotropy.

Table 1.2. Polynuclear cyanide complex along with their T_c values.

Complex	Tc	Magnetic Interactions	ref
$[Mn(en)]_3[Cr(CN)_6]_2 \cdot 4H_2O$	69	ferri	28
$[Mn^{II}_6(H_2O)_9\{W^V(CN)_8\}_4] \cdot 13H_2O]_n$	54	ferri	32a
$K_2Mn_3(H_2O)_6[Mo(CN)_7]_2 \cdot 6H_2O$	39	ferro	32b
$[Ni(1,1\text{-}dmen)_2]_2[Fe(CN)_6]NO_3 \cdot 4H_2O$	16.2	ferro	32c
$[Ni(1,1\text{-}dmen)_2]_2[Fe(CN)_6]I \cdot 4H_2O$	15.2	ferro	32c
$[Ni(1,1\text{-}dmen)_2]_2[Fe(CN)_6]BF_4 \cdot 3H_2O$	14.6	ferro	32c
$[Ni(N\text{-}men)_2]_3[Fe(CN)_6]_2$	10.8	ferro	25
$[Ni(pn)_2]_2[Fe(CN)_6]ClO_4 \cdot 2H_2O$	10	ferro	32d
$[Ni(1,1\text{-}dmen)_2]_2[Fe(CN)_6]N_3 \cdot 4H_2O$	9.7	ferro	32c
$[Ni(1,1\text{-}dmen)_2]_2[Fe(CN)_6]CF_3SO_3 \cdot 2H_2O$	9.5	ferro	32c
$[Ni(1,1\text{-}dmen)_2]_2[Fe(CN)_6]BzO \cdot 6H_2O$	9.3	ferro	32c

Table 1.2. con't

$[Ni(L_1)]_3[Fe(CN)_6]_2 \bullet 12H_2O$	9.1	ferro	32e
$[Ni(tren)]_3[Fe(CN)_6]_2 \bullet 6H_2O$	8	ferri	27
$[Ni(L_2)]_3[Fe(CN)_6]_2 \bullet 9H_2O$	5	ferro	32f
$[Mn^{II}(L_3)]_6[Mo^{III}(CN)_7][Mo^{IV}(CN)_8]_2 \bullet 19.5\ H_2O$	3	ferro	32g
$[Et_4N]_2[Mn(acacen)][Fe(CN)_6]$	1.9	ferro	32h

en = ethylenediamine
1,1-dmen = 1,1-dimethylethylenediamine
N-men = N-methylethylenediamine
pn = 1,2-diaminopropane
L_1 = 3,10-diethyl-1,3,5,8,10,12-hexaazacyclotetradecane
tren = tris(2-aminoethyl)amine)
L_2 = 3,10-dimethyl-1,3,5,8,10,12-hexaazacyclotetradecane
L_3 = 2,13-dimethyl-3,6,9,12,18-pentaazabicyclo[12.3.1]octadeca-1(18),2,12,14,16-pentane
acacen = N,N'-ethylenebis(acetylacetonylideneaminato)

38

6. References

1. (a) Gardner, G. B.; Venkataraman, D.; Moore, J. S.; Lee, S. *Nature* **1995**, *374*, 792. (b) Venkataraman, D.; Gardner, G. B.; Lee, S.; Moore, J. S. *J. Am. Chem. Soc.* **1995**, *117*, 11600. (c) Yaghi, O. M.; Li, H. *J. Am. Chem. Soc.* **1995**, *117*, 10401.

2. (a) Manriquez, J. M.; Yee, G. T.; McLean, S.; Epstein, A. J.; Miller, J. S. *Science* **1991**, *252*, 1415. (b) Tamaki, H.; Zhuang, Z. J.; Matsumoto, N.; Kida, S.; Koikawa, M.; Achiwa, Hashimoto, Y.; Okawa, H. *J. Am. Chem. Soc.* **1992**, *114*, 6974. (c) Stumpf, H. O.; Pei, Y.; Kahn, O.; Sletten, J.; Renard, J. P. *J. Am. Chem. Soc.* **1993**, *115*, 6738. (d) Inoue, K.; Iwamura, H. *J. Am. Chem. Soc.* **1994**, *116*, 3173. (e) Ohba, M.; Maruono, N.; Okawa, H.; Enoki, T.; Latour, J.-M. *J. Am. Chem. Soc.* **1994**, *116*, 11566. (f) Decurtins, S.; Schmalle, H. W.; Schneuwly, P.; Zheng, Li-M.; Ensling, J.; Hauser, A. *Inorg. Chem.* **1995**, *34*, 5501. (g) Miyasaka, H.; Matsumoto, N.; Okawa, H.; Re, N.; Gallo, E.; Floriani, C. *Angew. Chem. Int. Ed. Engl.* **1995**, *34*, 1446. (h) Ohba, M.; Okawa, H.; Ito, T.; Ohto, A. *J. Chem. Soc. Chem. Commun.* **1995**, 1545. (i) Michaut, C.; Ouahab, L.; Bergerat, P.; Kahn, O.; Bosseksou, A. *J. Am. Chem. Soc.* **1996**, *118*, 3610. (j) De Munno, G.; Poerio, T.; Viau, G.; Julve, M.; Lloret, F.; Journaux, Y.; Riviere, E. *J. Chem. Soc., Chem. Commun.* **1996**, 2587.

3. (a) Bechgaard, K.; Carneiro, K.; Rasmussen, F. B.; Olsen, M. *J. Am. Chem. Soc.* **1981**, *103*, 2440. (b) Wudl, F. *Acc. Chem. Res.* **1984**, *17*, 227. (c) Lacroix, P.; Kahn., O.; Gliezes, A.; Valade, L.; Cassoux, P. *Nouv. J. de Chimie* **1985**, 643. (d) Gross, R.; Kaim, W. *Angew. Chem. Int. Ed. Engl.* **1987**, *26*, 251. (e) Ballester, L.; Barral, M.; Gutiérrez, A.; Jiménez-Aparicio, R.; Martinez-Muyo, J.; Perpiñan, M.; Monge, M.; Ruiz-Valero, C. *J. Chem. Soc.,Chem. Commun.* **1991**, 1396. (f) Humphrey, D. G.; Fallon, G. D.; Murray, K. S. *J. Chem. Soc., Chem. Commun.* **1988**, 1356. (g) Cornelissen, J. P.; Van Diemen, J. H.; Groeneveld, L. R.; Haasnoot, J. G.; Spek, A. L.; Reedijk, J. *Inorg. Chem.* **1992**, *31*, 198. (h) Oshio, H.; Ino, E.; Mogi, I.; Ito, T. *Inorg. Chem.* **1993**, *32*, 5697. (i) Ballester, L.; Barral, M.; Gutiérrez, A.; Monge, A.; Perpiñan, M. F.; Ruiz-Valero, C.; Sánchez-Pélaez, A. *Inorg. Chem.* **1994**, *33*, 2142. (j) Oshio, H.; Ino, E.; Ito, T.; Maeda, Y. *Bull. Chem. Soc. Jpn.* **1995**, *68*, 889. (k) Azcondo, M. T.; Ballester, L.; Gutiérrez, A.; Perpiñan, F.; Amador, U.; Ruiz-Valero, C.; Bellitto, C. *J. Chem. Soc., Dalton Trans.* **1996**, 3015.

4. Aumüller, A.; Erk, P.; Klebe, G.; Hünig, S.; Von Schütz, J.; Werner, H. *Angew. Chem. Int. Ed. Engl.* **1986**, *25*, 740. (b) Aumüller, A.; Erk, P.; Hünig, S. *Mol. Cryst. Liq. Cryst. Inc. Nonlinear. Opt.* **1988**, *156*, 215. (c) Erk, P.; Gross, H.-J.; Hünig, U. L.; Meixner, H.; Werner, H.-P.; Von Schütz,

J. U.; Wolf, H. C. *Angew. Chem. Int. Ed. Engl.* **1989**, *28*, 1245. (d) Kato, R.; Kobayashi, H.; Kobayashi, A. *J. Am. Chem. Soc.* **1989**, *111*, 5224. (e) Aumüller, A.; Erk, P.; Hünig, S.; Hädicke. E.; Peters, K.; Von Schnering, H. G. *Chem. Ber.* **1991**, *124*, 2001. (f) Sinzger, K.; Hünig, S.; Jopp, M.; Bauer, D.; Bietsch, W.; Von Schütz, J. U.; Wolf, H. C.; Kremer, R. K.; Metzenthin, T.; Bau, R.; Khan, S. I.; Lindbaum, A.; Lengauer, C. L.; Tillmanns, E. *J. Am. Chem. Soc.* **1993**, *115*, 7696. (g) Gomez-Garcia, C. J.; Gimenez-Saiz, C.; Triki, S.; Coronado, E.; Magueres, P. L.; Ouahab, L.; Ducasse, L.; Sourisseau, C.; Delhaes, P. *Inorg. Chem.* **1995**, *34*, 4139. (h) Day, P.; Kurmoo, M. *J. Mat. Chem.* **1997**, *7*, 1291. (i) Clemente-León, M.; Mingotaud, C.; Agricole, B.; Gómez-Garcia, C.; Coronado, E.; Delhaés, P. *Angew. Chem. Int. Ed. Engl.* **1997**, *36*, 1114. (j) Canfield, P. C.; Gammel, P. L.; Bishop, D. J. *Physics Today* **1998**, 40. (k) Petruska, M. A.; Talham, D. R. *Chem. Mater.* **1998**, *10*, 3672.

5. (a) Wickman, H. H.; Trozzolo, A. M.; Williams, H. J.; Hull, G. W.; Merritt, F. R. *The Physical Review* **1967**, *155*, 563. (b) DeFotis, G. C.; Palacio, F.; O'Connor, C. J.; Bhatia, S. N.; Carling, R. L. *J. Am. Chem. Soc.* **1977**, *99*, 8314.

6. Pei, Y.; Kahn, O.; Nakatani, K.; Codjovi, E.; Mathonière, C.; Sletten, J. *J. Am. Chem. Soc.* **1991**, *113*, 6558. (b) Pei, Y.; Veraguer, M.; Sletten, J.; Renard, J. P. *J. Am. Chem. Soc.* **1986**, *108*, 7428.

7. Miller, J. S.; Calabresse, J. C.; Epstein, A. J.; Bigelow, W.; Zhang, J. H.; Reiff, W. M. *J. Chem. Soc., Chem. Commun.* **1986**, 1026.

8. (a) Gadet, V.; Mallah, T.; Castro, I.; Berdaguer, M. *J. Am. Chem. Soc.* **1992**, *114*, 9213. (b) Verdaguer, M. *Science* **1996**, *272*, 698, and references therein. (c) Bushmann, W. E.; Paulson, S. C.; Wynn, C. M.; Girtu, M. A.; Epstein, A. J.; White, H. S.; Miller, J. S. *Chem. Mat.* **1998**, *10*, 1386. (d) Ferlay, S.; Mallah, T.; Ouachés, R.; Veillet, R.; Verdaguer, M. *Inorg. Chem.* **1999**, *38*, 229.

9. (a) Miller, J. S.; Epstein, A. J.; *Chem. Commun.* **1998**, 1319. (b) Zhang, J.; Liable-Sands, L. M.; Rheingold, A. L.; Del Sesto, R. E.; Gordon, D. C.; Burkhart, B. M.; Miller, J. S. *Chem. Commun.* **1998**, 1385. (c) Zhang, J.; Ensling, J.; Ksenofontov, V.; Gütlich, P.; Epstein, A. J.; Miller, J. S. *Angew. Chem. Int. Ed.* **1998**, *37*, 637.

10. (a) Kurmoo, M.; Graham, A. W.; Day, P.; Coles, S. J.; Hursthouse, M. B.; Caulfield, J. L.; Singleeton, J.; Pratt, S. J.; Hayes, W.; Ducasse, L.; Guionneau, P. *J. Am. Chem. Soc.* **1995**, *117*, 12209. (b) Martin, L.; Tumer,

S. S.; Day, P. *Chem. Commun.* **1997**, 1367. (c) Day, P. *Physica Scripta* **1993**, *T49*, 726.

11. (a) Caneschi, A.; Gatteschi, D.; Sessoli, R. *J. Am. Chem. Soc.* **1991**, *113*, 5873. (b) Sessoli, R.; Tsai, H. L.; Schake, A. R.; Wang, S.; Vincent, J. B.; Folting, K.; Gatteschi, D.; Christou, G.; Hendrickson, D. N. *J. Am. Chem. Soc.* **1993**, *115*, 1804. (c) Sessoli, R.; Gatteschi, D.; Caneschi, A.; Novak, M. A. *Nature* **1993**, *365*, 141. (d) Abbati, G. L.; Cornia, A.; Fabretti, A. C.; Caneschi, A.; Gatteschi, D. *Inorg. Chem.* **1998**, *37*, 3759. (e) Abbati, G. L.; Cornia, A.; Fabretti, A. C.; Caneschi, A.; Gatteschi, D. *Inorg. Chem.* **1998**, *37*, 1430. (f) Schmid, G. *J. Chem. Soc., Dalton Trans.* **1998**, 1077. (g) Brechin, E. K.; Clegg, W.; Murrie, M.; Parsons, S.; Teat, S. J.; Winpenny, R. E. P. *J. Am. Chem. Soc.* **1998**, *120*, 7365. (h) Müller, A.; Krickemeyer, E.; Bögge, H.; Schmidtmann, M.; Beugholt, C.; Kögerler, P.; Lu, C. *Angew. Chem. Int. Ed. Engl.* **1998**, *37*, 1220. (i) Watton, S. P.; Fuhrmann, P.; Pence, L. E.; Caneschi, A.; Cornia, A.; Abbati, G. L.; Lippard, S. J. *Angew. Chem. Int. Ed. Engl.* **1997**, *36*, 2774. (j) Tran, N. T.; Kawano, M.; Powell, D. R.; Dahl, L. F. *J. Am. Chem. Soc.* **1998**, *120*, 10986. (k) Müller, A.; Shah, S.Q. N.; Bögge, H.; Schmidtmann, M. *Nature* **1999**, *397*, 48.

12. (a) Keggin, J. F.; Miles, F. D. *Nature* **1936**, *137*, 577. (b) Holtzman, H. *Ind. Eng. Chem.* **1945**, *37*, 855. (c) El-Sayed, M. F. A.; Sheline, R. K. *J.*

Inorg. Nucl. Chem. **1958**, *6*, 187. (d) Dows, D. A.; Haim, A.; Wilmarth, W.

K. *J. Inorg. Nucl. Chem.*, **1961**, *21*, 33. (e) Griffith, W. P. *Q. Rev.*, **1962**, *16*,

188. (f) Shriver, D. F. *Structure Bonding*, **1966**, 32. (g) Chadwick, B. M.;

Sharpe, A. G. *In Advances in Inorganic Chemistry and Radiochemistry*

1966, *8*, 83. (h) Britton, D. *In Perspectives in Structural Chemistry* **1967**, *1*,

109. (i) Ludi, A.; Gudel, H. U. *Structure Bonding*, **1973**, *14*, 1.

13. (a) Buser, J. H.; Ludi, A. *J. Chem. Soc. Chem. Commun.*, **1972**, 1299. (b)

Buser, H. J.; Schwarzenbach, D.; Petter, W.; Ludi, A. *Inorg. Chem.* **1977**,

16, 2704.

14. (a) Sharpe, A. G. The Chemistry of Cyano Complexes of the Transition

Metals, Academic Press Inc. New York **1976**. (b) Dunbar, K. R.; Heintz, R.

A. *Progress in Inorg. Chem.* **1997**, *45*, 283. (c) Vahrenkamp, H.; Geiss, A.;

Richardson, G. N. *J. Chem. Soc. Dalton*, **1997**, *20*, 3643.

15. Ito, A.; Suenaga, M.; Ono, K. *J. Chem. Phys.*, **1968**, *48(8)*, 3597.

16. Chappert, J.; Sawicka, B.; Sawicki, J. *Phys. Stat. Sol.*, **1975**, *B72*, K139.

17. Mayoh, B.; Day, J. *J. Chem. Soc. Dalton Trans.*, **1976**, 1483.

18. (a) Kahn, O. *Molecular Magnetism*, VCH, Weinheim, **1993**. (b) Carlin,

R. L. *Magnetochemistry*, Springer-Verlag Berlin Heidelberg, **1986**. (c)

Babel, D. *Comments Inorg. Chem.*, **1986**, *5(6)*, 2.

19. Klenze, R.; Kanellakoupuolos, B.; Trageser, G.; Eysel, H. H. *J. Chem*

Phys., **1980**, *72(11)*, 5819.

20. (a) Phillips, R. F.; Powell, H. M. *Proc. R. Soc. London* **1993**, *173*, 147. (b) Shaw, B. L.; Shaw, G. *J. Chem. Soc. A.* **1971**, 3533. (c) Slone, R. V.; Hupp, J. T.; Stern, L. C.; Albretch-Schmidt, T. E. *Inorg. Chem.* **1996**, *35*, 4096. (d) Stang, P. J.; Olenyuk, B. *Acc. Chem. Res.* **1997**, *30*, 502. (e) Olenyuk, B.; Fechtenkötter, A.; Stang, P. J. *J. Chem. Soc. Dalton Trans.* **1998**, 1707. (f) Hupp, J. T. *Coord. Chem. Rev.* **1998**, *171*, 221. (g) Belnkstein, K. D.; Hupp, J. T.; Stern, L. C. *Inorg. Chem.* **1998**, *37*, 5404 (h) Woessner, S. M.; Helms, J. B.; Shen, Y.; Sullivan, B. P. *Inorg. Chem.* **1998**, *37*, 5406. (i) Oshio, H.; Tamada, O.; Onodera, H.; Ito, T.; Ikomo, T.; Tero-Kubota, S. *Inorg. Chem.* **1999**, *38*, 5686.

21. Klausmeyer, K. K.; Rauchfuss, T. B.; Wilson, S. R. *Angew. Chem. Int. Ed. Engl.* **1998**, *37*, 1694.

22. Klausmeyer, K. L.; Wilson, S. R.; Rauchfuss, T. B. *J. Am. Chem. Soc.* **1999**, *121*, 2705.

23. Heinrich, J. L.; Berseth, P. A.; Long, J. R. *Chem. Commun.* **1998**, 1231.

24. (a) Friedman, J. R.; Sarachik, M. P.; Tejada, J.; Ziolo, R. *Phys. Rev. Lett.* **1996**, *76*, 3830. (b) Thomas, L.; Lionti, F.; Ballou, R.; Gatteschi, D.; Sessoli, R.; Barbara, B. *Nature* **1996**, *383*, 145. (c) Aubin, S. M. J.; Wemple, M. W.; Adams, D. M.; Tsai, H. L.; Christou, G.; Hendrickson, D. N. *J. Am. Chem.*

Soc. **1996**, *118*, 7746. (d) Aubin, S. M. J.; Spagna, S.; Eppley, H. J.; Sager, R. E.; Folting, K.; Christou, G.; Hendrickson, D. N. *Mol. Cryst. and Liq. Cryst. Science and Tech. Sec. A.-Mol. Cryst. Liq. Cryst.* **1997**, *305*, 181. (e) Aromi, G.; Aubin, S. M. J.; Spagna, S.; Bolcar, M. A.; Eppley, H. J.; Folting, K.; Christou, G.; Hendrickson, D. N.; Huffman, J. C.; Squire, R. C.; Tsai, H. L.; Wang, S.; Wemple, M. W. *Polyhedron* **1998**, *17*, 3005. (f) Ruiz, D.; Sun, Z.; Albela, B.; Folting, K.; Ribas, J.; Christou, G.; Hendrickson, D. N. *Angew. Chem. Int. Ed. Engl.* **1998**, *37*, 300.

25. Ohba, M.; Okawa, H. *Coord. Chem. Rev.* **2000**, *198*, 313.

26. Ohba, M.; Okawa, H.; Ito, T.; Ohto, A. *J. Chem. Soc., Chem. Commun.* **1995**, 1545.

27. Salah, M.; Fallah, E.; Rentschler, E.; Caneschi, A.; Sessoli, R.; Gatteschi, D. *Angew. Chem. Int. Ed. Engl.* **1996**, *35*, 1947.

28. Ohba, M.; Usuki, N.; Fukita, N.; Okawa, H. *Angew. Chem. Int. Ed.Engl.* **1999**, *38*, 1795.

29. Langenberg, K. V.; Batten, S. R.; Berry, K. J.; Hockless, D. C. R.; Moubaraki, B.; Murray, K. S. *Inorg. Chem.* **1997**, *36*, 5006.

30. Marvilliers, A.; Pei, Y.; Boquera, J. C.; Vostrikova, K. E.; Paulsen, C.; Rivière, E.; Audière, J.-P.; Mallah, T. *Chem. Commun.* **1999**, 1951.
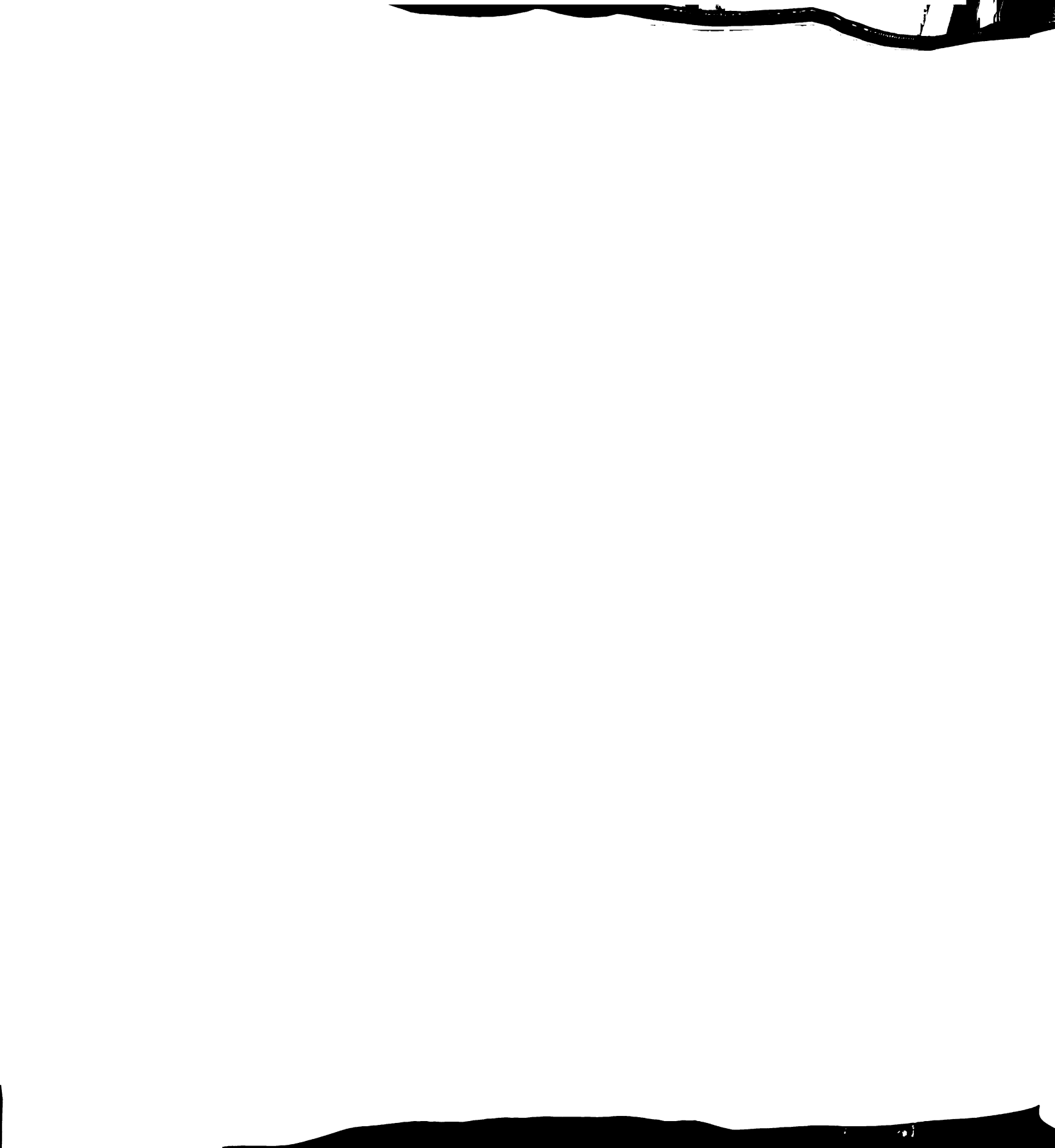
31. Vostrikova, K. E.; Luneau, D.; Wernsdorfer, W.; Rey, P.; Verdaguer, M. *J. Am. Chem. Soc.* **2000**, *122*, 718.

32. (a) Holmes, S. M.; Girolami, G. S. *J. Am. Chem. Soc.* **1999**, *121*, 5593. (b) Hatlevik, O.; Buschmann, W. E.; Zhang, J.; Manson, J. L.; Miller, J. S. *Adv. Mater.* **1999**, *11*, 914. (c) Dujardin, E.; Ferlay, S.; Phan, X.; Desplances, C.; d. Moulin, C. C.; Sainctavit, P.; Baudelet, F.; Dartyge, E.; Veillet, P., Verdaguer, M. *J. Am. Chem. Soc.* **1998**, *120*, 11347. (d) Ferlay, S.; Mallah, T.; Ouahes, R.; Veillet, P.; Verdaguer, M. *Nature (London)*, **1995**, *378*, 701. (e) Mallah, T.; Thiébaut, S.; Verdaguer, M.; Veillet, P. *Science* **1993**, *262*, 1554. (f) Entley, W. R.; Girolami, G. S. *Science* **1995**, *268*, 397. (g) Babel, D. *Comments Inorg. Chem.* **1986**, *5(6)*, 285., Greibler, W. D.; Babel, D. *Z Naturforsch.* **1982**, *87b*, 832. (h) Entley, W. R.; Girolami, G. S. *Inorg. Chem.* **1994**, *33*, 5165. (i) Juszczyk, S.; Johansson, C.; Hanson, M.; Ratuszna, A.; Malecki, G. *J. Phys.: Condens. Matter* **1994**, *6*, 5697.

33. (a) Zhong, Z. J.; Seino, H.; Mizobe, Y.; Hidai, M.; Verdaaguer, M.; Ohkoski, S.-I.; Hashimoto, K. *Inorg. Chem.* **2000**, *39*, 5095. (b) Larionova, J.; Kahn, O.; Gohlen, S.; Ouahab, L.; Clérac, R. *J. Am. Chem. Soc.* **1999**, *121*, 3349. (c) Ohba, M.; Okawa, H.; Fukita, N.; Hashimoto, Y. *J. Am. Chem. Soc.* **1997**, *119*, 1011. (d) Ohba, M.; Okawa, H.; Ito, T.; Ohto, A. *J.*

Chem. Soc., Chem. Commun. **1995**, 1545. (e) Kou, H.-Z.; Gao, S.; Ma, B.-Q.; Liao, D.-Z. *Chem. Commun.* **2000**, 1309. (f) Kou, H.-Z.; Gao, S.; Bu, W.-M.; Liao, D.-Z.; Ma, B.-Q.; Jiang, Z.-H.; Yan, S.-P.; Fan, Y.-G.; Wang, G.-L. *J. Chem. Soc., Dalton Trans.* **1999**, *15*, 2477. (g) Sra, A. K.; Andruh, M.; Kahn, O.; Golhen, S.; Ouahab, L.; Yakhmi, J. V. *Angew. Chem. Int. Ed.* **1999**, *38*, 2606. (h) Re, N.; Gallo, E.; Floriani, C.; Miyasaka, H.; Matsumoto, N. *Inorg. Chem.* **1996**, *35*, 6004.

Chapter II

Synthesis, Characterization and Reactivity Studies of

Square Precursors of the Type *cis*-[(N-N)$_2$M(S)$_2$]$^{n+}$

(S = H$_2$O, (CF$_3$SO$_3$)$^-$, CH$_3$CN, (NO$_3$)$^-$, (CN)$^-$)

1. INTRODUCTION

Many magnetic materials, most notably the three dimensional Prussian blue cubic solids depicted in Figure 1.1, are based on the cyanide ligand due to its effectiveness for providing an efficient pathway for magnetic communication between paramagnetic metal centers[1]. The prototype for the field is Prussian blue, $Fe_4[Fe(CN)_6]_3 \cdot xH_2O$ (x = 14-16), which contains Fe^{II} and Fe^{III} metal centers bridged by cyanide[2]. The strong field, carbon end, of CN^- is bound to Fe^{II} which is low-spin, and the weak-field, nitrogen end, is bound to Fe^{III} which is high-spin (S = 5/2). The physical properties of Prussian blue have been under investigation for many decades, and it is now widely recognized that the mixed-valency is responsible for the intense blue color of the solid as well as for the observed ferromagnetic ordering at 5.5 K[3]. Within the past ten years, researchers have opened up new venues for Prussian-blue type chemistry by introducing a variety of metal atoms into the cubic structure afforded by octahedral $[M(CN)_6]^{n-}$ building blocks. The aim is to increase the magnetic ordering temperature, and, indeed, several Prussian blue analogs have been observed to have T_c values above room temperature (Table 1.1.).[4] Unfortunately, the characterization and general usefulness of the PB solids is severely hampered by their total lack of solubility, thus researchers are seeking new ways to apply cyanide chemistry

50

to magnetism.

A completely different approach to cyanide chemistry from that mentioned above is to reduce the dimensionality by using capping ligands to avoid the growth of a three dimensional network. Okãwa and co-workers were the first group to apply this strategy by using ethylenediamine ligands in combination with hexacyanometallates to form 1-D chains, 2-D layers and 3-D motifs.[5] It is possible to use capping ligands to further lower the dimensionality to favor discrete molecules such as the first documented tetranuclear cyanide-based cluster [{$closo$-3-PPh$_3$-3(μ-CN)-3,1,2-RhC$_2$B$_9$H$_{11}$}$_4$] reported by Hawthorne and co-workers[6]. This molecule consists of four $closo$ phosphinorhodacarborane moieties joined through their respective metal centers by linear cyanide bridges to give a cyclic structure. Another example, provided by Maitlis and co-workers, is the cluster [{(C$_5$(CH$_3$)$_5$Rh-μ-CH$_2$)$_2$}$_2$(μ-CN)$_2$](PF$_6$)$_2$ composed of two {(C$_5$(CH$_3$)$_5$Rh-μ-CH$_2$)$_2$} units bridged by two cyanide ligands.[7] Additional examples of organometallic molecular squares, and even triangles, have emerged in recent years[8], but there are no examples of paramagnetic cyanide squares with two exceptions. During the course of our studies, Oshio and co-workers[9] reported [Fe$^{II}_2$Cu$^{II}_2$(μ-CN)$_4$(bpy)$_6$](PF$_6$)$_4$•2H$_2$O•4CHCl$_3$ and [Fe$^{III}_2$Cu$^{II}_2$(μ-CN)$_4$(bpy)$_6$](PF$_6$)$_6$•4CH$_3$CN•2CHCl$_3$ with Cu(II) and Fe(III)

paramagnetic metal centers. Magnetic susceptibility studies revealed that the $Fe^{II}_2Cu^{II}_2$ square based on low-spin Fe^{II} and $S = \frac{1}{2}$ Cu^{II} ions is a simple paramagnet with noninteracting Cu^{II} centers. The $Fe^{III}_2Cu^{II}_2$ square with two $S = \frac{1}{2}$ Fe^{III} centers in addition to two $S = \frac{1}{2}$ Cu^{II} centers exhibits ferromagnetic coupling which gives rise to a ground state of $S = 2$.

In order to design a convergent synthesis of molecular squares from octahedral metal ions, one must cap four coordination sites with two *cis* chelating ligands or use a tetradentate ligand that leaves two *cis* sites open for substitution chemistry. These compounds, then, will have an angle of 90° between the labile sites as displayed in Figure 2.1. Inexpensive choices for bidentate capping ligands are 2,2'-bipyridine or 1,10-phenanthroline which, because of the steric hindrance afforded by the opposing hydrogen atoms, bind exclusively as *cis* ligands. The other building block can be a precursor also tailored to have four sites blocked by innocent capping ligands but, in this case, the other two sites are occupied by cyanide ligands at 90°. One can envisage that the reaction between *cis*-$[(N-N)_2M(S)_2]^{n+}$ and *cis*-$[(N-N)_2M'(CN)_2]$ can yield either a molecular square (Figure 2.2.) or a one-dimensional zigzag chain, depending on kinetic versus thermodynamic control. In this chapter, the preparation and characterization of the two this different types of precursors are presented and discussed.

$$\left[\begin{array}{c} \text{N} \\ \text{N} \end{array} \text{M} \begin{array}{c} \text{N} \\ \text{N} \end{array} \begin{array}{c} \text{Cl} \\ \text{Cl} \end{array} \right]^{0/+} + 2\text{AgX} \longrightarrow \left[\begin{array}{c} \text{N} \\ \text{N} \end{array} \text{M} \begin{array}{c} \text{N} \\ \text{N} \end{array} \begin{array}{c} \text{S} \\ \text{S} \end{array} \right]^{0/n+}$$

$X = [CF_3SO_3]^-$, $[BF_4]^-$, $[PF_6]^-$

$S = OH_2$, CH_3OH, $[NO_3]^-$, $[O_3SCF_3]^-$ or CH_3CN

N⌒N = 2,2'-bipyrimidine, 2,2'-bipyridine or 1,10-phenanthroline
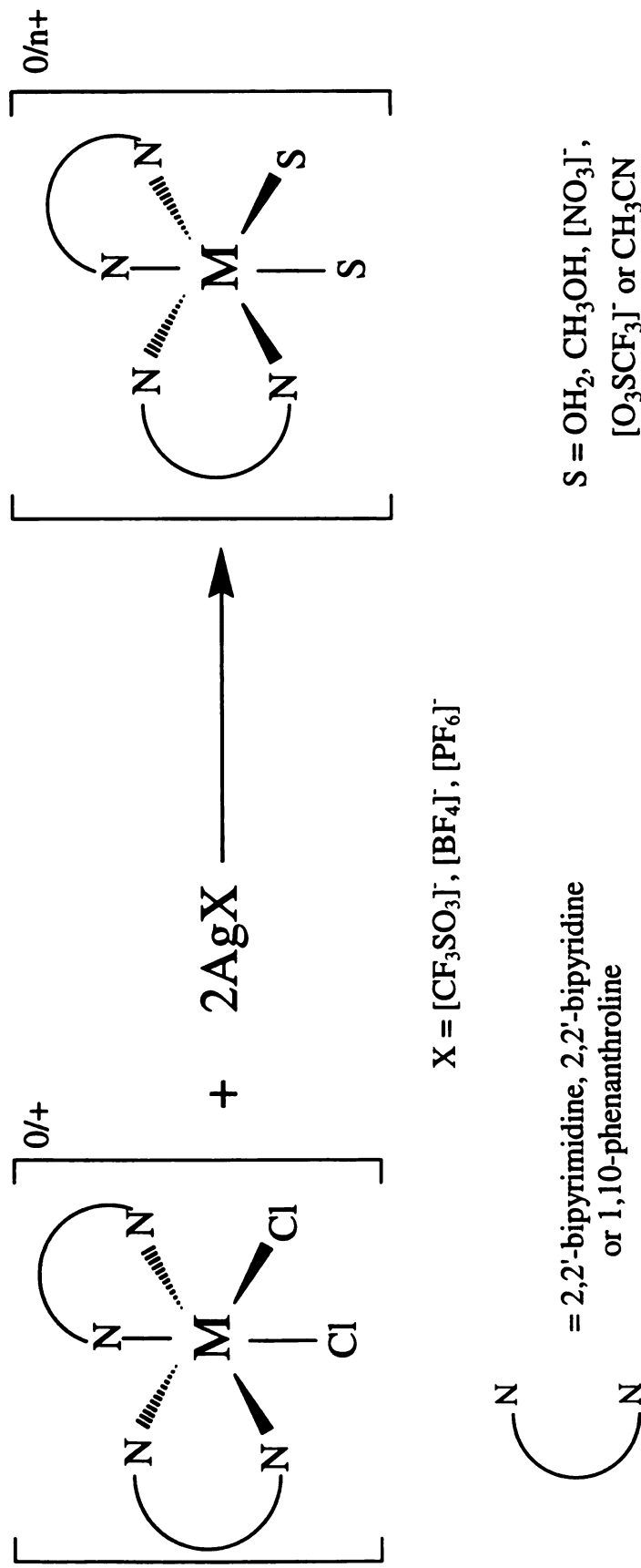
Figure 2.1. Schematic representation of halide abstraction from $[(N-N)_2MCl_2]$ to yield $[(N-N)_2M(S)_2]$ species.
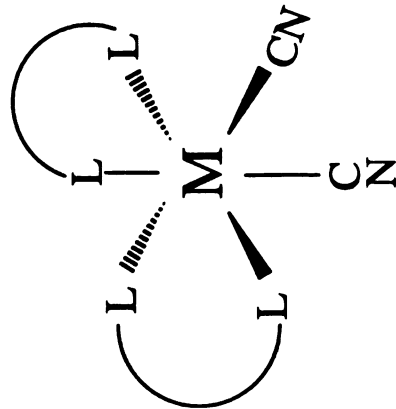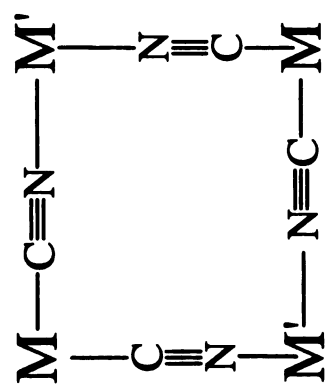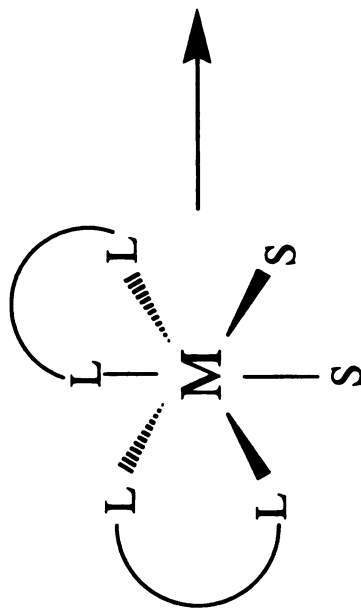
$$S = OH_2, CH_3OH, NO_3^-,$$
$$O_3SCF_3^- \text{ or } CH_3CN$$

$$\frown_L^L = \text{2,2'-bipyrimidine, 2,2'-bipyridine}$$
$$\text{or 1,10-phenanthroline}$$

Figure 2.2. Schematic representation of the molecular square assembly process.

2. EXPERIMENTAL

A. PHYSICAL METHODS

Infrared spectra were recorded on a Nicolet 42 spectrophotometer either in the Chemistry Department at Michigan State University or on a Nicolet 470 instrument in the Chemistry Department at Texas A&M University. Infrared spectra were recorded at 4 cm^{-1} resolution and 32 scans unless otherwise stated. Solid samples were measured as KBr pellets or Nujol mulls on KBr or CsI plates. Elemental analyses were performed at Desert Analytics, Tucson, AZ or in the chemistry department at Michigan State University with a Perkin and Elmer Series II CHNS/O analyzer 2400. Magnetic measurements were performed on a Quantum Design MPMS-5 equipped with a SQUID sensor housed in the Physics and Astronomy Department at Michigan State University or a MPMS-XL SQUID magnetometer located in the Chemistry Department at Texas A&M University.

B. SYNTHESES

The starting materials MCl_3 (M = Cr, Fe) and MCl_2, (M = Mn, Fe, C, Ni) and their analogous hydrates were purchased from Aldrich Chemical Company and used without further purification. $FeCl_2$ was prepared by literature methods.[10] The ligand 4,4'-dimethyl-2,2'-bipyridine was purchased from Aldrich and used without further purification. The ligands 2,2'-

bipyridine and 1,10-phenanthroline were purchased from Fisher or Aldrich and recrystallized before use. The ligand 2,2'-bipyrimidine was prepared according to published methods or a slight modification thereof.[11] The ligand 4,4'-^{t}Bu-2,2'-bpy was prepared according to published methods or a slight modification thereof.[12] Thallium hexafluorophosphate, silver tetrafluoroborate, silver nitrate and silver triflate were purchased from either Strem or Aldrich and used without further purification. The starting material, (THF)$_3$CrCl$_3$, was prepared according to literature methods.[13] Acetone and acetonitrile were distilled over 3 Å sieves, whereas benzene, diethyl ether, THF and toluene were distilled over sodium-potassium/benzophenone. Methylene chloride was distilled over P$_2$O$_5$ under a nitrogen atmosphere whereas methanol and ethanol were dried using magnesium alkoxide. Unless otherwise specified, all reactions were carried out under a nitrogen atmosphere using standard Schlenk-line techniques.

(1) [(2,2'-bpym)$_2$M(OH$_2$)$_2$](BF$_4$)$_2$ (M = Mn^{II}(1), Fe^{II}(2), Co^{II}(3), Ni^{II}(4)).

Preparation of [(2,2'-bpym)$_2$Mn(OH$_2$)$_2$](BF$_4$)$_2$ (1).

A quantity of AgBF$_4$ (0.698 g, 3.59 mmol) in 40 mL of acetonitrile was added via cannula techniques to (2,2'-bpym)$_2$MnCl$_2$•2H$_2$O (0.856 g, 1.79 mmol) in 40 mL of acetonitrile.[14] An immediate white precipitate of AgCl formed, which was separated from the yellow solution by filtration through

Celite and centrifugation. The volume of solution was reduced to ~5-10 mL, and 40 mL of diethyl ether were added to precipitate a pale yellow solid. The diethyl ether was removed by cannula techniques, and the yellow solid was dried *in vacuo*. Slow evaporation in air yielded crystals. (0.108 g, 10%) IR (KBr pellet, cm^{-1}): 1574 (s), 1493 (m), 1452 (m), 1408 (s), 1300 (m), 1242 (w), 1217 (w), 1084 (s, br), 823 (m), 756 (s), 696 (m), 667 (m), 657 (m), 534 (m), 522 (m), 265 (m), 240 (m).

Preparation of [(2,2'-bpym)$_2$Fe(OH$_2$)$_2$](BF$_4$)$_2$ (2).

The reagent AgBF$_4$ (0.952 g, 4.89 mmol) dissolved in 40 mL of acetonitrile was added via cannula techniques to a 40 mL acetonitrile solution of (2,2'-bpym)$_2$ FeCl$_2$ (1.08 g, 2.44 mmol). The AgCl by-product was removed by filtration through Celite and collected by centrifugation. The red filtrate was reduced in volume to 5-10 mL and treated with 40 mL of diethyl ether. A red solid was separated from the acetonitrile/ diethyl ether solution by cannula techniques and dried *in vacuo*. Yield: (0.306 g, 22%). IR data (KBr pellet, cm^{-1}): 3443 (s, br), 3082 (w), 3026 (w), 2924 (m), 2853 (w), 1628 (w), 1577 (s), 1556 (m), 1493 (m), 1457 (m), 1406 (s), 1300 (m), 1084 (s, br), 819 (m), 788(w), 754 (s), 696 (s), 659 (m), 534 (m), 523 (m).

Preparation of [(2,2'-bpym)$_2$Co(OH$_2$)$_2$](BF$_4$)$_2$ (3).

An acetonitrile solution (40 mL) of AgBF$_4$ (0.597 g, 3.07 mmol) was added dropwise to a 40 mL acetonitrile solution of (2,2'-bpym)$_2$CoCl$_2$•3H$_2$O (0.762 g, 1.53 mmol).[14] The AgCl was removed from an orange solution by filtration through Celite and centrifugation. The orange filtrate was reduced to ~5-10 mL and treated with 40 mL of diethyl ether to yield an orange solid. The diethyl ether was removed by cannula techniques, and the orange solid was dried *in vacuo*. Yield: (0.129 g, 15%) IR data (KBr pellet and CsI plates with Nujol (2 cm^{-1} resolution), cm^{-1}): 3084 (w), 3026 (w), 2963 (w), 2922 (w), 1631 (w), 1576 (s), 1558 (s), 1452 (w), 1408 (s), 1261 (m), 1211 (w), 1084 (s, br), 819 (m). 760 (s), 698 (m), 688 (m), 675 (w), 659 (m), 534 (m), 523 (m), 428 (w), 396 (w, br), 303 (w), 288 (m), 265 (m), 228 (w), 216 (w), 209 (w), 203 (w).

Preparation of [(2,2'-bpym)$_2$Ni(OH$_2$)$_2$](BF$_4$)$_2$ (4).

An acetonitrile solution (40 mL) of AgBF$_4$ (0.731 g, 3.76 mmol) was added via cannula techniques to a 40 mL acetonitrile solution of (2,2'-bpym)$_2$NiCl$_2$•3H$_2$O (0.871 g, 1.88 mmol).[14] The AgCl was removed from a pale-pink solution by filtration through Celite and centrifugation. The volume of solution was reduced to ~5-10 mL, and 40 mL of diethyl ether was added to precipitate a pale pink solid. The diethyl ether was removed by cannula techniques, and the pink solid was dried *in vacuo*. Yield: (0.370 g,

34%). IR data (KBr pellet, cm⁻¹): 3084 (w), 3026 (w), 2963 (w), 2924 (w), 1632 (w), 1577 (s), 1560 (s), 1452 (m), 1408 (s), 1300 (w), 1261 (m), 1084 (s, br), 819 (m), 758 (s), 696 (m), 690 (m), 679 (w), 661 (m), 534 (m), 523 (m).

(2) [(2,2'-bpy)₂M(CH₃CN)₂](BF₄)₂ for M = Mn^{II}(5), Co^{II}(6) and Ni^{II}(7).

Preparation of [(2,2'-bpy)₂Mn(CH₃CN)₂](BF₄)₂ (5).

A sample of AgBF₄ (1.31 g, 6.76 mmol) dissolved in 40 mL acetonitrile was added via cannula techniques to a 40 mL acetonitrile of (2,2'-bpy)₂MnCl₂•2H₂O (1.60 g, 3.37 mmol). The AgCl was removed by passing the pale yellow solution through Celite. The volume of solution was reduced to ~5-10 mL, and 40 mL of diethyl ether were added to induce precipitation of a pale yellow solid. The diethyl ether was removed by cannula techniques, and the yellow solid was dried *in vacuo*. Yield: (1.803 g, 86%) IR data (CsI plates with Nujol, cm⁻¹): 3508 (m), 2312 (s), 2285 (s), 1650 (m), 1599 (s), 1577 (s), 1495 (m), 1441 (s), 1365 (m), 1319 (m), 1286 (m), 1248 (m), 1221 (w), 1064 (s, br), 769 (s), 738 (m), 652 (m), 625 (m), 579 (w), 550 (w), 521 (s), 461 (w), 412 (s), 394 (w), 355 (w), 251 (s), 239 (w), 219 (w), 202 (w).

Preparation of [(2,2'-bpy)₂Co(CH₃CN)₂](BF₄)₂ (6).

A sample of AgBF₄ (2.35 g, 12.12 mmol) in 40 mL of acetonitrile was added

via a cannula to a 40 mL acetonitrile solution of (2,2'-bpy)$_2$CoCl$_2$ (2.67 g, 6.05 mmol). The AgCl by-product was removed by passing the orange solution through Celite. The volume of solution was reduced to ~5-10 mL, and 40 mL of diethyl ether was added to induce precipitation of an orange solid. The diethyl ether was decanted, and the orange solid was dried *in vacuo*. Yield: (2.92 g, 77%) IR data (KBr and CsI plates with Nujol, cm^{-1}): 3480 (m), 3134 (w), 3096 (w), 2312 (s), 2280 (s), 1608 (s), 1601 (s), 1580 (m), 1570 (m), 1504 (w), 1493 (m), 1319 (m), 1284 (m), 1250 (m), 1180 (w), 1163 (m), 1059 (s, br), 895 (w), 765 (s), 734 (m), 653 (m), 626 (m), 581 (w), 572 (w), 559 (w), 520 (s), 497 (w), 479 (w), 465 (w), 446 (w), 421 (m), 391 (w), 375 (w), 360 (w, br), 280 (m), 244 (w), 208 (w).

Preparation of [(2,2'-bpy)$_2$Ni(CH$_3$CN)$_2$](BF$_4$)$_2$ (7).

A 20 mL acetonitrile solution of (2,2'-bpy)$_2$NiCl$_2$ (0.592 g, 1.34 mmol)[15] was treated with an acetonitrile solution of AgBF$_4$ (0.522 g, 2.69 mmol) in 20 mL). The AgCl was collected on a Celite plug and the pale pink/purple filtrate was reduced under vacuum. Once the solution volume had been reduced to ~5-10 mL, 40 mL of diethyl ether were added to precipitate a pale pink/purple solid. The diethyl ether was decanted through a cannula, and the resulting pale pink/purple solid was dried *in vacuo*. Yield: (0.463 g, 55%) IR data (CsI plates with Nujol, cm^{-1}): 3495 (m), 1637 (m, br), 1603 (s),

1577 (s), 1568 (s), 1496 (m), 1444 (s), 1315 (m), 1286 (w), 1250 (m), 1224 (w), 1178 (w), 1060 (s, br), 895 (w), 769 (s), 736 (m), 655 (m), 636 (m), 554 (w), 521 (s), 445 (w), 418 (s), 394 (w), 355 (w), 282 (s), 252 (w).

(3) Preparation of [(phen)$_2$Ni(CH$_3$CN)$_2$](BF$_4$)$_2$ (8).

A sample of (phen)$_2$NiCl$_2$•H$_2$O (0.573 g, 1.13 mmol)[15] in 40 mL of acetonitrile was treated with a solution of AgBF$_4$ (0.411 g, 2.12 mmol) to give a AgCl precipitate and a purplish colored solution. The solution was allowed to stir overnight (~12 h) to ensure complete removal of the chloride ligands. The AgCl was removed by filtration through Celite under a nitrogen atmosphere. The resulting pale pink-purple solution was reduced in volume to ~5-10 mL, and a 40 mL portion of diethyl ether was added to induce precipitation of a pale pink/purple solid. The diethyl ether was removed by cannula techniques and the pale pink/purple solid was dried *in vacuo*. Yield: (0.584 g, 77%) IR (Nujol, cm^{-1}): 2318 (s), 2289 (s), 1645 (m, br), 1628 (m), 1606 (m), 1587 (m), 1520 (s), 1496 (w), 1429 (s), 1344 (m), 1307 (m), 1286 (w), 1226 (m), 1212 (w), 1198 (w), 1151 (m), 1086 (s), 1060 (s), 1053 (s), 1034 (s), 871 (m), 846 (s), 807 (w), 777 (m), 769 (w), 645 (m), 520 (w), 508 (w), 484 (w), 426 (w).

(4) Preparation of [(2,2'-bpy)$_2$Ni(CH$_3$CN)$_2$](PF$_6$)$_2$ (9).

A quantity of TlPF$_6$ (1.13 g, 3.24 mmol) was dissolved in 40 mL of

acetonitrile and treated with a 40 mL acetonitrile solution of $(2,2'\text{-bpy})_2NiCl_2$ (0.714 g, 1.62 mmol) which was added through a cannula.[15] The AgCl was removed by filtration though Celite, the pale pink/purple filtrate was reduced under vacuum to 5-10 mL, and 40 mL of diethyl ether were added to precipitate a pale pink/purple solid. The diethyl ether was removed by cannula techniques and the pale pink/purple solid was dried *in vacuo*. Yield: (1.02 g, 85%) IR data (Nujol, cm^{-1}): 2314 (s), 2284 (s), 1608 (m), 1602 (s), 1579 (s), 1571 (m), 1495 (m), 1446 (s), 1412 (m), 1365 (m), 1315 (m), 1251 (m), 1220 (w), 1178 (m), 1166 (m), 1106 (w), 1046 (w), 1024 (m), 1016 (m), 966 (w), 937 (w), 841 (s, br), 760 (s), 736 (s), 653 (m), 634 (m), 607 (m), 557 (s), 483 (w), 468 (w), 444 (w), 416 (m).

(5) Preparation of $(2,2'\text{-bpy})_2M(CF_3SO_3)_2$ (M = Mn^{II} (10) and Co^{II} (11)).

Preparation of $[(2,2'\text{-bpy})_2Mn(CF_3SO_3)_2]$ (10).

A sample of $(2,2'\text{-bpy})_2MnCl_2 \bullet 2H_2O$ (0.681 g, 1.44 mmol) was dissolved in 40 mL of acetonitrile and treated with two equivalents of $Ag(CF_3SO_3)$ (0.975 g, 3.80 mmol) dissolved in 40 mL of acetonitrile. The reaction was stirred for 12 h, after which time the AgCl was removed by filtration through Celite. The solution was reduced in volume to ~5-10 mL, and 40 mL of diethyl ether were added to precipitate the yellow product. Yellow crystals were grown by slow diffusion of diethyl ether and hexanes into an

acetonitrile solution of the compound. Yield: (0.774 g, 78%) *Anal.* Calc. for

$C_{22}H_{16}N_4S_2O_6F_6Mn$: C 39.71; H 2.42; N 8.42. Found: C 39.87; H 2.64; N

7.60. IR (Nujol, cm^{-1}): 1606 (s), 1599 (s), 1577 (m), 1493 (m), 1444 (s, br),

1311 (s), 1242 (s), 1234 (s), 1215 (s), 1180 (s), 1165 (s), 1024 (s), 769 (s),

738 (m), 653 (m), 636 (s), 581 (w), 572 (w, br), 516 (m), 416 (m), 358 (w,

br), 249 (m), 221 (w).

Preparation of [(2,2'-bpy)$_2$Co(CF$_3$SO$_3$)$_2$] (11).

A quantity of (2,2'-bpy)$_2$CoCl$_2$•3H$_2$O (0.841 g, 1.10 mmol) was dissolved in

40 mL of acetonitrile and combined with two equivalents of Ag(CF$_3$SO$_3$)

and (0.872 g, 3.39 mmol) in 40 mL of acetonitrile. The reaction was stirred

for 12 h, after which time the AgCl was removed by filtration through

Celite. The solution was reduced in volume to ~5-10 mL, and 40 mL of

diethyl ether were added to precipitate the product. The compound was

isolated as a dark orange solid. Orange crystals were obtained by slow

evaporation of an acetonitrile solution. Yield: (0.922 g, 78%) IR (CsI plates

with Nujol, cm^{-1}): 1608 (s), 1601 (s), 1577 (m), 1493 (m), 1444 (s, br), 1311

(s), 1242 (s), 1232 (s), 1213 (s), 1176 (m), 1157 (s, br), 1024 (s), 769 (s),

738 (m), 653 (m), 636 (s), 581 (w), 572 (w, br), 516 (m), 419 (m), 359 (w,

br), 280 (m), 244 (w, br), 208 (w).

(6) Preparation of [(phen)$_2$Mn(CF$_3$SO$_3$)$_2$] (12).

A sample of (phen)$_2$MnCl$_2$•2H$_2$O[16] (0.540 g, 1.04 mmol) was dissolved in

40 mL of acetonitrile and reacted with two equivalents of Ag(CF$_3$SO$_3$)

(0.603 g, 2.35 mmol) in 40 mL of acetonitrile. The reaction was stirred for

12 h, after which time the AgCl was removed by filtration through Celite.

The solution was reduced in volume to ~5-10 mL, and 40 mL of diethyl

ether were added to precipitate the yellow product. Yield: (0.379 g, 51%). IR

(Nujol, cm^{-1}): 1625 (m), 1605 (w), 1592 (m), 1581 (m), 1522 (m), 1513 (m),

1496 (m), 1429 (s), 1347 (m), 1307 (s), 1259 (s), 1234 (s), 1215 (s), 1182

(s), 1167 (s), 1143 (s), 1105 (m), 1042 (s), 1022 (s), 997 (m), 966 (w), 868

(m), 848 (s), 815 (m), 804 (m), 785 (m), 761 (m), 731 (s), 636 (s), 584 (m),

572 (m), 516 (m), 501 (w), 422 (m).

(7) Preparation of [Ni(2,2'-bpy)$_2$(H$_2$O)$_2$](CF$_3$SO$_3$)$_2$•2H$_2$O (13).

A sample of (2,2'-bpy)$_2$NiCl$_2$•H$_2$O (0.873 g, 1.90 mmol)[15] was dissolved in

40 mL of acetonitrile and reacted with two equivalents of Ag(CF$_3$SO$_3$)

(0.975 g, 3.80 mmol) in 40 mL of acetonitrile. The reaction was stirred for

12 h, the AgCl was removed by filtration through Celite, and the solution

was reduced in volume to ~10 mL. Treatment of the solution with 40 mL of

diethyl ether led to the precipitation of a purple solid. Purple crystals were

grown by slow evaporation of a water solution in air. Yield: (1.00 g, 75%).

Anal. Calc. for C$_{22}$H$_{24}$N$_4$S$_2$O$_{10}$F$_6$Ni: C 35.65; H 3.26; N 7.55. Found: C

64

36.93; H 2.49; N 7.21. IR (CsI plates with Nujol, cm^{-1}): 1610 (s), 1603 (s), 1579 (m), 1493 (m), 1448 (s, br), 1307 (s), 1244 (s), 1232 (s), 1217 (s), 1176 (s), 1161 (s), 1028 (s), 771 (s), 738 (m), 653 (m), 636 (s), 581 (w), 572 (w), 517 (m), 420 (m), 359 (w, br), 297 (m), 260 (m), 220 (w).

(8) Preparation of (phen)$_2$Mn(NO$_3$)$_2$ (14).

A sample of (phen)$_2$MnCl$_2$•2H$_2$O[16] (0.308 g, 0.590 mmol) was dissolved in 20 mL of acetonitrile and combined with two equivalents of AgNO$_3$ (0.207 g, 1.22 mmol) in 20 mL of acetonitrile. The reaction was stirred for 12 h, after which time the AgCl was removed by filtration through Celite. The solution was reduced in volume to ~5-10 mL, and 40 mL of diethyl ether were added to precipitate the product, which was collected by filtration and dried. The compound was isolated as a yellow solid. Yield: (0.211 g, 67%) IR data (Nujol, cm^{-1}): 1641 (w), 1624 (m), 1591 (m), 1577 (m), 1518 (s), 1494 (m), 1428 (s), 1412 (s), 1349 (s), 1328 (s), 1303 (s), 1298 (s), 1261 (s), 1223 (m), 1208 (w), 1100 (s, br), 1018 (s, br), 864 (m), 844 (s), 798 (s, br), 702 (w), 686 (w), 660 (w), 638 (m), 554 (w), 510 (w), 496 (w), 478 (w), 416 (w).

(9) Preparation of (phen)$_2$Co(NO$_3$)$_2$ (15).

A quantity of (phen)$_2$CoCl$_2$•2H$_2$O (0.237 g, 0.451 mmol) was dissolved in 20 mL of acetonitrile and treated with two equivalents of AgNO$_3$ (0.153 g,

0.901 mmol) in 20 mL of acetonitrile. The reaction was stirred for 12 h, after which time the AgCl was removed by filtration through Celite. The solution was reduced in volume to ~5-10 mL, and 40 mL of diethyl ether were added to precipitate the product. The compound was isolated by filtration as an orange solid. Yield: (0.210 g, 86%) IR (Nujol, cm^{-1}): 1625 (m), 1605 (w), 1582 (m), 1518 (s), 1494 (m), 1423 (s), 1292 (s, br), 1142 (s), 1101 (s), 1034 (m), 1024 (m), 993 (w), 972 (w), 959 (w), 869 (m), 847 (s), 826 (w), 776 (m), 750 (w), 643 (m), 554 (w), 508 (w), 479 (w), 443 (w), 424 (m).

(10) Preparation of $(2,2'-bpy)_2M(CN)_2$ ($M = Mn^{II}$ (16) and Co^{II} (17)).

Preparation of $(2,2'-bpy)_2Mn(CN)_2$ (16).

The literature preparation of $(phen)_2Mn(CN)_2 \bullet 3H_2O$ was modified by replacing 1,10-phenanthroline with 2,2'-bipyridine.[16] A solution of $MnSO_4 \bullet 4H_2O$ (0.525 g, 2.35 mmol) in 6 mL of CH_3OH and 24 mL of H_2O was added to a solution of 2,2'-bpy (0.971 g, 6.23 mmol) in a mixture of 20 mL of CH_3OH and 80 mL of H_2O. This mixture was heated to $80°C$ under a nitrogen atmosphere to prevent aerial oxidation, and maintained at this temperature during the gradual addition of a KCN (0.606 g, 9.33 mmol) solution (16 mL CH_3OH/64 mL H_2O). As the product slowly cooled, air-sensitive yellow needles were observed to form. Yield: (0.619 g, 56%) IR (Nujol, cm^{-1}) on KBr plates: 2114 (m), 1595 (s), 1574 (m), 1491 (m), 1441

(s), 1315 (m), 1261 (m), 1097 (m, br), 1060 (m), 1014 (s), 802 (m, br), 769

(s), 736 (m), 646 (m), 625 (m), 489 (w, br).

Preparation of (2,2'-bpy)$_2$Co(CN)$_2$ (17).

A procedure similar to the one described above for (2,2-bpy)$_2$Mn(CN)$_2$ (16),

was followed for the preparation of the Co(II) derivative. A solution of

CoSO$_4$•4H$_2$O (0.549 g, 1.96 mmol) in 6 mL of CH$_3$OH and 24 mL of H$_2$O

was added to a solution of 2,2'-bpy (0.610 g, 3.91 mmol) in a mixture of 20

mL of CH$_3$OH and 80 mL of H$_2$O. This mixture was heated to 80°C under a

nitrogen atmosphere to prevent aerial oxidation, and maintained at this

temperature during the slow addition of a KCN (0.255 g, 3.92 mmol)

solution (16 mL CH$_3$OH/64 mL H$_2$O). The product was slowly cooled to

yield yellow needles. Yield: (0.292 g, 35%) IR (KBr plates with Nujol, cm^{-1}): 2156 (w), 2123 (m), 1635 (m), 1599 (m), 1576 (m), 1315 (m), 1248 (m),

1157 (m), 1020 (m), 769 (s), 736 (m), 652 (m), 630 (w), 412 (m).

(11) Preparation of [(4,4'-(CH$_3$)$_2$-2,2'-bpy)$_2$CrCl$_2$]Cl (18).

Two equivalents of 4,4'-(CH$_3$)$_2$-2,2'-bpy (0.987 g, 5.37 mmol) in 25 mL of

acetonitrile were added dropwise into an acetonitrile solution of

(THF)$_3$CrCl$_3$ (1.01 g, 2.69 mmol). An instantaneous color change from

purple to green ensued with the formation of a green precipitate in a green

solution. The green precipitate was collected by filtration and washed with 2

x 20 mL of diethyl ether. The green filtrate was reduced in volume to ~10 mL, and 40 mL of diethyl ether were added to precipitate the green product. The solution was removed by cannula techniques and the green solid was dried *in vacuo*. Yield: (1.12 g, 80%) IR (Nujol, cm^{-1}): 1615 (m), 1591 (m), 1551 (m), 1486 (w), 1408 (w), 1364 (m), 1340 (w), 1321 (w), 1303 (m), 1279 (m), 1260 (w), 1239 (m), 1219 (m), 1102 (w), 1026 (m), 991 (m), 970 (w), 922 (m), 911 (m), 823 (s), 738 (m), 669 (m), 607 (w), 589 (w), 563 (m), 516 (s), 488 (w), 466 (w), 421 (m), 418 (m).

(12) Preparation of [(4,4'-(CH$_3$)$_2$-2,2'-bpy)$_2$FeCl$_2$]Cl (19).

Two equivalents of 4,4'-(CH$_3$)$_2$-2,2'-bpy (1.58 g, 8.58 mmol) in 25 mL of acetonitrile were added dropwise to an acetonitrile solution of FeCl$_3$ (0.695 g, 4.29 mmol) which effected an instantaneous color change from red/orange to yellow with the deposition of a yellow precipitate from a yellow solution. The yellow precipitate was removed by filtration and washed with 2 x 20 mL of diethyl ether. The yellow filtrate was reduced in volume to ~5-10 mL. Diethyl ether (40 mL) was added to precipitate the yellow product and the solution was decanted. The yellow product was dried *in vacuo*. Yield: (1.60 g, 70%) IR (Nujol, cm^{-1}): 1612 (s), 1554 (m), 1407 (w), 1304 (m), 1281 (w), 1242 (m), 1219 (w), 1203 (w), 1166 (w), 1153 (w), 1121 (w), 1078 (w), 1035 (w), 1018 (s), 968 (w), 922 (m), 897 (w), 845 (m), 831 (m), 770 (w),

740 (m), 669 (w), 553 (m), 518 (m), 482 (w), 422 (m), 418 (m).

(13) [(4,4'-(CH₃)₂-2,2'-bpy)₂Fe(CN)₂](PF₆) (20).

Two equivalents of AgCN (0.093 g, 0.694 mmol) in 10 mL of acetonitrile/10

mL methanol were added to a 10 mL acetonitrile/10 mL methanol solution

of [(4,4'-(CH₃)₂-2,2'-bpy)₂FeCl₂]Cl (0.184 g, 0.347 mmol). This was allowed

to react for 30 minutes, after which time one equivalent of TlPF₆ (0.122 g,

0.349 mmol) in 10 mL acetonitrile was added. After two days of stirring, the

solution was filtered, and the red filtrate was reduced in volume; addition of

40 mL of diethyl ether led to the precipitation of a red solid. The diethyl

ether was removed using cannula techniques and the red product was dried

in vacuo. Yield: (0.065 g, 30%) IR (Nujol, cm⁻¹): 2064 (m), 1618 (s), 1556

(m), 1412 (w), 1352 (w), 1305 (m), 1286 (w), 1264 (w), 1242 (m), 1225 (w),

1202 (w), 1166 (m), 1155 (m), 1078 (w), 1038 (w), 1024 (m), 971 (w), 924

(m), 908 (w), 843 (s, br), 773 (w), 736 (w), 670 (w), 557 (s), 531 (m), 518

(m), 494 (w), 486 (w), 467 (w), 424 (m).

C. Reactivity Studies

(1) Reaction of (2,2'-bpy)₂Co(CN)₂ with [(2,2'-bpy)₂Co(CH₃CN)₂](BF₄)₂.

One equivalent of [(2,2'-bpy)₂Co(CH₃CN)₂](BF₄)₂ (0.123 g, 0.298 mmol)

dissolved in 20 mL of acetonitrile was combined with one equivalent of

(2,2'-bpy)₂Co(CN)₂ (0.187 g, 0.298 mmol) in 20 mL of acetonitrile. A tan/

light-brown precipitate formed in a colorless solution, and was decanted from the solid. The precipitate was washed with 40 mL of diethyl ether and dried *in vacuo*. IR (Nujol, cm^{-1}): 2248 (w), 2147 (m), 1666 (m), 1608 (s), 1568 (m), 1504 (m), 1321 (m), 1284 (m), 1261 (s), 1180 (m), 1057 (s, br), 895 (w), 800 (s), 771 (s), 673 (w), 651 (w), 559 (w), 520 (m), 497 (w), 480 (w), 460 (w), 422 (m).

(2) Reaction of (2,2'-bpy)$_2$Co(CN)$_2$ with [(phen)$_2$Ni(CH$_3$CN)$_2$](BF$_4$)$_2$.

One equivalent of [(phen)$_2$Ni(CH$_3$CN)$_2$](BF$_4$)$_2$ (0.167 g, 0.248 mmol) in 5 mL of acetonitrile was reacted with one equivalent of (2,2'-bpy)$_2$Co(CN)$_2$ (0.105 g, 0.248 mmol) in 5 mL of acetonitrile. The solution turned green with the formation of a blue precipitate. The solution was decanted, and the blue precipitate was washed with 40 mL of diethyl ether and dried *in vacuo*. IR data (Nujol, cm^{-1}): 2166 (m), 1672 (w), 1628 (w), 1606 (m), 1518 (m), 1315 (w), 1147 (w), 1062 (s, br), 870 (w), 848 (m), 769 (m), 652 (w).

(3) Reaction of (2,2'-bpy)$_2$Co(CN)$_2$ with [(phen)$_2$Mn(CF$_3$SO$_3$)$_2$].

One equivalent of (phen)$_2$Mn(CF$_3$SO$_3$)$_2$ (0.133 g, 0.187 mmol) in 20 mL of acetonitrile was reacted with one equivalent of (2,2'-bpy)$_2$Co(CN)$_2$ (0.071 g, 0.168 mmol) in 20 mL of acetonitrile. The solution slowly turned gold with the deposition of a yellow/tan precipitate from a colorless solution. The solution was removed via a cannula, and the tan solid was washed with 20

70

mL of diethyl ether. The solvent was removed by cannula techniques and the solid was dried *in vacuo*. IR (Nujol, cm^{-1}): 2158 (s), 1604 (m), 1520 (m), 1427 (m), 1344 (w), 1304 (m), 1261 (s), 1238 (s), 1223 (s), 1157 (m), 1103 (m), 1030 (s), 848 (m), 769 (m), 729 (m), 636 (s), 451 (m).

(4) Reaction of (4,4'-^{t}Bu-2,2'-bpy)$_2$Co(CN)$_2$ with [(2,2'-bpy)$_2$Ni (CH$_3$CN)$_2$](PF$_6$)$_2$.

One equivalent of [(2,2'-bpy)$_2$Ni(CH$_3$CN)$_2$](PF$_6$)$_2$ (0.098 g, 0.131 mmol) in 15 mL acetonitrile was added to a 15 mL acetonitrile solution of (4,4'-^{t}Bu-2,2'-bpy)$_2$Co(CN)$_2$ (0.102 g, 0.157 mmol). The reaction was performed aerobically in wet acetonitrile, and allowed to stir for 12 h during which time the solvent evaporated. The yellow/orange solid was redissolved in acetonitrile, and the solution was slowly evaporated to yield yellow/orange crystals. IR (Nujol, cm^{-1}): 3400 (s, br), 2177 (m), 1608 (s), 1577 (m), 1550 (m), 1446 (s), 1412 (s), 1315 (s), 1251 (s), 1186 (m), 1161 (m), 1024 (s), 841 (s, br), 736 (s), 653 (s), 634 (s), 607 (s), 557 (s), 416 (m).

D. SINGLE CRYSTAL X-RAY STRUCTURAL STUDIES

Crystallographic data for compounds **7**, **10** and **16** were collected on a SMART 1K and for **13** and **21** on a SMART 2000 CCD diffractometer equipped with monchromated Mo Kα (λ_α = 0.71069 Å) radiation. The source is a Mo sealed tube with a 3 KW generator. The frames were

integrated in the Bruker SAINT software package[17] and the data were corrected for absorption using the SADABS program.[18] The SIR97[19] and SHELX-97[20] crystallographic software packages were used to solve and refine the crystal structures. Crystal parameters and basic information pertaining to data collection and structure refinement are summarized in Tables 2.1-2.3.

(1) [(2,2'-bpy)$_2$Ni(CH$_3$CN)$_2$](BF$_4$)$_2$ (7).

Single crystals of **7** were grown by reducing the volume of an acetonitrile solution of the compound under vacuum. A purple crystal of dimensions 0.25 x 0.20 x 0.15 mm^3 was mounted on the tip of a glass fiber with Dow Corning silicone grease and placed in a cold N$_2$ stream. Least squares refinement using well-centered reflections in the range $2.70 < 2\theta < 46.60$ gave a cell corresponding to a triclinic crystal system. A total of 9289 data (3908 unique) with F(000) = 624 were collected at 173(2) K using the ω-2θ scan technique to a maximum 2θ value of 46.60. The space group was determined as P-1. The final full-matrix, least-squares refinement was based on data with $F_o^2 > 4\sigma(F_o^2)$ and parameters to give $R_1 = 0.0414$ (w$R_2 =$ 0.1077) and $R_{int} = 0.0328$. The goodness-of-fit index was 0.710, and the highest peak in the final difference map was 0.512 e$^-$/Å^3. All non-hydrogen atoms were refined anisotropically. The hydrogen atoms were placed in

Table 2.1. Crystallographic information for [(2,2'- bpy)$_2$Ni(CH$_3$CN)$_2$](BF$_4$)$_2$ (7) and [(2,2'-bpy)$_2$Ni(OH$_2$)$_2$](O$_3$SCF$_3$)$_2$ (13) •2H$_2$O.

	7	13 •2H$_2$O
Formula	C$_{24}$H$_{16}$F$_8$NiN$_6$B$_2$	C$_{22}$H$_{24}$F$_6$N$_4$NiO$_{10}$S$_2$
Formula weight	620.76	741.28
Temperature (K)	173(2)	110(2)
Space group	P-1	P-1
a (Å)	9.990(5)	11.325(5)
b (Å)	10.255(5)	11.968(5)
c (Å)	15.290(5)	12.791(5)
α (°)	90.975(5)	81.134(5)
β (°)	96.600(5)	71.290(5)
γ (°)	119.051(5)	64.114(5)
Volume (Å^3)	1355.5(10)	1477.1(11)
Z	2	2
D$_{calc}$ (Mg m^{-3})	1.521	1.667
Absorption coefficient(mm^{-1})	0.797	0.896
Crystal size (mm)	0.25x0.20x0.15	0.30x0.372x0.063
Reflections collected	9289	6716
Independent reflections	3908	5448
R$_{int}$	0.0328	0.0182
Final R indices	R$_1$ = 0.0414	R$_1$ = 0.0447
	wR$_2$ = 0.1077	wR$_2$ = 0.1058

R$_1$ = $\Sigma[||F_o| - |F_c||] / \Sigma|F_o|$. wR$_2$ = $\{\Sigma[w(F_o^2 - F_c^2)^2 / \Sigma[w(F_o^2)^2]]\}^{1/2}$. GOF = $\{\Sigma[w(F_o^2 - F_c^2)^2] / (n - p)\}^{1/2}$ where n = total number of reflections and p = total number of parameters.

Table 2.2. Summary of crystallographic data for $Mn(O_3SCF_3)_2(2,2'\text{-bpy})_2$ **(10)** and for $Mn(CN)_2(2,2'\text{-bpy})_2$ **(16)** $\bullet 3H_2O$.

	10	**16** $\bullet 3H_2O$
Formula	$C_{22}H_{16}F_6MnN_4O_6S_2$	$C_{22}H_{22}MnN_6O_3$
Formula weight	665.45	473.40
Temperature (K)	173(2)	173(2)
Space group	C2/c	P2$_1$/n
a (Å)	10.024(1)	8.544(1)
b (Å)	14.237(1)	19.989(1)
c (Å)	18.922(1)	13.448(1)
α (°)	90	90
β (°)	101.32(1)	90.065(1)
γ (°)	90	90
Volume (Å^3)	647.9(4)	2296.87(11)
Z	4	4
D_{calc} (Mg m^{-3})	1.669	1.369
Absorption coefficient(mm^{-1})	0.745	0.610
Crystal size (mm)	0.52 x 0.47 x 0.18	0.25 x0.25 x 0.10
Reflections collected	8163	13655
Independent reflections	3118	5333
R_{int}	0.0267	0.0362
Final R indices	$R_1 = 0.0379$	$R1 = 0.0448$
	$wR_2 = 0.1035$	$wR2 = 0.0796$

$R_1 = \Sigma[||F_o| - |F_c||] / \Sigma|F_o|.$ $wR_2 = \{\Sigma[w(F_o^2 - F_c^2)^2 / \Sigma[w(F_o^2)^2]\}^{1/2}.$ GOF $= \{\Sigma[w(F_o^2 - F_c^2)^2] / (n - p)\}^{1/2}$ where n = total number of reflections and p = total number of parameters.

Table 2.3. Crystallographic Information for [Co(CN)$_2$(4,4'-^{t}Bu-2,2'-bpy)$_2$](PF$_6$) (**21**) •H$_2$O

	21 •H$_2$O
Formula	C$_{38}$H$_{50}$CoN$_6$OP$_1$F$_6$
Formula weight	805.73
Temperature (K)	100(2)
Space group	P -1
a (Å)	10.888(5)
b (Å)	16.059(5)
c (Å)	24.917(5)
α (°)	105.612(5)
β (°)	90.225(5)
γ (°)	97.899(5)
Volume (Å^3)	4152(2)
Z	4
D$_{calc}$ (Mg m^{-3})	1.295
Absorption coefficient(mm^{-1})	0.515
Crystal size (mm)	0.16 x 0.034 x 0.020
Reflections collected	21089
Independent reflections	16214
R$_{int}$	0.2171
Final R indices	R1 = 0.0815
	wR2 = 0.1760

R$_1$ = Σ[||F$_o$| - |F$_c$||] / Σ|F$_o$|. wR$_2$ = {Σ[w(F$_o^2$ - F$_c^2$)^2 / Σ[w(F$_o^2$)^2]}$^{1/2}$. GOF = {Σ[w(F$_o^2$ - F$_c^2$)^2] / (n - p)}$^{1/2}$ where n = total number of reflections and p = total number of parameters.

calculated positions and treated as riding atoms. A thermal ellipsoid plot is presented in Figure 2.3.

(2) (2,2'-bpy)$_2$Mn(CF$_3$SO$_3$)$_2$ (10).

Single crystals of **10** were grown by slow diffusion of diethyl ether/hexanes into an acetonitrile solution of the compound at room temperature. A pale-yellow crystal of dimensions 0.52 x 0.47 x 0.18 mm^3 was mounted on the tip of a glass fiber with Dow Corning silicone grease and placed in a cold N$_2$ stream. Least squares refinement using well-centered reflections in the range $4.40 < 2\theta < 56.40$ gave a cell corresponding to a monoclinic crystal system. A total of 8163 data (3118 unique) with F(000) = 1340 were collected at 173(2) K using the ω-2θ scan technique to a maximum 2θ value of 56.40. Systematic absences from the data led to the choice of C2/c as the space group. The final full-matrix, least-squares refinement was based on data with $F_o^2 > 4\sigma(F_o^2)$ and parameters to give $R_1 = 0.0379$ ($wR_2 = 0.1035$) and $R_{int} = 0.0267$. The goodness-of-fit index was 1.024, and the highest peak in the final difference map was 0.684 e$^-$/Å^3. All non-hydrogens atoms were refined anisotropically. Hydrogen atoms were placed in calculated positions as riding atoms. A thermal ellipsoid plot is presented in Figure 2.4.

(3) [(2,2'-bpy)$_2$Ni(OH$_2$)$_2$](CF$_3$SO$_3$)$_2$ (13).

Single crystals of **13** were grown by slow evaporation of an acetonitrile

solution of the compound at room temperature. A purple crystal of dimensions 0.30 x 0.37 x 0.063 mm^3 was mounted on the tip of a glass fiber with Dow Corning silicone grease and placed in a cold N_2 stream. Least squares refinement using well-centered reflections in the range 3.36 < 2θ < 56.48 gave a cell corresponding to a triclinic crystal system. A total of 11001 data (6716 unique) with F(000) = 756 were collected at 110(2) K using the ω-2θ scan technique to a maximum 2θ value of 56.48. The space group was determined to be P-1. The final full-matrix, least-squares refinement was based on data with $F_o^2 > 4\sigma(F_o^2)$ and parameters to give $R_1 = 0.0449$ ($wR_2 = 0.1058$) and $R_{int} = 0.0182$. The goodness-of-fit was 1.069, and the highest peak in the final difference map was 1.490 e$^-$/Å^3. All non-hydrogen atoms were refined anisotropically. Hydrogen atoms were placed in calculated positions as riding atoms. A thermal ellipsoid plot is depicted in Figure 2.5.

(4) (2,2'-bpy)$_2$Mn(CN)$_2$ (16) •3H$_2$O.

Single crystals of **16** were grown by slow cooling of the methanol/water solution from 80 °C to room temperature. A pale-yellow crystal of dimensions 0.25 x 0.25 x 0.10 mm^3 was mounted on the tip of a glass fiber with Dow Corning silicone grease and placed in a cold N_2 stream. Least squares refinement using well-centered reflections in the range 3.66 < 2θ < 56.48 gave a cell corresponding to a monoclinic crystal system. A total of

13655 data (5333 unique) with F(000) = 980 were collected at 173(2) K using the ω-2θ scan technique to a maximum 2θ value of 56.48. Systematic absences from the data led to the choice of P2$_1$/n as the space group. The final full-matrix, least-squares refinement was based on data with F_o^2 > 4$\sigma(F_o^2)$ to give R_1 = 0.0448 (wR_2 = 0.0796) and R_{int} = 0.0362. The goodness-of-fit was 1.052, and the highest peak in the final difference map was 0.277 e$^-$/Å^3. A thermal ellipsoid plot is shown in Figure 2.6.

(5) [(4,4'-^{t}Bu-2,2'-bpy)$_2$Co(CN)$_2$](PF$_6$) (21)

Single crystals of **21** were grown by slow evaporation of an acetonitrile solution at room temperature. A pale orange-yellow crystal of dimensions 0.16 x 0.034 x 0.020 mm^3 was mounted on the tip of a glass fiber with Dow Corning silicone grease and placed in a cold N$_2$ stream. Least squares refinement using well-centered reflections in the range 2.66 < 2θ < 56.56 gave a cell corresponding to a monoclinic crystal system. A total of 21089 (16214 unique) data were collected at 100(2) K using the ω-2θ scan technique to a maximum 2θ value of 56.56. The final full-matrix, least-squares refinement was based on data with F_o^2 > 4$\sigma(F_o^2)$ and parameters to give R_1 = 0.0815 (wR_2 = 0.1760) and R_{int} = 0.2171. The transmission factors are in the range of 0.577 to 1.00. The goodness-of-fit index was 0.732, and the highest peak in the final difference map was 0.728 e$^-$/Å^3. A thermal
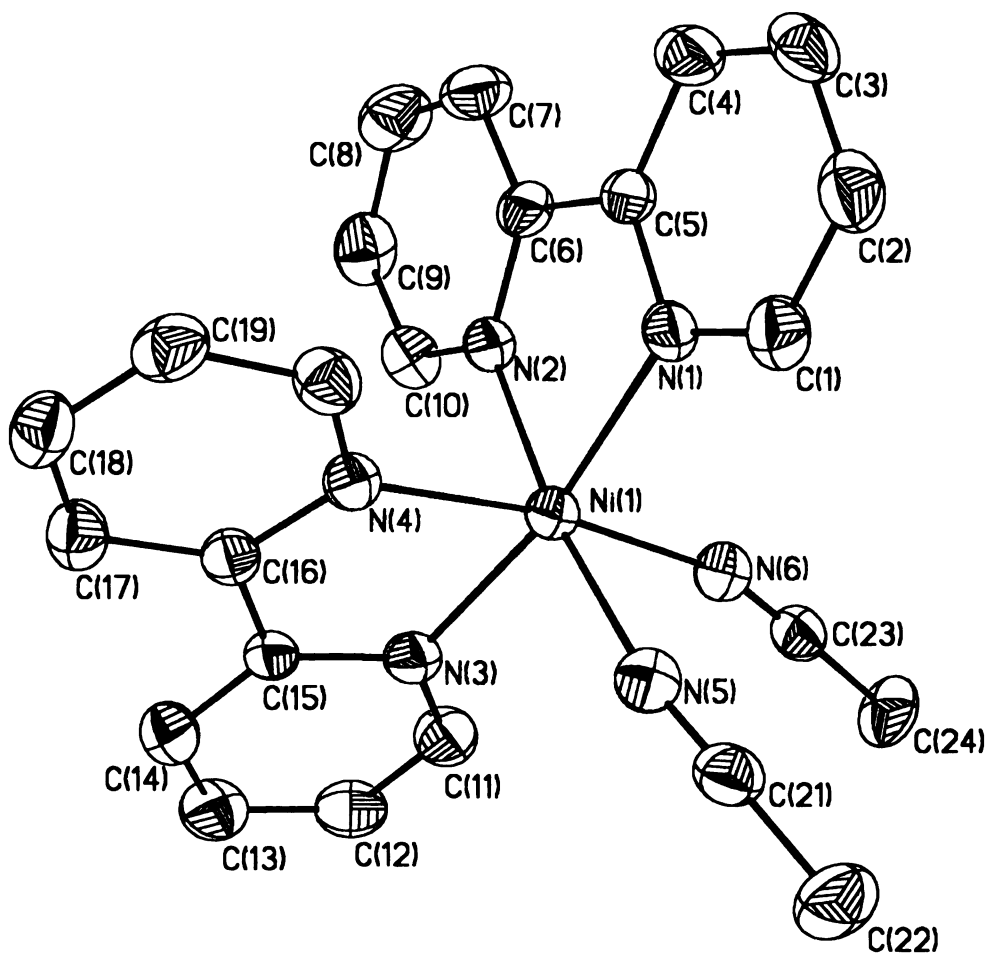
Figure 2.3. Thermal ellipsoid representation of the cation,
[(2,2'-bpy)$_2$Ni(CH$_3$CN)$_2$]$^{2+}$, in (7) at the 50 % probability level.
The hydrogen atoms were omitted for the sake of clarity.
(Image is presented in color)
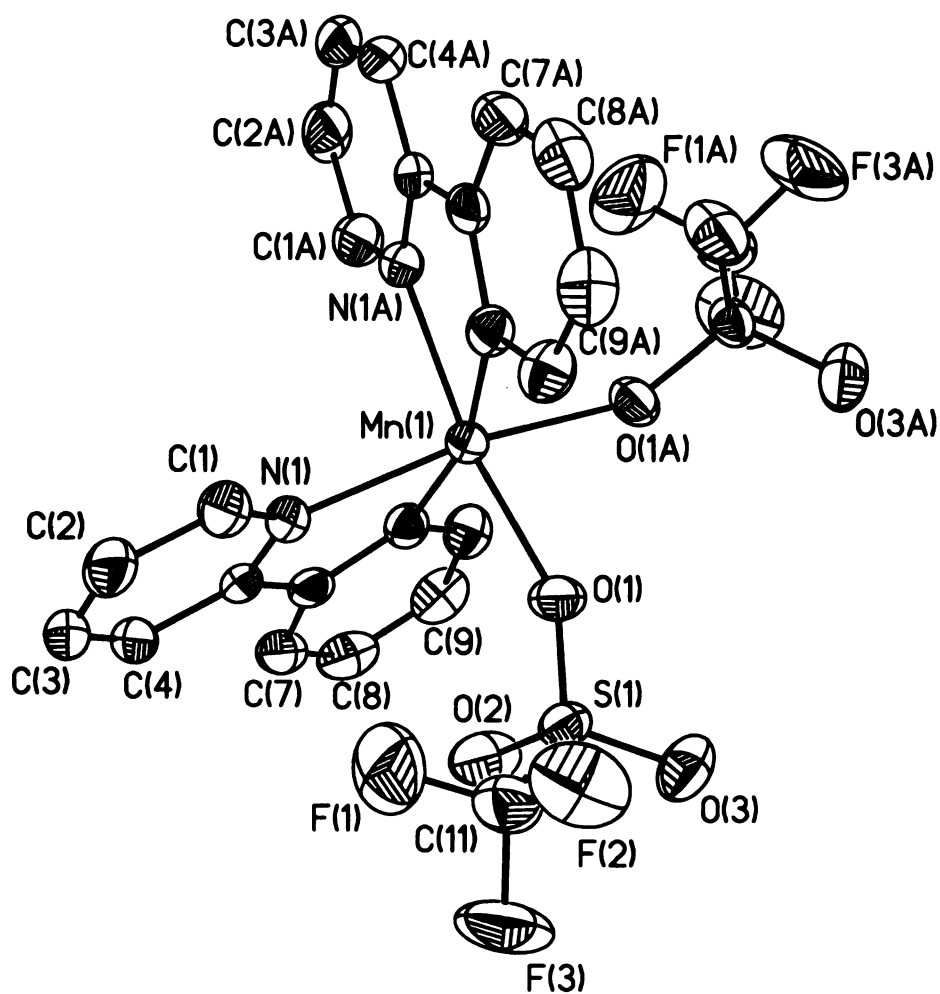
Figure 2.4. Thermal ellipsoid representation of (2,2'-bpy)$_2$Mn(CF$_3$SO$_3$)$_2$, (**10**), at the 50 % probability level. Hydrogen atoms were omitted for the sake of clarity.
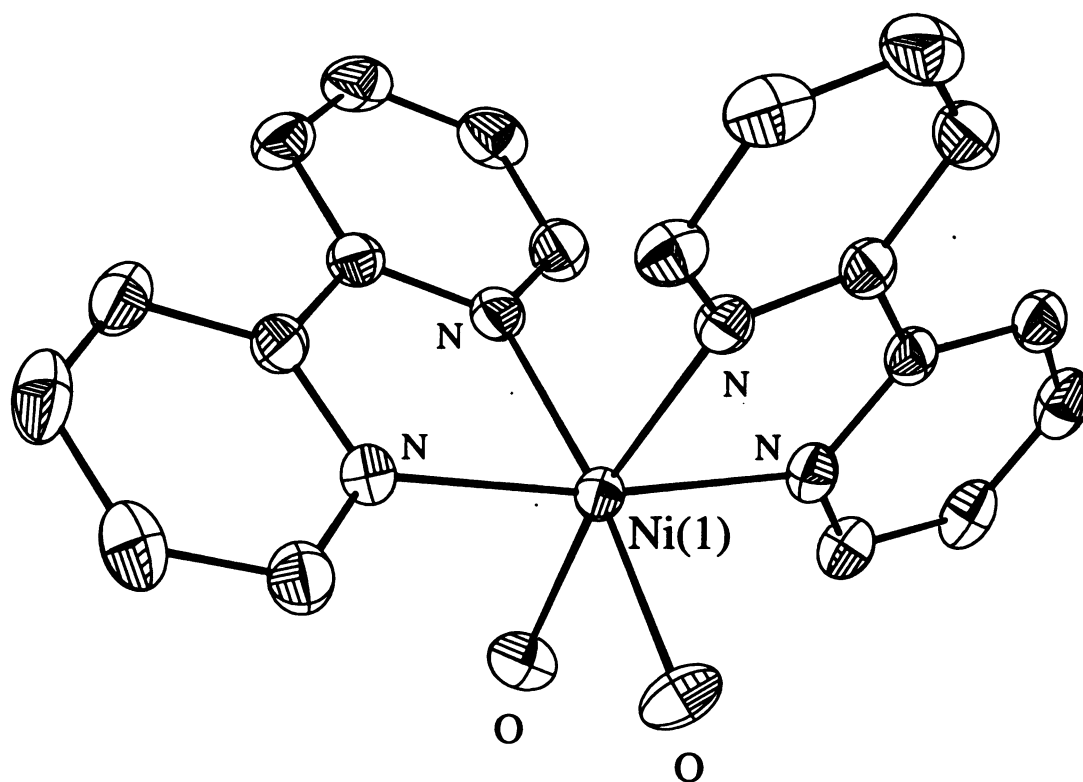
Figure 2.5. Thermal ellipsoid representation of the cation,
[Ni(2,2'-bpy)$_2$(OH$_2$)$_2$]$^{2+}$, in (13) at the 50% probability level.
Hydrogen atoms are omitted for the sake of clarity.
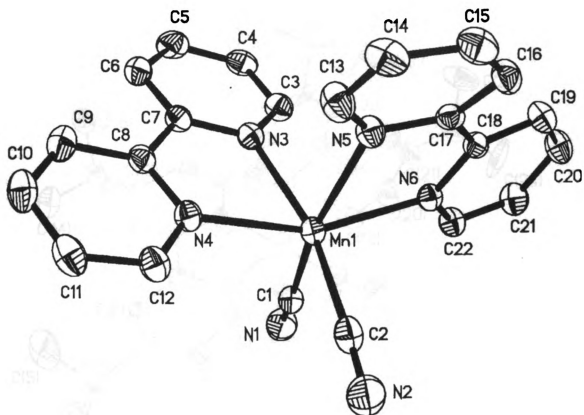
Figure 2.6. Thermal ellipsoid representation of (2,2'-bpy)$_2$Mn(CN)$_2$ (**16**) at the 50 % probability level. The hydrogen atoms were omitted for the sake of clarity.
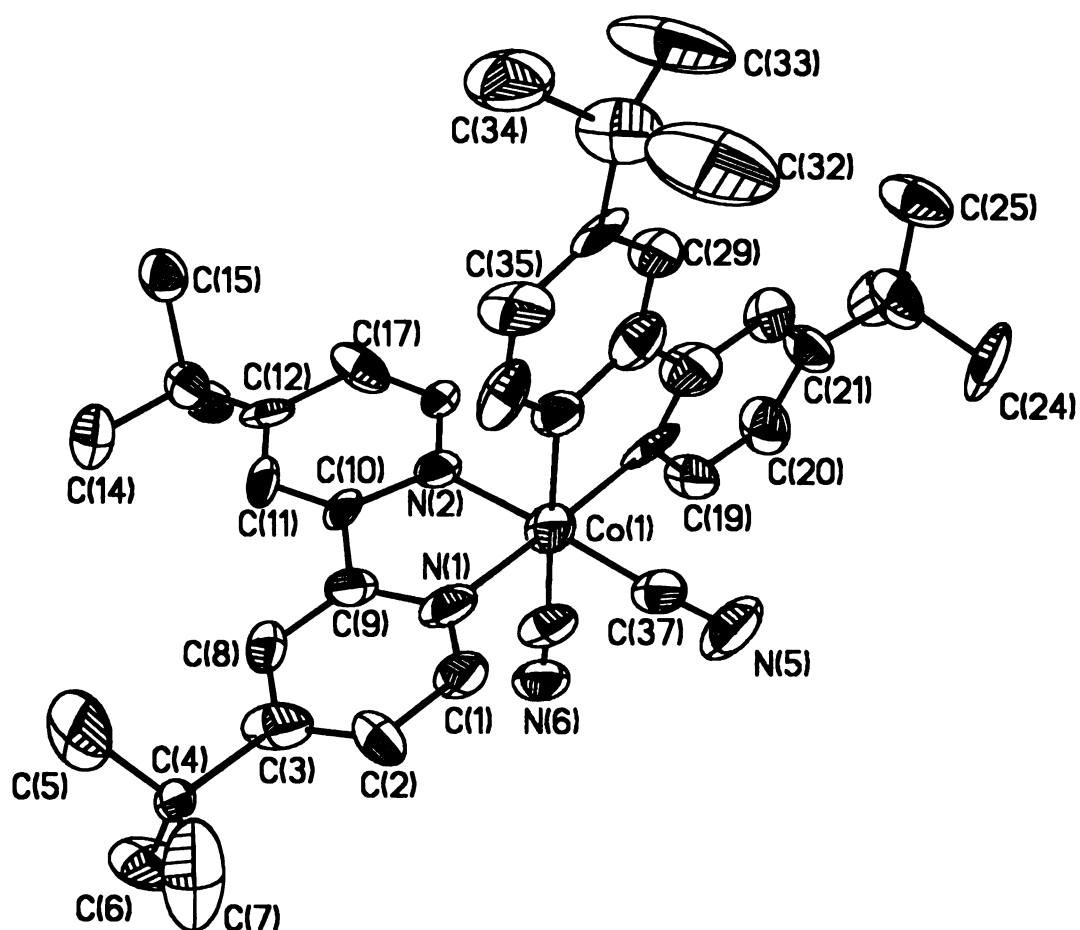
Figure 2.7. Thermal ellipsoid representation of the cation, [(4,4'-^{t}Bu-2,2'-bpy)$_2$Co(CN)$_2$]$^+$, in (21) at the 50 % probability level. The hydrogen atoms were omitted for the sake of clarity. (Image is presented in color)

ellipsoid plot is presented in Figure 2.7.

3. RESULTS AND DISCUSSION

A. Syntheses of $[(N-N)_2M(S)_2]^{2+}$ salts (N-N = 2,2'-bipyridine, 2,2'-bipyrimidine or 1,10-phenanthroline and S = H_2O, CH_3CN, CH_3OH or NO_3^-).

The preparation of compounds of the type $(2,2'-bypm)_2MCl_2$ in 1986 by Ruminiski and co-workers[14] paved the way for using such complexes as precursors for building larger clusters. The addition of two equivalents of a halide abstraction agent such as $AgBF_4$, $Ag(CF_3SO_3)$, $AgNO_3$ or $TlPF_6$ allows for two sites on the octahedral metal ion to be made available. (Figure 2.1.) These labile sites are occupied by either solvent molecules or weakly coordinating anions, which are readily displaced by stronger donors. We reasoned that if this chemistry works with the 2,2'-bpym ligand, then analogous chemistry should also be possible with 1,10-phenanthroline or 2,2'-bipyridine just as well. The coordination chemistry of these diimine ligands has been studied extensively, and it is known that steric interactions between the α-hydrogen atoms of opposite ligands for two 1,10-phenanthroline or 2,2'-bipyridine ligands disfavors a *trans* planar arrangement. Two 2,2'-bpy or phen ligands are, therefore, forced to adopt a *cis* configuration on an octahedral metal ion.[21]

(1) $[(2,2'\text{-bpym})_2M(OH_2)_2](BF_4)_2$ ($M = Mn^{II}$ (1), Fe^{II} (2), Co^{II} (3) and Ni^{II} (4).

The $[(2,2'\text{-bpym})_2M(OH_2)_2](BF_4)_2$ series of compounds were the first group of this type to be synthesized. Unfortunately, the products were obtained in poor yields and have not been able to be crystallized as suitably large single crystals for X-ray diffraction studies. These complexes are more difficult to synthesize due to the relatively high lability of the 2,2'-bpym groups in the presence of water molecules, which participate in hydrogen bonding at the uncoordinated N-N units. This increases the lability of the ligand and hence the rates of ligand redistribution, the ultimate result of which is the formation of the $[M(2,2'\text{-bpym})_3]^{2+}$ species. This problem is particularly prevalent in reactions with $FeCl_2$, which is difficult to dry and prone to oxidation.

The compounds were characterized by infrared spectroscopy, which is a good diagnostic tool for investigating the mode of the 2,2'-bpym ligand. The 2,2'-bpym molecule exhibits ring stretching $v(C=C)$, $v(C=N)$ modes at 1570, 1545 and 1400 cm^{-1}.[22] If the 1570 and 1545 cm^{-1} stretches appear as doublets then the 2,2'-bpym is bound in the mono-chelating mode. If the two stretches are quasi-symmetric, the 2,2'-bpym ligand is acting as a bis-chelator. In the case of uncoordinated 2,2'-bpym, an intense stretch (combination of $v(C=C)$,

$v(C=N)$) appears at 1420 cm^{-1}. Table 2.4 summarizes the IR data for the series [(2,2'-bpym)$_2$M(OH$_2$)$_2$](BF$_4$)$_2$. Electrospray mass spectrometry was conducted on [(2,2'-bpym)$_2$Ni(OH$_2$)$_2$](BF$_4$)$_2$ in a water/acetonitrile mixture. The parent ion peak in the spectrum appears at 187 m/z which corresponds to the [M(2,2'-bpym)$_2$]$^{2+}$ fragment. The bound water molecules are apparently easily lost under these conditions.

(2) [(N-N)$_2$M(CH$_3$CN)$_2$](BF$_4$)$_2$ (M = Mn^{II} (5), Co^{II} (6) and Ni^{II} (7 and 8) with N-N = 2,2'-bpy or phen).

These compounds were synthesized from their anhydrous chloride counterparts, viz., (N-N)$_2$MCl$_2$. The IR data reveal two acetonitrile stretches, which is consistent with the *cis* arrangement of CH$_3$CN ligands on a molecule with a C$_{2v}$ point group. The 2,2'-bpy or 1,10-phen stretches as well as the acetonitrile stretches are summarized in Table 2.5. In the presence of water, the CH$_3$CN ligands are displaced in favor of H$_2$O. The 2,2'-bpy stretches $v(C=C)$, $v(C=N)$ are typically in the range 1400-1600 cm^{-1} and a ring torsion (τ) occurs in the range 410-420 cm^{-1}.[23] The torsional ring motion appears at about 20 cm^{-1} higher than that of the free ligand.[23] There is an out-of-plane hydrogen bend δ(C-H) at ~ 725 cm^{-1}.

(3) [(2,2'-bpy)$_2$Ni(CH$_3$CN)$_2$](PF$_6$)$_2$ (9).

This complex was synthesized from (2,2'-bpy)$_2$NiCl$_2$ by removal of the

86

Table 2.4. IR data for compounds $[(2,2'\text{-bpym})_2M(OH_2)_2](BF_4)_2$ (M = Mn^{II} (**1**), Fe^{II} (**2**), Co^{II} (**3**) and Ni^{II} (**4**)).

$[(2,2'\text{-bpym})_2M(OH_2)_2](BF_4)_2$	2,2'-bpym ring ν (C=N) and ν(C=C) (cm^{-1})	ν(B-F) (cm^{-1})	Compound Color
Mn^{II}	1574 (s) 1408 (s)	1084 (s, br) 756 (s) 522 (m)	Yellow
Fe^{II}	1577 (s) 1556 (m) 1406 (s)	1084 (s, br) 754 (s) 523 (m)	Red
Co^{II}	1576 (s) 1558 (s) 1408 (s)	1084 (s, br) 760 (s) 523 (m)	Orange/Peach
Ni^{II}	1577 (s) 1560 (s) 1408 (s)	1084 (s, br) 758 (s) 523 (m)	Pale Pink

87

Table 2.5. IR data for compounds $[(N-N)_2M(CH_3CN)_2](BF_4)_2$ ($M = Mn^{II}$ (**5**), Co^{II} (**6**) and Ni^{II} (**7** and **8**) and $N-N = 2,2'$-bpy or 1,10-phenanthroline)

$[(N-N)_2M(CH_3CN)_2]^{2+}$	CH_3CN v (C≡N) (cm^{-1})	2,2'-bpym ring v (C=N), v(C=C) (cm^{-1})	v (B-F) (cm^{-1})	Compound Color
$[(2,2'\text{-bpy})_2Mn(CH_3CN)_2]^{2+}$	2312 (s) 2285 (s)	1599 (s) 1577 (s) 412 (s)	1064 (s, br) 769 (s) 521 (m)	Yellow
$[(2,2'\text{-bpy})_2Co(CH_3CN)_2]^{2+}$	2312 (s) 2280 (s)	1608 (s) 1601 (s) 1580 (m) 1570 (m) 421 (m)	1059 (s, br) 765 (s) 520 (m)	Orange
$[(2,2'\text{-bpy})_2Ni(CH_3CN)_2]^{2+}$		1603 (s) 1577 (s) 1568 (s) 418 (m)	1060 (s, br) 769 (s) 521 (m)	Purple/pink
$[(\text{phen})_2Ni(CH_3CN)_2]^{2+}$	2318 (s) 2289 (s)	1606 (m) 1587 (m)	1060 (s) 769 (w) 520 (w)	Purple/pink

88

chloride ligands with $TlPF_6$ in dry acetonitrile. Although the chloride complex does not appear to be soluble in acetonitrile, the green suspension is gradually replaced by a pink/purple solution upon addition of $TlPF_6$, with the deposition of white TlCl. IR data of the product reveals two acetonitrile stretches (2314 (s) and 2284 (s) cm^{-1}) as expected for the *cis* arrangement of a C_{2v} molecule. The 2,2'-bpy stretches $v(C=C)$, $v(C=N)$ appear at 1608 (m), 1602 (s), 1579 (s), 1571 (m) and ring torsion (τ) at 416 (m) cm^{-1}. The torsional ring motion appears about 20 cm^{-1} higher than that of the free ligand.[23] The $v(P-F)$ stretch appears as a strong and broad peak at 841 cm^{-1}.

(4) $(N-N)_2M(CF_3O_3S)_2$ ($M = Mn^{II}$ and Co^{II}; $N-N = 2,2'$-bpy or phen).

The triflate complexes were synthesized from $(N-N)_2MCl_2$ by removing the chlorides with $Ag(CF_3SO_3)$. The coordinated phen and 2,2'-bpy ligands exhibit stretches $v(C=C)$, $v(C=N)$ in the 1400-1600 cm^{-1} region. There is also a 2,2'-bpy ring torsion (τ) appearing at 420 cm^{-1}. The torsional ring motion appears about 20 cm^{-1} higher than that of the free ligand.[23] Unambiguous assignments of vibrational modes for $[CF_3SO_3]^-$ is not possible due to the mixing of CF_3 and SO_3 vibrational modes and accidental coincidences of these modes arising particularly in the stretching region. The triflate anion exhibits a characteristic symmetric stretch at $v_s(S-O)$ ~1024 cm^{-1} and an asymmetric stretch $v_{as}(S-O)$ at ~1287 cm^{-1}.[24] Potential energy calculations

indicate a high contribution of v(C-S) to a band in the IR at 320 cm^{-1}. The band at 770 cm^{-1} is due primarily to δ(C-F). The infrared data for these complexes are summarized in Table 2.6.

(5) [(2,2'-bpy)$_2$Ni(OH$_2$)$_2$](CF$_3$SO$_3$)$_2$ (13).

The reaction was performed in acetonitrile, but slow evaporation of the acetonitrile solution in moist laboratory air produced purple crystals of the water adduct. The purple crystals were verified by single crystal X-ray diffraction to be [(2,2'-bpy)$_2$Ni(OH$_2$)$_2$](CF$_3$SO$_3$)$_2$. This complex exhibits 2,2'-bpy stretches v(C=C), v(C=N) at 1610, 1603 and 1579 cm^{-1} along with 2,2'-bpy ring torsion (τ) at 420 cm^{-1} and a v_s(S-O) stretch at 1028 cm^{-1}. The torsional ring motion appears about 20 cm^{-1} higher than that of the free ligand.[23]

(6) (phen)$_2$M(NO$_3$)$_2$ (M = Mn^{II} (14) and Co^{II} (15)).

These complexes were synthesized from the (phen)$_2$MCl$_2$ species by removal of chlorides with silver nitrate. The 1,10-phen ligand stretches v(C=C), v(C=N) for each complex are in the range of 1400-1600 cm^{-1}. The broad nitrate stretches span the region of the spectrum around 1200 cm^{-1}.

(7) (2,2'-bpy)$_2$M(CN)$_2$ (M = Mn^{II} (16) and Co^{II} (17).

The cyanide complexes were prepared from a deoxygenated water-methanol solution according to a literature preparation of (phen)$_2$Mn(CN)$_2$. After slow

Table 2.6. IR data for [(N-N)$_2$M(CF$_3$SO$_3$)$_2$] (M = Mn^{II} (**10** and **12**), Co^{II} (**11**) and N-N = 2,2'- bpy or phen).

[(N-N)$_2$M(CF$_3$SO$_3$)$_2$]	N-N ring v (C=N), v(C=C) (cm^{-1})	v (S-O) stretch (cm^{-1})	Compound Color
[(2,2'-bpy)$_2$Mn(CF$_3$SO$_3$)$_2$]	1606 (s) 1599 (s) 1577 (m) 416 (m)	1024 (s)	Yellow
[(phen)$_2$Mn(CF$_3$SO$_3$)$_2$]	1581 (m) 1592 (m) 1522 (m) 1513 (m)	1024 (s)	Yellow
[(2,2'-bpy)$_2$Co(CF$_3$SO$_3$)$_2$]	1608 (s) 1601 (s) 1577 (m) 419 (m)	1022 (s)	Orange

addition of the cyanide solution at 80 °C, the reaction is slowly cooled by keeping the flask immersed in the silicone oil bath with a nitrogen purge. In this manner, yellow crystals of $(2,2'-bpy)_2Mn(CN)_2\cdot 3H_2O$ admixed with yellow precipitate can be obtained. Upon exposure of the product to air, an immediate color change to brown ensues, signifying that the product is decomposing. The corresponding Co reaction yields a tan/brownish precipitate. The reaction with Ni(II) led to ligand redistribution as evidenced by the isolation of pink crystals of the salt $[Ni(2,2'-bpy)_3][Ni(CN)_4]\cdot 2,2'-bpy$ which was characterized by X-ray crystallography. The iron (II) reaction produced red needle crystals from an intensely colored red solution, but they diffracted too poorly for a complete X-ray study to be performed. In addition, a small quantity of a blue precipitate was observed which is assumed to be Prussian blue due to loss of 2,2'-bpy from all the Fe centers and oxidation of some of the Fe^{II} to Fe^{III}.

A. Syntheses of Trivalent Precursors

The divalent metal precursors with cyanide such as complexes **16** and **17** of the type $(2,2'-bpy)_2M(CN)_2$ are neutral species which makes them fairly insoluble. One way to circumvent the neutrality is to prepare cis-dicyanide complexes of trivalent metals, which renders them monocations, of the type, $[(2,2'-bpy)_2M(CN)_2]^+$. Possible candidates for this chemistry are d^5 Fe(III)

92

and d^3 Cr(III) complexes, which possess one and three unpaired electrons respectively. In addition to the cationic charge, another option for improving the solubility of the neutral compounds is to synthesize complexes with substituted 2,2'-bpy or 1,10-phen ligands.

(1) [(4,4'-(CH$_3$)$_2$-2,2'-bpy)$_2$MCl$_2$]Cl (M = Cr^{III} (18) and Fe^{III} (19)).

The addition of two equivalents of 4,4'-(CH$_3$)$_2$-2,2'-bpy to (THF)$_3$CrCl$_3$ leads to a green solution and a green precipitate which were judged to be the same compound by infrared spectroscopy. Infrared data indicate the presence of characteristic 4,4'-(CH$_3$)$_2$-2,2'-bpy stretches v(C=C), v(C=N) at 1615, 1591 and 1551 cm^{-1}. The 4,4'-(CH$_3$)$_2$-2,2'-bpy ring torsion (τ) appears at 420 cm^{-1}.

In the case of the reaction of 4,4'-(CH$_3$)$_2$-2,2'-bpy with FeCl$_3$, a yellow solution and a yellow precipitate were obtained. Infrared spectral data indicated that the yellow solution and precipitate are the same complex. IR data reveals the presence of 4,4'-(CH$_3$)$_2$-2,2'-bpy activity in the form of v(C=C), v(C=N) stretches that appear at 1612 and 1554 cm^{-1} and a ring torsion (τ) mode at 420 cm^{-1}.

(2) [(4,4'-(CH$_3$)$_2$-2,2'-bpy)$_2$Fe(CN)$_2$](PF$_6$) (20).

This reaction was designed to replace Cl$^-$ with CN$^-$, thus AgCN was used as the Cl$^-$ abstraction reagent as well as the CN$^-$ delivery agent. Since AgCN is not very soluble in neat acetonitrile, a mixture of acetonitrile and methanol

was used. The reaction proceeded very slowly by visual inspection, and after

~30 minutes, one equivalent of thallium hexafluorophosphate was added.

Before the addition of the thallium complex the solution had turned light red.

Once the thallium was added, however, the solution became much more

deep red in color. The isolated red product was obtained in poor yield at

30%. The infrared data indicate that both cyanide (2064 cm^{-1}) and 4,4'-

$(CH_3)_2$-2,2'-bpy, with $v(C=C)$, $v(C=N)$ stretches at 1618 and 1556 cm^{-1}, are

present. The 4,4'-$(CH_3)_2$-2,2'-bpy ring torsion (τ) mode appears at 424 cm^{-1}.

There is also a strong, broad feature at 843 cm^{-1} due to $v(P-F)$ of the $[PF_6]^-$

anion. Although this reaction appears to be working, the yield is poor and is

obviously not a preferred route to the desired dicyanide precursor.

C. Reactivity Studies

The formation of molecular squares of the type $[(2,2'\text{-bpy})_8M_2M_2'(CN)_4]^{n+}$

requires that one equivalent of a solvated precursor be combined with one

equivalent of a cyanide precursor. This type of reaction is depicted in Figure

2.2.

(1)   Reaction between $(2,2'\text{-bpy})_2Co(CN)_2$ and

       $[(2,2'\text{-bpy})_2Co(CH_3CN)_2](BF_4)_2$.

The cobalt reagents were combined in acetonitrile, but the reaction was slow

due to the insolubility of the neutral species. Over the course of one day, a

brown precipitate was isolated and found to exhibit a single cyanide stretch at 2147 cm^{-1}. This observation is taken as an indication that either a molecular square has formed or that a polymer with only one type of cyanide ligand is produced. Unfortunately, the brown precipitate is insoluble in most common solvents, so no further characterization was possible.

(2) Reaction between (2,2'-bpy)$_2$Co(CN)$_2$ and [(phen)$_2$Ni(CH$_3$CN)$_2$](BF$_4$)$_2$

One equivalent of each of these complexes was combined in a small volume of acetonitrile. The color of the solution turned green, and a blue precipitate formed within 15 min. The blue precipitate, which is insoluble in most common solvents, exhibits a single cyanide stretch at 2166 cm^{-1}, which, as stated earlier, could be either a molecular square or a symmetrical polymer. The blue precipitate was sent to the University of California at Berkeley for electrospray mass spectrometry, but the results were inconclusive.

(3) Reaction between (2,2'-bpy)$_2$Co(CN)$_2$ and (phen)$_2$Mn(CF$_3$SO$_3$)$_2$.

A reaction of (2,2'-bpy)$_2$Co(CN)$_2$ and (phen)$_2$ Mn(CF$_3$SO$_3$)$_2$ in a 1:1 ratio was performed in acetonitrile. The solution turned gold, and within hours a yellow-tan precipitate was present. The infrared data revealed a single, strong, and very sharp, cyanide stretch at 2158 cm^{-1}. The triflate anion was also evident from the v_s(S-O) mode located at 1030 cm^{-1}. The golden colored solution was layered with hexanes and diethyl ether but it did not yield

crystals. The yellow-tan precipitate was also sent to the University of California at Berkeley for electrospray mass spectrometry, but the results were inconclusive.

(4) Reaction between (4,4'-^{t}Bu-2,2'-bpy)$_2$Co(CN)$_2$ and

[(2,2'-bpy)$_2$Ni(CH$_3$CN)$_2$](PF$_6$)$_2$.

The reaction was carried out in a 1:1 ratio of the parent compounds in acetonitrile in air. No spontaneous formation of precipitate was observed, but after slow evaporation of the acetonitrile solution, pale orange/yellow crystals were obtained. The crystals indicated that the cobalt complex had been oxidized from Co^{II} to Co^{III} to yield [(4,4'-^{t}Bu-2,2'-bpy)$_2$Co(CN)$_2$](PF$_6$) (21). Obviously, since (4,4'-^{t}Bu-2,2'-bpy)$_2$Co(CN)$_2$ was prepared in air, and with a methanol/water solution, this is sufficient to cause oxidation of the metal center.

D. Molecular Structures.

(1)   [(2,2'-bpy)$_2$Ni(CH$_3$CN)$_2$](BF$_4$)$_2$ (7).

The [(2,2'-bpy)$_2$Ni(CH$_3$CN)$_2$]$^{2+}$ cation possesses two 2,2'-bpy ligands acting as typical bidentate ligands bound to Ni(1) through the nitrogen atoms. Two acetonitrile molecules complete the octahedral environment around Ni(1). The Ni(1)–N(2,2'-bpy) bond lengths are in the range of 2.075(3)–2.082(3)Å, and the Ni(1)-N(CH$_3$CN) bond lengths are 2.091(4) and 2.094(4)Å. The Ni-

96

N(CH₃CN) distances are longer than the corresponding distances to the 2,2'-bipyridine, indicating that they are, as expected, poorer ligands than the 2,2'-bpy N atoms. The angles subtended by the five-membered rings created by the bidentate 2,2'-bipyridine ligands are 78.99(12)° and 79.10(12)°. The angle between the coordinated acetonitriles is 84.15(14)°. The C-N bonds lengths in the acetonitrile ligands are 1.142(5)Å and 1.141(5)Å. Selected bond distances and angles are given in Table 2.7.

(2) (2,2'-bpy)₂Mn(CF₃SO₃)₂ (10).

The compound possesses two 2,2'-bpy ligands and two triflate anions bound to the Mn atom through their respective oxygen atoms. The Mn(1)-N(2,2'-bpy) bond lengths are 2.2355(16) and 2.2330(15)Å while the Mn-O(CF₃SO₃) bond distance is 2.1957(14)Å. The bite angle of the 2,2'-bpy chelate is 73.52(6)°. The angle between the two coordinated water molecules is 86.61(8)°. Selected bond distances and angles are given in Table 2.8.

(3) [(2,2'-bpy)₂Ni(OH₂)₂](CF₃SO₃)₂ (13).

The structure consists of a Ni atom in an environment with four nitrogen atoms from the two 2,2'-bipyridine ligands and two oxygen atoms from the water molecules. The Ni(1)-N(2,2'-bpy) bond distances are in the range of 2.064(2)Å and 2.086(2)Å and the Ni(1)-O distances are 2.059(2)Å and 2.061(2)Å. The angle between the two water molecules is 84.55(9)°. The

bite angles for the 2,2'-bpy chelates are 78.89(9)° and 79.29(9)°. There is a slight distortion in **13** with the Ni(1)-N(10) bond being longer at 2.086(2)Å and the Ni(1)-N(9) being shorter at 2.064(2)Å. By comparison, the structure of the related compound, [Ni(C$_6$H$_2$O$_4$)(dmbpy)$_2$]•H$_2$O,[25] with one *o*-benzoquinone ligand exhibits Ni-N(dmbpy) bond lengths in the range of 2.035(7)–2.072(8) Å, which are slightly shorter than those for **13**. The bite angle is 79.1(3)°. The Ni-O bond lengths are in the range of 2.044(7)–2.055(7) Å, which are slightly shorter than for complex **13** indicating that the *o*-benzoquinone is a better donor than a water molecule. The angle between the two oxygen atoms is 79.4(3)°, which is less than the angle between the water molecules of complex **13**; this is likely due to the rigidity of the chelate ligand. Selected bond distances and angles for compound **13** are provided in Table 2.9.

Another example similar to complex **13** is a dimeric species,[26] [Ni$_2$(H$_2$O)$_8$(µ-2,2'-bpym)]$^{4+}$, in which the nickel atoms are bridged by the bis-chelate, 2,2'-bipyrimidine. The Ni-N(2,2'-bpym) bond distances are 2.092(3) and 2.097(3) Å which are much longer than complex **13**. The longer distance is attributed to the fact the 2,2'-bpym ligand is acting as a bis-chelate and the monochelate 2,2'-bpy is a stonger ligand than is 2,2'-bpym. The bite angle for the 2,2'-bpym ligand is 79.2(1)°, which is similar to what was found for

2,2'-bpy complexes. The remaining four sites on each Ni atom are composed of water molecules. The Ni-O(water) bond distances are in the range of 2.044(3) – 2.063(3) Å, which are similar to those found in complex **13**. The angle between the water molecules is 92.3°, which is greater than the O-Ni-O angle for complex **13**.

(4) (2,2'-bpy)₂Mn(CN)₂ (16)•3H₂O.

The structure consists of a pseudo-octahedral Mn^{II} atom coordinated to the N atoms of two *cis*-2,2'-bpy ligands and two carbon atoms from the cyanide ligand. The Mn-N(2,2'-bpy) bond lengths are in the range 2.2844(16) – 2.3503(17) Å, whereas the Mn-C distances are 2.239(2) and 2.248(2) Å. The C≡N bond lengths for the two cyanide ligand are 1.150(3) and 1.144(3) Å and the angle between the cyanide ligands is 96.92(8)°. The bite angles for the 2,2'-bpy bidentate ligands are 71.19(6) and 71.26(6)°. Selected bond distances and angles are presented in Table 2.10. Metrical parameters for the similar compound (2,2'-bpy)₂MnCl₂•2H₂O•CH₃CH₂OH[27] are Mn-N(2,2'-bpy) at 2.275(3) and 2.287(3) Å which are slightly shorter than in **16**. The bite angle for the 2,2'-bpy ligand is similar to the one found in **16** at 71.93(10)°. The Mn-Cl bond distances are 2.4834(11) Å. The angle between the chloride atoms is slightly larger than what is expected for a perfectly octahedral environment at 92.72(5)° due to the larger radii of the chloride atom.

99

(4)   [(4,4'-(CH₃)₂-2,2'-bpy)₂Co(CN)₂](PF₆) (21)

The structure consists of a pseudo-octahedral Co^{III} atom coordinated to the N

atoms of two *cis*-4,4'-(CH₃)₂-2,2'-bpy ligands and two carbon atoms from the

cyanide ligands. The asymmetric unit is composed of two [(4,4'-(CH₃)₂-2,2'-

bpy)₂Co(CN)₂]⁺ molecules, one of each isomer (Δ and Λ). The Co-N(4,4'-

(CH₃)₂-2,2'-bpy) bond lengths are in the range 1.875(15)-1.985(13) Å,

whereas the Co-C distances are in the range 1.80(2)-1.882(18) Å. The C≡N

bond lengths are in the range 1.164(18)-1.20(2) Å and the angle between the

cyanide ligands are 89.0(8)° and 91.9(8)°. The bite angles for 4,4'-(CH₃)₂-

2,2'-bpy bidentate ligands are 83.8(7)°, 83.6(5)°, 80.9(6)°, 84.1(7)°. Selected

bond distances and angles are presented in Table 2.11-2.12.

E. Magnetic Properties

Magnetic susceptibility studies were conducted to establish the ground state

spin values for the new paramagnetic molecular building blocks. The

magnetic moments at room temperature for the compounds are summarized

in Table 2.13. The magnetic susceptibility for the Mn^{II} center in [(2,2'-

bpym)₂Mn(OH₂)₂](BF₄)₂ (1) leads to μ_{eff} and g values that are in good

agreement with the predicted spin-only values of 5.9 B.M. g ~ 1.9 (S = 5/2).

The complex, [(2,2'-bpym)₂Co(OH₂)₂](BF₄)₂ (3), exhibits values of μ_{eff} = 4.4

and g ~ 2.0. An octahedral, high-spin d^7 Co^{II} complex with S = 3/2 has a

Table 2.7. Selected bond distances [Å] and angles [°] for [Ni(2,2'-bpy)$_2$(CH$_3$CN)$_2$](BF$_4$)$_2$ (7).

Bond Distances

A	B	A-B [Å]
Ni(1)	N(1)	2.077(3)
Ni(1)	N(3)	2.079(3)
Ni(1)	N(6)	2.091(4
N(6)	C(23)	1.142(5)
C(23)	C(24)	1.453(5)

Bond Angles

A	B	C	A-B-C [°]
N(4)	Ni(1)	N(3)	78.99(12)
N(2)	Ni(1)	N(5)	171.98(12)
N(3)	Ni(1)	N(5)	94.45(12)
N(1)	Ni(1)	N(5)	93.17(13)
N(6)	Ni(1)	N(5)	84.15(14)
C(21)	N(5)	Ni(1)	167.1(3)
N(5)	C(21)	C(22)	178.7(5)

Table 2.8. Selected bond distances [Å] and angles [°] for (2,2'-bpy)$_2$Mn(CF$_3$SO$_3$)$_2$ (10).

Bond Distances

A	B	A-B [Å]
Mn(1)	N(1)	2.2355(16)
Mn(1)	N(2)	2.2330(15)
Mn(1)	O(1)	2.1957(14)
S(1)	O(1)	1.4616(14)
S(1)	O(2)	1.4330(16)

Bond Angles

A	B	C	A-B-C [°]
N(1)	Mn(1)	N(2)	73.52(6)
O(1)	Mn(1)	N(1)	90.74(6)
O(1)	Mn(1)	N(2)	97.64(5)
O(1A)	Mn(1)	O(1)	86.61(8)
Mn(1)	O(1)	S(1)	137.10(9)

Table 2.9. Selected bond distances [Å] and angles [°] for [(2,2'-bpy)₂Ni(OH₂)₂](CF₃SO₃)₂ (13).

Bond Distances

A	B	A-B [Å]
Ni(1)	N(9)	2.064(2)
Ni(1)	N(10)	2.086(2)
Ni(1)	O(5)	2.059(2)
N(6)	O(7)	2.061(2)

Bond Angles

A	B	C	A-B-C [°]
N(4)	Ni(1)	N(9)	79.29(9)
N(8)	Ni(1)	N(10)	78.89(9)
O(5)	Ni(1)	O(7)	84.55(9)
N(4)	Ni(1)	N(8)	94.96(9)
O(5)	Ni(1)	N(10)	93.90(9)
O(7)	Ni(1)	N(4)	91.01(9)

Table 2.10. Selected bond distances [Å] and angles [°] for [(2,2'-bpy)$_2$Mn(CN)$_2$] (16).

Bond Distances

A	B	A-B [Å]
Mn(1)	N(5)	2.3503(17)
Mn(1)	N(6)	2.2844(16)
Mn(1)	C(1)	2.248(2)
Mn(1)	C(2)	2.239(2)
C(1)	N(1)	1.150(3)

Bond Angles

A	B	C	A-B-C [°]
N(3)	Mn(1)	N(4)	71.26(6)
N(5)	Mn(1)	N(6)	71.19(6)
N(3)	Mn(1)	C(1)	86.03(7)
N(3)	Mn(1)	N(6)	94.89(6)
C(1)	Mn(1)	C(2)	96.92(8)
Mn(1)	C(1)	N(1)	172.5(2)
Mn(1)	C(2)	N(2)	175.2(2)

Table 2.11. Selected bond distances [Å] for [(4,4'-^{t}Bu-2,2'-bpy)$_2$Co(CN)$_2$]
(PF$_6$) (21).

A	B	A-B [Å]
Co(1)	N(1)	1.930(15)
Co(1)	N(2)	1.919(16)
Co(1)	N(3)	1.982(15)
Co(1)	N(4)	1.946(13)
Co(1)	C(37)	1.86(2)
Co(1)	C(38)	1.865(19)
Co(2)	N(7)	1.921(15)
Co(2)	N(8)	1.875(15)
Co(2)	N(9)	1.928(13)
Co(2)	N(10)	1.985(13)
Co(2)	C(75)	1.882(18)
Co(2)	C(76)	1.80(2)
C(37)	N(5)	1.20(2)
C(38)	N(6)	1.197(19)
C(75)	N(11)	1.164(18)

Table 2.12. Selected bond angles [°] for [(4,4'-^{t}Bu-2,2'-bpy)$_2$Co(CN)$_2$](PF$_6$) (21).

A	B	C	A-B-C [°]
N(1)	Co(1)	N(2)	84.1(7)
N(3)	Co(1)	N(4)	80.9(6)
N(7)	Co(2)	N(8)	83.8(7)
N(9)	Co(2)	N(10)	83.6(5)
C(37)	Co(1)	C(38)	91.9(8)
C(75)	Co(2)	C(76)	89.0(8)
Co(1)	C(37)	N(5)	175.1(18)
Co(1)	C(38)	N(6)	174.6(18)
Co(2)	C(75)	N(11)	174.3(17)
Co(2)	C(76)	N(12)	178.0(17)

Table 2.13. Summary of magnetic data at room temperature for molecular square precursors.

Complex		μ_{eff} (B. M.)	g value
[(2,2'-bpym)$_2$Mn(OH$_2$)$_2$](BF$_4$)$_2$	(1)	5.9	1.9
[(2,2'-bpym)$_2$Co(OH$_2$)$_2$](BF$_4$)$_2$	(3)	4.4	2.0
[(2,2'-bpym)$_2$Ni(OH$_2$)$_2$](BF$_4$)$_2$	(4)	2.7	2.0
[(2,2'-bpy)$_2$Mn(CH$_3$CN)$_2$](BF$_4$)$_2$	(5)	5.9	1.9
[(2,2'-bpy)$_2$Co(CH$_3$CN)$_2$](BF$_4$)$_2$	(6)	4.0	2.0
[(2,2'-bpy)$_2$Ni(CH$_3$CN)$_2$](BF$_4$)$_2$	(7)	3.25	2.0
[(2,2'-bpy)$_2$Mn(CF$_3$SO$_3$)$_2$]	(10)	5.9	1.9
[(phen)$_2$Mn(CF$_3$SO$_3$)$_2$]	(12)	6.0	1.9
[(2,2'-bpy)$_2$Ni(OH$_2$)$_2$](CF$_3$SO$_3$)$_2$	(13)	3.0	2.0
(2,2'-bpy)$_2$Co(CN)$_2$	(17)	2.54	2.91

spin-only moment of μ_{eff} = 3.87 B.M. for g = 2.[28] The observed μ_{eff} value

deviates from the predicted spin-only value due to spin-orbit coupling that is

typical of high-spin Co^{II}.[28] The experimentally observed values are

consistent with literature reports of other octahedral Co^{II} compounds. The

complex, $[(2,2'-bpym)_2Ni(OH_2)_2](BF_4)_2$ (4), exhibits a moment of μ_{eff} = 2.7

B.M. with g ~2.0. The experimentally observed μ_{eff} and g values deviate

only slightly from the predicted spin-only value of 2.83 B.M. and g = 2.

The magnetic susceptibility data for $[(2,2'-bpy)_2Mn(CH_3CN)_2](BF_4)_2$ (5)

gave μ_{eff} and g values of 5.9 B.M. g ~ 1.9. The compound $[(2,2'-bpy)_2Co(CH_3CN)_2](BF_4)_2$ (6), exhibits μ_{eff} = 4.0 and g ~ 2.0. The complex

$[(2,2'-bpy)_2Ni(CH_3CN)_2](BF_4)_2$ (7), exhibits a moment of μ_{eff} = 3.25 B.M.

with g ~2.0. These values deviate slightly from the predicted spin-only value

of 2.83 B.M. and g = 2, but are consistent with literature reports of other

octahedral Ni^{II} compounds.[28] The magnetic susceptibility data for the high-

spin S = 5/2 Mn^{II} center in $(2,2'-bpy)_2Mn(CF_3SO_3)_2$ (10) and

$(phen)_2Mn(CF_3SO_3)_2$ (12) gave μ_{eff} and g values that are in good agreement

with the predicted spin-only values of 5.9 B.M. and 6.0 B.M. with g ~1.9

respectively. The moment for $[(2,2'-bpy)_2Ni(OH_2)_2](CF_3SO_3)_2$ (13), is 3.0

B.M. with g ~2.0. The experimentally observed μ_{eff} and g values deviate

from the predicted spin- only value of 2.83 B.M. and g = 2. The

experimental moment of the low-spin d^7 Co^{II} complex, $[(2,2'-bpy)_2Co(CN)_2]$ (17), with $S = 1/2$ is $\mu_{eff} = 2.54$ with a $g = 2.91$. The observed μ_{eff} value deviates from the predicted spin-only values due to spin-orbit coupling.

4. SUMMARY AND CONCLUSIONS

The compounds $(2,2'-bpy)_2MCl_2$ undergo chloride abstraction to yield the $cis-[(2,2'-bpy)_2M(S)_2]^{2+}$, solvated precursors. These precursors are obtained in good yield whereas the $cis-[(2,2'-bpym)_2M(OH_2)_2](BF_4)_2$ complexes are prepared in a much lower yield. Attempts to synthesize an iron(II) precursor with either 2,2'-bpym or 2,2'-bpy yielded only a mixture of Fe^{II} and Fe^{III}. The dicyanide species, $(2,2'-bpy)_2M(CN)_2$ ($M = Mn^{II}$ and Co^{II}), prepared by the water/methanol are crystalline. The trivalent chloride precursors were synthesized in good yield, but further synthetic work needs to be carried out to prepare the trivalent cyanide precursors. Silver cyanide is not a good choice for introducing cyanide into a reaction since its solubility is low. The successful synthesis of several divalent and trivalent precursors provides an opportunity to explore different charges for the resulting molecular squares. The molecular squares will be cationic, but the charge can be reduced if trivalent cyanide precursors are successfully synthesized. The self-assembly reactions of the two types of precursors were investigated. Based on infrared spectroscopic data, the most promising of these reactions is the 1:1 reaction

of [(2,2'-bpy)$_2$Co(CN)$_2$] (**17**) and [(2,2'-bpy)$_2$Mn(CF$_3$SO$_3$)$_2$] (**10**) which led

to a product with a single strong cyanide stretch in the infrared spectrum.

5. REFERENCES

1. Dunbar, K. R.; Heintz, R. A. *Prog. Inorg. Chem.* **1997**, *45*, 283.

2. Holtzaman, H. *Ind. Eng. Chem.* **1945**, *37*, 855.

3. (a) Ito, A.; Suenaga, M.; Ono, K. *J. Chem. Phys.* **1968**, *48(8)*, 3597. (b) Chappert, J.; Sawicka, B.; Sawicki, J. *Phys. Stat. Sol.* **1975**, *B72*, K139.

4. (a) Hatlevik, Ø; Buschmann, W. E.; Zhang, J.; Manson, J. L.; Miller, J. S. *Adv. Mater.* **1999**, *11*, 914. (b) Ferlay, S; Mallah, T.; Ouahés, R; Veillet, P; Verdaguer, **1995**, *378*, 701. (c) Holmes, S. M.; Girolami, G. S. *J. Am. Chem. Soc.* **1999**, *121*, 5593.

5. (a) Ohba, M.; Maruono, N.; Okawa, H; Enoki, T.; Latour, J. M. *J. Am. Chem. Soc.* **1994**, *116*, 11566. (b) Ohba, M.; Okawa, H.; Ito, T.; Ohto, A. *J. Chem. Soc., Chem. Commun.* **1995**, 1545. (c) Ohba, M.; Fukita, N.; Okawa, H. *J. Am. Chem. Soc.* **1997**, *119*, 1011. (d) Fukita, N.; Ohba, H.; Okawa, H.; Matsuda, K.; Iwamura, H. *Inorg. Chem.* **1998**, *37*, 842.

6. Kalb, W. C.; Demidowicz, Z.; Speckman, D. M.; Knobler, C.; Teller, R. G.; Hawthorne, M. F. *Inorg.Chem.* **1982**, *21*, 4027.

7. Martinez, J.; Adams, H.; Bailey, N. A.; Maitlis, P. M. *J. Organomet. Chem.* **1991**, *405*, 393.

8. (a) Fujita, M.; Yazaki, J.; Ogura, K. *J. Am. Chem. Soc.* **1990**, *112*, 5645. (b) Fujita, M.; Ibukura. F.; Hagihara, H.; Ogura, K. *Nature* **1994**, *367*, 720.

111

(c) Stang, P. J.; Cao, D. H. *J. Am. Chem. Soc.* **1994**, *116*, 4981. (d) Olenyuk, B.; Whiteford, J. A.; Stang, P. J. *J. Am. Chem. Soc.* **1996**, *118*, 8221. (e) Blake, A. J.; Hill, S. J.; Hubberstey, P.; Li, W.-S. *J. Chem. Soc. Dalton Trans.* **1997**, 913. (f) Baxter, P. N. W.; Lehn, J.-M.; Kneisel, B. O.; Fenske, D. *Chem. Commun.* **1997**, 2231. (g) Stang, P. J.; Olenyuk, B. *Acc. Chem. Res.* **1997**, *30*, 502. (h) Olenyuk, B.; Fechtenktter, A.; Stang, P. J. *J. Chem. Soc., Dalton Trans.* **1998**, 1707. (i) Constable, E. C.; Schofield, E. *Chem. Commun.* **1998**, 403. (j) Fujita, M.; Aoyagi, M.; Ibukura, F.; Pgura, K.; Yamaguchi, K. *J. Am. Chem. Soc.* **1998**, *120*, 611. (k) Boyle, P. D.; Cross, W. I.; Godfrey, S. M.; McAuliffe, C. A.; Pritchard, R. G.; Sarwar, S.; Sheffield, J. M. *Angew. Chem. Int. Ed.* **2000**, *39*, 1796. (l) Rajendran, T.; Manimaran, B.; Lee, F.-Y.; Lee, G.-H.; Peng, S.-M.; Wang. C. M.; Lu, K.-L. *Inorg. Chem.* **2000**, *39*, 2016. (m) Sugiura, K.-I.; Fujimoto, Y.; Sakata, Y. *Chem. Commun.* **2000**, 1105. (n) Schnebeck, R.-D.; Freisinger, E.; Lippert, B. *Eur. J. Inorg. Chem.* **2000**, 1193.

9. Oshio, H.; Tamada, O.; Onodera, H.; Ito, T.; Ikoma, T.; Tero-Kubota, S. *Inorg. Chem.* **1999**, *38*, 5686.

10. Edited by Brauer, G. *Handbook of Preparative Inorganic Chemistry* **1965**, *2*, second edition, Academic Press New York: London.

11. Fort, Y.; Becker, S.; Caubere; P. *Tetrahedron* **1994**, *50*, 11893.

12. Badger, G. M.; Sasse, W. H. F. *J.* **1956**, 616.

13. Kern, R. J. *J. Inorg. Nucl. Chem.* **1962**, *24*, 1105.

14. Hiskey, M. A.; Ruminski, R. R. *Inorg. Chim. Acta* **1986**, *112*, 189.

15. Harris, C. M.; McKenzie, E. D. *J. Inorg. Nucl. Chem.* **1967**, *29*, 1047.

16. Morcom, R. E.; Bell, C. F. *J. Inorg. Nucl. Chem.* **1973**, *35*, 1865.

17. Saint 1000 and 6.0, Bruker Analytical X-ray Instruments, Madison, WI 53719 (**1999** and **2000**)

18. Sheldrick, G. M. "SADABS, Siemens Area Detector Absorption Correction", Univ. of Göttingen, Göttingen, Germany (**1998**).

19. Altomare, A.; Burla, M. C.; Camalli, M.; Cascarano, G. L.; Giacovazza, C.; Guagliardi, A.; Moliterni, A. G. G.; Polidori, G.; Spagna, R. *J. Appl. Crystallogr.* **1999**, *32*, 115.

20. Sheldrick, G. M. SHELXTL version 5.10, Reference Manuel, Bruker Industrial Automation, Analytical Instrument, Madison, WI 53719 (**1999**). Program for Refinement of Crystal Structure, University of Göttingen, Göttingen, Germany.

21. McKenzie, E. D. *Coord. Chem. Rev.* **1971**, *6*, 187.

22. (a) Julve, M.; Verdaguer, M.; De Munno, G.; Real, J. A.; Bruno, G. *Inorg. Chem.* **1993**, *32*, 795. (b) Andrés, E.; De Munno, G.; Julve, M.; Real, J. A.; Lloret, F. *J. Chem. Soc. Dalton Trans.* **1993**, 2169. (c) De Munno, G.;

Julve, M.; Lloret, F.; Faus, J.; Caneschi, A. *J. Chem. Soc. Dalton Trans.* **1994**, 1175. (d) De Munno, G.; Poerio, T.; Viau, G.; Julve, M.; Lloret, F.; Journaux, Y.; Rivière, E. *Chem. Commun.* **1996**, 2587. (e) De Munno, G.; Armentano, D.; Julve, M.; lloret, F.; Lescouëzec, R.; Faus, J. *Inorg. Chem.* **1999**, *38*, 2234.

23. Strukl, J. S.; Walter, J. L. *Spectrochim. Acta* **1971**, *27A*, 223.

24. (a) Lawrance, G. A. *Chem. Rev.* **1986**, *86*, 17. (b) Boumizane, K.; Herzog-Cance, M. H.; Jones, D. J.; Pascal, J. L.; Potier, J.; Roziere, J. *Polyhedron* **1991**, *10*, 2757.

25. Decurtins, S.; Schmalle, H. W.; Schneuwly, P.; Zheng, L.-M. *Acta Cryst.* **1996**, *C52*, 561.

26. De Munno; G.; Julve, M.; Lloret, F.; Derory, A. *J. Chem. Soc. Dalton Trans.* **1993**, 1179.

27. McCann, S.; McCann, M.; Casey, M. T.; Jackman, M.; Devereux, M.; McKee, V. *Inorg. Chim. Acta* **1998**, *279*, 24.

28. (a) Carlin, R. L. Magnetochemistry, Springer-Verlag Berlin Heidelberg **1986**. (b) Mabbs, F. E.; Machin, D. J. Magnetism and Transition Metal Complexes, London Chapman and Hall **1973**.

Chapter III

Molecular Cube Precursors and Reactivity Studies

1. INTRODUCTION

The well-known material Prussian Blue, $Fe_4{}^{III}[Fe^{II}(CN)_6]\cdot xH_2O$ is readily prepared by addition of $[Fe^{II}(CN)_6]^{4-}$ to $[Fe^{III}(H_2O)_6]^{3+}$ in water. The three-dimensional structure adopted by this compound is based on a simple face-centered cubic arrangement of alternating metal atoms M and M' connected by cyanide.[1] One possible way to limit the growth of the 3-D phase is to use trigonal capping ligands to protect one side of the metal ion. In this way, the building blocks fac-$[L_3M(CN)_3]^{n-}$ and fac-$[L_3M(S)_3]^{n+}$ can be used to build cubes as depicted in Figure 3.1. A discrete molecular cube with cyanide edges was synthesized by Rauchfuss and co-workers[2], who prepared the tricyanide precursor, $[Et_4N]_3[CpRh(CN)_3]$, and reacted it with $(\eta^6$-$C_6H_3Me_3)Mo(CO)_3$ in the presence of alkali metal cations to form $[Et_4N]_3\{M[Cp*Rh(CN)_3]_4[Mo(CO)_3]_4\}$ (M = K or Cs) (Figure 1.8.). The cube contains twelve external CO and four C_5Me_5 ligands. In addition, the same group has synthesized other tricyanide precursors[3] which, when combined with non-cyanide complexes, lead to molecular geometries other than a cube. Another group working in this area, namely that of Long and co-workers, has reported the crystal structures of two molecular cubes [4] based on the tricyanide precursor, $[(tacn)Co(CN)_3]$ tacn = 1,4,7-triazacyclononane. These are $[Cr_4Co_4(CN)_{12}(tacn)_8]^{12+}$ and

$[Co_8(CN)_{12}(tacn)_8]^{12+}$. The homometallic cobalt(III) cube was characterized by single crystal X-ray crystallography whereas the mixed metal analogue was characterized by positive ion electrospray mass spectrometry.

It should be obvious from the previous discussion, that in order to design a convergent synthesis of molecular cubes from octahedral metal ions, one must cap three coordination sites with one facial tridentate ligand that leaves three mutually orthogonal sites free for substitution chemistry as indicated in Figure 3.1. Possible choices for tridentate, facially capping ligands are *tris*-pyrazolylborate (Tp), diethylenetriamine (dien), 1,4,7-triazacyclononane (tacn) and 1,4,7-trithiacyclononane (9S3). The second building block must also be a precursor that is tailored to have three sites blocked by an innocent capping ligand but, in this case, the other three sites are occupied by three cyanide ligands at 90° from one another. One can envisage that the reaction between fac-$[(L_3)M(S)_3]^{n+}$ and fac-$[(L_3)M'(CN)_3]$ can either yield a molecular cube, a part of a cube, or any number of open polymeric species depending on the kinetics and thermodynamics of the reaction. In this chapter, the preparation and characterization of the two different types of precursors are presented and discussed. The main point of this thesis, in
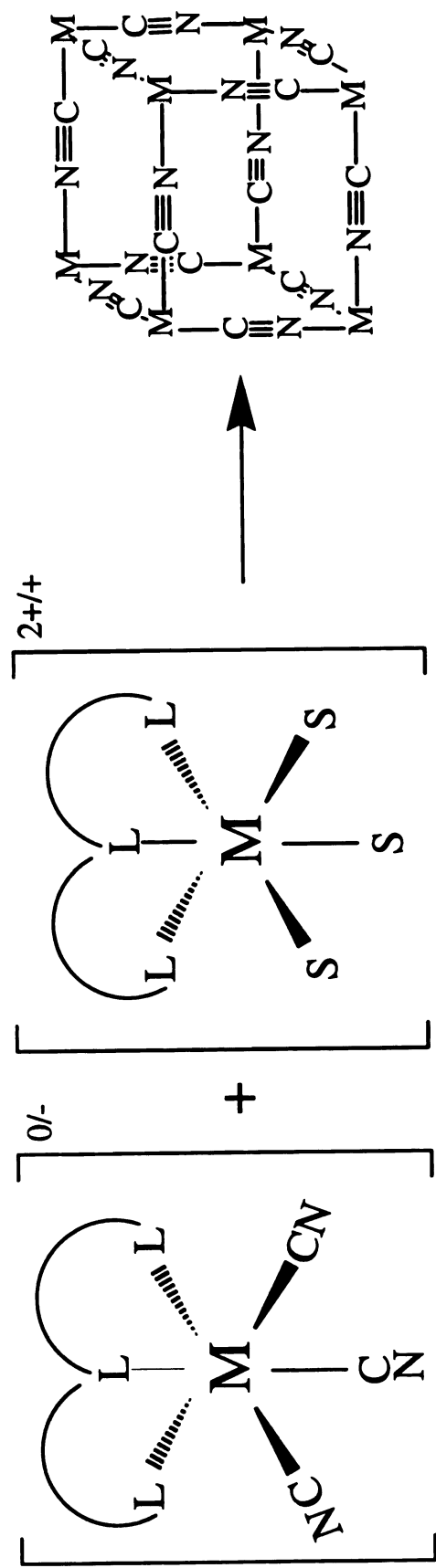
Figure 3.1. Schematic representation of the molecular cube assembly process.

contrast to the work of Rauchfuss where diamagnetic metal ions are used, is to use two different paramagnetic metal ions M and M' to build mixed metal $[M_4M'_4(CN)_{12}(L_3)_8]^{n+/n-}$ clusters with high spin ground states.

2. EXPERIMENTAL

A. PHYSICAL MEASUREMENTS

Infrared spectra were recorded on a Nicolet 42 spectrophotometer in the Chemistry Department at Michigan State University or on a Nicolet 470 instrument in the Chemistry Department at Texas A&M University. Infrared spectra were recorded at 4 cm^{-1} resolution and 32 scans unless otherwise stated. Solid samples were measured as KBr pellets or Nujol mulls on KBr or CsI plates. Elemental analyses were performed at Desert Analytics, Tucson, AZ or in the Chemistry Department at Michigan State University on a Perkin and Elmer Series II CHNS/O analyzer 2400. Magnetic measurements were performed on a Quantum Design MPMS-5 instrument equipped with a SQUID sensor housed in the Physics and Astronomy Department at Michigan State University or a MPMS-XL SQUID magnetometer located in the Chemistry Department at Texas A&M University.

B. SYNTHESES

The starting materials $[M(CH_3CN)_6]X_2$ (M = Fe^{II}, Co^{II}, Ni^{II}, and X = (BF$_4$)$^-$, (CF$_3$SO$_3$)$^-$, (PF$_6$)$^-$) were synthesized according to literature methods.[6] The metal complexes and ligands, $CoCl_2$, $FeCl_3$, KCN, [Et$_4$N]CN, 1,4,7-trithiacyclononane (9S3) and diethylenetriamine (dien), were purchased from Aldrich and used without further purification. Sodium *tris*-pyrazolylborate, NaTp, was prepared according to literature methods.[7] Silver hexafluorophosphate, silver tetrafluoroborate, silver nitrate and silver triflate were purchased from either Strem or Aldrich, and used without further purification. Acetone and acetonitrile were distilled over 3 Å sieves. Benzene, diethyl ether, THF and toluene were distilled over sodium-potassium/benzophenone, whereas methylene chloride was distilled over P_2O_5 under a nitrogen atmosphere. Methanol and ethanol were dried over magnesium alkoxide. Unless otherwise specified, all reactions were carried out under a nitrogen atmosphere using standard Schlenk-line techniques.

(1) Preparation of [TpFe(CH$_3$CN)$_3$](CF$_3$SO$_3$) (22).

One equivalent of NaTp (0.137 g, 0.582 mmol) in 30 mL of methanol was added via cannula techniques to a methanol solution (20 mL) of $[Fe(CH_3CN)_6](CF_3SO_3)_2$ (0.289 g, 0.482 mmol). Upon addition of the NaTp reagent, an immediate change in color ensued from colorless to red. The

reaction was left to stir for 12 h, after which time the solution was reduced in volume to ~10 mL and allowed to stand overnight in the refrigerator. A crop of colorless crystals of $Na(CF_3SO_3)$ was removed by filtration in an inert atmosphere. The remaining red solution was treated with 40 mL of diethyl ether to yield a red product. The diethyl ether was removed by cannula techniques, and red solid was dried *in vacuo*. Yield: (0.193 g, 74%). IR data (Nujol, cm^{-1}): 2480 (w), 2312 (m), 2284 (m), 2264 (w), 1504 (m), 1406 (m), 1307 (s), 1271 (s), 1242 (s), 1230 (s), 1209 (s), 1170 (s), 1115 (m), 1047 (s, br), 978 (m), 798 (m), 767 (m), 636 (m), 522 (m).

(2) Preparation of K[TpFe(CN)₃] (23).

Three equivalents of KCN (0.736 g, 11.32 mmol) in 50 mL of methanol were added via cannula techniques to a 50 mL methanol solution of Na[TpFeCl₃] (1.50 g, 3.78 mmol) over a 1 h period. The reaction was stirred for 12 h, after which time the by-product KCl was removed by filtration under an inert atmosphere and trapped in Celite. The resulting red filtrate was reduced in volume to ~5-10 mL, and treated with 40 mL of diethyl ether to precipitate a red product. The diethyl ether was removed by cannula techniques, and the red solid was dried *in vacuo*. Yield: (0.654 g, 53%) IR data (Nujol, cm^{-1}): 2490 (w), 2118 (w), 2054 (w), 2035 (m), 1408 (w), 1311 (m), 1261 (m), 1215 (m), 1153 (w), 1111 (m), 1072 (w), 1047 (m), 798 (m),

750 (w).

(3) Preparation of [TpCo(CH₃CN)₃]X (X = (BF₄)⁻ (24) , (CF₃SO₃)⁻ (25),

(PF₆)⁻ (27)).

Preparation of [TpCo(CH₃CN)₃](BF₄) (24).

An acetonitrile solution (20 mL) of NaTp (0.148 g, 0.628 mmol) was added

via cannula techniques to an acetonitrile (20 mL) solution of

[Co(CH₃CN)₆](BF₄)₂ (0.301 g, 0.628 mmol). The solution, which gradually

turned more orange in color, was stirred for 12 h, after which time the

solution was reduced in volume to about 10 mL and placed overnight in the

freezer at 0 °C. The solution was then filtered under an inert atmosphere to

remove the crystalline NaBF₄, and washed with cold CH₃CN (2 x 10 mL).

The solution was reduced to ~5-10 mL and treated with 40 mL of diethyl

ether to precipitate an orange product. The diethyl ether was removed by

cannula techniques, and the orange solid was dried *in vacuo*. Yield: (0.253 g,

84%) IR data (Nujol, cm⁻¹): 2517 (w), 2487 (w), 2314 (m), 2287 (m), 1732

(m), 1504 (m), 1406 (m), 1309 (s), 1261 (s), 1213 (s), 1112 (s), 1074 (s),

1047 (s, br), 1029 (s), 981 (m), 939 (w), 890 (w), 873 (w), 800 (s), 770 (m),

663 (m), 622 (w), 551 (w), 525 (w), 518 (w), 466 (w), 454 (w), 440 (w).

Preparation of [TpCo(CH₃CN)₃](CF₃SO₃) (25).

An acetonitrile solution (20 mL) of NaTp (0.118 g, 0.500 mmol) was added via cannula techniques to an acetonitrile (20 mL) solution of $[Co(CH_3CN)_6](CF_3SO_3)_2$ (0.301 g, 0.500 mmol). The solution gradually turned more orange in color. The reaction was stirred for 12 h, after which time the solution was reduced in volume to ~10 mL and placed in the refrigerator overnight. The solution was then filtered under an inert atmosphere to remove crystalline $Na(CF_3SO_3)$ and washed with cold CH_3CN (2 x 5 mL). The solution was reduced in volume to ~5 mL, and 40 mL of diethyl ether were added to precipitate an orange product. The diethyl ether was removed by cannula techniques, and the orange solid was dried *in vacuo*. Yield: (0.173 g, 64%) IR data (Nujol, cm^{-1}): 2509 (w), 2477 (m), 2314 (m), 2285 (m), 2264 (w), 1504 (m), 1404 (m), 1309 (s), 1265 (s, br), 1228 (s), 1211 (s), 1153 (s), 1113 (s), 1068 (w), 1047 (s), 1032 (s), 978 (m), 938 (w), 927 (w), 891 (w), 810 (w), 797 (w), 785 (m), 760 (m), 726 (m), 663 (m), 636 (s), 620 (m), 584 (w), 574 (m), 516 (m).

Preparation of [TpCo(CH$_3$CN)$_3$](PF$_6$) (26).

One equivalent of NaTp (0.072 g, 0.307 mmol) in 20 mL of acetonitrile was added via cannula techniques to an acetonitrile (20 mL) solution of $[Co(CH_3CN)_6](PF_6)_2$ (0.182 g, 0.338 mmol). The solution, which gradually turned more orange in color, was stirred for 12 h, after which time the

solution was reduced in volume to ~10 mL and placed in the refrigerator overnight. The solution was then filtered in an inert atmosphere to remove the crystalline $NaPF_6$ by-product and washed with cold CH_3CN (2 x 5 mL). The solution was reduced to ~5 mL, and 40 mL of diethyl ether were added to precipitate an orange product. The diethyl ether was removed by cannula techniques, and the orange solid was dried *in vacuo*. Yield: (0.120 g, 66%)

IR data (Nujol, cm^{-1}): 2474 (m), 2316 (m), 2287 (m), 1506 (m), 1404 (w), 1307 (m), 1213 (m), 1115 (m), 1070 (w), 1047 (m), 978 (m), 839 (s), 752 (m), 715 (m), 665 (m), 619 (m), 559 (m).

(4) Preparation of $[Et_4N]_2[TpCo(CN)_3]$ (27).

Three equivalents of [Et_4N]CN (0.297 g, 1.91 mmol) dissolved in 40 mL of acetonitrile were added via cannula techniques over a 2 h period to an acetonitrile solution (40 mL) of $[TpCo(CH_3CN)_3](PF_6)$ (0.339 g, 0.629 mmol). The color of the solution turned green then blue before reverting back to an orange color. The reaction was stirred for 12 h, after which time the solution was reduced in volume to ~10-15 mL and placed in the refrigerator overnight. The solution was filtered to remove the crystalline [Et_4N]PF_6 by-products and washed with cold CH_3CN (2 x 10 mL) in an inert atmosphere. The solution was reduced in volume to ~5 mL and treated with 50 mL diethyl ether to precipitate an orange product. The diethyl ether was

removed by cannula techniques, and the orange solid was dried *in vacuo*. Yield: (0.298 g, 78%). IR data (Nujol, cm^{-1}): 2511 (w), 2428 (w), 2127 (m), 2112 (m), 1404 (m), 1309 (m), 1294 (m), 1259 (w), 1211 (m), 1186 (m), 1172 (m), 1115 (m), 1078 (m), 1046 (m), 1037 (m), 1003 (m), 976 (w), 960 (w), 923 (w), 880 (m), 839 (s), 787 (m), 762 (m), 727 (m), 669 (w), 629 (w), 559 (m), 408 (m).

(5) Preparation of [TpNi(CH$_3$CN)$_3$]X (X = (BF$_4$)$^-$ (28), (CF$_3$SO$_3$)$^-$ (29), (PF$_6$)$^-$ (30)).

Preparation of [TpNi(CH$_3$CN)$_3$](BF$_4$) (28).

One equivalent of NaTp (0.254 g, 1.08 mmol) dissolved in 40 mL of acetonitrile was added via cannula techniques to an acetonitrile (40 mL) solution of [Ni(CH$_3$CN)$_6$](BF$_4$)$_2$ (0.515 g, 1.08 mmol). The solution gradually turned pale-purple in color. The reaction was stirred for 12 h, after which time the solution was reduced in volume to ~10 mL and placed in the freezer for at least 12 h. The solution was then filtered in an inert atmosphere to remove crystalline NaBF$_4$ by-product and washed with cold CH$_3$CN (2 x 10 mL). The solution was reduced to ~5-10 mL and treated with 40 mL of diethyl ether to precipitate a purple product. The diethyl ether was removed by cannula techniques, and the purple solid was dried *in vacuo*. Yield: (0.455 g, 88%) IR data (Nujol, cm^{-1}): 2476 (m), 2314 (m), 2296 (m), 1504

(m), 1408 (m), 1396 (m), 1311 (s), 1261 (w), 1213 (s), 1111 (s), 1047 (s, br),

983 (m), 936 (w), 893 (w), 815 (w), 798 (m), 783 (m), 765 (m), 756 (m),

746 (m), 726 (m), 665 (m), 623 (m), 552 (w), 525 (w), 519(w).

Preparation of [TpNi(CH$_3$CN)$_3$](CF$_3$SO$_3$) (29).

An acetonitrile solution (40 mL) of NaTp (0.119 g, 0.506 mmol) was added

via cannula techniques to an acetonitrile (40 mL) solution of

[Ni(CH$_3$CN)$_6$](CF$_3$SO$_3$)$_2$ (0.305 g, 0.506 mmol). The solution gradually

turned pale purple in color. The reaction was stirred for 12 h, after which

time the solution was reduced in volume to ~10 mL and placed in the freezer

at 0 °C for at least 12 h. The solution was filtered to the remove crystalline

NaOTf by-product and washed with cold CH$_3$CN (2 x 5 mL) under an inert

atmosphere. The solution was reduced to ~5 mL and treated with 40 mL of

diethyl ether to effect the precipitation of a purple product. The diethyl ether

was removed by cannula techniques, and the purple solid was dried *in*

vacuo. Yield: (0.237 g, 86%) IR data (Nujol, cm^{-1}): 2474 (m), 2467 (m),

2318 (m), 2309 (m), 2291 (m), 2284 (m), 2264 (m), 1504 (w), 1423 (w),

1410 (m), 1398 (m), 1311 (s), 1273 (s, br), 1259 (s, br), 1230 (s), 1211 (s),

1184 (m), 1155 (m, br), 1113 (m), 1093 (w), 1076 (m), 1047 (s), 1032 (s),

982 (m), 940 (w), 927 (w), 791 (m), 771 (m), 763 (s), 755 (m), 745 (m), 724

(m), 663 (m), 642 (s), 638 (s), 622 (m), 584 (w), 574 (w), 520 (m), 464 (w),

126

452 (w), 438 (w).

Preparation of [TpNi(CH$_3$CN)$_3$](PF$_6$) (30).

One equivalent of NaTp (0.122 g, 0.520 mmol) in 40 mL of acetonitrile was added via cannula techniques to an acetonitrile (40 mL) solution of [Ni(CH$_3$CN)$_6$](PF$_6$)$_2$ (0.323 g, 0.543 mmol). The solution gradually turned pale purple in color. The reaction was stirred for 12 h, after which time the solution was reduced in volume to ~10 mL and placed in the refrigerator overnight. The solution was filtered to remove the crystalline NaPF$_6$ by-product and washed with cold CH$_3$CN (2 x 10 mL) in an inert atmosphere. The solution was reduced to ~5-10 mL, and 40 mL of diethyl ether were added to precipitate the purple product. The diethyl ether was removed by cannula techniques, and the purple solid was dried *in vacuo*. Yield: (0.250 g, 85%) IR data (Nujol, cm^{-1}): 2478 (m), 2318 (m), 2291 (m), 1630 (m), 1504 (m), 1404 (s), 1311 (s), 1213 (s), 1149 (m), 1113 (s), 1070 (m), 1047 (s), 979 (m), 833 (s, br), 788 (m), 752 (s), 727 (m), 663 (m), (m), 559 (s).

(6) Preparation of NiTp$_2$ (32).

Two equivalents of NaTp (0.099 g, 0.422 mmol) dissolved in 20 mL of acetonitrile were added via cannula techniques over a 10 min period to an acetonitrile solution of [Ni(CH$_3$CN)$_6$](BF$_4$)$_2$ (0.100 g, 0.210 mmol). The reaction stirred for 12 h, after which time a pink precipitate was present in a

pale pink solution. The solution was removed via cannula techniques, and the precipitate was washed with acetonitrile (2 x 10 mL) followed by diethyl ether (2 x 20 mL). The diethyl ether was removed by cannula techniques, and the pale pink solid was dried *in vacuo*. Yield: (0.043 g, 43%). IR (Nujol, cm^{-1}): 2476 (m), 1502 (m), 1423 (w), 1404 (m), 1394 (m), 1309 (s), 1211 (s), 1109 (s), 1047 (s), 1030 (s), 976 (m), 881 (w), 790 (w), 765 (w), 754 (s), 746 (s), 727 (m), 667 (m), 640 (w), 621 (m), 550 (w), 526 (w), 518 (w).

(7) Preparation of [(9S3)Co(CH₃CN)₃](PF₆)₂ (32).

One equivalent of 9S3 (0.130 g, 0.726 mmol) dissolved in 15 mL of dichloromethane was slowly added to a 15 mL dichloromethane solution of [Co(CH₃CN)₆](PF₆)₂ (0.431 g, 0.726 mmol) over a 10-15 min period under an inert nitrogen atmosphere. The color of the solution gradually turned more orange and a bit pinkish (salmon). When the volume of the solution was ~10 mL, the addition of 40 mL of diethyl ether produced an orange/pink product, which was collected by filtration. The product is soluble in most common solvents. Yield: (0.289 g, 61%) IR data (Nujol, cm^{-1}): 1480 (s), 1410 (m), 1364 (m), 1340 (w), 1312 (m), 1301 (w), 1260 (w), 1186 (m), 1170 (w), 1153 (w), 1078 (m), 1033 (m), 105 (m), 937 (w), 881 (s), 835 (s, br), 794 (s), 789 (s), 668 (w), 557 (s), 467 (w).

(8) Preparation of (9S3)CoCl₂ (33).

One equivalent of 9S3 (0.257 g, 1.43 mmol) dissolved in 25 mL of acetonitrile was reacted with $CoCl_2$ (0.199 g, 1.53 mmol) in 25 mL of acetonitrile. A navy precipitate was observed to form immediately. The reaction was stirred for 12 h under an inert nitrogen atmosphere, after which time a navy precipitate and pale green solution were observed to be present. The precipitate was collected by filtration and washed with 20 mL of diethyl ether. The pale green solution was discarded. Yield: (0.44 g, 94%) IR data (Nujol, cm^{-1}): 2279 (w), 2244 (w), 1439 (s), 1410 (s), 1396 (m), 1366 (m), 1286 (m), 1274 (w), 1247 (w), 1182 (m), 1131 (w), 1120 (w), 1041 (m), 1014 (w), 937 (m), 917 (w), 904 (s), 825 (s), 820 (m), 690 (m), 669 (m), 635 (w), 623 (m), 488 (m), 449 (m).

(9) Preparation of [Co(9S3)₂]Cl₂ (34).

Two equivalents of 9S3 (0.279 g, 1.55 mmol) dissolved in 25 mL of acetonitrile were combined with $CoCl_2$ (0.100 g, 0.769 mmol) in 25 mL of acetonitrile which led to the immediate precipitation of a navy product. The reaction was allowed to stir for ~12 h under an inert nitrogen atmosphere after which time a navy precipitate and a pale red/pink solution were present. The precipitate was collected by filtration and washed with 20 mL of diethyl ether. The red/pink solution was discarded. Yield: (0.125 g, 33%). IR data

(Nujol, cm⁻¹): 1455 (m), 1441 (m), 1405 (m), 1346 (m), 1295 (m), 1279 (m), 1260 (m), 1172 (m), 1141 (m), 1097 (m), 1016 (s), 936 (m), 902 (s), 870 (w), 820 (s), 803 (s), 794 (s), 688 (m), 668 (w), 631 (m), 623 (m), 490 (m), 447 (m), 395 (m).

3. REACTIVITY STUDIES

(1) Reaction of [TpFe(CH₃CN)₃](CF₃SO₃) with K[TpFe(CN)₃].

A solution of [TpFe(CH₃CN)₃](CF₃SO₃) (0.107 g, 0.197 mmol) dissolved in 20 mL of methanol was slowly added via a cannula to a 20 mL methanol solution of K[TpFe(CN)₃] (0.076 g, 0.196 mmol) over a 15 min period. A green precipitate formed immediately in an orange/red solution. The orange/red solution was separated from the green solid and transferred to another flask where it was reduced in volume to 10 mL, at which point it was treated with 40 mL of diethyl ether to precipitate an orange/red product. The diethyl ether was removed by cannula techniques and the orange/red solid was dried *in vacuo*. IR data for the orange/red solid (Nujol, cm⁻¹): 2474 (w), 1504 (w), 1406 (m), 1307 (m), 1296 (s), 1248 (s), 1204 (m), 1180 (m), 1113 (m), 1047 (s), 979 (w), 763 (m), 740 (w), 659 (m), 648 (m), 520 (m). The green precipitate was washed with 20 mL of diethyl ether and dried *in vacuo*. The amount of green precipitate was negligible ~ 0.009 g. IR data for the green precipitate (Nujol, cm⁻¹): 2090 (m), 2066 (m), 1572 (w), 1410 (w),

1261 (m), 1215 (m), 1113 (m), 1041 (s), 800 (m), 754 (w), 642 (w), 621 (w), 466 (w).

(2) Reaction of [Et$_4$N]$_2$[TpCo(CN)$_3$] with [(dien)Ni(NO$_3$)$_2$].

A 10 mL acetonitrile/15 mL methanol solution of [(dien)Ni(NO$_3$)$_2$] (0.113 g, 0.395 mmol) was added via a cannula to a 10 mL acetonitrile/15 mL methanol solution of [Et$_4$N]$_2$[TpCo(CN)$_3$] (0.168 g, 0.275 mmol). After 30 min, a green precipitate formed in a colorless solution. The green precipitate was removed by filtration and washed with 10 mL of diethyl ether. IR (Nujol, cm^{-1}): 3358 (s), 3290 (s), 3171 (w), 2164 (s), 1647 (m), 1595 (s), 1406 (m), 1309 (s), 1215 (m), 1169 (w), 1111 (w), 1041 (s), 979 (m), 889 (w), 843 (s), 773 (w), 738 (w), 557 (m), 443 (m).

(3) Reaction of [Et$_4$N]$_3$[(CO)$_3$Mo(CN)$_3$] with [(9S3)Co(CH$_3$CN)$_3$](PF$_6$)$_2$

An excess of [(9S3)Co(CH$_3$CN)$_3$](PF$_6$)$_2$ (0.270 g, 0.414 mmol) dissolved in 25 mL acetonitrile was reacted dropwise with [Et$_4$N]$_3$[(CO)$_3$Mo(CN)$_3$] (0.110 g, 0.212 mmol) in 25 mL of acetonitrile. The reaction was stirred for 12 h, at which point a black precipitate in an orange solution was observed to be present. The black precipitate was removed by filtration and washed with 10 mL of diethyl ether. The orange filtrate was reduced to ~10 mL at which point 40 mL of diethyl ether were added to precipitate an orange product. The diethyl ether was decanted and the orange product was dried *in*

vacuo. The IR data of the orange solid was identical to the IR spectrum of the cobalt starting material. IR data (Nujol, cm^{-1}): 2310 (w), 2284 (w), 2248 (w), 2098 (s, br), 2027 (s), 1888 (s, br), 1792 (s, br), 1635 (s, br), 1287 (s, br), 1170 (m), 1021 (m, br), 936 (m), 902 (m), 843 (s), 622 (w), 597 (m), 557 (w), 446 (m), 404 (m).

(4) Reaction of [Et$_4$N]$_3$[(CO)$_3$Mo(CN)$_3$] with (THF)$_3$CrCl$_3$.

An excess of (THF)$_3$CrCl$_3$ (0.245 g, 0.654 mmol) dissolved in 25 mL of acetonitrile was added dropwise to a 20 mL acetonitrile solution of [Et$_4$N]$_3$[(CO)$_3$Mo(CN)$_3$] (0.171 g, 0.330 mmol) for 15 min. The solution, which turned red immediately, was stirred for 12 h, reduced in volume and treated with 40 mL of diethyl ether to precipitate a red product. The diethyl ether was removed by cannula techniques and the red solid was dried *in vacuo*. IR data (Nujol, cm^{-1}): 2318 (w), 2288 (w), 2240 (w), 2101 (s), 1995 (s), 1876 (s, br), 1760 (s, br), 1649 (m), 1572 (m), 1361 (s), 1301 (m), 1179 (m), 1171 (s), 1113 (w), 1076 (w), 1064 (w), 1051 (w), 1029 (w), 999 (m), 953 (w), 917 (w), 890 (w), 846 (w), 821 (w), 782 (m), 735 (w), 627 (w), 599 (m, sh), 546 (m), 489 (m, br), 387 (w), 323 (m), 315 (m), 308 (m), 302 (m), 287 (w), 275 (w), 260 (w), 254 (w), 245 (w), 233 (w), 227 (m), 219 (m), 211 (w), 206 (m), 202 (m).

(5) Reaction of [Et$_4$N]$_3$[(CO)$_3$Mo(CN)$_3$] with Na[TpCrCl$_3$].

Greater than a two-fold excess of Na[TpCrCl$_3$] (0.184 g, 0.491 mmol) dissolved in 25 mL acetonitrile was added dropwise over a 15 min period to a 25 mL acteonitrile solution of [Et$_4$N]$_3$[(CO)$_3$Mo(CN)$_3$] (0.121 g, 0.233 mmol). The resulting red solution was stirred for 12 h, after which time it was reduced in volume and treated with 40 mL of diethyl ether to precipitate a red product. The diethyl ether was removed by cannula techniques and the red solid was dried *in vacuo*. IR data (Nujol, cm^{-1}): 2096 (m), 2073 (m), 1996 (w), 1946 (w), 1883 (m), 1782 (m, br), 1702 (w), 1634 (w), 1618 (w), 1576 (w), 1500 (w), 1405 (m), 1310 (m), 1261 (w), 1210 (m), 1181 (w), 1170 (m), 1154 (w), 1115 (w), 1097 (w), 1074 (w), 1050 (m), 1000 (m), 889 (w), 843 (w), 818 (w), 771 (m), 659 (w), 621 (w), 598 (w), 545 (w), 491 (w).

(6) Reaction of [Et$_4$N]$_3$[(CO)$_3$Mo(CN)$_3$] with [(dien)Ni(NO$_3$)$_2$].

A slight excess of [(dien)Ni(NO$_3$)$_2$] (0.082 g, 0.287 mmol) dissolved in 25 mL of methanol was added dropwise for 15 min to a 25 mL methanol solution of [Et$_4$N]$_3$[(CO)$_3$Mo(CN)$_3$] (0.127 g, 0.245 mmol) which effected an instantaneous formation of a yellow precipitate in a pale yellow solution. The reaction was stirred for 12 h, after which time the yellow precipitate was collected by filtration and washed with 10 mL of diethyl ether. The pale yellow solution was combined with KPF$_6$ and evaporated to yield purple crystals. IR data (Nujol, cm^{-1}): 3342 (m), 3291 (m), 2247 (w), 2147 (m),

2125 (m), 2093 (w), 1891 (s), 1764 (s, br), 1590 (s), 1134 (m), 1058 (m), 958 (m), 889 (w), 771 (w), 596 (w), 512 (w), 441 (m), 220 (m), 208 (m).

4. SINGLE CRYSTAL X-RAY STRUCTURAL STUDIES

Crystallographic data were collected on a 1K (SMART 1000) CCD for **35** and on a 2K (SMART 2000) CCD diffractometer for **30**. Both are equipped with monchromated Mo Kα (λ_α = 0.71069 Å) radiation. The source is a Mo sealed tube with a 3KW generator. The frames were integrated in the Bruker SAINT software package[8] and the data were corrected for absorption using the SADABS program.[9] The SIR97[10] and SHELX-97[11] crystallographic software packages were used. Crystal parameters and basic information pertaining to data collection and structure refinement are summarized in Tables 3.1-3.2.

(1) [TpNi(CH₃CN)₃](PF₆) (30).

Single crystals of **30** were grown from a concentrated acetonitrile solution of the complex at low temperatures (~ -15 °C). A pale-purple crystal of dimensions 0.24 x 0.12 x 0.065 mm^3 was mounted on the tip of a glass fiber with Dow Corning silicone grease and placed in a cold N₂ stream. Least squares refinement using well-centered reflections in the range 4.04° < 2θ < 46.60° gave a cell corresponding to a rhomohedral/hexagonal crystal system. A total of 7319 data (1101 unique) with F(000) = 3288 were collected at

Table 3.1. Crystallographic information for [TpNi(CH$_3$CN)$_3$](PF$_6$) (**30**)

	30
Formula	C$_{15}$H$_{19}$F$_6$PNiN$_9$B
Formula weight	539.28
Temperature (K)	110(2)
Space group	R-3c
a (Å)	11.4050(16)
b (Å)	11.4050(16)
c (Å)	60.470(12)
α (°)	90
β (°)	90
γ (°)	120
Volume (Å^3)	6811.8(19)
Z	12
D$_{calc}$ (Mg m^{-3})	1.579
Absorption coefficient(mm^{-1})	0.996
Crystal size (mm)	0.236 x 0.122 x 0.065
Reflections collected	7319
Independent reflections	1101
R$_{int}$	0.1486
Final R indices	R$_1$ = 0.1196
	wR$_2$ = 0.3642

R$_1$ = $\Sigma[||F_o| - |F_c||] / \Sigma|F_o|$. wR$_2$ = $\{\Sigma[w(F_o{}^2 - F_c{}^2)^2 / \Sigma[w(F_o{}^2)^2]\}^{1/2}$. GOF = $\{\Sigma[w(F_o{}^2 - F_c{}^2)^2] / (n - p)\}^{1/2}$ where n = total number of reflections and p = total number of parameters.

Table 3.2. Crystallographic information for [FeTp$_2$](BF$_4$) (35).

	35
Formula	C$_{18}$H$_{20}$B$_3$F$_4$FeN$_{12}$
Formula weight	568.74
Temperature (K)	173(2)
Space group	P-1
a (Å)	11.694(5)
b (Å)	11.888(5)
c (Å)	11.889(5)
α (°)	115.825(5)
β (°)	116.478(5)
γ (°)	94.832(5)
Volume (Å^3)	1249.6(9)
Z	2
D$_{calc}$ (Mg m^{-3})	1.512
Absorption coefficient(mm^{-1})	0.667
Crystal size (mm)	0.20 x 0.30 x 0.15
Reflections collected	10745
Independent reflections	4969
R$_{int}$	0.1349
Final R indices	R1 = 0.0970
	wR2 = 0.2574

$R_1 = \Sigma[||F_o| - |F_c||] / \Sigma|F_o|$. $wR_2 = \{\Sigma[w(F_o^2 - F_c^2)^2 / \Sigma[w(F_o^2)^2]\}^{1/2}$. GOF = $\{\Sigma[w(F_o^2 - F_c^2)^2] / (n - p)\}^{1/2}$ where n = total number of reflections and p = total number of parameters.

110(2) K using the ω-2θ scan technique to a maximum 2θ value of 46.60°. Systematic absences from the data led to the choice of R-3c as the space group. The final full-matrix, least-squares refinement was based on data with $F_o^2 > 4\sigma(F_o^2)$ and parameters to give R1 = 0.1196 (wR$_2$ = 0.3642) and R$_{int}$ = 0.1486. The transmission factors were in the range 0.585 to 1.00. The goodness-of-fit index was 1.723, and the highest peak in the final difference map was 2.992 e$^-$/Å^3 which is located near the phosphorus atom of a disordered (PF$_6$)$^-$ anion. The hydrogen atoms were placed in calculated positions and treated as riding atoms. A thermal ellipsoid plot is presented in Figure 3.2.

(2) [FeTp$_2$](BF$_4$) (35).

Single crystals of **35** were grown by slow evaporation of the acetonitrile mother liquor. A red crystal of dimensions 0.20 x 0.30 x 0.15 mm^3 was mounted on the tip of a glass fiber with Dow Corning silicone grease and placed in a cold N$_2$ stream. Least squares refinement using well-centered reflections in the range 4.06° < 2θ < 57.54° gave a cell corresponding to a triclinic crystal system. A total of 10745 data (4969 unique) with F(000) = 578 were collected at 173(2) K using the ω-2θ scan technique to a maximum 2θ value of 57.54°. The space group is P-1. The final full-matrix, least-

137

squares refinement was based on data with $F_o^2 > 4\sigma(F_o^2)$ and parameters to give $R1 = 0.0970$ ($wR_2 = 0.2574$) and $R_{int} = 0.2574$. The transmission factors ranged from 0.0106 to 1.00. The goodness-of-fit index was 0.571, and the highest peak in the final difference map was 0.970 $e^-/Å^3$. The hydrogen atoms were placed in calculated positions and treated as riding atoms. A thermal ellipsoid plot is presented in Figure 3.3.

3. RESULTS AND DISCUSSION

A. Syntheses

Much of the research in this area with the *tris*-pyrazolylborate (Tp) ligand was fleshed out by Trofimenko who prepared numerous MTp_2 complexes with divalent metals in water.[12] This facially coordinating tridentate ligand is of great utility because it is anionic and therefore helps to reduce the cationic charge on the metal complex. The ligand can be used in both aqueous and non-aqueous media, which is convenient for our goal to prepare a molecular cube in a solvent such as acetonitrile. The Tp ligand is a tridentate, monoanionic ligand that has been used extensively in transition metal and main group coordination chemistry.[13] It is similar to the Cp family of ligands which has been used successfully by Rauchfuss to prepare molecular cubes. Both Cp⁻ and Tp⁻ donate 6 electrons, occupy three coordination sites, and are monanionic. Complexes of the *fac*-$[(L_3)M(S)_3]^{n+}$ type possess three labile

138
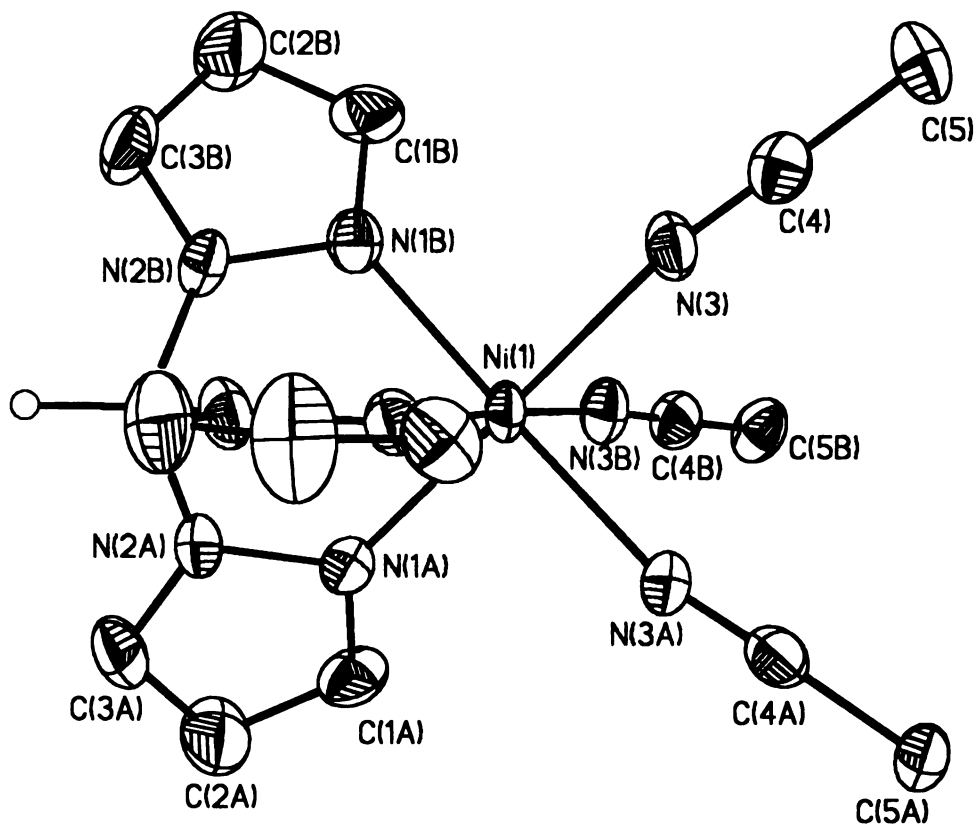
Figure 3.2. Thermal ellipsoid plot of cation [TpNi(CH₃CN)₃]⁺ in (30) at the 50 % probability level. The hydrogen atoms were omitted for the sake of clarity. (Image is presented in color)
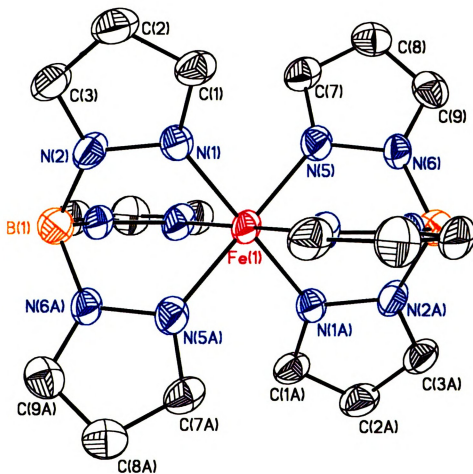
Figure 3.3. Thermal ellipsoid representation of the cation $[FeTp_2]^+$ in (**35**) at the 50 % probability level. The hydrogen atoms were omitted for the sake of clarity. (Image is presented in color)

sites occupied by either solvent molecules or weakly coordinating anions. Transition metal tricyanide complexes, fac-[(L$_3$)M'(CN)$_3$], were synthesized with only iron(III) and cobalt(II) with the $tris$-pyrazolylborate ligand. Transition metal complexes, fac-[(L$_3$)M(S)$_3$]$^{n+}$, were synthesized with a variety of 3d metals and counterions. One can envisage that the reaction between fac-[(L$_3$)M(S)$_3$]$^{n+}$ and fac-[(L$_3$)M'(CN)$_3$] could yield a molecular cube (Figure 3.1.). The molecular cube is of particular interest, but a reaction of this type could yield a portion of a cube or any number of open polymeric species that could also be of interest.

(1) Complexes of [TpM(CH$_3$CN)$_3$]X   M = Fe^{II}, Co^{II} and Ni^{II}; X$^-$= (BF$_4$)$^-$, (PF$_6$)$^-$ and (CF$_3$SO$_3$)$^-$.

The complexes, [TpM(CH$_3$CN)$_3$]$^+$, were synthesized from their solvated precursors [M(CH$_3$CN)$_6$]X$_2$ and one equivalent of NaTp as depicted in Figure 3.4. This chemistry is difficult to control, as the possibility for obtaining the bis-substituted complexes, MTp$_2$, is always an issue, since they are quite stable once formed. One other synthetic issue is that the halide abstraction reaction leads to a by-product NaX. This by-product is difficult to remove, but it can be separated from the product of interest, namely [TpM(CH$_3$CN)$_3$]$^+$, by reducing the volume of the reaction solution and chilling it to ~0 °C for up to a few days. Colorless crystals of the by-product

$$[M(CH_3CN)_6]^{2+} \quad + \quad L_3 \longrightarrow$$

$$\left[\begin{array}{c} \text{L} \quad \text{L} \quad \text{L} \\ \text{S} \quad \text{M} \quad \text{S} \\ \text{S} \end{array} \right]^{2+/+}$$

$$\overset{\frown}{\underset{L}{\bigcup}}_{L} = L_3 =$$

Tripodal ligand such as
Tp, *tris*-pyrazolylborate,
1,4,7-trithiacyclononane

$S = CH_3CN$

$M = Fe(II)$, Co(II), Ni(II)
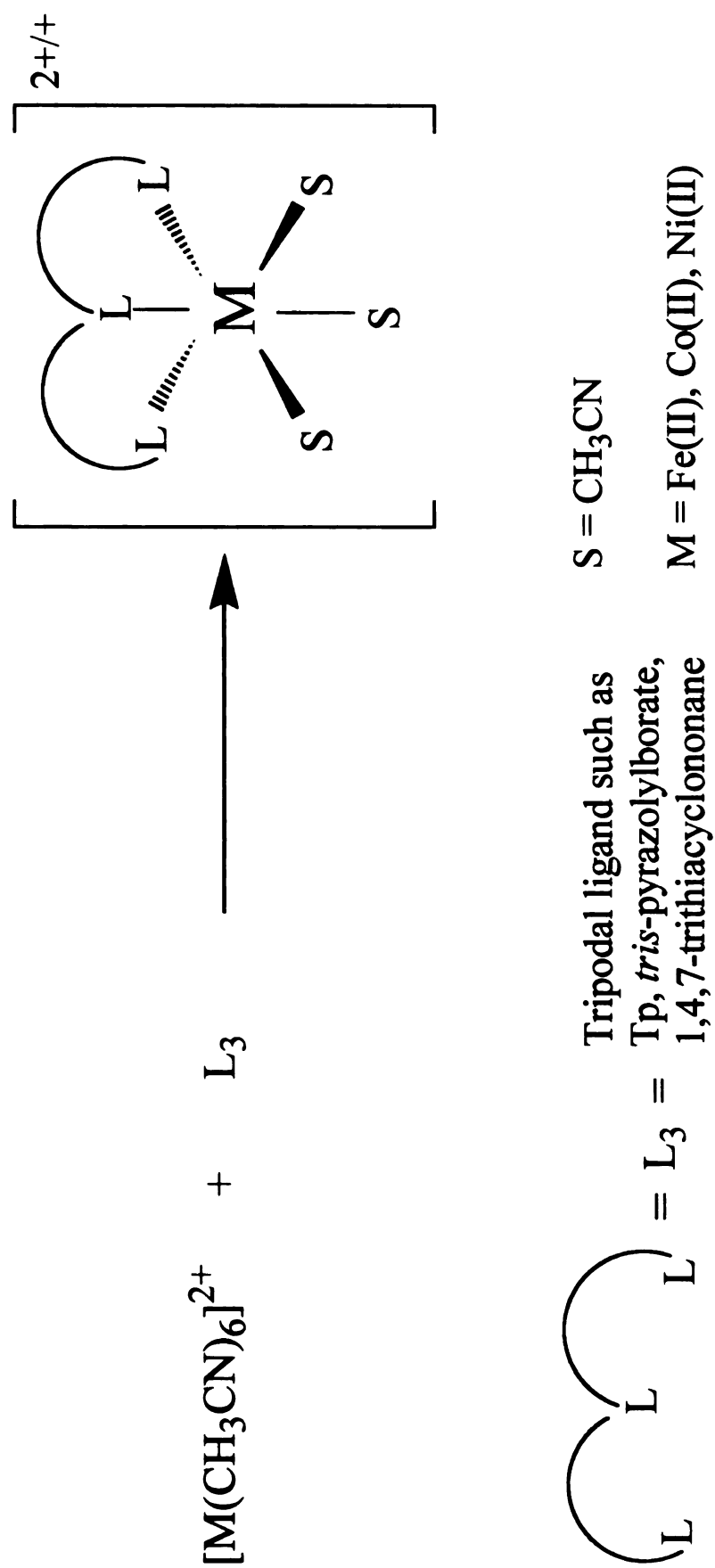
Figure 3.4. Schematic representation of reactions with the solvated precursors, $[M(CH_3CN)_6]^{2+}$, with a facial tridentate ligand to yield $[L_3M(S)_3]^{n+}$.

142

salts are formed under these conditions and can be removed by filtration. In the cases of the $(BF_4)^-$ and $(PF_6)^-$ salts, the $[TpM(CH_3CN)_3]^+$ products exhibit two CH_3CN stretches in the IR spectrum, while the triflate counterion typically gives rise to three stretches. All complexes exhibit at least one v(B-H) stretching mode in the range of 2450 – 2550 cm^{-1}. The IR spectral data are summarized in Table 3.3. The compounds, $[NiTp(CH_3CN)_3](PF_6)$ (30) and $[CoTp(CH_3CN)_3](PF_6)^{14}$ are the only precursors of this type for which we were able to obtain single crystals and fully characterized by X-ray methods.

The reaction of $[Ni(CH_3CN)_6](BF_4)_2$ with one equivalent of NaTp was performed on a large scale, and, after reducing the volume, pink crystals formed. The crystals are $NiTp_2$, which poses a problem for synthesizing $[TpNi(CH_3CN)_3]^+$ on a large scale. Evidently, the $NiTp_2$ complex is highly favored under concentrated conditions. The reaction was refluxed in acetonitrile overnight and, after reduction of the solvent, neither a pink precipitate nor pink crystals formed. The pink color is indicative of the $NiTp_2$ product, whereas the pale purple color is a sign of the desired $[TpNi(CH_3CN)_3]^+$ complex.

(2) K[TpFe(CN)₃].

The reaction of $Na[TpFeCl_3]$ and three equivalents of cyanide was

143

Table 3.3. IR data for [TpM(CH$_3$CN)$_3$]X M = Fe (**22**), Co (**24-26**) and Ni (**28-30**); X$^-$ = (BF$_4$)$^-$, (CF$_3$SO$_3$)$^-$, (PF$_6$)$^-$

[TpM(CH$_3$CN)$_3$](X)	ν(B-H) (cm^{-1})	ν(C≡N) (cm^{-1})	X$^-$ = ν(B-F), ν(P-F), ν(S-O) (cm^{-1})	Compound Color
[TpFe(CH$_3$CN)$_3$](CF$_3$SO$_3$)	2480 (w)	2312 (m) 2284 (m) 2264 (w)	1047 (s, br)	red
[TpCo(CH$_3$CN)$_3$](BF$_4$)	2517 (w) 2487 (w)	2314 (m) 2287 (m)	1047 (s)	orange
[TpCo(CH$_3$CN)$_3$](CF$_3$SO$_3$)	2509 (w) 2477 (m)	2314 (m) 2285 (m) 2264 (w)	1047 (s) 1032 (s)	orange
[TpCo(CH$_3$CN)$_3$](PF$_6$)	2474 (m)	2316 (m) 2287 (m)	839 (s)	orange
[TpNi(CH$_3$CN)$_3$](BF$_4$)	2476 (m)	2314 (m) 2296 (m)	1047 (s, br)	pale purple
[TpNi(CH$_3$CN)$_3$](CF$_3$SO$_3$)	2474 (m) 2467 (m)	2318 (m) 2284 (m) 2264 (m)	1047 (s) 1032 (s)	pale purple
[TpNi(CH$_3$CN)$_3$](PF$_6$)	2478 (m)	2318 (m) 2291 (m)	833 (s, br)	pale purple

performed in methanol, based on the fact that ligand redistribution occurs in an acetonitrile medium to form the thermodynamically stable complex, $[Fe^{III}Tp_2]^+$ and the anion $[Fe^{III}Cl_4]^-$.[15] Kim and co-workers[15] managed to crystallize $[Et_4N][TpFeCl_3]$ from THF due to its low solubility in this solvent. The $[FeTp_2]^+$ complex is blood-red in color which is typical of low-spin iron(III) complexes with nitrogen donor ligands. The $[TpFeCl_3]^-$ complex is high-spin and is lighter red/orange in color. In order to prepare $[TpFe(CN)_3]^-$, the KCN was added very slowly to avoid substitution of the Tp^- ligand for CN^- ligands (both reactions are depicted in Figure 3.5-3.6). In addition, the reaction was carried out under an inert atmosphere to prevent reduction of the Fe^{III} centers. IR data measured on the red solid revealed cyanide stretches as well as the $v(B-H)$ stretch at 2490 cm^{-1}. This supports the formulation of the product as the tricyanide complex $[TpFe(CN)_3]^-$. The cation could be either K^+ or Na^+, since the starting material was $Na[TpFeCl_3]$ but CN^- was introduced as KCN. Another approach to synthesizing the tricyanide species is to react $Na[TpFeCl_3]$ with 3 equivalents of AgX, X= $(BF_4)^-$, $(PF_6)^-$ and $(CF_3SO_3)^-$, in methanol and then reacting the partially solvated complex and reacting that with 3 equivalents of cyanide. This approach was not successful, however, since it invariably led to the formation of the $[FeTp_2]^+$ complex. The $[FeTp_2](BF_4)$ (35) salt was

FeCl$_3$ + NaTp

$$[\text{TpFeCl}_3]^-$$

= Tp, *tris*-pyrazolylborate
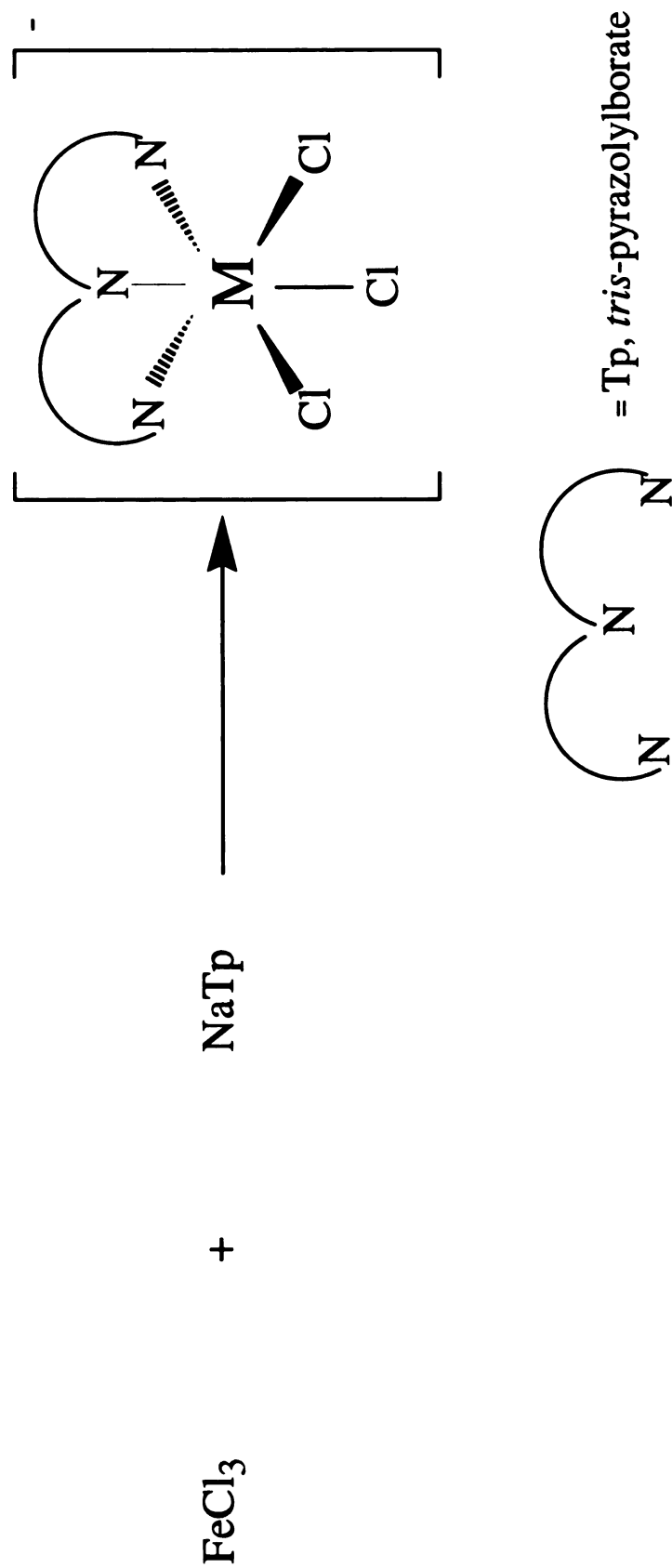
Figure 3.5. Schematic representation of the reaction between FeCl$_3$ and NaTp to yield [TpFeCl$_3$]$^-$

$$M = Cr(III),\ Fe(III)$$

= Tp, *tris*-pyrazolylborate
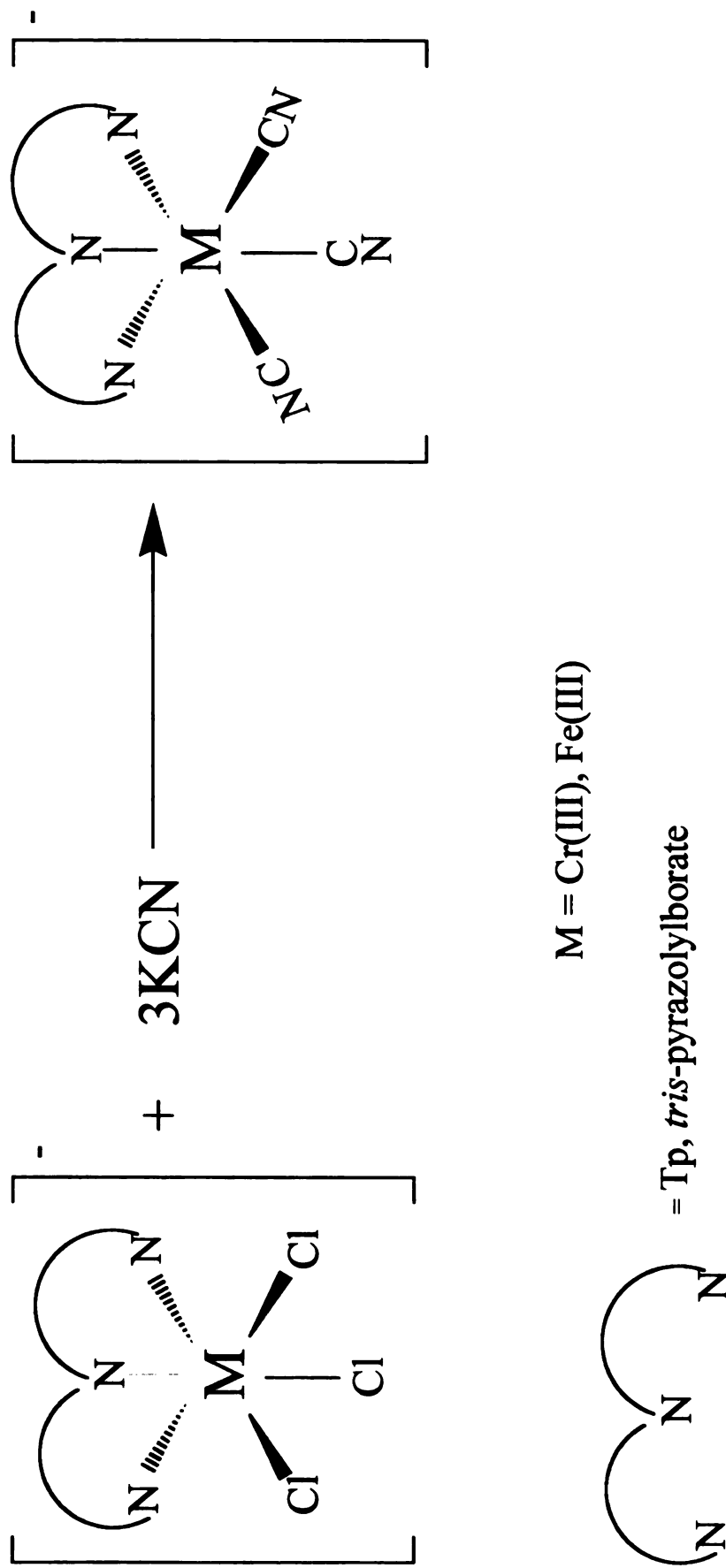
Figure 3.6. Schematic representation of the reaction of [TpMCl₃]⁻ with cyanide to yield [TpM(CN)₃]⁻

isolated from this type of reaction.

(3) [Et₄N]₂[CoTp(CN)₃].

The tricyanide complex was formed by adding three equivalents of cyanide to the $[TpCo(CH_3CN)_3]^+$ complex. The problem with this reaction is that $[TpCo(CH_3CN)_3]^+$ is difficult to purify, and the by-product salts NaX (X = $(BF_4)^-$, $(CF_3SO_3)^-$ and $(PF_6)^-$) are often present. This is the reason why satisfactory elemental analyses could not be obtained for the product. Moreover, it is difficult to be precisely stoichiometric with the CN⁻ addition; excess CN⁻ inevitably leads to the formation of $CoTp_2$ and $[Co^{II}(CN)_6]^{4-}$ and/or other undesired cyanide complexes. The IR data for the product $[Et_4N]_2[TpCo(CN)_3]$ consists of two cyanide stretches located at 2127 and 2112 cm⁻¹ which is consistent with the D_3 symmetry of the proposed molecular structure. The v(B-H) stretches appear at 2511 and 2428 cm⁻¹.

(4) NiTp₂.

The neutral $NiTp_2$ complex is known in the literature, but the synthetic route is slightly different from the one that led to the product in this work. In the present case, the complex was formed by reacting two equivalents of NaTp with $[Ni(CH_3CN)_6](BF_4)_2$ in acetonitrile. The synthetic route previously reported by Trifimenko was performed in water. The crystal structure was reported by Bandoli[16] and co-workers and is isostructural with its cobalt

148

analogue.[17]

(5) (9S3)Co(CH$_3$CN)$_3$](PF$_6$)$_2$.

The 1,4,7-thiacyclononane ligand is known to bind to a metal center as a facially tridentate ligand. The cations [M(9S3)$_2$]$^{2+}$ (M = Co, Ni and Cu) salts have been fully characterized as the (BF$_4$)$^-$ salts.[18] The solvated starting material, [Co(CH$_3$CN)$_6$](PF$_6$)$_2$, was reacted with one equivalent of the 9S3 ligand with no evidence for precipitation. The color of the [Co(9S3)$_2$](BF$_4$)$_2$ complex is purple, whereas the reaction of the one equivalent of 9S3 with [Co(CH$_3$CN)$_6$](PF$_6$)$_2$ salt leads to an orange colored product. It is obvious that the compound [Co(9S3)$_2$]$^{2+}$ is not forming under these conditions. The 9S3 ligand can be identified by the presence of several bands[19] in the IR spectrum at 1480 (s), 1410 (m), 1260 (w), 937 (m), and 881 (s) cm^{-1}. There are a few other peaks relevant to the 9S3 ligand, but they overlap with the Nujol or (PF$_6$)$^-$ modes. The IR data were measured both in air and in an inert atmosphere. The v(C$\equiv$N) stretches were present only in the IR data for the anaerobic sample, which implies the CH$_3$CN ligands are readily lost in favor of water molecules. The three CH$_3$CN stretches are present at 2324 (m), 2296 (m) and 2248 (w) cm^{-1}.

(6) (9S3)CoCl$_2$ and [Co(9S3)$_2$]Cl$_2$.

An acetonitrile solution of CoCl$_2$ was treated with both one and two

equivalents of 9S3 under an inert atmosphere. The results were essentially the same in both cases, namely a navy precipitate immediately formed. In both cases, the chloride salts are not readily soluble in acetonitrile but are soluble in water. The (9S3)CoCl$_2$ (**33**) complex exhibits stretches in the IR for the 9S3 ligand at 1439 (s), 1410 (s), 1274 (w), 937 (m), 904 (s), 825 (s) and 820 (m) cm^{-1}. Assuming the environment around the cobalt(II) metal center is octahedral, either one site for this complex is open or else it is occupied by solvent. The reaction carried out in acetonitrile led to a product with two weak ν(C≡N) stretches at 2279 and 2244 cm^{-1}. The [Co(9S3)$_2$]Cl$_2$ (**34**) complex exhibits stretches in the IR spectrum for the 9S3 ligand at 1455 (m), 1441 (m), 1405 (m), 1279 (m), 936 (m), 902 (s), 820 (s) cm^{-1}. In both cases, the IR data demonstrates the presence of the 9S3 ligand.

B. Reactivity Studies

(1) Reaction between [TpFe(CH$_3$CN)$_3$](CF$_3$SO$_3$)$_2$ and K[TpFe(CN)$_3$].

Equimolar solutions of [TpFe(CH$_3$CN)$_3$](CF$_3$SO$_3$)$_2$ and K[TpFe(CN)$_3$] were reacted by addition of the solvated precursor into the cyanide complex. A green precipitate formed almost immediately leaving behind a red solution. The IR data for the green precipitate indicates that redistribution of the ligands has occurred. The IR data consist of two peaks in the cyanide region at 2090 (m) and 2066 (m) cm^{-1}. No ν(B-H) stretch was observed. The

v(C≡N) mode for K[TpFe(CN)$_3$] is located at 2118 cm^{-1}, therefore the cyanide species in the product is either in a different environment or the metal center is Fe^{II} instead of Fe^{III}. A v(B-H) stretch (2474 cm^{-1}) appears in IR data for the orange/red solution with no cyanide stretches being evident. This implies that [FeTp$_2$]$^+$ is being formed, because if neutral FeTp$_2$ had formed, it would have precipitated from solution due to its low solubility. The green precipitate contains an iron(II) cyanide species as judged by the fact that the cyanide stretches occur at lower energies than the corresponding modes for the original Fe^{III} starting material.

(2) Reaction between [Et$_4$N]$_2$[TpCo(CN)$_3$] and (dien)Ni(NO$_3$)$_2$.

An excess of (dien)Ni(NO$_3$)$_2$ was combined with [Et$_4$N]$_2$[TpCo(CN)$_3$] which led to the production of a green precipitate and a colorless solution. The IR spectrum of the green precipitate contains a strong v(C≡N) mode at 2164 cm^{-1}, but no v(B-H) stretch was evident. The v(C≡N) is shifted to higher energy from the [Et$_4$N]$_2$[TpCo(CN)$_3$] starting material at 2127 (m) and 2112 (m) cm^{-1}, which is an indication that the nitrogen end of the cyanide ligand is bound to another metal.

(3) Reaction of [Et$_4$N]$_3$[(CO)$_3$Mo(CN)$_3$] with [(9S3)Co(CH$_3$CN)$_3$](PF$_6$)$_2$.

An excess of [(9S3)Co(CH$_3$CN)$_3$](PF$_6$)$_2$ was added dropwise to an

acetonitrile solution of [Et$_4$N]$_3$[(CO)$_3$Mo(CN)$_3$] to yield a black precipitate.

The IR data of the black precipitate indicates the presence of cyanide, carbonyl and 9S3 ligands. A polymer could have formed, since the black precipitate formed immediately. The v(C≡O) stretches are shifted to higher energy from the parent complex to 1888 (s, br), 1792 (s, br) and 1635 (s, br) cm^{-1} from 1850 (s), 1706 (s, br) cm^{-1} which is an indication of less π-backbonding. The v(C≡N) stretch in the parent complex is located at 2065 (s) cm^{-1}, whereas the black precipitate exhibits two features at 2098 (s, br) and 2027 (s) cm^{-1}. The 9S3 modes appear at 1287 (s, br), 936 (m) and 902 (m) cm^{-1}. The v(C≡N) modes of CH$_3$CN in the cobalt starting material, have shifted from 2324 (m), 2296 (m) and 2248 (w) cm^{-1} to 2310 (w), 2284 (w) and 2248 (w) cm^{-1}. Efforts to grow crystals of the black precipitate by slow diffusion of the cobalt complex dissolved in methanol into a solution of the molybdenum complex dissolved in acetonitrile led to the immediate deposition of a black precipitate.

(4) Reaction of [Et$_4$N]$_3$[(CO)$_3$Mo(CN)$_3$] with (THF)$_3$CrCl$_3$ and Na[TpCrCl$_3$].

The complex [Et$_4$N]$_3$[(CO)$_3$Mo(CN)$_3$] was reacted with an excess of (THF)$_3$CrCl$_3$ or Na[TpCrCl$_3$] in acetonitrile. The solutions turn red with the addition of the Cr(III) complexes and both red products exhibit similar IR

data. The (THF)$_3$CrCl$_3$ starting material produced a red product with a single cyanide stretch located at 2101 (s), and carbonyl stretches at 1995 (s), 1876 (s, br) and 1760 (s, br) cm^{-1}. The product from the reaction of [TpCrCl$_3$]$^+$ complex exhibits similar cyanide and carbonyl stretches at 2096 (m), 2073 (m), 1996 (w), 1946 (w), 1883 (m) and 1782 (m, br) cm^{-1}. No v(B-H) stretches are present in the latter case indicating that the cyanide on the molybdenum complex must have displaced the Tp$^-$ ligand. Since the red product is soluble in acetonitrile, it is unlikely to be a polymer. The cyanide stretches in both cases are shifted to higher energies indicating that the nitrogen end of the cyanide ligand is bound to another metal atom. Efforts to grow crystals by slow diffusion of diethyl ether/hexanes layer into an acetonitrile solution containing the red product failed. The three carbonyls should be good facially capping ligands in much the same manner as a Tp$^-$ ligand, which would leave three orthogonal sites with cyanide for the formation of a molecular cube.

(5) Reaction between [Et$_4$N]$_3$[(CO)$_3$Mo(CN)$_3$] and (dien)Ni(NO$_3$)$_2$.

A slight excess of (dien)Ni(NO$_3$)$_2$ was added dropwise to a solution of [Et$_4$N]$_3$[(CO)$_3$Mo(CN)$_3$] to produce a yellow precipitate and a pale yellow solution. The IR spectrum of the yellow precipitate indicates the presence of both cyanide and carbonyl stretches. The cyanide stretches of

$[Et_4N]_3[(CO)_3Mo(CN)_3]$ appear at 2065 (s) cm^{-1} while that of the precipitate have shifted to higher energies, namely to 2147 (m) and 2125 (m) cm^{-1}. The carbonyl stretches for the precipitate appear at 1891 (s) and 1764 (s, br) cm^{-1}, which are higher in energy than the molybdenum starting material (1850 (s) and 1706 (s, br) cm^{-1}). A small amount of KPF$_6$ was added to the pale yellow solution in an attempt to grow crystals of the yellow precipitate. The pale yellow solution with the KPF$_6$ was removed from the dry box and evaporated with the vial cap slightly ajar to allow for slow evaporation. The purple crystals that formed were analyzed by X-ray crystallography and found to be $[Ni(dien)_2](NO_3)_2$, which is a result of a rearrangement of the starting material. The yellow precipitate, which is insoluble in most common solvents, did not change color in air. Most likely, if the compound contained Mo(0), it would readily oxidize, so it is likely that the Mo oxidation state in this yellow precipitate is higher, and, since the compound is insoluble, it may be a polymer. Efforts to grow crystals by layering $[Et_4N]_3[(CO)_3Mo(CN)_3]$ in acetonitrile with the $[(dien)Ni(NO_3)_2]$ dissolved in methanol in test tubes in the dry box yielded only yellow precipitate but no crystals.

C. Molecular Structures

(1) [TpNi(CH₃CN)₃](PF₆) (30).

The $[TpNi(CH_3CN)_3]^+$ cation possesses one Tp⁻ ligand acting as a typical facial tridentate ligand bound to Ni(1) through the nitrogen atoms. Three acetonitrile molecules complete the octahedral environment around Ni(1). The Ni and (PF₆)⁻ anions are located on special positions. The asymmetric unit is composed of one third of the molecule. The Ni(1)-N(Tp) bond length is 2.066(6) Å while the Ni(1)-N(CH₃CN) distance is 2.088(7) Å. For comparison, the Ni-N(Tp) bond distances in NiTp₂ are in the range of 2.104(3) to 2.087(2) Å. The Ni(1)-N(CH₃CN) bond distances are longer than the corresponding distances to the Tp, indicating that they are not coordinated as tightly to the metal. The angle between the coordinated acetonitrile molecules is 87.4°, whereas the angle between the pyrazole rings is 88.1(2)°. The trans angle between a pyrazolylborate nitrogen atom and an acetonitrile molecule is 166.3(6)°. The angle C(5)-C(4)-N(3), subtended by the CH₃CN ligand is nearly ideal at 177.8°. The C-N bonds within the acetonitrile ligands are typical (e.g. 1.135(10) Å). Selected bond distances and angles are given in Table 3.4.

(2) [FeTp₂](BF₄) (35).

The $[FeTp_2]^+$ cation in (35) possesses two Tp ligands that act as tridentate facial ligands coordinated to Fe(1) through the nitrogen atoms. The Fe(1)-

N(Tp) bond lengths are in the range of 1.930(5) – 1.979(6) Å and the Fe(2)-N(Tp) distances are in the range of 1.933(5) – 1.966(6) Å. The angles between pyrazole rings around Fe(1) are in the range 88.6(2) – 91.4(2)°. The angles between the pyrazole rings around Fe(2) are between 88.8(2) and 91.2(2)°. The asymmetric unit of this molecule is one-half of the two iron atoms Fe(1) and Fe(2) and one $[BF_4]^-$ anion. In the asymmetric unit, the environment around Fe(1) consists of one complete Tp^- ligand. The environment around Fe(1) consists of four Fe(1)-N(Tp) bonds, two of each at 1.930(5) and 1.939(5) Å and two longer Fe(1)-N(Tp) bond lengths of 1.979(6) Å. In contrast, the environment around Fe(2) has four longer Fe(2)-N(Tp) bond lengths with two each at 1.966(5) and 1.960(5) Å, and two Fe(2)-N(Tp) bond distances that are slightly shorter at 1.933(5) Å. Selected bond distances and bond angles are listed in Table 3.5.

D. Magnetic Data

Magnetic susceptibility studies were conducted to establish the ground state spin values for the new paramagnetic molecular building blocks. This information is useful for predicting the number of unpaired electrons that one might expect for a given molecular cube assembly reaction.[20] Magnetic moments at room temperature for molecular cube precursors are summarized in Table 3.6.

Table 3.4. Selected bond distances [Å] and angles [°] for [TpNi(CH₃CN)₃](PF₆) (30).

$[TpNi(CH_3CN)_3](PF_6)$

Bond Distances

A	B	A-B [Å]
Ni(1)	N(1)	2.066(6)
Ni(1)	N(3)	2.088(6)
C(3)	N(3)	1.135(10)

Bond Angles

A	B	C	A-B-C [°]
N(1)	Ni(1)	N(1a)	88.1(2)
N(1)	Ni(1)	N(3)	94.0(2)
Ni(1)	N(3)	C(4)	166.3(6)
N(3)	C(4)	C(5)	177.8(8)

Table 3.5. Selected bond distances [Å] and angles [°] for [FeTp$_2$](BF$_4$) (**35**).

Bond Distances

A	B	A-B [Å]
Fe(1)	N(1)	1.930(5)
Fe(1)	N(3)	1.939(5)
Fe(1)	N(5)	1.979(6)
Fe(2)	N(9)	1.960(5)
Fe(2)	N(11)	1.966(5)

Bond Angles

A	B	C	A-B-C [°]
N(1)	Fe(1)	N(3)	89.5(2)
N(1)	Fe(1)	N(5)	91.3(2)
N(3)	Fe(1)	N(5)	91.4(2)
N(7)	Fe(2)	N(11)	90.2(2)
N(9)	Fe(2)	N(11)	91.2(2)
N(7)	Fe(2)	N(9)	89.6(2)

Table 3.6. Summary of magnetic susceptibility data for cube precursors at room temperature.

Complex		μ_{eff} (B. M.)	g value
[TpCo(CH$_3$CN)$_3$](BF$_4$)	(24)	3.69	2.0
[TpCo(CH$_3$CN)$_3$](CF$_3$SO$_3$)	(25)	4.33	2.0
[Et$_4$N]$_2$[TpCo(CN)$_3$]	(27)	1.68	1.9
[TpNi(CH$_3$CN)$_3$](BF$_4$)	(28)	2.7	2.0
[FeTp$_2$](BF$_4$)	(35)	1.86	2.16

159

The $t_{2g}^6 e_g^2$ electron configuration for a Ni^{II} center in [TpNi(CH$_3$CN)$_3$](BF$_4$) (**28**) leads to a μ_{eff} = 2.7 B.M. and g = 2. The experimentally observed μ_{eff} and g values deviate slightly from the predicted spin-only value of 2.83 B.M. and g = 2, but are consistent with literature reports of other octahedral Ni^{II} complexes.[21] The $t_{2g}^5 e_g^2$ electron configuration for a Co^{II} center in [TpCo(CH$_3$CN)$_3$]X with X = (BF$_4$)$^-$ (**24**), (CF$_3$SO$_3$)$^-$ (**25**) lead to a μ_{eff} = 3.69 and 4.33 B.M. with a g = 2 respectively, which are typical values for the Co^{II} configuration.[20]

The low-spin $t_{2g}^6 e_g^1$ electron configuration for the Co^{II} center in [TpCo(CN)$_3$]$^{2-}$ leads to a μ_{eff} = 1.68 B.M. and g = 1.9, in good agreement with the predicted spin-only values of μ_{eff} = 1.73 B.M. and g = 2. The low-spin $t_{2g}^5 e_g^0$ electron configuration for a Fe^{III} center in [FeTp$_2$](BF$_4$) (**35**) leads to μ_{eff} = 1.86 B.M. with a g = 2.16 which are slightly higher than the predicted spin-only values of 1.73 B.M. and g ~ 2.0. The observed values deviate due to spin-orbit coupling.[20]

4. SUMMARY AND CONCLUSIONS

The reaction of NaTp with the solvated precursors, [M(CH$_3$CN)$_6$]X$_2$, is a convenient non-aqueous route to the corner 'building blocks" [TpM(CH$_3$CN)$_3$]$^{n+}$. It is difficult to avoid the formation of the MTp$_2$ complexes, as they are stable products once formed. A problem with these

types of reactions is that the by-product salt NaX is difficult to remove completely. This excess salt poses a problem for the next step, namely preparation of $[TpM(CN)_3]^{n-}$ from $[TpM(CH_3CN)_3]^{n+}$ because the contaminated sample of the latter precludes the use of a stoichiometric addition of CN^-. The synthetic approach to $K[TpFe(CN)_3]$ is more straightforward, since three equivalents of cyanide can be added directly to the $Na[TpFeCl_3]$ complex, thereby leading to the formation of $[TpFe(CN)_3]^-$ and KCl. If the $[TpM(CN)_3]^{n-}$ complexes can be obtained in sufficient quantity, reactions of these anions with metal ions in water, the solvent of choice used for the corresponding tacn chemistry of Long and co-workers, is a promising avenue for future work.

5. REFERENCES

1. Dunbar, K. R.; Heintz, R. A. *Prog. Inorg. Chem.* **1997**, *45*, 283 and references therein.

2. Klausmeyer, K. K.; Wilson, S. R.; Rauchfuss, T. B. *J. Am. Chem. Soc.* **1998**, *121*(*12*), 2705.

3. (a) Contakes, S. M.; Klausmeyer, K. K.; Milberg, R. M.; Wilson, S. R.; Rauchfuss, T. B. *Organometallics* **1998**, *17*, 3633. (b) Contakes, S. M.; Schmidt, M.; Rauchfuss, T. B. *Chem. Commun.* **1999**, 1183. (c) Contakes, S. M.; Klausmeyer, K. K.; Rauchfuss, T. B. *Inorg. Chem.* **2000**, *39*, 2069.

4. (a) Heinrich, J. L.; Berseth, P. A.; Long, J. R. *Chem. Commun.* **1998**, 1231.

5. (a) Shores, M. P.; Beauvais, L. G.; Long, J. R. *J Am. Chem. Soc* **1999**, *121*, 775. (b) Shores, M. P.; Beauvais, L. G.; Long, J. R. *Inorg. Chem.* **1999**, *38*, 1648. (c) Bennett, M. V.; Shores, M. P.; Beauvais, L. G.; Long, J. R. *J. Am. Chem. Soc.* **2000**, *122*, 6664.

6. Heintz, R. A.; Smith, J. A.; Szalay, P. S.; Weisgerber, A.; Dunbar, K. R. submitted to Inorganic Syntheses.

7. Trofimenko, S. Inorganic Syntheses 1970, 12, 99.

8. SAINT 1000 and 6.0, Bruker Analytical X-ray Instruments, Madison, WI, 53719 (**1999** and **2000**)

9. Sheldrick, G. M. "SADABS, Siemens Area Detector Absorption Correction", Univ. of Gottingen, Gottingen, Germany (**1998**).

10. Altomare, A.; Burla, M. C.; Camalli, M.; Cascarano, G. L.; Giacovazza, C.; Guagliardi, A.; Moliterni, A. G. G.; Polidori.G.; Spagna, R. *J. Appl. Crystallogr.* **1999**, *32*, 115.

11. Sheldrick, G. M. SHELXTL version 5.10, Reference Manuel, Bruker Industrial Automation, Analytical Instrument, Madison, WI 53719 (**1999**). Program for Refinement of Crystal Structure, University of Göttingen, Göttingen, Germany.

12. Trofimenko, S. *J. Am. Chem. Soc.* **1967**, *89*, 3170.

13. Trofimenko, S. *Chem. Rev.* **1993**, *93*, 943.

14. For details regarding [TpCo(CH₃CN)₃](PF₆) please refer to the Dissertation of P. S. Szalay Jr, Michigan State University August, 2001.

15. Cho, S.-H.; Whang, D.; Han, K.-N.; Kim, K. *Inorg. Chem.* **1992**, *31*, 519.

16. Bandoli, G.; Clemente, D. A.; Paolucci, G.; Doretti, L. *Cryst. Struct. Comm.* **1979**, *8*, 965.

17. Churchill, M. R.; Gold, K.; Maw, C. E. *Inorg. Chem.* **1970**, *9*, 1597.

18. Setzer, W. N.; Ogle, C. A.; Wilson, G. S.; Glass, R. S. *Inorg. Chem.* **1983**, *22*, 266.

19. (a) Hartman, J. A. R.; Hintsa, E. J.; Cooper, S. R. *J. Am. Chem. Soc.* **1986**, *108*, 1208. (b) Baker, P. K.; Drew, M. G. B.; Meehan, M. M. *Inorg. Chem,* **1999**, *2*, 442.

20. (a) Carlin, R. L. Magnetochemistry, Springer-Verlag Berlin Heidelberg **1986**. (b) Mabbs, F. E. Machin, D. J. Magnetism and Transition Metal Complexes, London Chapman and Hall **1973**.

Chapter IV

Cyanide Assemblies and Clusters

1. INTRODUCTION

Prussian blue, $Fe_4[Fe(CN)_6]_3 \cdot 14H_2O$, is an example of a 3-D cyanide structure that exhibits ferromagnetic ordering at 5.5 K.[1] Analogues of Prussian blue have been prepared with numerous other metals as illustrated by the list provided in Table 1.1.[2] These materials have also been the inspiration for new architectures that involve the use of capping groups to lower the dimensionality.[3] For example, if hexacyanometallate anions are reacted with metal centers capped with various bidentate, tridentate or tetradentate ligands, new motifs can be formed. In this vein, Okãwa and co-workers reported early results in this field including 1-D, 2-D and 3-D architectures.[4] One of the first reported examples is a 1-D rope-ladder motif, $[Ni(en)_2]_3[Fe(CN)_6]_2 \cdot 2H_2O$, in which Ni atoms are coordinated to two ethylenediamine (en) molecules in both the *cis* and *trans* arrangements. This group has reported a series of compounds with this rope-ladder motif simply by replacing the Fe^{III} center with Mn^{III}, Cr^{III} or Co^{III}. The magnetic data reveal no magnetic ordering with the Mn^{III}, Cr^{III} or Co^{III} compounds but the Fe^{III} complex is metamagnetic.[5] More recently the material $[Mn(en)]_3[Cr(CN)_6]_2 \cdot 4H_2O$ was prepared which exhibits a 3-D structure orders at 69 K; this is the highest ordering temperature among structurally

characterized molecular based magnets.[6]

In our laboratory, efforts are being made to synthesize motifs such as molecular squares and cubes by using pre-designed precursors. The main approach is to react the precursors cis-$[(N\text{-}N)_2M(S)_2]^n$ or fac-$[(L_3)M(S)_3]^n$, with hexacyanometallate anions to prepare discrete structures with interesting magnetic properties.

2. EXPERIMENTAL

A. PHYSICAL METHODS

Infrared spectra were recorded on a Nicolet 42 spectrophotometer in the Chemistry Department at Michigan State University or on a Nicolet 470 in the Chemistry Department at Texas A&M University. Infrared spectra were recorded at 4 cm^{-1} resolution and 32 scans unless otherwise stated. Solid samples were measured as Nujol mulls on KBr or CsI plates. Elemental analyses were performed at Desert Analytics, Tucson, AZ or in the Chemistry Department at Michigan State University; in the latter case a Perkin and Elmer Series II CHNS/O analyzer 2400 was used. Magnetic measurements were performed on a Quantum Design MPMS-5 instrument equipped with a SQUID sensor housed in the Physics and Astronomy Department at Michigan State University or a MPMS-XL SQUID magnetometer located in the Chemistry Department at Texas A&M University. Scanning electron

micrographs (SEM) were obtained on a JEOL 6400 instrument at the Electron Microscopy Center at Texas A & M University.

B. SYNTHESES

The starting materials $K_3[Fe(CN)_6]$ and $K_4[Fe(CN)_6]$ were purchased from Aldrich and used without further purification. Acetone and acetonitrile were distilled over 3 Å molecular sieves. Benzene, diethyl ether, THF and toluene were distilled over sodium-potassium/benzophenone, whereas methylene chloride was distilled over P_2O_5 under nitrogen atmosphere. Methanol and ethanol were dried over magnesium alkoxide.

(1) Synthesis of $\{Mn(H_2O)_2[Mn(2,2'-bpym)(H_2O)]_2[Fe(CN)_6]_2\}_\infty$ (36)

Three equivalents of $[(2,2'-bpym)_2Mn(H_2O)_2](BF_4)_2$ (0.049 g, 0.084 mmol) or $[(2,2'-bpym)_2Mn(H_2O)_2](SO_4)^7$ in 25 mL of water were reacted with two equivalents of $K_3[Fe(CN)_6]$ (0.018 g, 0.056 mmol) in aqueous (25 mL) solution to yield a brown precipitate and a yellow filtrate after 12 h. The brown precipitate was collected by filtration and washed with water (2 x 10 mL) followed by acetone (2 x 10 mL). The filtrate was slowly evaporated to give a brown crystalline material, which was washed with water to remove soluble by-products. Combined yield: (0.020 g, 64%) IR data (Nujol, cm^{-1}): 2146 (s), 2119 (s), 2065 (w), 1609 (m), 1591 (w), 1572 (s), 1558 (s), 1407

(s), 1301 (w), 1267 (w), 1208 (w), 1146 (w), 1103 (m), 1010 (m), 960 (m),

825 (m), 761 (m), 689 (w), 657 (m), 526 (w), 419 (m), 226 (w).

(2) Syntheses of {[Co(2,2'-bpy)₂]₃[Fe(CN)₆]₂}⁺ (37)

A. Reaction of (2,2'-bpy)₂Co(CF₃SO₃)₂ with [Et₄N]₃[Fe(CN)₆]

Three equivalents of (2,2'-bpy)₂Co(CF₃SO₃)₂ (0.103 g, 0.154 mmol)

dissolved in 20 mL of water were reacted with two equivalents of

[Et₄N]₃[Fe(CN)₆] (0.062 g, 0.103 mmol) dissolved in 25 mL of water. The

reaction was stirred overnight, after which time a blue precipitate was

obtained by filtration and washed with water (2 x 10 mL) followed by

acetone (2 x 10 mL). IR data for the blue precipitate (Nujol, cm⁻¹): 2137 (w),

2106 (m), 2096 (m), 2066 (s), 1635 (w, br), 1605 (m), 1567 (w), 1498 (m),

1325 (w), 1313 (m), 1276 (w), 1243 (m), 1162 (m), 1110 (w), 1074 (w),

1037 (w), 1027 (w), 966 (w, br), 936 (w), 917 (w), 890 (w), 844 (w), 801

(w), 770 (m), 737 (m), 671 (w), 651 (w), 589 (w), 545 (m), 503 (w), 467 (w),

440 (w), 424 (w), 415 (w), 374 (w), 351 (w).

B. Reaction of [Co(2,2'-bpy)₃](ClO₄)₂ with K₄[Fe(CN)₆]

Three equivalents of [Co(2,2'-bpy)₃](ClO₄)₂ (0.233 g, 0.321 mmol) dissolved

in 25 mL of water and K₄[Fe(CN)₆] (0.090 g, 0.213 mmol) in aqueous (25

mL) solution were added together and stirred overnight to yield a blue

precipitate. The navy blue precipitate was collected by filtration, washed with

169

water (2 x 10 mL) followed by acetone (2 x 10 mL). Yield: 95.4 mg IR data

of the blue precipitate (Nujol, cm^{-1}): 2138 (m), 2108 (m), 2094 (m), 2068 (s),

1639 (w, br), 1606 (m), 1567 (m), 1498 (m), 1314 (m), 1274 (w), 1243 (m),

1162 (m), 1110 (w), 1074 (m), 1033 (w), 1029 (w), 968 (w), 935 (w), 917

(w), 890 (w), 843 (w), 802 (w), 768 (m), 669 (w), 652 (w), 589 (w), 545 (m),

503 (w), 468 (w), 415 (w), 377 (w), 351 (w), 282 (w), 254 (w), 240 (w).

C. Reaction of (2,2'-bpy)$_2$Co(CF$_3$SO$_3$)$_2$ with K$_3$[Fe(CN)$_6$]

A deoxygenated water solution (25 mL) of K$_3$[Fe(CN)$_6$] (0.085 g, 0.258

mmol) was treated with three equivalents of (2,2'-bpy)$_2$Co(CF$_3$SO$_3$)$_2$ (0.258 g,

0.386 mmol) in 25 mL of deoxygenated water. After stirring for 12 h, the

resulting navy blue precipitate was filtered under nitrogen, washed with water

(2 x 10 mL) followed by 10 mL of diethyl ether, and finally dried in air.

Yield: 206 mg. IR data of the navy blue precipitate. (Nujol, cm-^{1}): 2141 (w),

2108 (m), 2094 (m), 2067 (s), 1653 (w), 1606 (m), 1605 (m), 1575 (w), 1569

(w), 1560 (w), 1558 (w), 1544 (w), 1365 (s), 1309 (m), 1274 (w), 1244 (w),

1169 (m), 1159 (m), 1108 (w), 1074 (m), 1037 (m), 1030 (m), 966 (m), 934

(w), 918 (w), 891 (w), 840 (w), 769 (m), 733 (m), 668 (w), 652 (w), 587 (w),

542 (m), 500 (w), 470 (w), 459 (w), 416 (w).

D. Reaction of (2,2'-bpy)$_2$Co(CF$_3$SO$_3$)$_2$ with [K-18-C-6]$_3$[Fe(CN)$_6$]

Three equivalents of (2,2'-bpy)$_2$Co(CF$_3$SO$_3$)$_2$ (0.200 g, 0.299 mmol)

dissolved in 25 mL of acetonitrile were reacted with two equivalents of [K-18-C-6]₃[Fe(CN)₆] (0.224 g, 0.199 mmol) in acetonitrile (25 mL). The reaction was stirred for 12 h, after which time a navy blue precipitate was collected by filtration, washed with acetonitrile (2 x 10 mL) followed by acetone (2 x 10 mL), and dried in air. The filtrate was colorless. Yield: 174.5 mg. IR data of the navy blue precipitate (Nujol, cm^{-1}): 2138 (w), 2106 (s), 2063 (s, br), 1639 (m), 1606 (s), 1567 (m), 1500 (m), 1314 (m), 1244 (m), 1162 (m), 1109 (m), 1074 (m), 1038 (m), 968 (w), 890 (w), 769 (s), 653 (w), 590 (w), 546 (m), 468 (w), 415 (w), 351 (w).

E. Reaction of (2,2'-bpy)₂Co(CF₃SO₃)₂ with [K-18-C-6]₃[Fe(CN)₆]

A sample of (2,2'-bpy)₂Co(CF₃SO₃)₂ (0.201 g, 0.300 mmol) dissolved in 25 mL of methanol was combined with two equivalents of [K-18-C-6]₃[Fe(CN)₆] (0.225 g, 0.201 mmol) in 25 mL of methanol. After 12 h of stirring, the navy blue precipitate that had formed was collected by filtration, washed with methanol (2 x 10 mL) and diethyl ether (10 mL), and dried in air. The filtrate was colorless. Yield: 142.7 mg. IR data of the navy blue precipitate (Nujol, cm^{-1}): 2144 (w), 2105 (m), 2056 (s, br), 1636 (w, br), 1600 (s), 1566 (m), 1497 (w), 1359 (s), 1325 (w), 1312 (m), 1271 (m), 1241 (s), 1222 (m), 1154 (s), 1106 (m), 1069 (m), 1028 (s), 972 (w), 921 (w), 894 (w), 844 (w), 801 (w), 765 (s), 733 (m), 668 (w), 637 (m), 584 (m), 543 (m), 463 (m), 412 (m).

F. Reaction of (2,2'-bpy)$_2$Co(CF$_3$SO$_3$)$_2$ with K$_3$[Fe(CN)$_6$]

Three equivalents of (2,2'-bpy)$_2$Co(CF$_3$SO$_3$)$_2$ (0.275 g, 0.411 mmol) dissolved in 25 mL of water were treated with a water solution (25 mL) of K$_3$[Fe(CN)$_6$] (0.090 g, 0.273 mmol) which led to the production of an immediate navy blue precipitate. The solid was collected by filtration, washed with water (2 x 10 mL) followed by 10 mL of diethyl ether, and dried in air. Yield: 232 mg. IR data of the navy blue precipitate (Nujol, cm^{-1}): 2141 (w), 2106 (m), 2097 (m), 2066 (s), 1636 (w, br), 1606 (m), 1604 (m), 1574 (w), 1567 (w), 1365 (s), 1307 (m), 1273 (w), 1245 (w), 1171 (m), 1161 (m), 1110 (w), 1074 (m), 1032 (m), 968 (m), 938 (w), 921 (w), 891 (w), 845 (w), 801 (w), 769 (m), 737 (s), 648 (w), 588 (w), 545 (m), 463 (w), 412 (w).

G. Reaction of [Co(2,2'-bpy)$_3$](ClO$_4$)$_2$ with K$_3$[Fe(CN)$_6$]

A sample of [Co(2,2'-bpy)$_3$](ClO$_4$)$_2$ (0.218 g, 0.300 mmol) dissolved in 25 mL of water was reacted with two equivalents of K$_3$[Fe(CN)$_6$] (0.067 g, 0.204 mmol) in 25 mL of water. The resulting navy blue solid was collected by filtration, washed with water (2 x 10 mL) followed by 10 mL of diethyl ether, and dried in air. Yield: 170.1 mg. IR data of the navy blue precipitate (Nujol, cm^{-1}): 2139 (w), 2109 (m), 2094 (m), 2067 (s, br), 1650 (w, br), 1638 (w, br), 1606 (m), 1568 (w), 1500 (w), 1361 (s), 1332 (w), 1315 (m), 1276 (w), 1244 (m), 1163 (m), 1096 (m), 1076 (m), 1039 (m), 1018 (w), 969 (w),

890 (w), 839 (w), 801 (w), 767 (s), 733 (m), 670 (w), 652 (w), 625 (w), 588 (w), 545 (m), 501 (w), 464 (w), 415 (w).

H. Reaction of [Co(2,2'-bpy)$_3$](ClO$_4$)$_2$ with [K-18-C-6]$_3$[Fe(CN)$_6$]

An aqueous (25 mL) solution of [Co(2,2'-bpy)$_3$](ClO$_4$)$_2$ (0.219 g, 0.302 mmol) was reacted with [K-18-C-6]$_3$[Fe(CN)$_6$] (0.226 g, 0.201 mmol) in 25 mL of water. After 12 h, a navy blue precipitate was collected by filtration and washed with water (2 x 10 mL) followed by 10 mL of diethyl ether and finally dried in air. Yield: 148.6 mg. IR data of the navy blue precipitate (Nujol, cm^{-1}): 2139 (w), 2109 (m), 2094 (m), 2067 (s, br), 1645 (w, br), 1606 (m), 1568 (w), 1500 (m), 1362 (s), 1329 (w), 1315 (m), 1278 (w), 1244 (m), 1220 (w), 1175 (w), 1163 (m), 1110 (m), 1072 (m), 1039 (m), 1025 (w), 967 (w), 891 (w), 841 (w), 802 (w), 767 (s), 731 (m), 670 (w), 653 (w), 588 (w), 544 (m), 468 (w), 416 (w).

I. Reaction of (2,2'-bpy)$_2$Co(CF$_3$SO$_3$)$_2$ with K$_4$[Fe(CN)$_6$]

Three equivalents of (2,2'-bpy)$_2$Co(CF$_3$SO$_3$)$_2$ (0.253 g, 0.378 mmol) in 25 mL of water were reacted with K$_4$[Fe(CN)$_6$] (0.107 g, 0.254 mmol) in 25 mL of water. After 12 h of stirring, a navy blue precipitate was collected by filtration and washed with water (2 x 10 mL) followed by 10 mL of diethyl ether and dried in air. The intensely colored blue filtrate was slowly evaporated to yield a navy blue solid, which was washed with water (1 x 10 mL) and diethyl

ether (10 mL) and dried in air. IR data on both batches of blue solids indicate that the samples are the same product. Combined yield: 98.8 mg. IR data of the navy blue precipitate (Nujol, cm^{-1}): 2140 (w), 2108 (m), 2094 (m), 2067 (s, br), 1639 (w, br), 1606 (s), 1566 (w), 1499 (w), 1357 (s), 1331 (w), 1314 (m), 1278 (w), 1244 (m), 1178 (w), 1163 (m), 1131 (w), 1109 (m), 1073 (m), 1037 (m), 1030 (m), 968 (w), 891 (w), 845 (w), 801 (w), 769 (s), 735 (m), 672 (w), 651 (w), 618 (w), 588 (m), 542 (m), 467 (w), 417 (w).

(3) Synthesis of [Ni(2,2'-bpy)$_2$(OH$_2$)][Ni(2,2'-bpy)$_2$]$_2$[Fe(CN)$_6$]$_2$ (38)

Three equivalents of [(2,2'-bpy)$_2$Ni(OH$_2$)$_2$](CF$_3$SO$_3$)$_2$ (0.159 g, 0.238 mmol) in 25 mL of water were reacted with K$_3$[Fe(CN)$_6$] (0.052 g, 0.159 mmol) in 25 mL of water. An immediate yellow/brown precipitate formed. The reaction was stirred for 12 h, after which time the precipitate was collected by filtration and washed with (2 x 10 mL) of water followed by 10 mL of acetone and dried in air. The yellow filtrate was evaporated next to an oven, and after a certain period of time, a yellow brown precipitate was present admixed with dark orange/red/brown crystals. These crystals were identified as [Ni(2,2'-bpy)$_2$(OH$_2$)][Ni(2,2'-bpy)$_2$]$_2$[Fe(CN)$_6$]$_2$ (38). Yield of yellow/brown solid 68.7 mg. IR data of the initial yellow/brown precipitate (Nujol, cm^{-1}): 2142 (m), 2113 (s), 1630 (w), 1604 (s), 1598 (s), 1575 (m), 1567 (m), 1313 (s), 1247 (w), 1170 (w), 1156 (m), 1103 (w), 1060 (w), 1043

(w), 1022 (m), 971 (w), 891 (w), 847 (w), 811 (w), 765 (s), 736 (s), 652 (m), 632 (m), 413 (m), 283 (w), 251 (w), 247 (w), 221 (w), 215 (w), 212 (w), 208 (w), 205 (w), 201 (w).

(4) Synthesis of [Zn(phen)₃][Zn(phen)₂]₂[Fe(CN)₆]₂ (39)

An aqueous solution (25 mL) of (phen)$_2$Zn(NO$_3$)$_2$ (0.103 g, 0.187 mmol)[7] reacts instantaneously with K$_3$[Fe(CN)$_6$] (0.041 g, 0.124 mmol) in 25 mL of water to yield a yellow precipitate. After the reaction was stirred for 12 h, the yellow precipitate was collected by filtration. The yellow precipitate was washed with water (2 x 10 mL) followed by acetone (2 x 10 mL) and dried in air. The resulting yellow filtrate slowly evaporated to produce orange crystals of [Zn(phen)$_3$][Zn(phen)$_2$]$_2$[Fe(CN)$_6$]$_2$. Yield: 96.2 mg. IR data for the yellow precipitate (Nujol, cm^{-1}): 2150 (m), 2113 (m), 2062 (w), 1623 (m), 1579 (m), 1517 (m), 1425 (s), 1341 (w), 1305 (w), 1260 (w), 1224 (m), 1143 (m), 1103 (m), 966 (w), 867 (m), 850 (m), 774 (w), 640 (m), 421 (m), 288 (m), 241 (w), 225 (w), 208 (w). IR data of the orange crystals (Nujol, cm^{-1}): 2151 (m), 2143 (w), 2127 (w), 2108 (m), 1623 (m), 1578 (m), 1517 (m), 1142 (m), 1103 (m), 965 (w, br), 867 (m), 847 (s), 640 (m), 421 (m), 285 (w), 241 (w).

C. REACTIVITY STUDIES

(1) Reaction of (2,2'-bpy)₂Mn(CF₃SO₃)₂ with [K-18-C-6]₃[Fe(CN)₆]

Three equivalents of (2,2'-bpy)₂Mn(CF₃SO₃)₂ (0.072 g, 0.108 mmol) in 20 mL of acetonitrile/20 mL of methanol were reacted with two equivalents of [K-18-C-6]₃[Fe(CN)₆] (0.078 g, 0.076 mmol) in a mixture of acetonitrile and methanol (20mL/20mL) After 1 hour, a brown precipitate was present in a colorless filtrate. The brown precipitate was collected by filtration, washed with methanol (2 x 10 mL) followed by acetone (2 x 10 mL), and dried in air. Yield: 35.4 mg. IR data (Nujol, cm⁻¹): 2143 (s), 2119 (m), 2063 (m), 1622 (m), 1590 (m), 1517 (w), 1494 (w), 1424 (s), 1342 (w), 1302 (w), 1260 (m), 1222 (m), 1143 (m), 1102 (m), 1030 (m), 865 (m), 848 (s), 774 (w), 639 (m), 420 (m), 277 (w).

(2) Reaction of (2,2'-bpy)₂Mn(CF₃SO₃)₂ with K₃[Fe(CN)₆]

An aqueous solution (25 mL) of (2,2'-bpy)₂Mn(CF₃SO₃)₂ (0.076 g, 0.114 mmol) was mixed with K₃[Fe(CN)₆] (0.038 g, 0.115 mmol) in 25 mL of water. After 1 h, a brown precipitate had formed which was collected by filtration, washed with water (2 x 10 mL) and acetone (2 x 10 mL), and finally dried in air. Yield: 38.4 mg. IR data of the brown precipitate (Nujol, cm⁻¹): 3368 (s, br), 2155 (w), 2142 (s), 2133 (s), 2122 (s), 2112 (s), 2078 (w), 2061 (w), 2038 (w), 1631 (w), 1601 (s), 1595 (s), 1575 (m), 1566 (m), 1490 (m), 1439 (s), 1315 (m), 1245 (m), 1220 (w), 1174 (m), 1156 (m), 1116 (w), 1100 (w), 1061 (m), 1043 (w), 1016 (s), 977 (w), 965 (w), 902 (w), 890

(w), 814 (w), 767 (s), 737 (s), 647 (m), 626 (m), 411 (m), 351 (w), 227 (m).

(3) Reaction of (2,2'-bpy)$_2$Mn(CF$_3$SO$_3$)$_2$ with K$_3$[Fe(CN)$_6$]

Three equivalents of (2,2'-bpy)$_2$Mn(CF$_3$SO$_3$)$_2$ (0.034 g, 0.052 mmol) in 15

mL of water were reacted with K$_3$[Fe(CN)$_6$] (0.011 g, 0.034 mmol) in 15 mL

of water. A brown precipitate was apparent after 1 h. After 12 h of stirring,

the brown precipitate was collected by filtration, washed with water (2 x 10

mL) and acetone (2 x 10 mL), and dried in air. Yield: 9.2 mg. IR (Nujol, cm$^-$

^{1}): 2156 (w), 2142 (m), 2132 (m), 2119 (m), 2114 (m), 2080 (w), 2061 (w),

2026 (w), 1627 (w), 1601 (m), 1595 (s), 1575 (m), 1563 (m), 1489 (m), 1439

(s), 1365 (m), 1342 (w), 1314 (m), 1245 (w), 1170 (w), 1156 (m), 1101 (w),

1061 (w), 1042 (w), 1015 (m), 966 (w), 890 (w), 766 (s), 737 (m), 647 (m),

626 (w), 411 (m), 236 (w), 226 (w), 218 (w), 212 (m), 202 (s).

(4) Reaction of [Mn(2,2'-bpy)$_3$](ClO$_4$)$_2$ with K$_3$[Fe(CN)$_6$]

One equivalent of [Mn(2,2'-bpy)$_3$](ClO$_4$)$_2$ (0.077 g, 0.106 mmol) in 40 mL of

water was reacted with K$_3$[Fe(CN)$_6$] (0.035 g, 0.106 mmol) in 40 mL of

water. After 12 h of stirring, the resulting brown precipitate was collected by

filtration and washed with water (2 x 10 mL) followed by (2 x 10 mL)

acetone and dried in air. Yield: 10.3 mg. IR (Nujol, cm^{-1}): 2136 (m), 2120 (s),

2057 (m), 1631 (w), 1594 (s), 1575 (m), 1565 (m), 1485 (m), 1313 (m), 1246

(m), 1216 (w), 1174 (w), 1157 (m), 1100 (m), 1062 (w), 1040 (w), 1014 (m),

968 (w, br), 935 (w), 915 (w), 902 (w), 890 (w), 844 (w), 812 (w), 767 (s),

737 (m), 646 (m), 625 (m), 589 (w), 412 (m), 211 (w).

(5) Reaction of [Mn(2,2'-bpy)₃](ClO₄)₂ with [K-18-C-6]₃[Fe(CN)₆]

The precursors [Mn(2,2'-bpy)₃](ClO₄)₂ (0.160 g, 0.222 mmol) and [K-18-C-6]₃[Fe(CN)₆] (0.165 g, 0.161 mmol) were combined in a Schlenk flask under a nitrogen atmosphere, treated with 100 mL of acetonitrile, and refluxed for 12 h. During this time, a brown precipitate had formed in a colorless solution. The solution was removed via a cannula and the brown precipitate was washed with acetonitrile (2 x 20 mL) and diethyl ether (20 mL). The washings were removed each time via a cannula and the product was dried under vacuum. Yield 13.9 mg. IR data (Nujol, cm^{-1}): 2146 (s), 2118 (m), 2064 (m), 1603 (m), 1597 (m), 1575 (m), 1316 (w), 1245 (w), 1177 (w), 1157 (m), 1062 (w), 1019 (m), 772 (m), 737 (m), 651 (m), 628 (w), 420 (m), 412 (m), 230 (w), 226 (w), 219 (w), 214 (w), 212 (w), 207 (m), 206 (m), 203 (m), 202 (m).

(6) Reaction of (phen)₂Mn(CF₃SO₃)₂ with K₃[Fe(CN)₆]

Three equivalents of (phen)₂Mn(CF₃SO₃)₂ (0.067 g, 0.093 mmol) in 40 mL of water/10 mL of methanol were reacted with K₃[Fe(CN)₆] (0.021 g, 0.063 mmol) in 40 mL of water. After 1 h, a brown precipitate was observed to have formed. The reaction was stirred for a total of 12 h with no further

changes being observed. The brown precipitate was collected by filtration and washed with water (2 x 10 mL) followed by acetone (2 x 10 mL) and dried in air. Yield: 13.9mg. IR data (Nujol, cm^{-1}): 2142 (w), 2113 (m), 2090 (w), 2053 (w, br), 1733 (w), 1622 (m), 1589 (m), 1574 (m), 1514 (m), 1338 (m), 1303 (m), 1260 (w), 1219 (w), 1167 (w), 1143 (m), 1100 (m), 1087 (w), 1076 (w), 1029 (w), 1014 (w), 968 (m), 936 (w), 916 (w), 891 (m), 864 (m), 848 (s), 804 (w), 772 (m), 728 (m), 637 (w), 418 (w), 392 (w, br), 277 (w), 237 (w), 224 (w), 208 (w).

(7) Reaction of (phen)$_2$Mn(CF$_3$SO$_3$)$_2$ with [K-18-C-6]$_3$[Fe(CN)$_6$]

A water solution (25 mL) of (phen)$_2$Mn(CF$_3$SO$_3$)$_2$ (0.055 g, 0.077 mmol) was reacted with [K-18-C-6]$_3$[Fe(CN)$_6$] (0.086 g, 0.084 mmol) in 25 mL of water. After 1 h, a yellow/brown precipitate was present. After 12 h of stirring, the yellow/brown precipitate was collected by filtration and washed with 2 x 10 mL aliquots of water followed with 2 x 10 mL portions of acetone and dried in air. Yield: 14.4 mg. IR data (Nujol, cm^{-1}): 2142 (w), 2112 (m), 1622 (m), 1589 (m), 1573 (m), 1514 (m), 1422 (m), 1338 (m), 1302 (w), 1260 (w), 1221 (w), 1169 (w), 1142 (m), 1101 (m), 1022 (w, br), 970 (w), 892 (w), 864 (m), 848 (m), 804 (w), 773 (m), 727 (s), 637 (m), 513 (w, br), 438 (w), 418 (m), 393 (w), 278 (w), 219 (w), 208 (m).

(8) Reaction of (phen)$_2$Mn(CF$_3$SO$_3$)$_2$ with [K-18-C-6]$_3$[Fe(CN)$_6$]

The compound $(\text{phen})_2\text{Mn}(\text{CF}_3\text{SO}_3)_2$ (0.053 g, 0.075 mmol) was dissolved in a mixture of acetonitrile and methanol (15 mL/10 mL) and reacted with [K-18-C-6]$_3$[Fe(CN)$_6$] (0.056 g, 0.055 mmol) in 15 mL of acetonitrile/10 mL of methanol. After one hour, a brown precipitate was present which was collected by filtration after 12 h of continuous stirring. The precipitate was washed with 10 mL of acetonitrile, 10 mL of methanol and 2 x 10 mL of acetone, and finally dried aerobically. Yield: 15.2 mg. IR (Nujol, cm^{-1}): 2143 (w), 2114 (m), 2067 (w, br), 1622 (m), 1602 (w), 1590 (m), 1572 (m), 1515 (m), 1422 (m), 1340 (w), 1302 (w), 1254 (w), 1222 (w), 1168 (w), 1143 (m), 1101 (m), 1087 (m), 1050 (w), 1030 (w), 1016 (w), 970 (w), 934 (w), 916 (w), 892 (w), 864 (m), 848 (m), 806 (w), 773 (m), 728 (m), 637 (m), 589 (w), 554 (w), 510 (w), 436 (w), 418 (m), 395 (w), 277 (w), 238 (w), 219 (w), 212 (w), 206 (w).

(9) Reaction of [Co(2,2'-bpym)$_3$](BF$_4$)$_2$ with [K-18-C-6]$_3$[Fe(CN)$_6$]

Three equivalents of [Co(2,2'-bpym)$_3$](BF$_4$)$_2$ (0.058 g, 0.083 mmol) and two equivalents of [K-18-C-6]$_3$[Fe(CN)$_6$] (0.064 g, 0.055 mmol) were placed in a Schlenk flask, treated with 35 mL of acetonitrile, and refluxed for 3 days. No reaction was apparent until a few drops of water were added, after which time the solution turned purple and a purple precipitate appeared. The reaction was stirred for 12 h, after which time the colorless solution was removed via a

cannula. The purple precipitate was washed with 2 x 20 mL aliquots of acetonitrile and the washings were removed via a cannula. The solid was then washed with 20 mL of diethyl ether, the washings were removed via a cannula and discarded, and the solid was dried under vacuum. Yield: 12.8 mg. IR (Nujol, cm^{-1}): 2141 (w), 2119 (m), 2068 (s), 1638 (w, br), 1594 (w), 1576 (s), 1560 (m), 1408 (s), 1365 (m), 1352 (w), 1340 (w), 1305 (w), 1220 (w), 1168 (w), 1146 (w), 1105 (w), 1072 (w), 1026 (w), 1013 (w), 962 (w), 935 (w), 917 (w), 891 (w), 840 (w), 822 (w), 762 (m), 754 (w), 748 (w), 691 (w), 675 (w), 658 (w), 587 (w), 555 (w), 411 (w, br), 229 (w), 223 (w), 212 (m), 208 (w), 204 (m), 202 (m).

(10) Reaction of [Co(2,2'-bpym)₃](BF₄)₂ with K₃[Fe(CN)₆]

Three equivalents of [Co(2,2'-bpym)₃](BF₄)₂ (0.049 g, 0.070 mmol) in 15 mL of deoxygenated water were reacted with K₃[Fe(CN)₆] (0.015 g, 0.048 mmol) in 15 mL of deoxygenated water. The solution turned purple in color, and after 12 h, a gelatinous purple product was collected by filtration. The finely divided solid was washed with water (2 x 5 mL) followed by acetone (2 x 10 mL) and dried in air. Yield: 12.1 mg. IR data of the purple product (Nujol, cm^{-1}): 2117 (s), 2074 (s, br), 1629 (m, br), 1580 (s), 1575 (s), 1557 (s), 1407 (s), 1218 (m), 1029 (s, br), 822 (m), 760 (m), 747 (m), 689 (w), 675 (m), 659 (w), 541 (m), 466 (w), 212 (w).

(11) Reaction of (phen)₂Co(NO₃)₂ with K₃[Fe(CN)₆]

Three equivalents of $(phen)_2Co(NO_3)_2$ (0.090 g, 0.166 mmol) in 10 mL of deoxygenated water were combined with $K_3[Fe(CN)_6]$ (0.036 g, 0.111 mmol) in 15 mL of deoxygenated water. A green precipitate formed instantaneously, but the reaction was stirred for a total of 12 h to ensure that complete reaction had occurred. The green precipitate was collected by filtration, washed with water (2 x 10 mL) followed by acetone (2 x 10 mL), and dried in air. The filtrate was pale green colored and upon evaporation yielded no suitable crystals. Yield: 20.4 mg. IR (Nujol, cm^{-1}): 2144 (w), 2108 (s), 2074 (s), 1656 (m), 1629 (m, br), 1605 (m), 1584 (m), 1521 (m), 1494 (m), 1429 (s), 1413 (m), 1366 (s), 1347 (m), 1313 (m), 1262 (w), 1228 (m), 1207 (w), 1166 (w), 1153 (w), 1146 (m), 1111 (w), 1099 (w), 1039 (w), 1035 (w), 965 (w, br), 923 (w), 890 (w), 881 (w), 850 (s), 846 (s), 800 (w), 773 (w), 750 (m), 717 (s), 655 (w), 590 (w, br), 551 (w), 523 (w), 510 (w), 498 (w), 494 (w), 465 (w), 443 (w, sh), 393 (w, br), 246 (w), 239 (w), 228 (w), 222 (w), 218 (w), 214 (m), 211 (m), 209 (w), 207 (m), 205 (m), 200 (m).

(12) Reaction of (phen)₂Co(NO₃)₂ with K₃[Fe(CN)₆]

Three equivalents of $(phen)_2Co(NO_3)_2$ (0.024 g, 0.046 mmol) in 10 mL of water were combined with $K_3[Fe(CN)_6]$ (0.060 g, 0.184 mmol) in 15 mL of water to yield an instantaneous green precipitate. The reaction was stirred for

12 h, and the green precipitate was collected by filtration, washed with water (2 x 10 mL) followed by acetone (2 x 10 mL), and dried in air. The light blue filtrate was allowed to slowly evaporate which led to the formation of very thin light blue needles. Yield: 15.3 mg. IR (Nujol, cm^{-1}): 2108 (m), 2078 (m, br), 1632 (w, br), 1604 (m), 1584 (m), 1521 (m), 1491 (w), 1427 (m), 1412 (m), 1363 (m), 1345 (m), 1313 (m), 1227 (m), 1168 (w), 1154 (m), 1143 (m), 1110 (w), 1099 (w), 1040 (w), 1035 (w), 971 (w), 921 (w), 881 (w), 842 (m), 800 (w), 773 (w), 749 (m), 717 (s), 654 (w), 590 (w), 522 (w), 441 (w), 394 (w, br), 226 (w), 221 (w), 219 (w), 216 (w), 211 (m, br), 208 (m), 205 (m), 203 (m).

(13) Reaction of [TpCo(CH$_3$CN)$_3$](PF$_6$) with [K-18-C-6]$_3$[Fe(CN)$_6$]

A sample of [TpCo(CH$_3$CN)$_3$](PF$_6$) (0.073 g, 0.135 mmol) in 25 mL of acetonitrile was combined with [K-18-C-6]$_3$[Fe(CN)$_6$] (0.151 g, 0.135 mmol) in 25 mL of acetonitrile to give a blue/green solution. The solution was reduced in volume to ~10 mL, after which time 40 mL of diethyl ether was added to induce precipitation of a blue/green product. The colorless solution was removed via a cannula and the blue/green product was dried under vacuum. Yield: 0.543 mg. IR (Nujol, cm^{-1}): 3370 (s, br), 2109 (s), 2064 (s, br), 1639 (m), 1501 (w), 1408 (m), 1350 (s), 1324 (w), 1286 (m), 1248 (m), 1217 (w), 1107 (s, br), 1047 (m), 963 (s), 837 (s), 771 (w), 660 (w), 620 (w),

557 (m), 528 (w), 406 (w, br), 243 (w, br).

(14) Reaction of (dien)Ni(NO₃)₂ with [K-18-C-6]₃[Fe(CN)₆]

A sample of (dien)Ni(NO₃)₂ (0.044 g, 0.154 mmol) in 25 mL of CH₃OH/CH₃CN was reacted with [K-18-C-6]₃[Fe(CN)₆] (0.176 g, 0.157 mmol) in a mixture of CH₃OH/CH₃CN (25 mL v/v). A dark orange/brown solution resulted after 12 h of stirring. The volume of the solution was reduced to ~10 mL, and 40 mL of diethyl ether was added to precipitate a dark orange product. The colorless solution was decanted through a cannula, and the product dried under vacuum. IR data (Nujol, cm⁻¹): 3341 (w), 3281 (w), 3172 (w), 2405 (w), 2361 (w), 2244 (w), 2149 (m), 2101 (s), 1974 (w), 1748 (w), 1740 (w), 1601 (m), 1284 (s), 1248 (s), 1103 (s), 963 (s), 837 (s), 591 (w), 531 (m), 389 (m), 253 (m).

(15) Reaction of (2,2'-bpy)₂Ni(CF₃SO₃)₂ with [K-18-C-6]₃[Fe(CN)₆]

Three equivalents of (2,2'-bpy)₂ Ni(CF₃SO₃)₂ (0.183 g, 0.273 mmol) and two equivalents of [K-18-C-6]₃[Fe(CN)₆] (0.205 g, 0.183 mmol) were combined in a Schlenk flask with 50 mL of acetonitrile and refluxed overnight to give a yellow/brown precipitate in a colorless solution. The solution was removed via a cannula, and the product washed with 40 mL of diethyl ether which was removed by cannula and discarded. The yellow/brown product was dried under vacuum. Yield 54.2 mg. IR data (Nujol, cm⁻¹): 3391 (m), 2156 (m),

2144 (m), 2112 (m), 2107 (m), 1638 (w), 1599 (s), 1576 (m), 1567 (m), 1492 (m), 1314 (m), 1249 (m), 1224 (w), 1157 (m), 1104 (m), 1062 (w), 1044 (w), 1023 (m), 961 (w), 765 (s), 736 (s), 652 (m), 639 (m), 518 (w), 413 (m).

(16) Reaction of [(2,2'-bpy)$_2$Ni(CH$_3$CN)$_2$](PF$_6$)$_2$ with K$_3$[Fe(CN)$_6$]

Three equivalents of [(2,2'-bpy)$_2$Ni(CH$_3$CN)$_2$](PF$_6$)$_2$ (0.320 g, 0.430 mmol) in 40 mL acetonitrile were added to a 10 mL acetonitrile/50 mL water solution of K$_3$[Fe(CN)$_6$] (0.046 g, 0.139 mmol). An immediate brown precipitate formed in an orange/yellow solution. The solution was removed through a cannula, the brown precipitate was washed with 40 mL of diethyl ether, and dried under vacuum. IR data (Nujol, cm^{-1}): 2148 (s), 2126 (m), 2087 (m), 1601 (s), 1568 (m), 1313 (m), 1155 (m), 1060 (w), 1026 (m), 844 (m), 765 (s), 736 (s), 653 (m), 582 (w), 554 (w), 411 (m, br).

(17) Reaction of (phen)$_2$Zn(NO$_3$)$_2$ with K$_3$[Fe(CN)$_6$]

Three equivalents of (phen)$_2$Zn(NO$_3$)$_2$ (0.104 g, 0.189 mmol)[8] in 50 mL of water were reacted with K$_3$[Fe(CN)$_6$] (0.042 g, 0.127 mmol) in 50 mL of water. A yellow precipitate immediately formed which was collected by filtration, washed with water (2 x 10 mL) followed by acetone (2 x 10 mL), and dried in air. The yellow filtrate was slowly evaporated which led to the deposition of a minor quantity of a yellow/orange crystalline material. Yield: 92.7 mg. IR (Nujol, cm^{-1}): 2151 (m), 2114 (m), 2062 (w), 1623 (m), 1585

185

(m), 1578 (m), 1518 (m), 1425 (s), 1340 (w), 1307 (w), 1223 (m), 1144 (m),

1104 (m), 967 (w), 867 (m), 851 (m), 775 (w), 641 (m), 421 (m), 287 (m),

236 (w), 230 (w), 223 (w), 213 (m), 210 (m), 208 (m), 206 (m), 204 (m), 203

(m), 201 (w).

(18) Reaction of (phen)$_2$Zn(NO$_3$)$_2$ with K$_3$[Fe(CN)$_6$]

Three equivalents of (phen)$_2$Zn(NO$_3$)$_2$ (0.102 g, 0.185 mmol) in 25 mL of

methanol were reacted with K$_3$[Fe(CN)$_6$] (0.041 g, 0.124 mmol) in 25 mL of

methanol. An orange/yellow precipitate formed within 12 h of stirring. The

precipitate was collected by filtration, washed with methanol (2 x 10 mL)

followed by acetone (2 x 10 mL), and dried in air. The orange filtrate was

slowly evaporated which yielded orange crystals of K$_3$[Fe(CN)$_6$]. Yield: 67.2

mg. IR (Nujol, cm^{-1}): 2147 (m), 2114 (m), 2077 (m), 1626 (m), 1577 (m),

1517 (m), 1342 (w), 1306 (w), 1224 (w), 1145 (m), 1102 (m), 866 (m), 850

(m), 773 (w), 641 (m), 421 (m), 226 (w), 222 (w), 221 (w), 217 (w), 216 (w),

214 (w), 211 (m), 209 (w), 208 (w), 206 (w), 202 (m).

(19) Reaction of (phen)$_2$Zn(NO$_3$)$_2$ with K$_3$[Fe(CN)$_6$]

A sample of (phen)$_2$Zn(NO$_3$)$_2$ (0.134 g, 0.244 mmol) in 25 mL of water was

reacted with an aqueous solution (25 mL) of K$_3$[Fe(CN)$_6$] (0.020 g, 0.060

mmol). A yellow precipitate formed immediately which was collected by

filtration, washed with water (2 x 10 mL) followed by acetone (2 x 10 mL),

and dried in air. The colorless filtrate was discarded. Yield: 51.5 mg. IR (Nujol, cm^{-1}): 2150 (w), 2143 (w), 2114 (m), 2082 (w, br), 1623 (m), 1579 (w), 1518 (m), 1426 (m), 1305 (w), 1224 (w), 1144 (m), 1103 (m), 966 (w), 867 (m), 851 (m), 641 (w), 420 (w), 221 (w), 212 (w), 210 (w), 208 (m), 205 (m), 201 (m).

(20) Reaction of (phen)$_2$Zn(NO$_3$)$_2$ with K$_3$[Fe(CN)$_6$]

An aqueous solution (25 mL) of (phen)$_2$Zn(NO$_3$)$_2$ (0.130 g, 0.236 mmol) was reacted with K$_3$[Fe(CN)$_6$] (0.078 g, 0.237 mmol) in 25 mL of water. An immediate yellow precipitate formed, which was collected by filtration, washed with water (2 x 10 mL) followed by acetone (2 x 10 mL), and dried in air. The yellow filtrate was slowly evaporated in air to yield a mixture of colorless and very small orange/yellow crystals. Yield of yellow solid: 132.2 mg. IR (Nujol, cm^{-1}): 2150 (w), 2143 (w), 2127 (w), 2112 (m), 1623 (m), 1579 (w), 1517 (m), 1425 (m), 1306 (w), 1224 (w), 1143 (m), 1103 (m), 966 (w, br), 867 (m), 851 (m), 641 (w), 421 (w), 288 (w), 240 (w), 225 (w), 221 (w), 215 (w), 211 (m), 208 (m), 201 (m).

(21) Reaction of (phen)$_2$Zn(NO$_3$)$_2$ with K$_4$[Fe(CN)$_6$]

Three equivalents of (phen)$_2$Zn(NO$_3$)$_2$ (0.118 g, 0.214 mmol) in 25 mL of water were combined with K$_4$[Fe(CN)$_6$] (0.031 g, 0.073 mmol) in 25 mL of water. The immediate formation of a fluffy yellow/orange material occurred.

The orange/yellow product was isolated by filtration, washed with water (2 x 5 mL) followed by 10 mL of acetone, and dried in air. The colorless filtrate was discarded. Yield: 55.5 mg. IR data (Nujol, cm^{-1}): 2056 (s), 1623 (m), 1579 (m), 1517 (m), 1427 (s), 1343 (w), 1306 (w), 1224 (w), 1143 (m), 1103 (m), 867 (m), 849 (s), 772 (w), 640 (w), 589 (m), 422 (w), 290 (w), 220 (w), 219 (w), 215 (w), 212 (w), 209 (w), 207 (w), 204 (w), 201 (w).

(22) Reaction of (phen)$_2$Zn(NO$_3$)$_2$ with K$_4$[Fe(CN)$_6$]

Three equivalents of (phen)$_2$Zn(NO$_3$)$_2$ (0.204 g, 0.371 mmol) in 25 mL of water were reacted with K$_4$[Fe(CN)$_6$] (0.106 g, 0.251 mmol) in 25 mL of water. A pale yellow/white fluffy solid formed, which was collected by filtration, washed with water (2 x 5 mL) followed by 10 mL of acetone, and dried in air. The orange filtrate was evaporated, but no crystals were obtained. Yield: 76.4 mg. IR data (Nujol, cm^{-1}): 2074 (s, br), 1622 (m), 1223 (m), 1142 (m), 1103 (m), 868 (m), 849 (s), 771 (m), 593 (s), 423 (m), 292 (m), 216 (w), 207 (w).

(23) Reaction of (phen)$_2$ZnCl$_2$ with K$_3$[Fe(CN)$_6$]

Three equivalents of (phen)$_2$ZnCl$_2$ (0.104 g, 0.209 mmol) in 25 mL of water were added to K$_3$[Fe(CN)$_6$] (0.046 g, 0.139 mmol) in 25 mL of water. The resulting yellow precipitate was collected by filtration, washed with water (2 x 5 mL) followed by 10 mL of acetone, and dried in air. The colorless filtrate

was discarded. Yield: 121.5 mg. IR (Nujol, cm^{-1}): 3375 (m, br), 2151 (w), 2144 (w), 2126 (w), 2114 (m), 1624 (m), 1579 (w), 1518 (m), 1425 (m), 1224 (w), 1144 (m), 1104 (m), 967 (w), 867 (m), 851 (m), 641 (w), 421 (w), 225 (w), 219 (w) 216 (w), 212 (m), 210 (m), 207 (w), 204 (m), 202 (m).

(24) Reaction of (phen)$_2$ZnCl$_2$ with K$_3$[Fe(CN)$_6$]

Three equivalents of (phen)$_2$ZnCl$_2$ (0.101 g, 0.203 mmol) in 50 mL of water were reacted with K$_3$[Fe(CN)$_6$] (0.045 g, 0.136 mmol) in 50 mL of water. A yellow precipitate formed which was separated from a colorless filtrate, washed with water (2 x 5 mL) followed by 10 mL of acetone, and finally dried in air. The colorless filtrate was discarded. Yield: 121.6 mg. IR (Nujol, cm^{-1}): 3375 (m, br), 2151 (m), 2143 (m), 2127 (m), 2114 (s), 2088 (m), 1623 (m), 1579 (m), 1518 (s), 1495 (w), 1425 (w), 1340 (m), 1306 (w), 1224 (m), 1144 (m), 1104 (m), 967 (w), 889 (w), 867 (m), 851 (s), 773 (w), 641 (m), 421 (m), 288 (m), 241 (w), 232 (w), 227 (w), 219 (m), 215 (m), 212 (w), 211 (w), 209 (m), 208 (m), 207 (m), 204 (m), 203 (m), 201 (m).

(25) Reaction of [Zn(phen)$_3$]Cl$_2$ with K$_3$[Fe(CN)$_6$]

An aqueous sample (25 mL) of [Zn(phen)$_3$]Cl$_2$ (0.108 g, 0.159 mmol) was reacted with K$_3$[Fe(CN)$_6$] (0.034 g, 0.103 mmol) in 25 mL of water. An immediate yellow gel-like material formed, which was collected by filtration, washed with (2 x 5 mL) of water followed by 10 mL of acetone, and dried in

air. The colorless filtrate was discarded. Yield: 59.3 mg. IR data (Nujol, cm^{-1}): 3292 (m, br), 2174 (s), 2165 (s), 2133 (w), 2097 (m), 2084 (m), 1623 (w), 1586 (m), 1579 (m), 1519 (m), 1494 (w), 1426 (s), 1225 (w), 1145 (m), 1104 (m), 867 (m), 850 (s), 771 (m), 643 (w), 446 (m, br), 423 (w), 293 (w), 243 (w), 238 (w), 225 (w), 220 (w), 214 (w), 211 (w), 208 (w), 206 (m), 205 (m), 201 (m).

(26) Reaction of [Zn(phen)$_3$]Cl$_2$ with K$_3$[Fe(CN)$_6$]

Three equivalents of [Zn(phen)$_3$]Cl$_2$ (0.103 g, 0.152 mmol) in 50 mL of water were reacted with K$_3$[Fe(CN)$_6$] (0.032 g, 0.097 mmol) in 50 mL of water. A gelatinous yellow product formed which was collected by filtration, washed with water (2 x 5 mL) followed by 10 mL of acetone and dried in air. The colorless filtrate was discarded. Yield: 55.8 mg. IR data (Nujol, cm^{-1}): 2173 (m), 2165 (m), 2133 (w), 2096 (m), 2082 (m), 1622 (w), 1585 (w), 1577 (w), 1515 (m), 1306 (w), 1225 (w), 1147 (m), 1101 (m), 868 (m), 850 (m), 773 (w), 642 (w), 446 (w, br), 294 (m), 242 (w), 237 (w), 232 (w), 228 (w), 220 (w), 216 (w), 212 (m), 209 (m), 205 (m), 201 (m).

(27) Reaction of (2,2'-bpy)$_2$Zn(NO$_3$)$_2$ with K$_3$[Fe(CN)$_6$]

An aqueous solution (25 mL) of (2,2'-bpy)$_2$Zn(NO$_3$)$_2$ (0.157 g, 0.313 mmol) was reacted with K$_3$[Fe(CN)$_6$] (0.069 g, 0.210 mmol) in 25 mL of water. An immediate yellow precipitate formed which was collected by filtration,

washed with water (2 x 10 mL) followed by acetone (2 x 10 mL), and dried in air. The nearly colorless filtrate was discarded. Yield: 116.2 mg. IR data (Nujol, cm^{-1}): 2177 (s), 2168 (s), 2162 (s), 2124 (m), 2114 (m), 2108 (m), 2085 (s), 1607 (m), 1597 (s), 1577 (m), 1567 (m), 1492 (m), 1314 (m), 1249 (m), 1171 (m), 1156 (m), 1104 (w), 1062 (m), 1025 (m), 1013 (w), 966 (w), 890 (w), 844 (w), 767 (s), 734 (s), 652 (m), 630 (w), 597 (w), 526 (w), 447 (m), 414 (m), 239 (w), 211 (w), 209 (w).

(28) Reaction of (2,2'-bpy)$_2$Zn(NO$_3$)$_2$ with K$_4$[Fe(CN)$_6$]

Three equivalents of (2,2'-bpy)$_2$Zn(NO$_3$)$_2$ (0.123 g, 0.246 mmol) in 25 mL of water were reacted with K$_4$[Fe(CN)$_6$] (0.070 g, 0.166 mmol) in 25 mL of water. As the reaction proceeded, the solution became cloudy and gel-like in consistency and a yellow precipitate began to settle out. The yellow product was collected by filtration, washed with water (2 x 5 mL) followed by 10 mL of acetone, and dried in air. The filtrate was discarded. Yield: 86.5 mg. IR data (Nujol, cm^{-1}): 2085 (s), 2062 (w), 2048 (w), 2034 (s), 1623 (m), 1580 (m), 1517 (m), 1496 (w), 1425 (s), 1344 (w), 1306 (w), 1224 (m), 1142 (m), 1103 (m), 867 (m), 849 (s), 773 (w), 641 (w), 586 (m), 421 (w), 285 (w), 216 (w), 205 (w).

(29) Reaction of (2,2'-bpy)$_2$ZnCl$_2$ with K$_3$[Fe(CN)$_6$]

A deoxygenated water solution (10 mL) of (2,2'-bpy)$_2$ZnCl$_2$ (0.075 g, 0.167

mmol) was reacted with $K_3[Fe(CN)_6]$ (0.036 g, 0.109 mmol) in 15 mL of air-free water. After stirring for 12 h, the yellow precipitate was collected by filtration, washed with water (2 x 10 mL) followed by acetone (2 x 10 mL), and dried in air. The pale yellow filtrate was slowly evaporated in air but did not yield crystals. Yield: 42.2 mg. IR data (Nujol, cm^{-1}): 2162 (m), 2090 (s), 1607 (m), 1598 (m), 1578 (w), 1568 (w), 1492 (w), 1316 (m), 1249 (w), 1157 (m), 1061 (w), 1023 (m), 767 (m), 735 (m), 652 (m), 596 (m), 498 (w), 422 (w, br), 414 (m), 216 (w), 212 (w), 209 (w), 206 (m), 204 (w), 201 (w).

(30) Reaction of $(2,2'-bpy)_2ZnCl_2$ with $K_4[Fe(CN)_6]$

Three equivalents of $(2,2'-bpy)_2ZnCl_2$ (0.084 g, 0.188 mmol) in 10 mL of water were added to $K_4[Fe(CN)_6]$ (0.054 g, 0.128 mmol) in 15 mL of water. The solution became cloudy and a pale yellow/white gelatinous material was collected by filtration, washed with water (2 x 5 mL) followed by 10 mL of acetone, and dried in air. The filtrate was discarded. Yield: 54.6 mg. IR data (Nujol, cm^{-1}): 2160 (w), 2097 (s), 2086 (s), 2061 (s), 1605 (m), 1596 (s), 1576 (m), 1314 (m), 1250 (m), 1173 (m), 1156 (m), 1102 (w), 1060 (m), 1023 (m), 974 (w), 764 (s), 734 (s), 651 (m), 628 (w), 592 (s), 494 (m), 413 (m), 235 (w), 221 (w), 216 (w), 212 (w), 211 (w), 206 (m), 203 (w).

C. SINGLE CRYSTAL X-RAY STRUCTURAL STUDIES

Crystallographic data for compounds **36, 37, 38, 39** and **40** were collected on

a 2K (SMART 2000) CCD diffractometer equipped with monchromated Mo Kα(λ_α = 0.71069 Å) radiation. The source is a Mo sealed tube with a 3KW generator. The frames were integrated in the Bruker SAINT software package[9] and the data were corrected for absorption using the SADABS program.[10] The SIR97[11] and SHELX-97[12] crystallographic software packages were used. Crystal parameters and basic information pertaining to data collection and structure refinement are summarized in Tables 4.1-4.5.

(1) {Mn(H$_2$O)$_2$[Mn(2,2'-bpym)(H$_2$O)]$_2$[Fe(CN)$_6$]$_2$}$_\infty$ (36)

Single crystals of **36** were grown by layering an aqueous solution of K$_3$[Fe(CN)$_6$] with and acetonitrile solution of [(2,2'-bpym)$_2$Mn(H$_2$O)$_2$](BF$_4$)$_2$. A brown needle-like crystal of dimensions 0.083 x 0.017 x 0.010 mm^3 was mounted on the tip of a glass fiber with Dow Corning silicone grease and placed in a cold N$_2$ stream. Least squares refinement using well-centered reflections in the range 3.06° < 2θ < 56.66° gave a cell corresponding to a monoclinic crystal system. A total of 18,980 data (6134 unique) with F(000) = 1154 were collected at 110(2) K using the ω-2θ scan technique to a maximum 2θ value of 56.66°. Systematic absences from the data led to the choice of P2$_1$/c as the space group. The final full-matrix, least-squares refinement was based on data with F$_o^2$ > 4σ(F$_o^2$) and parameters to give R1 =

Table 4.1. Crystallographic information for
$\{Mn(H_2O)_2[Mn(2,2'\text{-}bpym)(H_2O)]_2[Fe(CN)_6]_2\}_\infty$ (36) •$9H_2O$

	36 •$9H_2O$
Empirical formula	$C_{28}H_{38}Fe_2Mn_3N_{20}O_{13}$
Formula weight	1139.30
Temperature (K)	110(2)
Space group	$P2_1/c$
a (Å)	13.209(3)
b (Å)	26.694(5)
c (Å)	7.443(2)
α (°)	90
β (°)	105.57(3)
γ (°)	90
Volume (Å^3)	2528.1(10)
Z	2
D_{calc} (Mg m^{-3})	1.497
Absorption coefficient(mm^{-1})	1.361
Crystal size (mm)	0.083 x 0.017 x 0.010
Reflections collected	18980
Independent reflections	6134
R_{int}	0.2250
Final R indices	$R_1 = 0.0715$
	$wR_2 = 0.1630$

$R_1 = \Sigma[||F_o| - |F_c||] / \Sigma|F_o|$. $wR_2 = \{\Sigma[w(F_o^2 - F_c^2)^2 / \Sigma[w(F_o^2)^2]]\}^{1/2}$. GOF = $\{\Sigma[w(F_o^2 - F_c^2)^2] / (n - p)\}^{1/2}$ where n = total number of reflections and p = total number of parameters.

Table 4.2. Crystallographic information for $\{[Co(2,2'\text{-bpy})_2]_3[Fe(CN)_6]_2\}^+$ (37)

	37
Formula	$C_{78}H_{71}Fe_2Co_3N_{24}O_{18}$
Formula weight	1926.39
Temperature (K)	90(2)
Space group	$P6_322$
a (Å)	18.540(5)
b (Å)	18.540(5)
c (Å)	30.710(5)
α (°)	90
β (°)	90
γ (°)	120
Volume (Å^3)	9142(4)
Z	2
D_{calc} (Mg m^{-3})	1.374
Absorption coefficient(mm^{-1})	0.918
Crystal size (mm)	0.053 x 0.04 x 0.021
Reflections collected	59352
Independent reflections	7537
R_{int}	0.1494
Final R indices	$R_1 = 0.067$
	$wR_2 = 0.2222$

$R_1 = \Sigma[||F_o| - |F_c||] / \Sigma|F_o|$. $wR_2 = \{\Sigma[w(F_o^2 - F_c^2)^2 / \Sigma[w(F_o^2)^2]\}^{1/2}$. GOF = $\{\Sigma[w(F_o^2 - F_c^2)^2] / (n - p)\}^{1/2}$ where n = total number of reflections and p = total number of parameters.

Table 4.3. Crystallographic information for {[Ni(2,2'-bpy)$_2$(OH$_2$)][Ni(2,2'-bpy)$_2$]$_2$[Fe(CN)$_6$]$_2$} (38)

	38
Formula	C$_{73}$H$_{48}$Fe$_2$Ni$_3$N$_{24}$O$_{18}$
Formula weight	1837.18
Temperature (K)	110(2)
Space group	P-1
a (Å)	13.251(3)
b (Å)	17.678(4)
c (Å)	18.057(4)
α (°)	94.57(3)
β (°)	103.81(3)
γ (°)	95.35(3)
Volume (Å^3)	4066.8(14)
Z	2
D$_{calc}$ (Mg m^{-3})	1.500
Absorption coefficient(mm^{-1})	1.112
Crystal size (mm)	0.053 x 0.04 x 0.021
Reflections collected	30014
Independent reflections	18520
R$_{int}$	0.0729
Final R indices	R$_1$ = 0.101
	wR$_2$ = 0.2543

$R_1 = \Sigma[||F_o| - |F_c||] / \Sigma|F_o|$. $wR_2 = \{\Sigma[w(F_o^2 - F_c^2)^2 / \Sigma[w(F_o^2)^2]\}^{1/2}$. GOF = $\{\Sigma[w(F_o^2 - F_c^2)^2] / (n - p)\}^{1/2}$ where n = total number of reflections and p = total number of parameters.

Table 4.4. Crystallographic information for {[Zn(phen)$_3$][Zn(phen)$_2$]$_2$ [Fe(CN)$_6$]$_2$} (39) •25H$_2$O

	39 •25H$_2$O
Formula	C$_{96}$H$_{106}$Fe$_2$Zn$_3$N$_{26}$O$_{25}$
Formula weight	2326.54
Temperature (K)	110(2)
Space group	C2/c
a (Å)	42.047(5)
b (Å)	13.541(5)
c (Å)	28.781(5)
α (°)	90
β (°)	120.232(5)
γ (°)	90
Volume (Å^3)	14158(6)
Z	4
D$_{calc}$ (Mg m^{-3})	1.354
Absorption coefficient(mm^{-1})	0.944
Crystal size (mm)	0.175 x 0.047 x 0.011
Reflections collected	22031
Independent reflections	11727
R$_{int}$	0.1126
Final R indices	R$_1$ = 0.0997
	wR$_2$ = 0.2617

$R_1 = \Sigma[||F_o| - |F_c||] / \Sigma|F_o|$. $wR_2 = \{\Sigma[w(F_o^2 - F_c^2)^2 / \Sigma[w(F_o^2)^2]\}^{1/2}$. GOF = $\{\Sigma[w(F_o^2 - F_c^2)^2] / (n - p)\}^{1/2}$ where n = total number of reflections and p = total number of parameters.

Table 4.5. Crystallographic information for $\{[Zn(phen)_2][Fe(CN)_6]\}_2$ $\{[Zn(phen)_2][Zn(phen)_2(OH_2)][Fe(CN)_6]\}_2$ **(40)** $\bullet 19H_2O\bullet 4CH_3OH$

	40 $\bullet 19H_2O\bullet 4CH_3OH$
Formula	$C_{172}H_{146}Fe_4Zn_6N_{48}O_{25}$
Formula weight	2826.4
Temperature (K)	110(2)
Space group	C2/c
a (Å)	48.139(10)
b (Å)	13.585(3)
c (Å)	34.131(7)
α (°)	90
β (°)	112.05(3)
γ (°)	90
Volume (Å^3)	20689(7)
Z	2
D_{calc} (Mg m^{-3})	1.134
Absorption coefficient(mm^{-1})	0.726
Crystal size (mm)	0.014 x 0.07 x 0.05
Reflections collected	75183
Independent reflections	24876
R_{int}	0.5283
Final R indices	$R_1 = 0.0997$
	$wR_2 = 0.2185$

$R_1 = \Sigma[\|F_o| - |F_c\|] / \Sigma|F_o|$. $wR_2 = \{\Sigma[w(F_o^2 - F_c^2)^2 / \Sigma[w(F_o^2)^2]\}^{1/2}$. GOF = $\{\Sigma[w(F_o^2 - F_c^2)^2] / (n - p)\}^{1/2}$ where n = total number of reflections and p = total number of parameters.

0.0715 (wR2 = 0.1630) and R_{int} = 0.2250. The goodness-of-fit index was 0.856, and the highest peak in the final difference map was 0.957 $e^-/\text{Å}^3$. All non-hydrogen atoms were refined anisotropically, except for the disordered interstitial water molecules. The hydrogen atoms were placed in calculated positions and treated as riding atoms. A structural representation is depicted in Figure 4.1.

(2) $\{[Co(2,2'\text{-bpy})_2]_3[Fe(CN)_6]_2\}^+$ (37)

Single crystals of 37 were grown by layering an aqueous solution of [K-18-C-6]$_3$[Fe(CN)$_6$] with an acetonitrile solution of [Co(2,2'-bpy)$_3$](ClO$_4$)$_2$ in a test tube. A hexagonal, navy-blue crystal of dimensions 0.053 x 0.04 x 0.021 mm^3 was mounted on the tip of a glass fiber with Dow Corning silicone grease and placed in a cold N_2 stream. Least squares refinement using well-centered reflections in the range 2.54° < 2θ < 56.52° gave a cell corresponding to a hexagonal crystal system. A total of 59352 data (7537 unique) with F(000) = 3834 were collected at 90(2) K using the ω-2θ scan technique to a maximum 2θ value of 56.52°. Systematic absences from the data led to the choice of P6$_3$22 as the space group. The final full-matrix, least-squares refinement was based on data with $F_o^2 > 4\sigma(F_o^2)$ and parameters to give R1 = 0.067 (wR2 = 0.2222) and R_{int} = 0.1494. The goodness-of-fit index was 1.151, and the

highest peak in the final difference map was 1.384 e$^-$/Å^3. All non-hydrogen atoms were refined anisotropically, except for the disordered interstitial water molecules. The hydrogen atoms were placed in calculated positions and treated as riding atoms. A thermal ellipsoid plot is presented in Figure 4.2.

(3) [Ni(2,2'-bpy)$_2$(OH$_2$)][Ni(2,2'-bpy)$_2$]$_2$[Fe(CN)$_6$]$_2$ (38)

Single crystals of **38** were grown by evaporation of a solution in a vial containing [(2,2'-bpy)$_2$Ni(OH$_2$)$_2$](CF$_3$SO$_3$)$_2$ and K$_3$[Fe(CN)$_6$] that had been placed near an oven. A dark orange-red crystal of dimensions 0.379 x 0.162 x 0.070 mm^3 was mounted on the tip of a glass fiber with Dow Corning silicone grease and placed in a cold N$_2$ stream. Least squares refinement using well-centered reflections in the range 2.32° < 2θ < 56.54° gave a cell corresponding to a triclinic crystal system. A total of 30014 data (18520 unique) with F(000) = 1868 were collected at 110(2) K using the ω-2θ scan technique to a maximum 2θ value of 56.54°. The space group is P-1. The final full-matrix, least-squares refinement was based on data with F$_o$^{2} > 4σ (F$_o$^{2}) and parameters to give R1 = 0.101 (wR2 = 0.2543) and R$_{int}$ = 0.0729. The goodness-of-fit index was 0.909, and the highest peak in the final difference map was 1.707 e$^-$/Å^3. All non-hydrogen atoms were refined anisotropically, except for the disordered interstitial water molecules. The

200

hydrogen atoms were placed in calculated positions and treated as riding atoms. A structural representation is depicted in Figure 4.3.

(4) [Zn(phen)$_3$]{[Zn(phen)$_2$][Fe(CN)$_6$]}$_2$ (39)

Single crystals of **39** were grown by slow evaporation of the yellow filtrate. An orange crystal of dimensions 0.175 x 0.047 x 0.110 mm^3 was mounted on the tip of a glass fiber with Dow Corning silicone grease and placed in a cold N$_2$ stream. Least squares refinement using well-centered reflections in the range 8.36° < 2θ < 51.08° gave a cell corresponding to a monoclinic crystal system. A total of 22031 data (11727 unique) with F(000) = 5864 were collected at 110(2) K using the ω-2θ scan technique to a maximum 2θ value of 51.08°. Systematic absences from the data led to the choice of C2/c as the space group. The final full-matrix, least-squares refinement was based on data with F$_o{}^2$ > 4σ(F$_o{}^2$) and parameters to give R1 = 0.997 (wR2 = 0.2617) and R$_{int}$ = 0.1126. The goodness-of-fit index was 1.083, and the highest peak in the final difference map was 2.081 e$^-$/Å^3. All non-hydrogen atoms were refined anisotropically, except for the disordered interstitial water molecules. The hydrogen atoms were placed in calculated positions and treated as riding atoms. A structural representation is presented in Figure 4.4.

(5){[Zn(phen)$_2$][Fe(CN)$_6$]}$_2$[Zn(phen)$_2$][Zn(phen)$_2$(OH$_2$)][Fe(CN)$_6$]}$_2$ (40)

Single crystals of **40** were grown by slow diffusion of an aqueous solution of $K_3[Fe(CN)_6]$ into a methanol solution of $(phen)_2Zn(NO_3)_2$. A yellow crystal of dimensions 0.014 x 0.07 x 0.05 mm^3 was mounted on the tip of a glass fiber with Dow Corning silicone grease and placed in a cold N_2 stream. Least squares refinement using well-centered reflections in the range $2.54° < 2\theta < 56.64°$ gave a cell corresponding to a monoclinic crystal system. A total of 75183 data (24876 unique) with F(000) = 7392 were collected at 110(2) K using the ω-2θ scan technique to a maximum 2θ value of 56.64°. Systematic absences from the data led to the choice of C2/c as the space group. The final full-matrix, least-squares refinement was based on data with $F_o^2 > 4\sigma(F_o^2)$ and parameters to give R1 = 0.099 (wR2 = 0.2185) and R_{int} = 0.5283. The goodness-of-fit index was 0.678, and the highest peak in the final difference map was 1.018 e$^-$/Å^3. All non-hydrogen atoms were refined anisotropically, except for the disordered interstitial water molecules. The hydrogen atoms were placed in calculated positions and treated as riding atoms. A structural representation is presented in Figure 4.5.
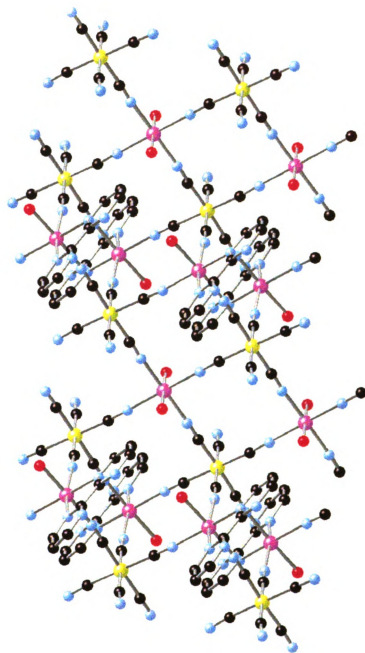
Figure 4.1. A structural representation of the 2-D polymer {Mn(H₂O)[Mn(2,2'-bpym)(H₂O)]₂[Fe(CN)₆]₂}∞ (36) taken from the coordinates of the X-ray structure. (Image is presented in color)
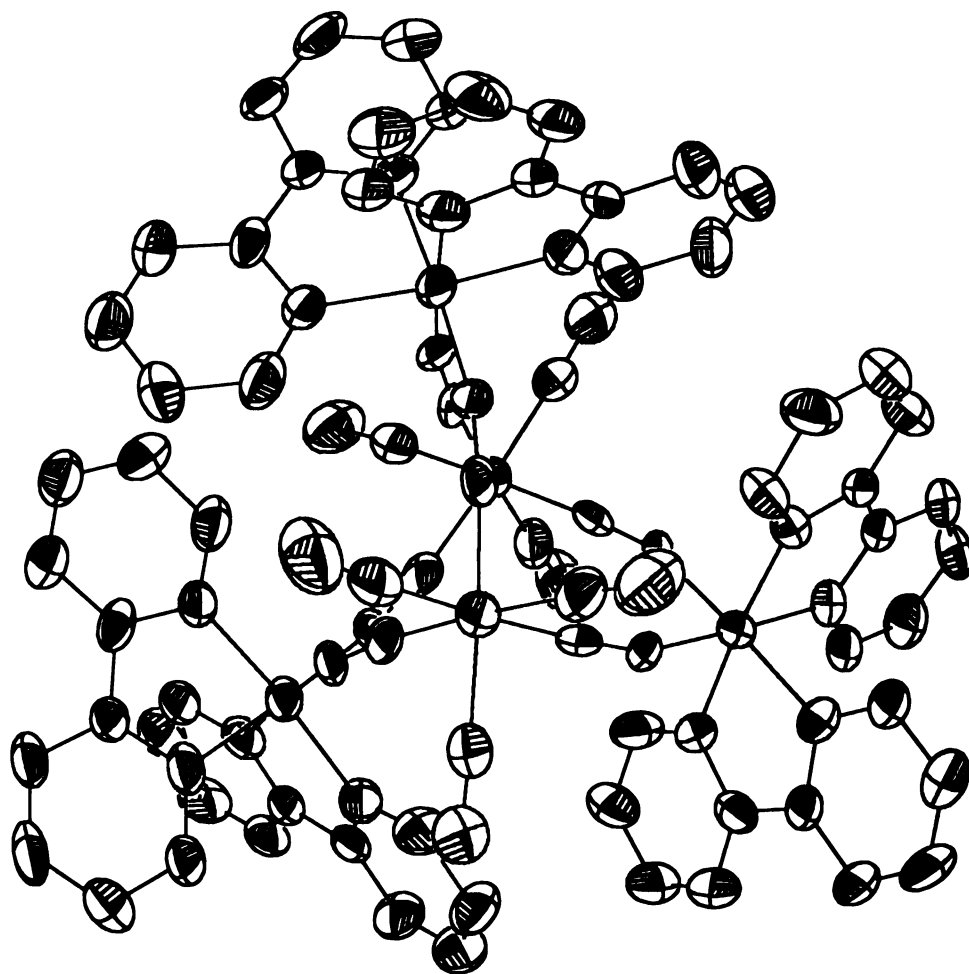
Figure 4.2. Thermal ellipsoid plot of $\{[Co(2,2'\text{-bpy})_2]_3[Fe(CN)_6]_2\}^+$ (37) at the 50 % probability level. The hydrogen atoms were omitted for the sake of clarity. (Image is presented in color)
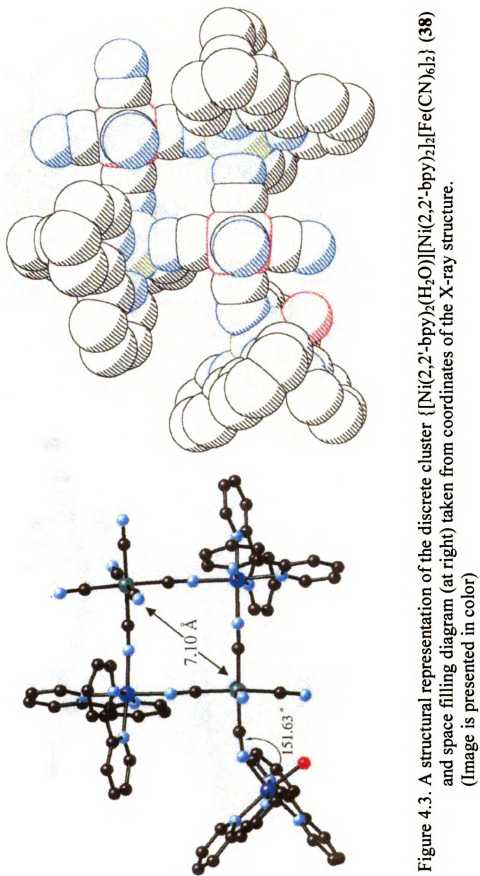
Figure 4.3. A structural representation of the discrete cluster {[Ni(2,2'-bpy)$_2$(H$_2$O)][Ni(2,2'-bpy)$_2$]$_2$[Fe(CN)$_6$]$_2$} (38) and space filling diagram (at right) taken from coordinates of the X-ray structure. (Image is presented in color)
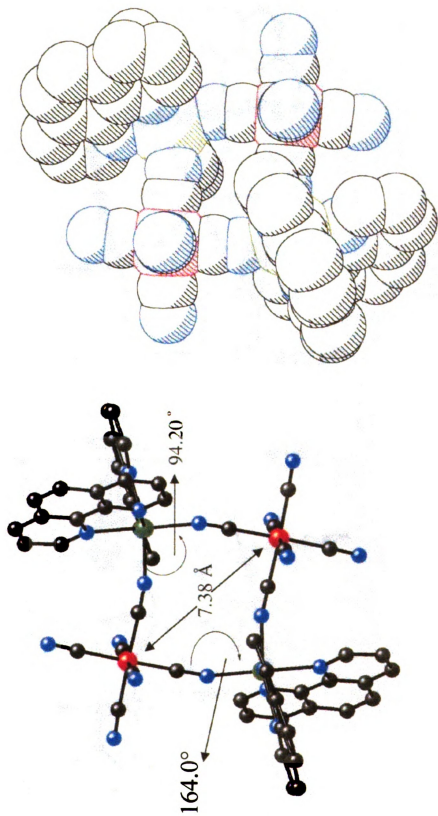
Figure 4.4. A structural representation of the anionic discrete cluster {[Zn(phen)₂]₂[Fe(CN)₆]₂}²⁻ (**39**) and the space filling model (at right) taken from coordinates of the X-ray structure. (Image is presented in color)
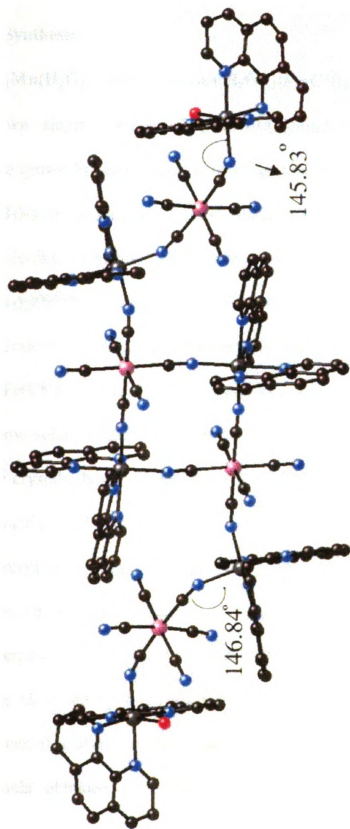
Figure 4.5. A structural representation of {[Zn(phen)₂][Fe(CN)₆]}₂{[Zn(phen)₂][Zn(phen)₂(H₂O)][Fe(CN)₆]}₂ (40) taken from coordinates of the X-ray structure. (Image is presented in color)

3. RESULTS AND DISCUSSION

A. Syntheses

(1) {Mn(H$_2$O)$_2$[Mn(2,2'-bpym)(H$_2$O)]$_2$[Fe(CN)$_6$]$_2$}$_($ (36) •9H$_2$O

Brown single crystals of {Mn(H$_2$O)$_2$[Mn(2,2'-bpym)(H$_2$O)]$_2$[Fe(CN)$_6$]$_2$}$_\infty$ were grown by slow diffusion of an acetonitrile solution of [(2,2'-bpym)$_2$Mn (OH$_2$)$_2$](BF$_4$)$_2$ into an aqueous solution of K$_3$[Fe(CN)$_6$]. The same brown needle-like crystals were obtained by replacing [(2,2'-bpym)$_2$Mn (OH$_2$)$_2$](BF$_4$)$_2$ with [(2,2'-bpym)$_2$Mn(OH$_2$)$_2$]SO$_4$. The reaction of three equivalents of [(2,2'-bpym)$_2$Mn(OH$_2$)$_2$](BF$_4$)$_2$ with two equivalents of K$_3$[Fe(CN)$_6$] yields a brown precipitate and a yellow solution. After the yellow solution had been slowly evaporated, brown crystals were obtained. The crystals, however, are not of a quality suitable for single crystal X-ray diffraction. IR data collected on both the brown crystals and the polycrystalline sample support the conclusion that the compounds are the same. Once the crystals and the polycrystalline sample had been washed with water, a pale yellow filtrate was obtained which produced yellow crystals that were identified by X-ray methods as being K$_3$[Fe(CN)$_6$](2,2'-bpym)$_5$(H$_2$O)$_5$. Elemental analysis on the polycrystalline sample did not fit well with the formula obtained from the single crystal data. The TGA data of the

polycrystalline sample yielded only 5 water molecules being released instead of 13 water molecules.

Attempts to synthesize the polymeric product from the combination of three equivalents of $MnSO_4 \cdot 7H_2O$ with two equivalents of $K_3[Fe(CN)_6]$ and one equivalent of 2,2'-bpym in water did not succeed. The reaction yielded a brown/yellow precipitate that was washed with water followed by acetone. The IR data reveal cyanide stretches at 2196 (w), 2147 (m), 2083 (w), 2062 (w) cm^{-1} which are at higher energies than the ones identified for *bona fide* batches of $\{Mn(H_2O)_2[Mn(2,2'-bpym)(H_2O)]_2[Fe(CN)_6]_2\}_\infty$ (36) $\cdot 9H_2O$.

(2) $\{[Co(2,2'-bpy)_2]_3[Fe(CN)_6]_2\}^+$ (37)

All nine reactions described in sections 2A-I were performed by adding the cobalt starting material into the solution of the hexacyanoferrate(III) anion. In all cases, the result was the formation of a navy blue precipitate. The IR data summarized in Tables 4.6 and 4.7 reveal that the seven reactions performed in 50 mL of water (regardless of the presence or absence of air) yield products with four $\nu(C\equiv N)$ stretches at ($\sim$ 2139, 2108, 2096 and 2067 cm^{-1}). IR data summarized in Table 4.7 also indicates the remaining two reactions between $[Co(2,2'-bpy)_3](ClO_4)_2$ or $[(2,2'-bpy)_2Co(CF_3SO_3)_2]$ and $[K-18-C-6]_3[Fe(CN)_6]$ in a 3:2 ratio in either acetonitrile or methanol gave rise to three

v(C≡N) stretches at ~2138, 2106, 2060 cm^{-1}. X-ray powder diffraction, SEM and Mössbauer studies were performed on selected samples in these studies. SEM and X-ray powder diffraction data clearly indicate that the reactions performed in water are more crystalline (Figure 4.6). The reactions carried out in acetonitrile or methanol led to essentially amorphous products as indicated by SEM and X-ray powder diffraction. Room temperature Mössbauer data for the eight prodcuts of reactions 2B-I indicate that all the Fe atoms are divalent. The isomer shifts and and quadrupole splittings are summarized in Table 4.8.

The preferred method for growing crystals of {[Co(2,2'-bpy)$_2$]$_3$[Fe(CN)$_6$]$_2$}$^+$ is to layer an aqueous solution of [K-18-C-6]$_3$[Fe(CN)$_6$] with an acetonitrile solution of either [Co(2,2'-bpy)$_3$](ClO$_4$)$_2$ or (2,2'-bpy)$_2$Co(CF$_3$SO$_3$)$_2$. Slow diffusion reactions of this type were set up in 6-8 m diameter glass tubes as well as in various sizes of test tubes. In all of these cases, large well-formed yellow crystals were obtained. These yellow crystals invariably were [(2,2'-bpy)$_2$Co(CN)$_2$](ClO$_4$) or [(2,2'-bpy)$_2$Co(CN)$_2$](CF$_3$SO$_3$) as evidenced by single crystal X-ray diffraction. This result points out the ease with which Co^{II} atoms oxidize to Co^{III} in these reactions.

Table 4.6. Summary of IR data for $\{[Co(2,2'-bpy)_2]_3[Fe(CN)_6]_2\}^+$ (37)

			$\nu(C{\equiv}N)$	atmosphere	Solvent
$3[(2,2'-bpy)_2Co(CF_3SO_3)_2]$	+	$2[Et_4N]_3[Fe(CN)_6]$	2137 (w) 2106 (m) 2096 (m) 2066 (s)	aerobic	50 mL water
$3[(2,2'-bpy)_2Co(CF_3SO_3)_2]$	+	$2K_3[Fe(CN)_6]$	2141 (w) 2108 (m) 2094 (m) 2067 (s)	anaerobic	50 mL water
$3[(2,2'-bpy)_2Co(CF_3SO_3)_2]$	+	$2K_3[Fe(CN)_6]$	2141 (w) 2106 (m) 2097 (m) 2066 (s)	aerobic	50 mL water
$3[Co(2,2'-bpy)_3](ClO_4)_2$	+	$2K_3[Fe(CN)_6]$	2139 (w) 2109 (m) 2094 (m) 2067 (s, br)	aerobic	50 mL water
$3[Co(2,2'-bpy)_3](ClO_4)_2$	+	$2[K-18-C-6]_3[Fe(CN)_6]$	2139 (w) 2109 (m) 2094 (m) 2067 (s, br)	aerobic	50 mL water

211

Table 4.7. Summary of IR data for $\{[\text{Co}(2,2'\text{-bpy})_2]_3[\text{Fe}(\text{CN})_6]_2\}^+$ (**37**)

		$\nu(\text{C}\equiv\text{N})$	Solvent
3[Co(2,2'-bpy)$_3$](ClO$_4$)$_2$	+ 2K$_4$[Fe(CN)$_6$]	2138 (w) 2108 (m) 2094 (m) 2068 (s)	50 mL water
3[(2,2'-bpy)$_2$Co(CF$_3$SO$_3$)$_2$]	+ 2K$_4$[Fe(CN)$_6$]	2140 (w) 2108 (m) 2094 (m) 2067 (s, br)	50 mL water
3[(2,2'-bpy)$_2$Co(CF$_3$SO$_3$)$_2$]	+ 2[K-18-C-6]$_3$[Fe(CN)$_6$]	2138 (w) 2106 (s) 2063 (s, br)	50 mL acetonitrile
3[Co (2,2'-bpy)$_3$](ClO$_4$)$_2$	+ 2[K-18-C-6]$_3$[Fe(CN)$_6$]	2144 (w) 2105 (m) 2056 (s, br)	50 mL methanol
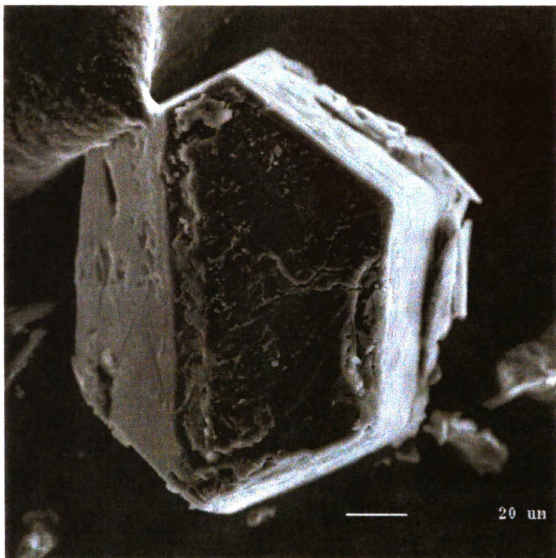
Figure 4.6. SEM photograph of {[Co(2,2'-bpy)$_2$]$_3$[Fe(CN)$_6$]$_2$}$^+$ (**37**).

Table 4.8. Mössbaur data summarized for $\{[Co(2,2'\text{-bpy})_2]_3[Fe(CN)_6]_2\}^+$ (37)

Reaction of		Isomer Shift (mm/s)	Quadrupole Shift (mm/s)
3[(2,2'-bpy)$_2$Co(CF$_3$SO$_3$)$_2$]	2K$_3$[Fe(CN)$_6$]	-0.08	0.08
3[(2,2'-bpy)$_2$Co(CF$_3$SO$_3$)$_2$]	2K$_3$[Fe(CN)$_6$]	-0.08	0.00
[(2,2'-bpy)$_2$Co(CF$_3$SO$_3$)$_2$]	K$_3$[Fe(CN)$_6$]	-0.08	0.06
3[(2,2'-bpy)$_2$Co(CF$_3$SO$_3$)$_2$]	2[K-18-C-6]$_3$[Fe(CN)$_6$]	-0.08	0.13
3[(2,2'-bpy)$_2$Co(CF$_3$SO$_3$)$_2$]	2[K-18-C-6]$_3$[Fe(CN)$_6$]	-0.09	0.13
3[Co (2,2'-bpy)$_3$](ClO$_4$)$_2$	2K$_3$[Fe(CN)$_6$]	-0.09	0.10
3[Co (2,2'-bpy)$_3$](ClO$_4$)$_2$	2K$_4$[Fe(CN)$_6$]	-0.08	0.15
3[Co (2,2'-bpy)$_3$](ClO$_4$)$_2$	2[K-18-C-6]$_3$[Fe(CN)$_6$]	-0.08	0.07
3[(2,2'-bpy)$_2$Co(CF$_3$SO$_3$)$_2$]	2K$_4$[Fe(CN)$_6$]	-0.08	0.06

(3) [Ni(2,2'-bpy)₂(OH₂)][Ni(2,2'-bpy)₂]₂[Fe(CN)₆]₂ (38)

When three equivalents of [(2,2'-bpy)$_2$Ni(OH$_2$)$_2$](CF$_3$SO$_3$)$_2$ were combined with 2 equivalents of K$_3$[Fe(CN)$_6$] in water, an initial yellow/brown precipitate formed. IR data of the yellow/brown precipitate revealed ν(C≡N) stretches located at 2142 and 2113 cm^{-1} and ligand ν(C=C) and ν(C=N) stretches for 2,2'-bpy at 1604 1598, 1575 and 1567 cm^{-1}. The yellow filtrate from this reaction was evaporated in a warm place in the lab (next to an oven) which led to the slow growth of dark orange/brown crystals admixed with a yellow/brown precipitate. A single crystal X-ray diffraction study identified the crystals to be the pentameric compound [Ni(2,2'-bpy)$_2$(OH$_2$)][Ni(2,2'-bpy)$_2$]$_2$[Fe(CN)$_6$]$_2$ (**38**). Attempts to grow crystals by slow diffusion of aqueous K$_3$[Fe(CN)$_6$] with [(2,2'-bpy)$_2$Ni(OH$_2$)$_2$](CF$_3$SO$_3$)$_2$ in acetonitrile led to yellow precipitate and tiny orange crystals.

(4) [Zn(phen)₃]{[Zn(phen)₂][Fe(CN)₆]}₂ (39)

An aqueous solution of (phen)$_2$Zn(NO$_3$)$_2$ (3 equiv) was reacted with K$_3$[Fe(CN)$_6$] (2 equiv) to yield a yellow precipitate whose IR spectrum contains ν(C≡N) modes at 2150, 2113 and 2062 cm^{-1} and 1,10-phenanthroline ν(C=C) and ν(C=N) stretches at 1623 and 1579 cm^{-1}. When the yellow filtrate was slowly evaporated, orange trigonal-shaped crystals of

the tetrameric compound [Zn(phen)$_3$]{[Zn(phen)$_2$][Fe(CN)$_6$]}$_2$ were obtained.

IR spectral properties of the orange crystals indicate the presence of v(C≡N) stretches at 2151, 2143, and 2127 and 2108 cm^{-1} and v(C=C) and v(C=N) modes at 1623 and 1578 cm^{-1} for the 1,10-phenanthroline ligand. The IR data for the yellow precipitate and orange crystals are very similar.

Additional studies on this reaction were carried out in attempts to grow crystals of the main product(s). Slow diffusion reactions were set up in 6 mm diameter tubes with an aqueous layer of hexacyanoferrate(III) on the bottom and a methanol solution of (phen)$_2$Zn(NO$_3$)$_2$ on top. These slow diffusions resulted in the formation of rectangular yellow crystals which are the unusual decameric compound {[Zn(phen)$_2$][Fe(CN)$_6$]}$_2${[Zn(phen)$_2$]-[Zn(phen)$_2$(OH$_2$)][Fe(CN)$_6$]}$_2$ (40) as determined by single crystal X-ray diffraction methods.

B. Reactions

(1) Reaction of (2,2'-bpy)$_2$Mn(CF$_3$SO$_3$)$_2$ with [K-18-C-6]$_3$[Fe(CN)$_6$]

The manganese complex was added directly to a solution of hexacyanoferrate(III) to give a brown precipitate with v(C≡N) stretches at 2143 (s), 2119 (m) and 2063 (m) cm^{-1}. Based on our experience with the compound {Mn(H$_2$O)$_2$[Mn(2,2'-bpym)(H$_2$O)]$_2$[Fe(CN)$_6$]$_2$}$_\infty$ (36), the v(C≡N)

216

mode at 2146 cm^{-1} is assigned to the Fe^{III} oxidation state and the activity at 1622 (m) and 1590 (m) cm^{-1} is assigned to v(C=C) and v(C=N) stretches of the 2,2'-bipyridine ligand. Attempts to grow crystals by layering [K-18-C-6]$_3$[Fe(CN)$_6$] in methanol with (2,2'-bpy)$_2$Mn(CF$_3$SO$_3$)$_2$ in acetonitrile were performed in 6-8 mm diameter glass tubes and test tubes, but no crystals were observed to form. A list of the cyanide stretches from various reactions is provided in Table 4.9.

(2) Reaction of (2,2'-bpy)$_2$Mn(CF$_3$SO$_3$)$_2$ and K$_3$[Fe(CN)$_6$]

These reactions were performed in water with different ratios of the starting materials. Equimolar quantities of each reactant 50 mL of water gave a brown precipitate which had a very complicated v(C≡N) region: 2155 (w), 2142 (s), 2133 (s), 2122 (s), 2112 (s), 2078 (w), 2061 (w) and 2038 (w) cm^{-1}. According to the results of the previous section, the use of [K-18-C-6]$_3$[Fe(CN)$_6$] in acetonitrile/methanol gave a product with only one strong stretch at 2143 cm^{-1}. This species may be forming in water, but there are many other products as well. The second reaction of this type was performed in a 3:2 ratio in 30 mL of water, which led to the deposition of a brown precipitate with numerous cyanide stretches as indicated by the IR data. It is obvious that more than one product is forming in these reactions. A comparison of the IR data for different reactions is provided in Table 4.9.

217

Table 4.9. IR data for reactions between [(2,2'-bpy)$_2$Mn(CF$_3$SO$_3$)$_2$] and [Fe(CN)$_6$]$^{3-}$.

		ν(C≡N)	Solvent
3[(2,2'-bpy)$_2$Mn(CF$_3$SO$_3$)$_2$]	2[K-18-C-6]$_3$[Fe(CN)$_6$]	2143 (s) 2119 (m) 2063 (m)	methanol/ acetonitrile
[(2,2'-bpy)$_2$Mn(CF$_3$SO$_3$)$_2$]	K$_3$[Fe(CN)$_6$]	2155 (w) 2142 (s) 2133 (s) 2122 (s) 2112 (s) 2078 (w) 2061 (w) 2038 (w)	water
3[(2,2'-bpy)$_2$Mn(CF$_3$SO$_3$)$_2$]	2K$_3$[Fe(CN)$_6$]	2156 (w) 2142 (m) 2132 (m) 2119 (m) 2114 (m) 2080 (w) 2061 (w) 2026 (w)	water

(3) Reaction of [Mn(2,2'-bpy)₃](ClO₄)₂ with K₃[Fe(CN)₆]

The reaction of equimolar quantites of [Mn(2,2'-bpy)₃](ClO₄)₂ and K₃[Fe(CN)₆] in 80 mL of water led to the formation of in a brown precipitate with cyanide stretches at 2136 (m), 2120 (s) and 2057 (m) cm^{-1}. The presence of 2,2'-bipyridine was indicated by the ν(C=C) and ν(C=N) stretches at 1594 (s), 1575 (m) 1565 (m) cm^{-1}. Attempts to grow crystals by layering an aqueous solution of K₃[Fe(CN)₆] with [Mn(2,2'-bpy)₃](ClO₄)₂ in acetonitrile in 6 mm glass tubing led to the isolation of brown needles. Although the crystals were small and diffracted poorly, an X-ray data set was collected which led to the identification of the product as {Mn(H₂O)₂[Mn(2,2'-bpym)(H₂O)]₂[Fe(CN)₆]₂}∞ (36). This polymeric material is identical to the 2-D structure with 2,2'-bpym ligand, and it's isolation with 2,2'-bpy ligand indicates that it is a stable, persistent architecture.

(4) Reaction of [Mn(2,2'-bpy)₃](ClO₄)₂ with [K-18-C-6]₃[Fe(CN)₆]

A 3:2 ratio of [Mn(2,2'-bpy)₃](ClO₄)₂ and [K-18-C-6]₃[Fe(CN)₆] in 100 mL of acetonitrile was refluxed for three days to give a brown precipitate with three ν(C≡N) stretches at 2146 (s), 2118 (m) and 2064 (m). This is essentially the same cyanide infrared stretching pattern observed for {Mn(H₂O)₂[Mn

(2,2'-bpym)(H₂O)]₂[Fe(CN)₆]₂}∞ (**36**).

(5) Reaction of (phen)₂Mn(CF₃SO₃)₂ and [Fe(CN)₆]³⁻

Reactions between of (phen)₂Mn(CF₃SO₃)₂and [Fe(CN)₆]³⁻ were performed with different ratios of reactants and in different solvents. Three equivalents of (phen)₂Mn(CF₃SO₃)₂ in a mixture of water and methanol were added to two equivalents of K₃[Fe(CN)₆] dissolved in water to give a brown precipitate. IR data in the v(C≡N) region are 2142 (w), 2113 (m), 2090 (w), 2053 (w, br) cm⁻¹. The presence of 1,10-phenanthroline was noted by the v(C=C) and v(C=N) stretches located at 1589 (m) and 1574 (m) cm⁻¹. A 1:1 ratio of (phen)₂Mn(CF₃SO₃)₂ with [K-18-C-6]₃[Fe(CN)₆] in water led to the formation of a yellow/brown precipitate with v(C≡N) modes at 2142 (w) and 2112 (m) cm⁻¹ and C=C and C=N stretches (1589 (m) and 1573 (m) cm⁻¹) for 1,10-phen. A third reaction of this type was performed with a 3:2 ratio of (phen)₂Mn(CF₃SO₃)₂ and [K-18-C-6]₃[Fe(CN)₆] in a mixture of acetonitrile and methanol. The reaction yielded a brown precipitate with cyanide stretches located at 2143 (w), 2114 (m) and 2067 (w, br) cm⁻¹ and 1,10-phen C=C and C=N stretches at 1590 (m) and 1572 (m) cm⁻¹ in the IR data. A comparison of the IR data for cyanide region is presented in Table 4.10. In all three of these reactions, the prominent v(C≡N) stretch is at ~2113 cm⁻¹. The 2-D strong

Table 4.10. Summary of IR data for reactions between [(phen)$_2$Mn(CF$_3$SO$_3$)$_2$] and K$_3$[Fe(CN)$_6$].

solvent	ν(C≡N) stretches
methanol/water	2142 (w)
	2113 (m)
	2090 (w)
	2053 (w, br)
water	2142 (w)
	2112 (m)
acetonitrile/methanol	2143 (w)
	2114 (m)
	2067 (w, br)

221

stretch as higher energies, namely 2146 cm^{-1}, which implies that the use of the 1,10-phen ligand leads to a different structure than the one with 2,2'-bpym. Unfortunately, attempts to crystallize this product were not successful.

(6) Reaction of [Co(2,2'-bpym)$_3$](BF$_4$)$_2$ with [K-18-C-6]$_3$[Fe(CN)$_6$]

Mixtures of [Co(2,2'-bpym)$_3$](BF$_4$)$_2$ and [K-18-C-6]$_3$[Fe(CN)$_6$] in a 3:2 ratio in acetonitrile did not react even after refluxing the reaction for three days. After three days, a few drops of water were added which led to the deposition of a purple precipitate in an intensely colored purple solution. An IR spectrum of the purple solid in the v(C≡N) region revealed stretches at 2141 (w), 2119 (m) and 2068 (s) cm^{-1}. The presence of the 2,2'-bipyrimidine ligand was indicated by the v(C=N) stretches located at 1576 (s) and 1560 (m) cm^{-1} in the IR. In comparison, {[Co(2,2'-bpy)$_2$]$_3$[Fe(CN)$_6$]$_2$}$^+$ (37), displays a strong cyanide stretch at ~2066 cm^{-1}. In (37), the metal ion oxidation states are Co^{III} and Fe^{II}. From this, it is logical to conclude that the same oxidation states are present in the purple product as well.

(7) Reaction of [Co(2,2'-bpym)$_3$](BF$_4$)$_2$ with K$_3$[Fe(CN)$_6$]

This reaction was performed in deoxygenated water in a 3:2 ratio of [Co(2,2'-bpym)$_3$](BF$_4$)$_2$ and K$_3$[Fe(CN)$_6$]. Upon mixing, the solution color instantaneously turned to an intense purple color and a filmy solid was

isolated by filtration in air. The $\nu(C\equiv N)$ stretches for the product are located at 2117 (s) and 2074 (s, br) cm^{-1}, and the presence of 2,2'-bpym was confirmed by the $\nu(C=N)$ stretches at 1580 (s), 1575 (s) and 1557 (s) cm^{-1}. As mentioned in the previous section, it is postulated that this product contains Co^{III} and Fe^{II} since the cyanide stretches appear at lower energies than what is observed for Co^{II} and Fe^{III} combinations. Attempts to grow crystals by layering an aqueous solution of $K_3[Fe(CN)_6]$ with [Co(2,2'-bpym)$_3$](BF$_4$)$_2$ invariably led to a gelatinous purple product.

(8) Reaction of (phen)$_2$Co(NO$_3$)$_2$ with $K_3[Fe(CN)_6]$

Reactions of (phen)$_2$Co(NO$_3$)$_2$ and $K_3[Fe(CN)_6]$ (3:2 ratio) in water lead to the formation of a green precipitate regardless of whether the reaction is performed in air or the absence of air. The filtrate for the reaction performed under nitrogen was pale green, while the reaction performed in air yielded a pale blue colored filtrate. Both green solids exhibit essentially the same cyanide stretches at ~2108 and 2076 cm^{-1}. The IR data also indicate the presence of the 1,10-phenanthroline ligand. A compilation of IR data in the $\nu(C\equiv N)$ region is summarized in Table 4.11. Crystal growing attempts included layering a solution of $K_3[Fe(CN)_6]$ in H$_2$O with a CH$_3$OH

223

Table 4.11. Summary of IR data for reactions between Co^{II} precursors and $K_3[Fe(CN)_6]$.

	$\nu(C{\equiv}N)$ stretches	solvent	environment
$3[(phen)_2Co(NO_3)_2]$ + $2K_3[Fe(CN)_6]$	2144 (w) 2108 (s) 2074 (s)	water	anaerobic
$3[(phen)_2Co(NO_3)_2]$ + $2K_3[Fe(CN)_6]$	2108 (m) 2078 (m, br)	water	aerobic
$3[Co(2,2'\text{-bpym})_3](BF_4)_2$ + $2[K\text{-}18\text{-}C\text{-}6]_3[Fe(CN)_6]$	2141 (w) 2119 (m) 2068 (s)	acetonitrile	anaerobic
$3[Co(2,2'\text{-bpym})_3](BF_4)_2$ + $2K_3[Fe(CN)_6]$	2117 (s) 2074 (s, br)	water	anaerobic

solution of (phen)$_2$Co(NO$_3$)$_2$. Hexagonal-shaped blue crystals formed as well as very thin blue needle-like crystals. Unfortunately, these crystals were not of a quality sufficient to collect a single-crystal X-ray data set.

(9) Reaction of [TpCo(CH$_3$CN)$_3$](PF$_6$) with [K-18-C-6]$_3$[Fe(CN)$_6$]

Equimolar quantitites of each reactant were combined in 50 mL of acetonitrile to give a blue/green solution with no precipitate. The lack of a precipitate indicates that the product is product is probably not a polymer or a neutral material, but rather a charged molecule. IR data revealed the presence of two cyanide stretches at 2109 (s) and 2064 (s, br) cm^{-1}. The low energies indicate that the product contains Co^{III} and Fe^{II}. The solution was slowly evaporated under a nitrogen purge, but unfortunately no crystals were obtained. A small amount of the acetonitrile solution was placed in a 5 mL vial without a cap and placed inside of a capped 20 mL vial that contained diethyl ether, but this attempt also failed to yield crystals.

(10) Reaction of (dien)Ni(NO$_3$)$_2$ with [K-18-C-6]$_3$[Fe(CN)$_6$]

Equimolar solutions of each reactant were dissolved in a mixture of acetonitrile and methanol, which led to a dark orange/brown colored solution. The IR spectrum of the product contains two cyanide stretches at 2149 (m) and 2101 (s) cm^{-1}. All attempts to grow crystals of the product by slow

evaporation and slow diffusion of diethyl ether into the reaction solution led only to powders.

(11) Reaction of [(2,2'-bpy)₂Ni(OH₂)₂](CF₃SO₃)₂ with [K-18-C-6]₃[Fe(CN)₆]

A 3:2 ratio of [(2,2'-bpy)$_2$Ni(OH$_2$)$_2$](CF$_3$SO$_3$)$_2$ to [K-18-C-6]$_3$[Fe(CN)$_6$] in 50 mL of acetonitrile was refluxed overnight to yield a yellow/brown precipitate. The IR spectrum contains v(C≡N) features at 2156, 2144, 2112 and 2107 cm^{-1}, and v(C=C)/v(C=N) features of 2,2'-bpy at 1599, 1576, 1567 cm^{-1}.

(12) Reaction of [(2,2'-bpy)₂Ni(CH₃CN)₂](PF₆)₂ with K₃[Fe(CN)₆]

Three equivalents of [(2,2'-bpy)$_2$Ni(CH$_3$CN)$_2$](PF$_6$)$_2$ in an acetonitrile solution were combined with the K$_3$[Fe(CN)$_6$] in a mixture of acetonitrile and water to give a brown precipitate with v(C≡N) modes at 2148 (s), 2126 (m) and 2087 (m) cm^{-1}. The 2,2'-bpy ligand was evident by the v(C=C)/v(C=N) stretches at 1585 (m) and 1578 (m) cm^{-1}.

(13) Reaction of [(phen)₂Zn(NO₃)₂ with K₃[Fe(CN)₆] in various ratios

Aqueous solutions of (phen)$_2$Zn(NO$_3$)$_2$ and K$_3$[Fe(CN)$_6$] were reacted in a 3:2 ratio to yield a yellow precipitate with v(C≡N) stretches at 2147 (m), 2114 (m) and 2077 (m) cm^{-1} for the reaction performed in 50 mL of water. The reaction performed at lower concentrations (100 mL) exhibited similar

cyanide stretches at 2151 (m), 2114 (m) and 2062 (w) cm^{-1}. The 1,10-phenanthroline ligand activity was evident by stretches at 1623 (m), 1585 (m) and 1578 (m) cm^{-1} for the 50 mL reaction and at 1626 (m) and 1577 (m) cm^{-1} for the 100 mL reaction. These IR data indicate that the reactions lead to the same yellow product. A 1:1 and a 4:1 reaction of (phen)$_2$Zn(NO$_3$)$_2$ and K$_3$[Fe(CN)$_6$] also yield yellow precipitates, but the IR data are more complicated, indicating that more than one product is being formed. A comparison of the IR data of the cyanide stretching region for these four reactions is in Table 4.12.

(14) Reaction of (phen)$_2$Zn(NO$_3$)$_2$ with K$_4$[Fe(CN)$_6$] in various ratios

The reaction of (phen)$_2$Zn(NO$_3$)$_2$ and K$_4$[Fe(CN)$_6$] in a 3:1 ratio produces a gelatinous yellow/orange product with cyanide stretches located at 2056 (s) and the signature of 1,10-phen at 1623 (m) and 1579 (m) cm^{-1}. When the ratio of reactants was changed to 3:2, a pale yellow/white gelatinous product was obtained which exhibits only one v(C≡N) stretch at 2074 (s, br) cm^{-1}. IR data of these two reactions are summarized in Table 4.12.

(15) Reaction of (phen)$_2$ZnCl$_2$ with K$_3$[Fe(CN)$_6$]

These reactions were performed in a 3:2 ratio of the reactants in both 50 mL and 100 mL of water. In both reactions, a yellow precipitate formed with v(C=C) and v(C=N) stretches from the 1,10-phenanthroline ligand located at

Table 4.12. Summary of IR data for reactions between [(phen)$_2$Zn(NO$_3$)$_2$] and [Fe(CN)$_6$]$^{3-/4-}$

Reaction			ν(C≡N)	Solvent
3[(phen)$_2$Zn(NO$_3$)$_2$]	+	2K$_3$[Fe(CN)$_6$]	2150 (m) 2113 (m) 2062 (w)	50 mL water
3[(phen)$_2$Zn(NO$_3$)$_2$]	+	2K$_3$[Fe(CN)$_6$]	2151 (m) 2144 (m) 2062 (w)	100 mL water
3[(phen)$_2$Zn(NO$_3$)$_2$]	+	2K$_3$[Fe(CN)$_6$]	2147 (m) 2114 (m) 2077 (m)	50 mL methanol
4[(phen)$_2$Zn(NO$_3$)$_2$]	+	K$_3$[Fe(CN)$_6$]	2050 (w) 2143 (w) 2114 (m) 2082 (w, br)	50 mL water
[(phen)$_2$Zn(NO$_3$)$_2$]	+	K$_3$[Fe(CN)$_6$]	2150 (w) 2127 (w) 2112 (m)	50 mL water
3[(phen)$_2$Zn(NO$_3$)$_2$]	+	K$_4$[Fe(CN)$_6$]	2056 (s)	50 mL water
3[(phen)$_2$Zn(NO$_3$)$_2$]	+	2K$_4$[Fe(CN)$_6$]	2074 (s, br)	50 mL water

228

Table 4.13. Summary of IR data for reactions between [(phen)$_2$ZnCl$_2$] or [Zn(phen)$_3$]Cl$_2$ and K$_3$[Fe(CN)$_6$].

	ν(C≡N) stretches	Total Volume of water
3[(phen)$_2$ZnCl$_2$] + 2K$_3$[Fe(CN)$_6$]	2151 (w) 2126 (w) 2114 (m)	50 mL
3[(phen)$_2$ZnCl$_2$] + 2K$_3$[Fe(CN)$_6$]	2151 (m) 2127 (m) 2114 (s) 2088 (m)	100 mL
3[Zn(phen)$_3$]Cl$_2$ + 2K$_3$[Fe(CN)$_6$]	2174 (s) 2165 (s) 2133 (w) 2097 (m) 2084 (m)	50 mL
3[Zn(phen)$_3$]Cl$_2$ + 2K$_3$[Fe(CN)$_6$]	2173 (m) 2165 (m) 2133 (w) 2096 (m) 2082 (m)	100 mL

1624 and 1579 cm^{-1} in the IR. Both reactions led to products with similar cyanide stretches. The IR data is summarized in Table 4.13.

(16) Reaction of [Zn(phen)$_3$]Cl$_2$ and K$_3$[Fe(CN)$_6$]

Reactions performed in a 3:2 ratio of the reactants in both 50 mL and 100 mL of water lead to yellow gelatinous products with numerous cyanide stretches in the IR spectrum (Table 4.13).

(17) Reaction of (2,2'-bpy)$_2$Zn(NO$_3$)$_2$ and K$_3$[Fe(CN)$_6$]

A 3:2 ratio of the reactants in H$_2$O leads to the immediate production of a yellow precipitate with v(C≡N) modes located at 2177 (s), 2168 (s), 2162 (s), 2124 (m), 2114 (m), 2108 (m) and 2085 (s) cm^{-1}. The presence of 2,2'-bipyridine was evident from the v(C=C)/v(C=N) stretches located at 1607, 1597, 1577 and 1567 cm^{-1}. The complicated nature of the v(C≡N) region is indicative of the formation of several products and possibly mixed Fe^{III} and Fe^{II} oxidation states.

(18) Reaction of (2,2'-bpy)$_2$Zn(NO$_3$)$_2$ and K$_4$[Fe(CN)$_6$]

The reactants were combined in a 3:2 ratio to yield a gelatinous yellow product in water. The IR data revealed v(C≡N) modes located at 2085, 2062, 2048, and 2034 cm^{-1}.

(19) Reaction of (2,2'-bpy)$_2$ZnCl$_2$ and K$_3$[Fe(CN)$_6$]

An aqueous solution of 3 equivalents of $(2,2'\text{-bpy})_2ZnCl_2$ were combined with two equivalents of $K_3[Fe(CN)_6]$ to give a yellow precipitate with $\nu(C\equiv N)$ stretches at 2162 and 2090 cm^{-1} and $\nu(C=C)/\nu(C=N)$ modes at 1607, 1598, 1578 and 1568 cm^{-1} for the 2,2'-bpy ligand.

(20) Reaction of $(2,2'\text{-bpy})_2ZnCl_2$ and $K_4[Fe(CN)_6]$

The reactants were combined in a 3:2 ratio to yield a pale yellow/white gelatinous material in water. The product exhibited $\nu(C\equiv N)$ stretches at 2160, 2097, 2086 and 2061 cm^{-1} and $\nu(C=C)/\nu(C=N)$ modes at 1605, 1596 and 1576 cm^{-1} for the 2,2'-bpy ligand.

C. Molecular Structures

(1) $\{Mn(H_2O)_2[Mn(2,2'\text{-bpym})(H_2O)]_2[Fe(CN)_6]_2\}_\infty$ (36)

The asymmetric unit of the structure consists of one $[Fe(CN)_6]^{3-}$ unit connected to two different types of Mn^{II} centers via cyanide bridges. One Mn atom (Mn2) has retained only one 2,2'-bpym ligand while the other one (Mn1) has lost both of its original 2,2'-bpym ligands. For simplicity in describing the repeat pattern, the building blocks of the layers are defined as $[Fe(CN)_6]^{3-}$ (Fe1), *trans*-$[Mn(OH_2)_2]^{2+}$ (Mn1) and *fac*-$[Mn(2,2'\text{-}$ bpym)(OH_2)]^{2+}$ (Mn2) units. Each Fe^{III} ion forms bridges to three Mn2 and two Mn1 centers, which leaves behind one terminal CN$^-$ ligand. The *trans-*

[Mn(OH$_2$)$_2$]$^{2+}$ units are linked to four Fe^{III} ions, and each *fac*-[Mn(2,2'-bpym)(OH$_2$)]$^{2+}$ building block is connected to three independent [Fe(CN)$_6$]$^{3-}$ anions. The resulting polymeric framework is best described as being composed of individual 1-D chains formed by edge-sharing {[Mn(2,2'-bpym)(OH$_2$)]$_2$[Fe(CN)$_6$]$_2$} squares. These chains, which exhibit a staircase motif, are stitched into layers by *trans*-[Mn(OH$_2$)$_2$]$^{2+}$ bridges that serve to link Fe atoms of adjacent chains and to create two new corner-sharing {[Mn(2,2'-bpym)(OH$_2$)][Fe(CN)$_6$]$_2$-[Mn(OH$_2$)]$_2$} squares (Figure 4.7a). A simplified diagram of this structure, depicted in Figure 4.7b, reveals that the framework resembles a 2-D array of fused Mn$_4$Fe$_3$ cubes missing one vertex. It is of further interest to point out that the 2,2'-bpym ligands of adjacent layers are interdigitated to form a stacked column along the *c* axis with a mean spacing of 3.35 Å (Figure 4.8.). The bond distances and bond angles are summarized in Tables 4.14 and 4.15.

(2) {[Co(2,2'-bpy)$_2$]$_3$[Fe(CN)$_6$]$_2$}$^+$ (37)

The structure consists of two [Fe(CN)$_6$]$^{3-}$ units, each connected to three Co^{III} centers in a facial arrangement by cyanide bridges. Each pseudo-octahedral Co^{III} atom is composed of two 2,2'-bpy ligands, with the remaining two sites being filled by the nitrogen end of the cyanide ligand from the [Fe(CN)$_6$]$^{3-}$ units. The Co-N(2,2'-bpy) distances are in the range 1.847(9)-1.953(8) Å.

(a)

(b)
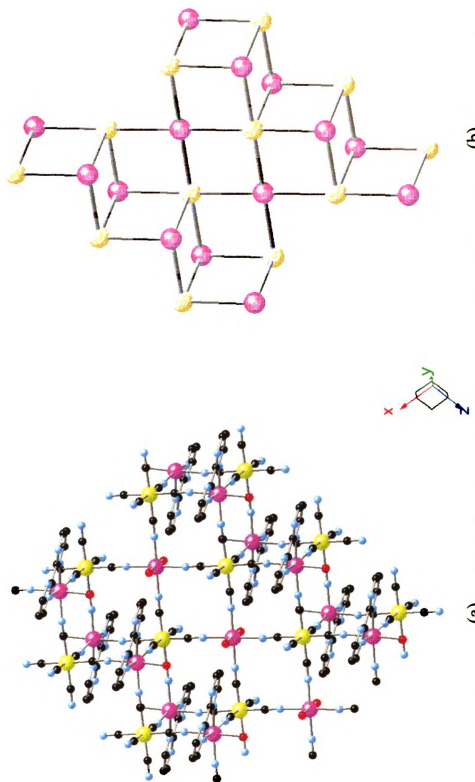
Figure 4.7. (a) View of the 2-D network of {Mn(H$_2$O)$_2$[Mn(2,2'-bpym)(H$_2$O)]$_2$[Fe(CN)$_6$]$_2$} (**36**) down the *b* axis (b) Scheme emphasizing the partial cubane motif in the 2-D network. (Image is presented in color)
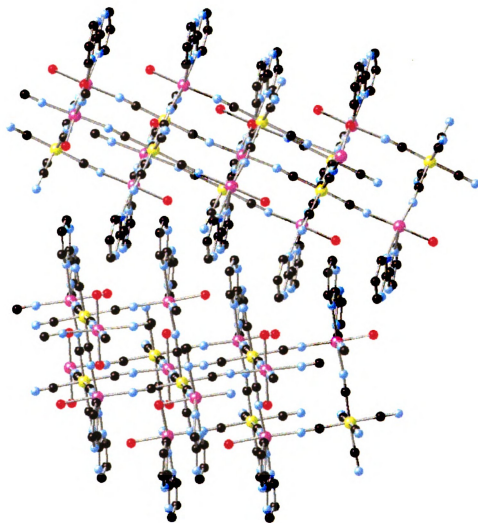
Figure 4.8. A view along the *c* axis of {Mn(H₂O)₂[Mn(2,2'-bpym)(H₂O)]₂[Fe(CN)₆]₂} (**36**). (Image in color)

Table 4.14. Selected bond distances [Å] for {Mn(H₂O)₂[Mn(2,2'-bpym)(H₂O)]₂[Fe(CN)₆]₂} (36)

A	B	A-B [Å]
Mn(1)	N(5)	2.177(10)
Mn(1)	O(1)	2.187(12)
Mn(1)	N(6)	2.193(11)
Mn(2)	N(3)	2.152(10)
Mn(2)	N(4)	2.148(13)
Mn(2)	N(2)	2.166(10)
Mn(2)	O(2)	2.282(8)
Mn(2)	N(8)	2.296(11)
Mn(2)	N(7)	2.275(10)
Fe(1)	C(5)	1.912(13)
Fe(1)	C(3)	1.953(12)
C(1)	N(1)	1.157(17)
C(3)	N(3)	1.131(13)
C(5)	N(5)	1.173(14)

Table 4.15. Selected bond angles [°] for
{Mn(H$_2$O)$_2$[Mn(2,2'-bpym)(H$_2$O)]$_2$[Fe(CN)$_6$]$_2$} (36)

A	B	C	A-B-C [°]
N(7)	Mn(2)	N(8)	71.5(4)
C(2)	N(2)	Mn(2)	172.0(10)
C(3)	N(3)	Mn(2)	174.5(12)
C(4)	N(4)	Mn(2)	169.4(11)
C(5)	N(5)	Mn(1)	179.7(15)
C(6)	N(6)	Mn(1)	174.1(11)
N(1)	C(1)	Fe(1)	178.4(15)
N(2)	C(2)	Fe(1)	177.8(13)
N(5)	C(5)	Fe(1)	176.3(11)
N(6)	C(6)	Fe(1)	177.4(11)

The bite angles for the 2,2'-bpy ligands are 82.0(4) and 82.7(4)°. The Fe-C(cyanide) bond distances are in the range 1.868(13)-1.949(12)Å. Bond distances and angles are given in Tables 4.16 and 4.17. Top and side views of the molecule are depicted in Figure 4.9 and the packing diagram is shown in Figures 4.10.

(3) [Ni(2,2'-bpy)$_2$(OH$_2$)][Ni(2,2'-bpy)$_2$]$_2$[Fe(CN)$_6$]$_2$ (38)

The structure of **38** consists of two [Fe(CN)$_6$]$^{3-}$ units connected to two (bpy)$_2$Ni^{II} centers to give a molecular square. One of the [Fe(CN)$_6$]$^{3-}$ units is connected to two Ni^{II} centers within the molecular square and is further coordinated to a third Ni^{II} molecule which contains two bpy ligands and a H$_2$O molecule. Bond distances and angles are given in Table 4.18 and 4.19. The packing of this structure is presented in Figure 4.11.

(4) [Zn(phen)$_3$][Zn(phen)$_2$]$_2$[Fe(CN)$_6$]$_2$ (39)

The structure of this compound is a molecular square with alternating [Zn(phen)$_2$]$^{2+}$ and [Fe(CN)$_6$]$^{3-}$ units connected by cyanide bridges. Each [Fe(CN)$_6$]$^{3-}$ possesses four terminal CN$^-$ ligands. The molecular square is anionic and therefore the [Zn(phen)$_3$]$^{2+}$ cation is present for charge neutrality. The Zn-N(phen) bond distances are in the range 2.081(13)-2.265(13)Å. The bite angles for the phen ligand are in the range 74.2(5)-
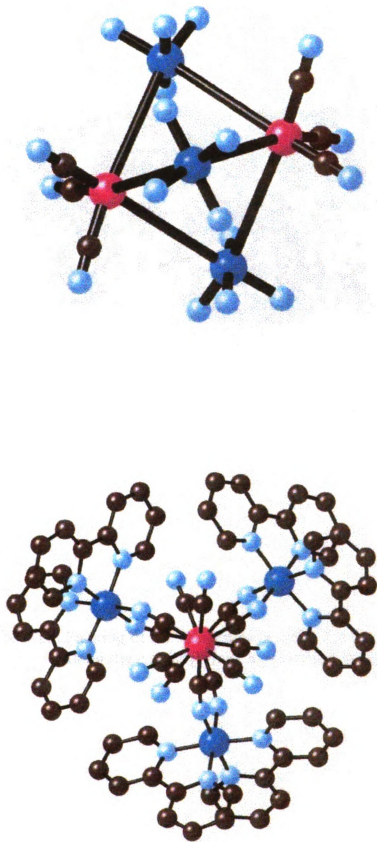
Figure 4.9. View of {[Co(2,2'-bpy)$_2$]$_3$[Fe(CN)$_6$]$_2$}$^+$ (37) from the top (left) and side (right) where the black rods represent CN$^-$ ligands and each 2,2'-bpy ligand is represented by two blue atoms attached to the cobalt atoms. (Image is presented in color)
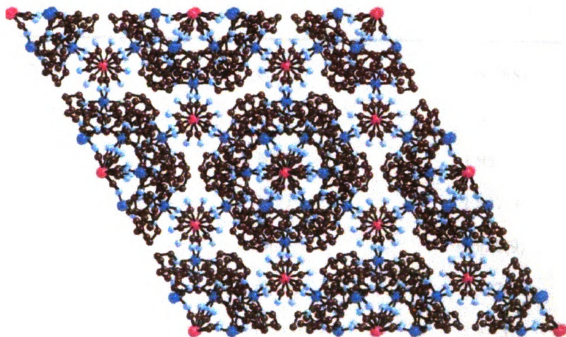
Figure 4.10. Packing of the molecules in $\{[Co(2,2'\text{-bpy})_2]_3[Fe(CN)_6]_2\}^+$ (**37**) along the *c* axis. (Image is presented in color)

Table 4.16. Selected bond distances [Å] for $\{[Co(2,2'\text{-bpy})_2]_3[Fe(CN)_6]_2\}^+$
(37)

A	B	A-B [Å]
Co(1)	N(6)	1.879(8)
Co(1)	N(10)	1.906(8)
Co(1)	N(9)	1.953(8)
Co(4)	N(7)	1.847(9)
Co(4)	N(8)	1.928(9)
Co(4)	N(16)	1.927(10)
Fe(1)	C(100)	1.93(3)
Fe(2)	C(22)	1.879(12)
Fe(2)	C(1)	1.949(12)
Fe(3)	C(26)	1.868(13)
Fe(3)	C(59)	1.888(10)
C(1)	N(1)	1.136(12)
C(59)	N(6)	1.191(11)
C(22)	N(7)	1.216(13)
C(100)	N(100)	1.35(3)

Table 4.17. Selected bond angles [°] for {[Co(2,2'-bpy)$_2$]$_3$[Fe(CN)$_6$]$_2$}$^+$ (37)

A	B	C	A-B-C [°]
N(9)	Co(1)	N(10)	82.0(4)
N(8)	Co(4)	N(16)	82.7(4)
C(59)	N(6)	Co(1)	161.8(7)
C(22)	N(7)	Co(4)	165.3(7)
N(7)	C(22)	Fe(2)	172.9(8)
N(1)	C(1)	Fe(2)	177.5(11)
N(60)	C(26)	Fe(3)	173.3(11)
N(6)	C(59)	Fe(3)	174.0(9)
N(100)	C(100)	Fe(1)	172(2)

Table 4.18. Selected bond distances [Å] for
{[Ni(2,2'-bpy)$_2$(H$_2$O)][Ni(2,2'-bpy)$_2$]$_2$[Fe(CN)$_6$]$_2$} (**38**)

A	B	A-B [Å]
Ni(1)	N(2)	2.119(6)
Ni(1)	N(3)	2.081(8)
Ni(1)	N(15)	2.047(7)
Ni(2)	N(5)	2.099(7)
Ni(2)	N(6)	2.068(8)
Ni(2)	N(16)	2.065(8)
Ni(5)	N(21)	2.037(8)
Ni(5)	N(24)	2.080(7)
Ni(5)	O(100)	2.104(6)
Fe(1)	C(52)	1.925(8)
Fe(1)	C(48)	1.950(9)
Fe(2)	C(46)	1.946(8)
Fe(2)	C(44)	1.963(9)
C(46)	N(9)	1.164(10)
C(49)	N(16)	1.149(11)

Table 4.19. Selected bond angles [°] for
{[Ni(2,2'-bpy)$_2$(H$_2$O)][Ni(2,2'-bpy)$_2$]$_2$[Fe(CN)$_6$]$_2$} (38)

A	B	C	A-B-C [°]
N(3)	Ni(1)	N(4)	78.4(3)
N(14)	Ni(1)	N(15)	90.4(3)
N(7)	Ni(2)	N(8)	78.1(3)
N(9)	Ni(2)	N(16)	89.9(3)
N(22)	Ni(5)	N(23)	78.6(3)
N(21)	Ni(5)	O(100)	86.2(3)
C(47)	N(15)	Ni(1)	169.3(7)
C(49)	N(16)	Ni(2)	171.3(7)
C(52)	N(21)	Ni(5)	151.4(7)
N(21)	C(52)	Fe(1)	172.7(8)
N(16)	C(49)	Fe(1)	174.1(8)
N(9)	C(46)	Fe(2)	175.9(8)
N(12)	C(42)	Fe(2)	178.5(8)

(a)

(b)
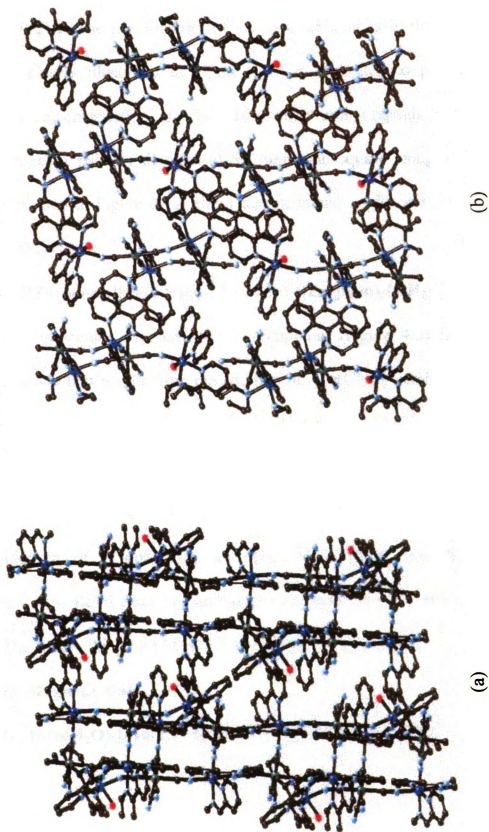
Figure 4.11. View of the packing diagram of {[Ni(2,2'-bpy)$_2$(H$_2$O)][Ni(2,2'-bpy)$_2$]$_2$[Fe(CN)$_6$]$_2$} (**38**) (a) along the ab plane and (b) along the bc plane. (Image in presented in color)

77.2(5)°. The Fe-C(cyanide) bond distances are in the range 1.882(15)-1.99(2)Å. The non-linearity of the cyanide ligands in this molecular square (as clearly illustrated in Figure 4.4.) is attributed to packing effects that involve $[Zn(phen)_3]^{2+}$ and the 1,10-phenanthroline ligands that cap the anionic square. A packing diagram of the molecular square along with the cation is presented in Figure 4.12. Bond distances and angles are presented in Table 4.20 and 4.21.

(5){[Zn(phen)₂][Fe(CN)₆]}₂{Zn(phen)₂][Zn(phen)₂(OH₂)][Fe(CN)₆]}₂ (40)

This molecular structure of this compound (Figure 4.5) is a very unusual decamer that results from the addition of $[Fe(CN)_6]^{3-}$ and $[Zn(phen)_2]^{2+}$ units to the molecular square $[Zn(phen)_3][Zn(phen)_2]_2[Fe(CN)_6]_2$. The square is composed of two $[Fe(CN)_6]^{3-}$ units connected to two $[Zn(phen)_2]^{2+}$ by cyanide bridges in a *cis* arrangement but, the molecule grows by further addition of $[Zn(phen)_2]^{2+}$ and $[Fe(CN)_6]^{3-}$ units through *trans* cyanide linkages. Bond distances and angles are presented in Tables 4.22 and 4.23. The space filling plot of (40) is presented in Figure 4.13.

D. Magnetic Data

(1) {Mn(H₂O)₂[Mn(2,2'-bpym)(H₂O)]₂[Fe(CN)₆]₂}∞ (36)

Table 4.20. Selected bond distances [Å] for {[Zn(phen)$_3$][Zn(phen)$_2$]$_2$[Fe(CN)$_6$]$_2$} (39)

A	B	A-B [Å]
Zn(1)	N(2)	2.186(13)
Zn(1)	N(4)	2.091(13)
Zn(2)	N(11)	2.065(15)
Zn(2)	N(8)	2.266(14)
Fe(3)	C(66)	1.933(17)
Fe(3)	C(64)	1.95(2)
Fe(3)	C(62)	1.97(2)
Fe(3)	C(61)	1.873(17)
C(66)	N(16)	1.143(18)
C(63)	N(13)	1.18(2)
C(64)	N(14)	1.164(19)
C(62)	N(11)	1.126(18)

Table 4.21. Selected bond angles [°] for
{[Zn(phen)$_3$][Zn(phen)$_2$]$_2$[Fe(CN)$_6$]$_2$} (39)

A	B	C	A-B-C [°]
N(1)	Zn(1)	N(23)	76.6(6)
N(3)	Zn(1)	N(2)	77.2(5)
N(5)	Zn(1)	N(4)	76.8(5)
N(7)	Zn(2)	N(8)	73.9(6)
N(9)	Zn(2)	N(10)	75.0(6)
C(61)	N(12)	Zn(2)	162.9(12)
C(62)	N(11)	Zn(2)	162.9(14)
N(16)	C(66)	Fe(3)	176.8(15)
N(13)	C(63)	Fe(3)	177.6(16)
N(11)	C(62)	Fe(3)	176.1(17)
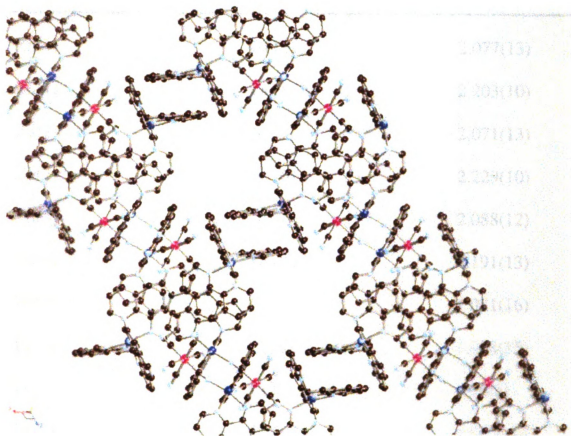
Figure 4.12. View of the packing diagram of {[Zn(phen)$_3$][Zn(phen)$_2$]$_2$ [Fe(CN)$_6$]$_2$} (**39**) down the *b* axis. (Image is presented in color)

Table 4.22. Selected bond distances [Å] for
{[Zn(phen)$_2$][Fe(CN)$_6$]}$_2${[Zn(phen)$_2$][Zn(phen)$_2$(OH$_2$)][Fe(CN)$_6$]}$_2$ **(40)**

A	B	A-B [Å]
Zn(1)	N(12)	2.077(13)
Zn(1)	O(1)	2.203(10)
Zn(2)	N(6)	2.071(13)
Zn(2)	N(16)	2.229(10)
Zn(3)	N(7)	2.088(12)
Zn(3)	N(120)	2.191(13)
Fe(4)	C(57)	1.981(16)
Fe(4)	C(68)	1.908(15)
Fe(5)	C(29)	1.98(2)
Fe(5)	C(81)	1.883(16)
C(82)	N(86)	1.147(17)
C(67)	N(5)	1.132(16)
C(57)	N(205)	1.102(16)
C(49)	N(1)	1.169(18)
C(39)	N(81)	1.175(18)

Table 4.23. Selected bond angles [°] for
{[Zn(phen)$_2$][Fe(CN)$_6$]}$_2${[Zn(phen)$_2$][Zn(phen)$_2$(OH$_2$)][Fe(CN)$_6$]}$_2$ (**40**)

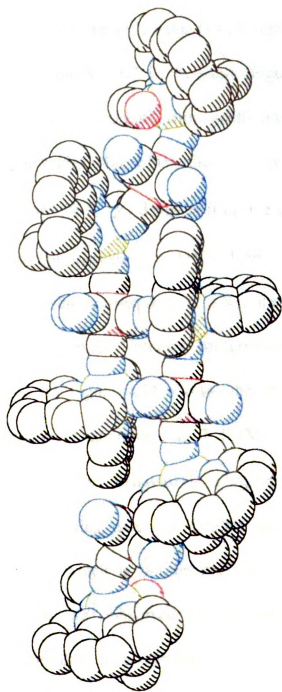| A	B	C	A-B-C [°]
N(121)	Zn(1)	N(122)	78.6(5)
N(2)	Zn(1)	N(14)	78.8(5)
N(9)	Zn(2)	N(10)	76.5(5)
N(8)	Zn(2)	N(16)	75.4(4)
N(15)	Zn(3)	N(120)	75.7(5)
C(81)	N(12)	Zn(1)	145.7(13)
C(37)	N(6)	Zn(2)	163.1(12)
C(82)	N(86)	Zn(2)	147.0(12)
C(68)	N(7)	Zn(3)	173.6(12)
N(7)	C(68)	Fe(4)	175.5(12)
N(5)	C(67)	Fe(5)	175.1(13)
N(13)	C(69)	Fe(5)	176.3(13)

Figure 4.13. Space filling diagram of {[Zn(phen)$_2$][Fe(CN)$_6$]}$_2$[Zn(phen)$_2$][Zn(phen)$_2$(H$_2$O)][Fe(CN)$_6$]}$_2$ (40) taken from coordinates of the X-ray structure. (Image is presented in color)

The molar susceptibity χ_m between 50 and 300 K was fit to a Curie-Weiss law with C = 13.8 K mol^{-1} and (θ = -12.8 K. The Curie constant is in good agreement with the expected spin-only value (13.875 emu K mol^{-1}) for three S = 5/2 Mn^{II} and two low-spin S = 1/2 Fe^{III} centers (Figure 4.14). The sign of the Weiss constant indicates local antiferromagnetic interactions as expected for Fe^{III}-CN-Mn^{II} spin bridges for which there is direct overlap of the t$_{2g}$ magnetic orbitals. Below 50 K, χ_m deviates from the Curie-Weiss behavior and undergoes an abrupt increase at ~11K which suggests the onset of magnetic ordering. This state corresponds to a ferromagnetic ordering, since the Fe^{III} and Mn^{II} spin centers interact antiferromagnetically with non-cancellation of spins. As Figure 4.14 shows, the magnetization increases gradually, but saturation is incomplete at 7 T (M = 11.6 μ_B versus the theoretical value 13 μ_B). This behavior is a signature of a complicated magnetic structure (competing magnetic interactions with possibly some degree of spin canting), which is not unexpected in view of the crystal structure. No hysteresis was observed in the field dependence of the magnetization. Susceptibility measurements of the ac type confirm the ferromagnetic ordering at 11 K (Figure 4.15) and reveal no significant frequency dependence.
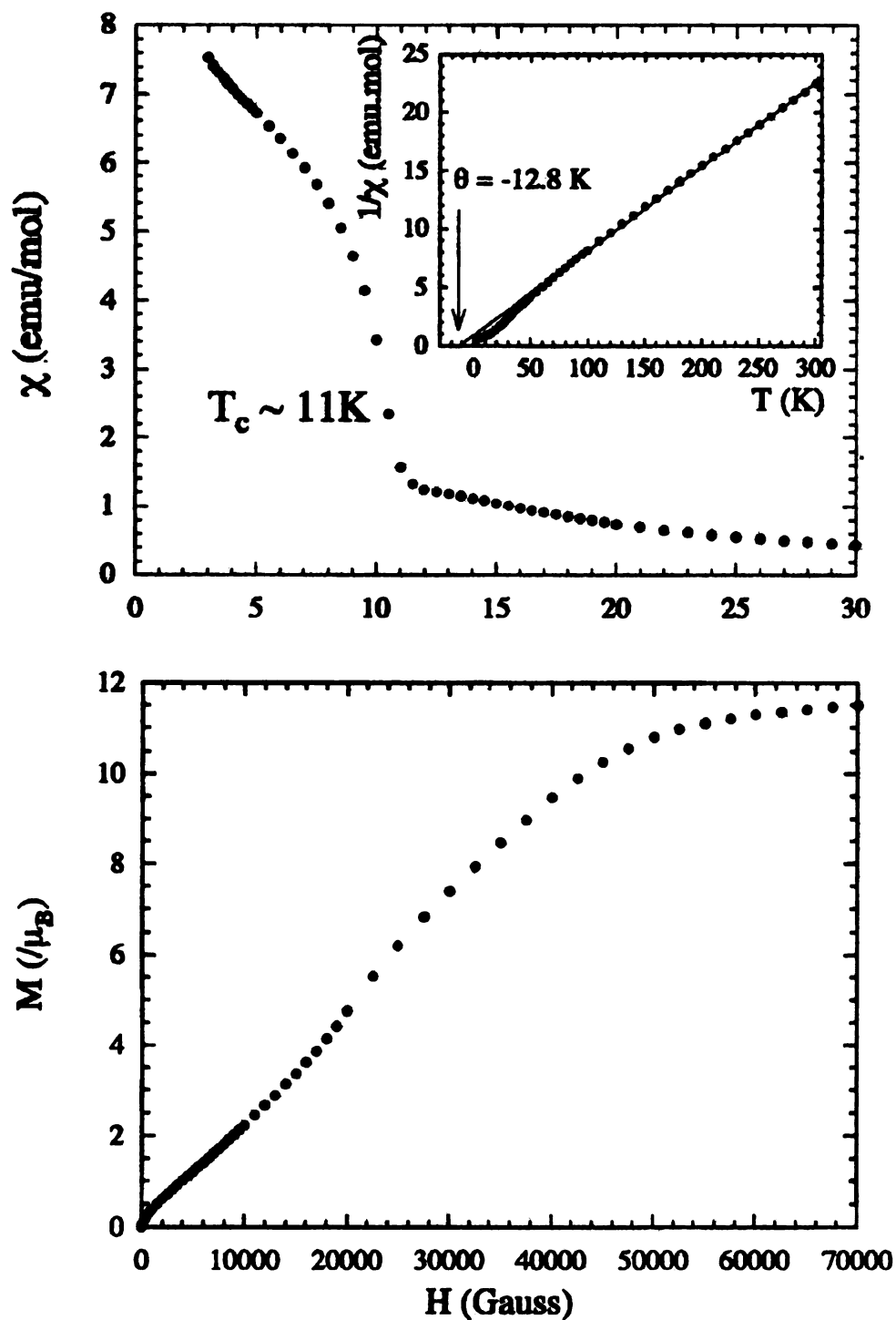
Figure 4.14. Thermal dependence below 30 K of χ_m at 100 G for complex
(36). Inset: temperature dependence of $1/\chi_m$ between 2-300 K.
The solid line indicates the best fit to the Curie-Weiss law. Field
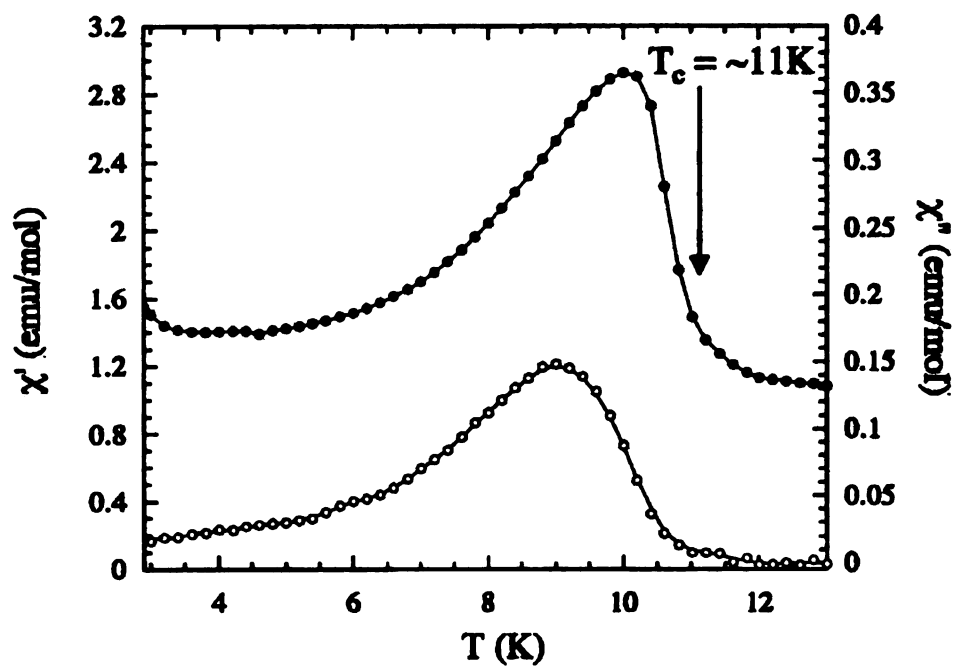dependence of the magnetization at 2 K (bottom)

Figure 4.15. Temperature dependence of the ac suceptibility (in-phase, χ', and out-of-phase, χ'') below 13 K (ac measuring field 1 G (10^{-4} T); frequency of 1 Hz; no external dc field).

4. SUMMARY AND CONCLUSIONS

Reactions between protected metal precursors and hexacyanometallate anions lead to interesting motifs and magnetic properties as judged by the results presented in this chapter. Only one discrete magnetic cluster was synthesized, namely the pentamer $[Ni(2,2'-bpy)_2(OH_2)][Ni(2,2'-bpy)_2][Fe(CN)_6]_2$ **(38)** which has an interesting, low symmetry structure. Future work in this area will involve other hexacyanometallate anions as well as cations with different protecting groups including tetradentate ligands instead of two *cis* bidentate ligands. The possibilities are numerous and the field will undoubtedly grow as more researchers opt to use the cyanide ligand to construct new magnetic molecules and materials.

5. REFERENCES

1. (a) Keggin, J. F.; Miles, F. D. *Nature* **1936**, *137*, 577. (b) Holtzman, H. *Ind. Eng. Chem.* **1945**, *37*, 855. (c) El-Sayed, M. F. A.; Sheline, R. K. *J. Inorg. Nucl. Chem.* **1958**, *6*, 187. (d) Dows, D. A.; Haim, A.; Wilmarth, W. K. *J. Inorg. Nucl. Chem.*, **1961**, *21*, 33. (e) Griffith, W. P. *Q. Rev.*, **1962**, *16*, 188. (f) Shriver, D. F. *Structure Bonding*, **1966**, 32. (g) Chadwick, B. M.; Sharpe, A. G. *In Advances in Inorganic Chemistry and Radiochemistry* **1966**, *8*, 83. (h) Britton, D. *In Perspectives in Structural Chemistry* **1967**, *1*, 109. (i) Ludi, A.; Gudel, H. U. *Structure Bonding*, **1973**, *14*, 1. (j) Sharpe, A. G. The Chemistry of Cyano Complexes of the Transition Metals, Academic Press Inc. New York **1976**. (k) Dunbar, K. R.; Heintz, R. A. *Progress in Inorg. Chem.* **1997**, *45*, 283. (l) Vahrenkamp, H.; Geiss, A.; Richardson, G. N. *J. Chem. Soc. Dalton*, **1997**, *20*, 3643.

2. (a) Gadet, V.; Mallah, T.; Castro, I.; Berdaguer, M. *J. Am. Chem. Soc.* **1992**, *114*, 9213. (b) Verdaguer, M. *Science* **1996**, *272*, 698, and references therein. (c) Bushmann, W. E.; Paulson, S. C.; Wynn, C. M.; Girtu, M. A.; Epstein, A. J.; White, H. S.; Miller, J. S. *Chem. Mat.* **1998**, *10*, 1386. (d) Ferlay, S.; Mallah, T.; Ouachés, R.; Veillet, R.; Verdaguer, M. *Inorg. Chem.* **1999**, *38*, 229. (e) Miller, J. S.; Epstein, A. J.; *Chem. Commun.* **1998**, 1319.

(f) Zhang, J.; Liable-Sands, L. M.; Rheingold, A. L.; Del Sesto, R. E.; Gordon, D. C.; Burkhart, B. M.; Miller, J. S. *Chem. Commun.* **1998**, 1385.

(g) Zhang, J.; Ensling, J.; Ksenofontov, V.; Gütlich, P.; Epstein, A. J.; Miller, J. S. *Angew. Chem. Int. Ed.* **1998**, *37*, 637. (h) Klenze, R.; Kanellakoupuolos, B.; Trageser, G.; Eysel, H. H. *J.Chem. Phys.*, **1980**, *72(11)*, 5819 (i) Holmes, S. M.; Girolami, G. S. *J. Am. Chem. Soc.* **1999**, *121*, 5593. (j) Hatlevik, O.; Buschmann, W. E.; Zhang, J.; Manson, J. L.; Miller, J. S. *Adv. Mater.* **1999**, *11*, 914. (k) Dujardin, E.; Ferlay, S.; Phan, X.; Desplances, C.; d. Moulin, C. C.; Sainctavit, P.; Baudelet, F.; Dartyge, E.; Veillet, P., Verdaguer, M. *J. Am. Chem. Soc.* **1998**, *120*, 11347. (l) Ferlay, S.; Mallah, T.; Ouahes, R.; Veillet, P.; Verdaguer, M. *Nature (London)*, **1995**, *378*, 701. (m) Mallah, T.; Thiébaut, S.; Verdaguer, M.; Veillet, P. *Science* **1993**, *262*, 1554. (n) Entley, W. R.; Girolami, G. S. *Science* **1995**, *268*, 397. (o) Babel, D. *Comments Inorg. Chem.* **1986**, *5(6)*, 285., Greibler, W. D.; Babel, D. *Z Naturforsch.* **1982**, *87b*, 832. (p) Entley, W. R.; Girolami, G. S. *Inorg. Chem.* **1994**, *33*, 5165. (q) Juszczyk, S.; Johansson, C.; Hanson, M.; Ratuszna, A.; Malecki, G. *J. Phys.: Condens. Matter* **1994**, *6*, 5697.

3. (a) Langenberg, K. V.; Batten, S. R.; Berry, K. J.; Hockless, D. C. R.; Moubaraki, B.; Murray, K. S. *Inorg. Chem.* **1997**, *36*, 5006. (b) Marvilliers,

A.; Pei, Y.; Boquera, J. C.; Vostrikova, K. E.; Paulsen, C.; Rivière, E.; Audière, J.-P.; Mallah, T. *Chem. Commun.* **1999**, 1951. (c) Vostrikova, K. E.; Luneau, D.; Wernsdorfer, W.; Rey, P.; Verdaguer, M. *J. Am. Chem. Soc.* **2000**, *122*, 718. (d) Salah, M.; Fallah, E.; Rentschler, E.; Caneschi, A.; Sessoli, R.; Gatteschi, D. *Angew. Chem. Int. Ed. Engl.* **1996**, *35*, 1947. (e) Ferlay, S.; Mallah, T.; Vaissermann, J.; Bartolome, F.; Veillet, P.; Verdaguer, M. *Chem. Commun.* 1996, 2481. (f) Re, N.; Gallo, E.; Floriani, C.; Miyasaka, H.; Matsumoto, N. Inorg. Chem. 1996, 35, 6004. (g) Colacio, E.; Dominguez-Vera, J. M.; Ghazi, M.; Kivekas, R.; Lloret, F.; Moreno, J. M.; Stoeckli-Evans, H. chem. Commun. 1999, 987. (h) Miyasaka, H.; Ieda, H.; Matsumoto, N.; Re, N.; Crescenzi, R.; Floriani, C. Inorg. Chem. 1998, 37, 255. (i) Kou, H.-Z.; Bu, W.-M.; Liao, D.-L., Jiang, Z.-H., Yan, S.-P.; Fan, Y.-G.; Wang, G.-L. J. Chem. Soc., Dalton Trans. 1998, 4161. (j) Marvilliers, A.; Parsons, S.; Riviere, E.; Audiere, J.-P.; Mallah, T. Chem. Commun. 1999, 2217.

4. (a) Ohba, M.; Okawa, H. *Coord. Chem. Rev.* **2000**, *198*, 313. (b) Miyasaka, H.; Okawa, H.; Miyazaki, A.; Enoki, T. Inorg. Chem. 1998, 37, 4878. (c) Fukita, N.; Ohba, M.; Okawa, H.; Matsuda, K.; Iwamura, H. Inorg. Chem. 1998, 37, 842. (d) Ohba, M.; Okawa, H.; Fukita, N.; Hashimoto, Y. J. Am. Chem. Soc. 1997, 119, 1011. (e) Ohba, M.; Okawa, H.; Ito, T.; Ohto, A.

J. Chem. Soc., Chem. Commun. **1995**, 1545.

5. Ohba, M.; Maruono, N.; Okawa, H.; Enoki, T.; Latour, J.-M. J. Am. Chem. Soc. 1994, 116, 11566.

6. Ohba, M.; Usuki, N.; Fukita, N.; Okawa, H. *Angew. Chem. Int. Ed.Engl.* **1999**, *38*, 1795.

7. [Mn(2,2-bpym)₂(H₂O)₂](SO₄) was synthesized by an adaptation of the procedure reported for the perchlorate salt: Hong, D. M.; Wei, H. H.; Gan, L. L.; Lee, G. H.; Wang, Y. *Polyhedron* **1996**, *15*, 2335.

8. Ohno, T.; Kato, S. Bull. Chem. Soc. Jpn **1974**, *47*(12), 2953.

9. SAINT 1000 and 6.0, Bruker Analytical X-ray Instruments, Madison, WI, 53719 (**1999** and **2000**)

10. Sheldrick, G. M. "SADABS, Siemens Area Detector Absorption Correction", Univ. of Gottingen, Gottingen, Germany (**1998**).

11. Altomare, A.; Burla, M. C.; Camalli, M.; Cascarano, G. L.; Giacovazza, C.; Guagliardi, A.; Moliterni, A. G. G.; Polidori.G.; Spagna, R. *J. Appl. Crystallogr.* **1999**, *32*, 115.

12. Sheldrick, G. M. SHELXTL version 5.10, Reference Manuel, Bruker Industrial Automation, Analytical Instrument, Madison, WI 53719 (**1999**). Program for Refinement of Crystal Structure, University of Göttingen, Göttingen, Germany.